EXPERIMENTAL APPROACHES TO MEASURING BRAIN EXPOSURE:

RATE, EXTENT AND REGIONAL DISTRIBUTION

Rong Zhao

A dissertation submitted to the faculty of the University of North Carolina at Chapel Hill in partial fulfillment of the requirements for the degree of Doctor of Philosophy in the School of Pharmacy.

Chapel Hill
2007

Approved by:

Advisor: Gary M. Pollack, Ph.D.

Reader: James E. Hall, Ph.D.

Reader: David S. Miller, Ph.D.

Reader: Adam Persky, Ph.D.

Reader: Thomas J. Raub, Ph.D.

ABSTRACT

RONG ZHAO: Experimental Approaches to Measuring Brain Exposure:
Rate, Extent and Regional Distribution
(Under the direction of Gary M. Pollack, Ph.D.)

The objective of this project was to understand the influence of physicochemical properties of compounds, biologic factors and physiologic factors on the kinetics (rate, extent and regional distribution) of brain uptake. The initial rate of brain uptake was determined using *in situ* brain perfusion in mice, and was found to vary widely among different compounds. Lipophilicity and ionization state, brain tissue unbound fraction, and P-gp-mediated efflux were important determinants of the rate of brain uptake. Fexofenadine was poorly permeable at the blood-brain barrier (BBB) and the slow equilibration of this compound between brain tissue and blood influenced the accuracy of measurement of kinetic parameters such as the P-gp efflux ratio. Pharmacokinetic simulations and continuous subcutaneous infusion with osmotic minipumps provided evidence of time-dependency in fexofenadine P-gp efflux ratio at the BBB. The more permeable precursor, terfenadine, was biotransformed to fexofenadine in brain tissue and increased fexofenadine brain exposure. The potential functional efficiency of breast cancer resistance protein (Bcrp), which shares similar expression pattern and substrate specificity with P-gp, was evaluated using *in vitro*, *in situ* and *in vivo* experimental approaches. While Bcrp effectively mediated substrate flux *in vitro*, it had limited impact on brain tissue exposure *in situ* or *in vivo*. The impact of local perfusion flow rate,

capillary density, and P-gp activity on regional exposure to colchicine, quinidine, verapamil, diazepam and loperamide was evaluated in *mdr1a(+/+)* and *mdr1a(-/-)* mice using the *in situ* brain perfusion and *in vivo* administration together with brain microdissection technique. The regional perfusion rate varied 7.5-fold, and capillary density varied 3.7-fold, among the thirteen brain regions examined. Regional flow correlated with capillary density (R^2=0.955). Regional P-gp-mediated efflux activity for colchicine and verapamil was directly proportional to local capillary density. Verapamil brain uptake was reduced with decreased blood perfusion rate, and P-gp-mediated efflux in less-perfused brain regions was influenced by changes in flow. In well-perfused brain structures, flow had no or little effect on P-gp activity. Taken together, these results provide a framework for understanding the multiplicity of interactive factors that determine regional brain exposure in intact animals.

ACKNOWLEDGEMENTS

I would like to sincerely thank my advisor Dr. Gary M. Pollack for his generous support of time, knowledge and patience. Most importantly, he gave me the freedom to explore on my own and encouraged me to become not only a pharmacokineticist but also an independent thinker. I am also grateful for having an exceptional committee and wish to thank Dr. James E. Hall for his generous analytical support, Dr. David S. Miller for his insightful discussion, Dr. Adam M. Persky for his modeling expertise, Dr. Thomas J. Raub for his inspiration of the work presented in Chapter 4, and his constructive suggestions in both experiments and manuscript writing.

I would like to extend many thanks to Dr. Arlene Bridges for her LC/MS/MS analysis expertise, Geri A. Sawada and Steven C. Kaspers from Eli Lilly and Company for the fine experiments with *in vitro* cell transport assays, Souzan Yanni for the help in brain metabolism experiment, Drs. Chris Wiesen and Heyward Hull for statistical consultation. I wish to thank my past and present fellow graduate students in our laboratory for their help, especially Dr. J. Cory Kalvass for his help in bioanalysis, protein binding assay and insightful scientific discussions and Dr. Candace Graff for showing me the elegance of pharmacokinetic modeling.

I am also thankful to my colleagues and friends, especially Jeannie Padowski, Emily Olson, Michael Wang, Xin Ming, Zhen Xu, Dongmei Lu, David L. Bourdet, Seowang Hong, Maciej J. Zamek-Gliszczynski and Xiaoyan Wang.

Finally, I want to thank my husband, Dr. Bubing Zeng for his support, encouragement, quiet patience and unwavering love. I thank my parents, for their unconditional love and support.

TABLE OF CONTENTS

LIST OF TABLES

LIST OF FIGURES

LIST OF ABBREVIATIONS

ABC	ATP-Binding Cassette
AUC	Area under the curve
BBB	Blood-brain barrier
Bcrp	Breast cancer resistance protein
BCSFB	Blood cerebrospinal fluid barrier
BMECs	Brain microvessel endothelial cells
BUI	Brain uptake index
$clogD_{7.4}$	Calculated octanol-water partition coefficient at pH 7.4
clogP	Calculated octanol-water partition coefficient in unionized state
CNS	Central nervous system
CSF	Cerebrospinal fluid
CYP	Cytochrome P450
DHEAS	Dehydroepiandrosterone sulfate
DPDPE	[D-penicillamine^{2,5}]-enkephalin
$f_{u,brain}$	Drug unbound fraction in brain tissue
$f_{u,plasma}$	Drug unbound fraction in plasma
GLUT1	Glucose transporter 1
HIV	Human immunodeficiency virus
HPLC	High performance liquid chromatography
$k_{p,brain}$	Brain partition coefficient
LC/MS/MS	Liquid chromatography - tandem mass spectrometry

LogBB	Logarithm of the brain-to-blood concentration ratio
MCT	Monocarboxylic acid transporter
MDR/Mdr	Multi-drug resistance gene
MRP/Mrp	Multi-drug resistance associated protein
Oat	Organic anion transporter
Oatp	Organic anion transporting polypeptide
PET	Positron emission tomography
P-gp	P-glycoprotein
PS	Permeability-surface area coefficient
$t_{1/2eq,brain}$	Brain equilibrium half-life
UGT	Uridine diphosphate glucuronosyltransferase

CHAPTER 1

INTRODUCTION

The time course of central nervous system (CNS) pharmacologic response is a complex function of CNS pharmacokinetics (drug exposure at the site of action) and pharmacodynamics (the relationship between the biologic response and drug concentration at the site of action). The presence of the blood-brain barrier (BBB) at the interface between the brain and the systemic circulation significantly restricts the entry of many molecules into the brain, including new chemical entities and potential drugs with intended central activity.

Drug presentation to CNS sites of action also is a complex multi-process phenomenon dependent upon movement of therapeutic agents from the site of administration to the bloodstream (systemic pharmacokinetics) and then from the bloodstream to the site of action (CNS pharmacokinetics). Understanding how, and at what rate, drugs access CNS target sites often is problematic due to the complexity of the organ per se, as well as to the limitations inherent in available experimental methodologies. These limitations are especially evident, albeit understandable, in clinical pharmacology studies.

The brain is a compartmentalized organ, in terms of both macro- and micro-architecture. The biophase (i.e., the specific location of the target receptor and the surrounding microenvironment) can be accessed from the extracellular fluid (ECF), intracellular fluid (ICF), or in some cases the cerebrospinal fluid (CSF). In addition, therapeutic targets are not distributed homogeneously throughout the brain. Thus, measurement of drug uptake into whole brain, which typically is performed in preclinical CNS pharmacokinetic studies, may not provide an accurate representation of drug exposure at the target site.

Recently, *in vitro*, *in situ*, and *in vivo* models have been developed to study many aspects of CNS pharmacokinetics, including the rate and extent of BBB penetration. Significant recent attention has been paid to the mechanisms that determine BBB permeation. However, factors that influence regional drug exposure in brain, and thereby determine drug presentation to the site of action following BBB penetration, are only beginning to be appreciated. Factors that influence the systemic (absorption, distribution, metabolism and elimination), and CNS (protein binding in plasma and brain tissue, BBB permeability, active transport and metabolism, CSF turnover, local cerebral blood flow rate, capillary density, and regional transporter and metabolizing enzymes expression level and functionality) all contribute to the determinants of drug exposure at the site of action and the resultant pharmacologic or toxic effect (Brodie et al., 1960; Fenstermacher et al., 1981; Schinkel et al., 1994; Kalvass and Maurer, 2002; Liu et al., 2004; Liu and Chen, 2005; Kalvass et al., 2007a).

THE BLOOD-BRAN BARRIER (BBB)

The BBB is the primary interface between the CNS and the systemic circulation. The BBB is formed by a continuous monolayer of brain capillary endothelial cells. The highly-developed tight junctions, as well as a lack of fenestrae and limited pinocytic or transcytotic activities, significantly limit brain penetration of many endogenous and exogenous compounds, including therapeutic agents. This physical barrier only allows compounds with lipid solubility to traverse it. Physicochemical properties such as molecular weight, pKa, lipophilicity, polar surface area, and the number of hydrogen bonds are important determinants of BBB penetration (Brodie et al., 1960).

The BBB is not only a structural barrier, but also a functional barrier regulating the turnover of endogenous and exogenous substrates by active transport and metabolism in the brain (Strobel et al., 2001; Begley, 2003; Begley, 2004a; Graff and Pollack, 2004; Terasaki and Ohtsuki, 2005). The most important physiologic role of BBB functionality is to control precisely CNS homeostasis. The BBB supplies amino acids, glucose, and creatine to the brain through the action of specific carrier systems expressed at the brain capillary endothelial cells. The BBB also is involved in the brain-to-blood efflux transport of neurotransmitters (e.g., γ-aminobutyric acid, dopamine) and metabolites of neurotransmitters and neurosteroids (e.g., dehydroepiandrosterone sulfate) (Graff and Pollack, 2004; Ohtsuki, 2004; Terasaki and Ohtsuki, 2005). The BBB functionality is regulated by the surrounding astrocytes, neurons, pericytes and microglial cells. The expression of transporters, GLUT1, MCT1, P-gp and Mrps at the BBB is modulated by dietary and pathological conditions (Koehler-Stec et al., 1998; Terasaki and Pardridge, 2000; Ohtsuki, 2004; Terasaki and Ohtsuki, 2005; Ohtsuki and Terasaki, 2007). An alteration in BBB function may lead to several CNS disease etiologies and neurodegenerative disorders, including recent speculation regarding Alzheimer's disease (Vogelgesang et al., 2004; Zlokovic, 2004).

THE BLOOD-CEREBROSPINAL FLUID BARRIER (BCSFB)

The BCSFB is a composite barrier comprised of the choroid plexi, the arachnoid membrane, and the periventricular organs (including the area postrema, median eminence, neurohypophysis, and pineal gland) (de Lange, 2004; Strazielle et al., 2004). The choroid plexus epithelium is sealed by tight junctions, and expresses various efflux transporters and metabolizing enzymes, in a manner similar to the BBB. The BCSFB provides a

functional barrier between blood and CSF, just as the BBB serves as a functional barrier between blood and brain ECF. The surface area of BCSFB is about three orders of magnitude less than that of the BBB (de Lange, 2004), and to date the BCSFB is understudied.

CSF is secreted by the choroid plexus, located anatomically in the lateral, third and fourth ventricles of the brain. The bulk flow of CSF moves from the site of formation, through the ventricles and subarachnoid spaces, then is reabsorbed into venous blood at the arachnoid villi. During this passage, CSF has direct communication with the brain ECF spaces close to the cortex surface (Shen et al., 2004). Little is known about the kinetics of solute exchange between these two fluid compartments. Such information is necessary to understand the distribution and clearance kinetics of drugs in the brain. The estimated bulk flow clearance in mice can be as high as 0.7 µl/min/g (Rudick et al., 1982). The CSF is turned over every 5-7 hr or about 4 times a day in human, whereas turnover is every 2 hr (twelve times a day) in mice (Shen et al., 2004). CNS bulk flow and constant CSF turnover may act as a significant clearing mechanism for polar hydrophobic molecules with low BBB permeability (Liu and Chen, 2005).

In the treatment of certain brain diseases such as meningitis, the therapeutic target is in close contact with the ventricular CSF. CSF concentrations therefore are directly related to the biophase concentration in these cases. Intracerebroventricular administration has been proposed to enhance the targeted delivery of therapeutic agents to specific brain regions (Johanson et al., 2005). For the treatment of most CNS diseases (e.g., Alzheimer's disease, Parkinson's disease, epilepsy, neurotropic pain), however, the brain ECF is assumed to be in direct contact or equilibrium with the unbound drug at the site of

action. The drug CSF concentration is sometimes taken as the surrogate measurement of brain ECF concentration due to easier accessibility and the assumption of direct communication and equilibrium between CSF and ECF. This assumption has been shown to be valid for many compounds, especially substrates with moderate to high lipophilicity (Liu et al., 2006). However, for drug targets distant from the ventricles, CSF concentrations will not necessarily provide useful information regarding drug presentation to the site of action due to the complexity of brain compartmentalization, especially for compounds that undergo active transport at the BBB and BCSFB. CSF concentrations may either under- or over-estimate brain ECF concentrations, depending on the specifics of the situation under examination (Wijnholds et al., 2000; Sun et al., 2001a; de Lange and Danhof, 2002; Anthonypillai et al., 2004; Venkatakrishnan et al., 2007).

Knowledge regarding active transport at the BCSFB is relatively limited. Many of the transport proteins found at the BBB also are expressed in the BCSFB (Graff and Pollack, 2004; Soontornmalai et al., 2006). P-gp and Mrp1 are reported to actively transport endogenous or exogenous compounds at the BCSFB. Mrp1 is expressed in the basolateral membrane of choroid plexus epithelial cells and transports the substrates towards the blood circulation, while P-gp is expressed in the apical side and has the opposite transport direction towards the CSF (de Lange, 2004). Transfer of endogenous thyroid hormones into the brain is mediated by P-gp and Oatps at the BCSFB (Kassem et al., 2007). Prevention of the entry of harmful compounds into the CSF and/or elimination of such compounds from the CSF potentially contribute to overall CNS protection.

The choroidal epithelial cells also express a high level of several metabolic enzymes. The coupled metabolism-efflux process results in synergistic protection of the choroids plexus. The metabolite of 1-naphthol, catalyzed via uridine diphosphate glucuronosyltransferase (UGT) conjugation, was actively transported into the blood circulation (Strazielle and Ghersi-Egea, 1999). Glutathione *S*-transferase and glutathione peroxidase have been found in high levels at the BCSFB. Epoxide hydrolase and UGTs also have been identified with high activities, similar to those in the liver. In addition, the BCSFB expresses high level of several cytochrome P450 isoenzymes, which might be important for the metabolism of therapeutic agents (Ghersi-Egea et al., 1994).

CARRIER-MEDIATED TRANSPORT AT THE BBB

Increasing evidence has shown that drug flux across the BBB is subject to active and facilitated transport processes, rather than simple passive diffusion alone (Taylor, 2002; Begley, 2003; Begley, 2004a; Ohtsuki and Terasaki, 2007). At least 15 mRNAs of drug transport proteins belonging to several subfamilies are expressed at the BBB (Bauer et al., 2003). These drug transporters consist of uptake and efflux transport systems. The uptake transporters at the BBB facilitate the influx of nutrients and endogenously-generated compounds such as glucose and amino acids. Major efflux transporters at the BBB belong to the ATP-binding cassette (ABC) superfamily. These efflux transporters decrease the effective brain ECF concentrations by attenuating brain uptake and/or enhancing brain efflux (Golden and Pollack, 1998; Syvanen et al., 2006). The members of the ABC superfamily of transport proteins relevant to the BBB include P-glycoprotein (P-gp), breast cancer resistance protein (Bcrp), and multidrug resistance associated proteins (Mrps). Other transporters, such as organic anion transport peptides (Oatps) and

organic anion transporters (Oats) also have been reported to be expressed and functional in the transport of endogenous and exogenous compounds (e.g., thyroxine, fexofenadine) into and/or out of the brain (Cvetkovic et al., 1999; Tohyama et al., 2004). P-gp knockout mice, as well as animals naturally deficient in the protein, have been in use for more than a decade, and the impact of P-gp on brain exposure and pharmacologic response has been well established. With recently-developed knockout mouse models for other transport proteins, it should be possible to probe the role of other efflux transporters at the BBB.

P-glycoprotein (P-gp)

P-gp is a 170-kDa membrane-bound protein encoded by multidrug resistance gene ABCB1 (formerly, *MDR1* in human, *mdr1a* and *mdr1b* in rodents). P-gp was first identified in multidrug resistant cancer cells, and mediates the efflux of anticancer drugs out of the cells and decreases their intracellular concentration (Kartner et al., 1983). P-gp subsequently was found to be expressed in normal tissues such as the small intestine, liver, kidney and brain. The functional efficiency of P-gp has been studied extensively using various *in vitro* cell-based models, *in situ,* and *in vivo* animal models, as well as in human clinical studies.

P-gp is involved in many aspects of drug exposure in the body, including intestinal secretion, hepatobiliary excretion, and renal elimination. However, P-gp appears to have only a modest influence on systemic clearance and/or plasma concentrations following intravenous administration (studies comparing wild-type and gene-knockout mice), suggesting that P-gp has minimal effect on systemic disposition (Chen et al., 2003b).

However, P-gp has a profound influence on distribution into certain sanctuary or protected tissues or organs, including the brain.

P-gp mediates the efflux of a wide range of substrates at the BBB, and net brain penetration of P-gp substrates has been reported to be decreased by 2- to nearly 100-fold in the presence of P-gp expression at the BBB (Schinkel et al., 1994; Kalvass et al., 2004). In the brain, P-gp is principally expressed at the luminal side of the brain capillary endothelial cells. Expression of the transport protein in microglia, astrocytic end feet and parenchymal neurons also has been demonstrated, especially under pathological condition when the transporter is upregulated (Seegers et al., 2002; Volk and Loscher, 2005). Several studies have confirmed that the P-gp expression level is enriched in the brain endothelial cell fraction, while it is undetectable in the endothelial cell-negative fraction or whole brain homogenate (Demeule et al., 2001).

P-gp is a gatekeeper at the BBB and limits the entry of many therapeutic agents into the brain. Direct evidence for this function came from drug distribution studies in genetic knockout or naturally-mutant P-gp-deficient *mdr1a(-/-)* and *mdr1a/1b*(-/-) mice (Schinkel et al., 1994; Kalvass et al., 2004), as well as selective or specific chemical inhibition (P-gp modulators such as quinidine, PSC 833, cyclosporine A) (Choo et al., 2000). The resultant change of pharmacologic response following P-gp knockout also has been revealed. The first evidence for a P-gp-dependent modulation of biologic response in the CNS came from administration of the antihelminthic drug ivermectin, which caused significant neurotoxicity and deaths in P-gp-deficient animals (Schinkel et al., 1994). In addition, the antinociceptive effect of a μ-opioid peptide, DPDPE ,was found to be attenuated by P-gp-mediated efflux at the BBB (Chen and Pollack, 1997; Chen and

Pollack, 1999). Loperamide, a potent μ-opioid agonist, evidenced significant central antinociceptive effect in *mdr1a(-/-)* mice, but brain uptake in P-gp-competent mice was so limited that a central effect could not be elicited (Kalvass et al., 2004).

The foregoing results suggested that the drug candidates for intended CNS therapy with adequate lipid solubility will stand a better chance of success in the drug development process if they are not substrates of P-gp. P-gp-mediated efflux was found to be one of the factors that differentiate CNS from non-CNS drugs using *in vitro* models (Mahar Doan et al., 2002). A recent review demonstrated that more than 20 marketed psychotropic drugs have no or very weak interaction with P-gp *in vivo* (Ejsing et al., 2007; Linnet and Ejsing, 2007). In contrast, for peripheral therapeutic targets, P-gp-mediated efflux at the BBB decreases the possibility of neurotoxic effects. As exemplified by the second-generation nonsedating antihistamines, fexofenadine and cetirizine, brain uptake limited by P-gp-mediated efflux can improve the therapeutic profile for a peripherally acting agent. In the case of anthistamines, efflux transport limits the potential for the undesirable sedative effect for second-generation drugs, while brain uptake of the first-generation antihistamine hydoxyzine is not limited by BBB P-gp, resulting in marked sedative side effects (Chen et al., 2003a; Polli et al., 2003). Another relevant example is, domperidone, a highly efficient and specific dopamine antagonist *in vitro*. Domperidone cannot be used as an antipsychotic (neuroleptic) because it does not cross the BBB readily. However, it is used clinically as an antiemetic agent to counteract the unwanted dose-limiting peripheral side effects of dopamine-agonist drugs (e.g., bromocriptine and levodopa) used for the treatment of Parkinson's disease, owing to its action on peripheral dopamine receptors (Schinkel et al., 1996).

The expression and function of P-gp at the BBB can be modulated by many factors, including pathological conditions and drug treatment (Bauer et al., 2005; Volk and Loscher, 2005). This is an important aspect of CNS therapy. However, only a few studies have addressed the importance of unintended functional BBB modulation. One relevant example is the up-regulation of P-gp at the BBB by rifampin treatment, which occurs via the human nuclear pregnane X receptor (PXR) pathway. In mice transfected with human PXR, up-regulation of P-gp by rifampin pretreatment reduced the central antinociceptive efficacy of methadone by ~70% (Bauer et al., 2006).

Breast Cancer Resistance Protein (Bcrp)

Bcrp is a recently-identified member of ABC efflux transporter encoded by gene *Abcg2* (Doyle et al., 1998). Bcrp is widely expressed in the intestine, liver, mammary gland, and placenta. The functional effects of Bcrp in these organs, such as intestinal secretion, fetal penetration, and secretion into breast milk of various compounds (e.g., topotecan, nitrofurantoin, and cimetidine) has been documented (Jonker et al., 2000; Jonker et al., 2005). Bcrp also is expressed on the luminal side of brain capillary endothelial cells, sharing the same localization as that of P-gp, and the Bcrp mRNA expression level is similar to that of P-gp. Bcrp mediates the efflux of a wide variety of substrates, from sulfoconjugated organic anions to various organic cations (Maliepaard et al., 1999; Cooray et al., 2002; Eisenblatter and Galla, 2002; Eisenblatter et al., 2003; Cisternino et al., 2004; Aronica et al., 2005; Lee et al., 2005; Tanaka et al., 2005). The extensive overlap of Bcrp with P-gp in expression pattern and substrate specificity led to the speculation that Bcrp, like P-gp, might have significant impact on the pharmacologic handling of substrate drugs in animals and humans. However, studies to date have shown

that Bcrp function at the BBB is speculative. Some results have indicated that Bcrp is an important functional component of the BBB, e.g., Bcrp completely abolished brain penetration of three phytoestrogens (Enokizono et al., 2007). Imatinib mesylate brain penetration was decreased by 2.5-fold in wild-type mice compared to Bcrp-deficient mice (Breedveld et al., 2005). However, other experiments have been unable to ascribe an effect of Bcrp on substrate permeation across the BBB. The initial rate of brain uptake of imatinib mesylate was comparable between wild-type and *Bcrp1(-/-)* mice, and treatment with GF120918 (elacridar, a P-gp and Bcrp inhibitor) did not change brain uptake of imatinib in *mdr1a/1b(-/-)* mice (Bihorel et al., 2007). Bcrp appears to play only a minor role in mitoxantrone and DHEAS brain uptake (Lee et al., 2005). Bcrp has also been reported to be upregulated in the brain of epileptic patients (Vander Borght et al., 2006). The pharmacologic relevance of this modulation, however, remains unknown. Interestingly, compared to P-gp, Bcrp has a more significant role in limiting systemic bioavailability after oral administration (Jonker et al., 2000; Sparreboom et al., 2005). The discrepancies in apparent Bcrp effects (or lack thereof) at the BBB require further investigation.

Multidrug Resistance Associated Proteins (Mrps)

Mrps also are reported to be expressed at the human and rodent BBB (Sun et al., 2003; Strazielle et al., 2004). Little is known about the functional efficiency of brain Mrps, in part because they consist of nine isoforms (Mrp1-9). The Mrps primarily transport organic anions. Mrp1, 2, 4, and 5 are expressed in human and rodent brains, as demonstrated using isolated microvessels and tissue sections. However, the localization and functional efficiencies of the BBB Mrps remain controversial (Berezowski et al.,

2004; Nies et al., 2004; Zhang et al., 2004). Mrp1 was found to be functional at the BBB by some (Sugiyama et al., 2003), but not by others (Cisternino et al., 2003; Sasabe et al., 2004). Mrp2 has been demonstrated to be functional at the BBB using isolated brain capillaries or brain microdialysis (Miller et al., 2000; Miller et al., 2002; Potschka et al., 2003), but several other groups failed to demonstrate Mrp2 expression or activity in the brain tissue (Sugiyama et al., 2003; Nies et al., 2004; Zhang et al., 2004). Recently, Mrp4 at the BBB was reported to mediate the efflux of nucleotide drugs such as PMEA and puromycin, with 2- to 3-fold higher brain penetration of these substrates in gene knockout animals (Zhang et al., 2000; Adachi et al., 2002a; Adachi et al., 2002b; Sampath et al., 2002). The difficulties associated with the study of Mrps at the BBB using gene knockout animals might be the development of compensatory mechanisms by one or more members of the same family. Similar problems are associated with chemical inhibition studies. MK571 was widely used to inhibit Mrps. However, no specific inhibitor for each member has been identified. Probenecid was considered as a selective Mrp inhibitor. However, probenecid has been found to inhibit Oatps and Oats as well as the Mrps (Wang et al., 1997), further emphasizing the difficulties inherent in the design and interpretation of transport inhibition studies in the intact BBB.

BBB DRUG METABOLIZING ENZYMES

The expression of drug metabolizing enzymes at the blood-brain and CSF-brain interfaces, glial cells and neurons indicates that the BBB can also be a metabolic barrier that provides an additional mechanism to protect the brain (Strobel et al., 2001; Miksys and Tyndale, 2002; Meyer et al., 2007). The importance of brain metabolism was not appreciated until recently because enzyme levels in the organ are relatively low compared

to the liver. However, the expression of metabolizing enzymes in the brain is region- and cell-specific. In some brain regions (e.g., choroid plexus), the expression level and functional activity of drug metabolizing enzymes are as high as, or even higher than, in liver (Ghersi-Egea et al., 1994).

Cytochromes P450, epoxide hydrolase, as well as conjugating enzymes are expressed in the brain. More than 75% of marketed drugs are metabolized by P450s. So it is reasonable to speculate that the P450s expressed in brain might influence the local metabolism of therapeutic agents after penetration of the BBB. Brain P450s are not likely to influence the overall clearance of substrates from the body, due to the low absolute expression level (only about 1-10% of liver content). Nonetheless, these biotransformation reactions may be important determinants of substrate (or active metabolite) presentation to central sites of action. Mouse CYP3A11 and CYP3A13, the counterparts of human CYP3A4, were responsible for 6β-hydroxylation of testosterone in the brain, and activity was inducible by antiepileptic drug phenytoin treatment (Hagemeyer et al., 2003; Meyer et al., 2006). Early studies also showed that codeine is metabolized to morphine in the brain, thereby exerting an analgesic effect (Chen et al., 1990). The data on regional metabolism in brain are scarce, however. The importance of local metabolism, regional modulation and perturbation on endogenous metabolic pathways due to drug treatment, are only beginning to be appreciated.

CENTRAL NERVOUS SYSTEM KINETICS

The onset and offset of CNS effect is determined by many factors that influence the movement of the drug from the site of administration to the site of action. It is assumed

that the unbound drug at the site of action drives the biologic effect. The rate and extent of drug presentation to the site of action are dependent on passive permeability at the BBB, nonspecific binding in blood and brain, and active transport and metabolism in the brain, any of which could be changed by pathophysiologic conditions (Klein et al., 1986; Kalvass and Maurer, 2002; Norinder and Haeberlein, 2002; Liu and Chen, 2005). For many centrally acting drugs, flux across the BBB is the rate-limiting step in the presentation of drug to the site of action. The importance of studying cerebral kinetics has been realized, especially for the analgesic drugs (Villesen et al., 2006a; Villesen et al., 2006b; Kalvass et al., 2007b).

The rate of brain uptake is dependent on the intrinsic permeability at the BBB, active transport and nonspecific binding in brain tissue (Hammarlund-Udenaes et al., 1997; Liu et al., 2005). The rate of brain equilibration is directly proportional to the product of permeability and unbound fraction ($PS \times f_{u,brain}$) under passive diffusion (Liu and Chen, 2005; Liu et al., 2005). Low passive permeability does not necessarily indicate that a compound will have a poor CNS distribution. If $f_{u,brain}$ is large, then it is possible for a compound with low passive permeability (e.g., theobromine) to have unimpaired and adequate CNS distribution (Liu et al., 2005).

The extent of brain penetration, commonly described by brain-to-plasma concentration ratio or brain partition coefficient $k_{p,brain}$, is determined by the relative binding in blood and brain tissue, active transport and metabolism at the BBB, as well as the sink action of CSF bulk flow (Liu and Chen, 2005). The *in vitro* unbound fraction ratio (plasma to brain tissue) and P-gp efflux ratio have been used successfully to predict brain penetration (Kalvass and Maurer, 2002; Maurer et al., 2005; Summerfield et al., 2006; Kalvass et al.,

2007a). However, it has been recognized that unbound brain concentration is the more relevant predictor of biological response (Martin, 2004; Pardridge, 2004). For compounds that undergo passive diffusion at the BBB, the unbound plasma and brain concentrations will be equal at steady-state or post distributional equilibrium. When CNS distribution is impaired by active efflux, metabolism, or CSF bulk flow, the unbound brain concentration will be normally lower than the unbound plasma concentration.

The brain is a highly anatomically- and functionally-specialized organ. Blood flow varies ~18-fold in different brain regions in rat (Fenstermacher et al., 1991). Brain capillary density, pharmacologic receptors, and expression of transporters are not homogeneously distributed in the brain (Sakurada et al., 1978; Duelli and Kuschinsky, 1993; Heiss and Herholz, 2006). To date, little is known about how drugs distribute within the brain to the site of action, and thus the ultimate fate of a given drug in the brain after the penetration through the BBB typically is unkown.

From a pharmacokinetic standpoint, the brain can be viewed as being compartmentalized into cerebral capillary, CSF, extracellular fluid, and intracellular fluid compartments. Most CNS targets are membrane receptors, and in these cases the brain ECF concentration will drive the effect. In contrast, for the treatment of HIV and brain tumors, the relevant driving-force will be the intracellular concentration. CSF concentration might be representative of the biophase concentration when the target resides in the ventricular organs. Depending on the localization of the target site, the assessment of local unbound concentration at the target site needs to be considered in experimental design.

Other factors that might influence regional drug exposure also need to be considered in CNS therapy. Clinical practice has shown variations in sensitivity to therapeutic effect or CNS side effects when the target site resides in different brain regions. For example, the hippocampus is especially vulnerable to ischemia and colchicine cytotoxicity (Goldschmidt and Steward, 1980; Cavaglia et al., 2001). Chemotherapeutic agents in combination with transient reversible hyperosmotic opening of the BBB have been used to treat brain tumors. Both *in vivo* and *in situ* studies have demonstrated that variations exist in BBB disruption in different brain regions following hyperosmotic treatment, suggesting that clinical efficacy of hyperosmolar disruption therapy may be affected by the location of the tumor within the brain (Chiueh et al., 1978; Brown et al., 2004). Region-specific overexpression of P-gp decreased phenytoin concentration in the temporal hippocampus and parahippocampal cortex region in chronic epileptic rats (van Vliet et al., 2007). Previous studies demonstrated that P-gp-mediated efflux at the BBB influenced regional distribution of ^{3}H-verapamil to different extents in different brain regions (Graff et al., 2005; Appendix). Knowledge of the regional cerebral vascular volume and blood flow rate, as well as regional P-gp activity, is of particular interest with regard to effective treatment of cerebral diseases.

EXPERIMENTAL APPROACHES

For CNS drug discovery and development, choosing the best experimental models for the BBB, as well as other aspects of drug distribution in the brain, depends on a variety of logistical issues (cost, time) as well as how closely a model needs to resemble *in vivo* conditions (Fenstermacher et al., 1981; Bonate, 1995). *In vitro* modeling of the BBB is a simplification of the *in vivo* situation. Cellular BBB assays are more cost-effective, and

represent high-throughput techniques in comparison to *in situ* and *in vivo* methods. There is, of course, concern as to how well such models mimic the structure and function of the BBB in the intact organism. *In situ* brain perfusion is an accurate method for studying the rate of BBB penetration, although it requires significant technical expertise. *In vivo* distribution studies provide direct measurement of BBB penetration, but are labor-intensive. *In situ* and *in vivo* methods are especially useful to assess transporter kinetics in gene knockout animal models.

In Vitro Models

The development and application of *in vitro* systems have facilitated important progress in understanding the biochemical properties of the BBB (Gumbleton and Audus, 2001; Terasaki et al., 2003; Cecchelli et al., 2007). *In vitro* cell-based models have provided efficient screening in the early phase of drug development, in addition to allowing the efficient generation of large data sets. Cultured brain microvessel endothelial cells (BMECs) from different species, as well as non-cerebral-origin cell lines such as MDCK and LLC-PK1, have been developed over the past several years. In many evaluations of BBB function and transport, the relevance of *in vitro* BBB models is justified by comparison with data obtained through the use of *in vivo* methodologies. The limitations of primary BMECs or cultured cell lines lie predominantly in the "leaky" tight junctions characteristic of these models, and thus paracellular permeability that is higher than *in vivo*. In addition, the regulation of efflux transporters in cultured BMECs may be different than in the intact animal. These cell-based models nevertheless have been successfully used to rank order the passive permeability of the screening compounds (Hansen et al., 2002; Mahar Doan et al., 2002).

A variety of *in vitro* assays have been developed to assess the potential for compounds to act as P-gp substrates, inhibitors and/or inducers, such as the monolayer efflux assay, the ATPase assay, and the calcein-AM fluorescence assay (Gumbleton and Audus, 2001; Carrara et al., 2007). Among these methods, the monolayer efflux assay employing P-gp-expressing polarized cell monolayers is considered a standard method for identifying compounds as P-gp substrates and/or inhibitors. This approach also can provide important information on drug transport kinetics. Efflux transporters such as P-gp, Mrps, and Bcrp stably single-, double-, and triple-transfected cell lines based on MCDK or LLC-PK1 cells have been developed for studying transport kinetics, especially in the identification and characterization of P-gp substrates and/or inhibitors, as well as potential drug-drug interactions at the level of active transport at the BBB (Polli et al., 2001; Rautio et al., 2006).

Isolated brain microvessels also have been used for the study of carrier-mediated transport at the BBB (Miller et al., 2000). However, this method is more technically challenging and time-consuming, and is not suitable for drug screening.

Gene Knockout vs. Chemical Inhibition

In situ or *in vivo* studies using gene knockout animal models have provided the most convincing evidence of active transport at the BBB (Schinkel et al., 1994; Sugiyama et al., 2003; Assem et al., 2004; Breedveld et al., 2005; Doran et al., 2005; Zelcer et al., 2005; Johnson et al., 2006). Gene knockout mice do not display clear physiologic abnormalities or a decreased life span (Schinkel, 1999). Single gene (P-gp, Mrp1, 2, 3, 4, or Bcrp) or double gene Abcg2/Mrp4(-/-) knockout mouse models have been developed and used in

the study of drug transport at the BBB (Chen et al., 2003b; Sugiyama et al., 2003; Lee et al., 2005; Takenaka et al., 2007). P-gp knockout, or the natural mutant P-gp-deficient mice *mdr1a(-/-)* and *mdr1a/1b*(-/-). have been in use for more than a decade, and P-gp is the most well studied efflux transporter at the BBB to date. P-gp knockout mice have become important tools used in the drug screening process (Cisternino et al., 2001; Chen et al., 2003b; Doran et al., 2005). P-gp can have a profound effect in attenuating the rate and extent of brain penetration, although the transport protein appears to have only a limited contribution to the systemic clearance of P-gp substrates (Chen et al., 2003b). The impact of a specific efflux transporter on the *in vivo* CNS distribution can be described by the ratio of $k_{p,brain}$ or uptake clearance (Cl_{up}) in gene-deficient mice relative to gene-competent mice (Kalvass and Pollack, 2007). The knockout of a single efflux transporter gene (Mrps, Bcrp or P-gp) significantly increased the brain penetration of substrates by 2- to nearly 100-fold (Chen et al., 2003b; Enokizono et al., 2007; Kalvass et al., 2007a; Takenaka et al., 2007).

One important disadvantage to gene knockout models is that compensatory mechanisms can develop in these animals that influence substrate flux (Cisternino et al., 2004; Takenaka et al., 2007). In addition to the modulation of transport proteins, the activity of other compensatory systems (metabolic enzymes, receptors, or post-receptor signaling) might change in response to loss of the target gene. Thus, careful control experiments must be conducted to rule out specific and non-specific changes in substrate pharmacokinetics and pharmacodynamics in response to the genetic perturbation.

Chemical inhibition with specific transport modulators also has provided useful information regarding the function and pharmacologic consequences of efflux transport at

the BBB (Kemper et al., 2003; Elsinga et al., 2004; Kemper et al., 2004). The most important problem associated with chemical inhibition as a probe of transport-mediated drug distribution across the BBB is the degree to which chemical inhibitors are specific for the target transporter. Verapamil and quinidine inhibit P-gp function, but also inhibit metabolic enzymes (Sikic et al., 1997). Cyclosporine A and GF120918 inhibit both P-gp and Bcrp (Breedveld et al., 2006). The degree to which inhibitors of efflux transport also might modulate uptake transporters suach as the Oatps is unclear, but obviously would yield confounded data that would be very difficult to interpret. It is good general practice to utilize both genetic models of transport deficiency and selective chemical inhibition as a cross-check.

Systemic Administration

Systemic administration [intravenous (i.v.), subcutaneous (s.c.), intraperitoneal (i.p.), or oral (p.o)] of a test compound is the most widely used approach for studying systemic pharmacokinetics. In terms of CNS kinetics, the rate and extent of brain uptake, as well as the regional distribution of test compounds, can be determined by sampling brain tissue at a specific time or several time points. The concentrations of substrate in whole brain homogenate or dissected specific brain regions can be determined. Systemic administration approaches can provide information at steady-state (during continuous presentation or multiple discrete dosing) or following the attainment of distribution equilibrium (after multiple passages through the systemic circulation). To determine drug distribution at steady-state, multiple dosing or continuous i.v. infusion through a venous cannula often is used. An alternative method that is particularly useful for compounds with long terminal elimination half-lives, or agents that require a long time to achieve

distribution equilibrium, is drug administration via osmotic minipumps. These pumps can be implanted intraperitoneally or subcutaneously, and release drug continuously at a constant rate over an extended time (up to 4 weeks) (www.alzet.com). The surgery procedure is relatively simple and time-efficient compared to other techniques.

Following systemic administration, the extent of brain uptake can be quantitated as the brain-to-plasma concentration ratio at steady-state or post distribution equilibrium. An equivalent metric, although one that requires a different information set, is the brain-to-plasma area under the concentration-time curve (AUC) ratio. Unbound drug concentrations can be determined based on the unbound fraction measured using *in vitro* equilibrium dialysis (Kalvass and Maurer, 2002; Kalvass et al., 2007a). *In silico* predictive models and high-throughput screening of brain tissue binding have been developed (Wan et al., 2007). The systemic administration approach also can be used to assess the rate of brain penetration, with a pharmacokinetic modeling approach (Liu et al., 2005; Kalvass et al., 2007b).

The effect of active transport at the BBB also can be evaluated using this approach in gene knockout animal models or in the presence of chemical inhibitors. The P-gp efflux ratio is defined as the ratio of uptake clearance or $k_{p,brain}$ in P-gp-deficient to P-gp-competent mice. In addition, the concentration dependence due to saturable processes at the BBB also can be evaluated using escalating dosing (substrate or inhibitor) regimens (Bart et al., 2005; Hsiao et al., 2006).

Regional drug distribution in different brain structures can be determined by microdissection or imaging techniques. Regional physiologic parameters such as blood

flow rate and capillary vascular space also can be determined using this method (Ohno et al., 1979; Duelli and Kuschinsky, 1993; Dagenais et al., 2000a). For example, the regional blood-to-brain glucose transfer in the rat was determined following systemic administration of double tracers (Gjedde and Diemer, 1985).

Among all of the preclinical methodologies, this method most closely resembles the clinical situation. However, it is not useful in understanding the specific mechanisms underlying brain uptake of a given substrate since the uptake process is a multi-factorial event including systemic disposition, nonspecific binding in brain tissue and blood, CSF bulk flow, and active transport and metabolism in the CNS.

Brain Uptake Index (BUI)

The BUI technique was first introduced for the study of drug penetration of the BBB (Oldendorf, 1970). A small-volume bolus of buffered saline or plasma containing tracer concentrations of test compound and a permeable reference (e.g., ^{3}H-H_2O) is injected rapidly into the carotid artery of an anesthetized animal. At a fixed time (~ 5 s) after injection, the brain is removed for substrate analysis. The BUI of the test compound then is determined as the fraction of test compound extracted from the injection mixture relative to the extraction fraction of the permeable reference.

The BUI method has been used for rank-ordering BBB permeability of a wide variety of compounds (Bonate, 1995). A good correlation between BUI and compound lipophilicity in adult rat BBB has been reported (Oldendorf, 1974). In addition, this technique can be used to examine concentration-dependent efflux transport at the BBB, or in conjunction with gene knockout animals or co-injection of chemical inhibitors to assess the impact of

loss of efflux transport activity on single-pass substrate uptake into brain. Regional distribution in different brain structures can be assessed after single-pass uptake following brain microdissection. The main disadvantage of this method is that, by definition, it focuses on single-pass permeability, and thus is insensitive for compounds with low BBB permeability. These are the very compounds of interest from the perspective of significant efflux transport.

In Situ Brain Perfusion

In situ brain perfusion was first developed to determine the intrinsic BBB permeability in rats (Takasato et al., 1984). In the original method, the brain hemisphere was perfused with physiologic buffer or artificial blood via retrograde perfusion through the external carotid artery for a time period up to 3 minutes. The rate of brain uptake is calculated as uptake clearance based on the initial unidirectional phase of brain uptake. Modification of the surgical procedure has been developed. The brain hemisphere of guinea pigs, for example, has been perfused for 30 minutes through the internal carotid artery. Subsequent capillary depletion allows assessment of drug trapped inside the capillary endothelium (Zlokovic et al., 1986). The first *in situ* mouse brain perfusion in *mdr1a(-/-)* animals extended the use of brain perfusion to the screening of P-gp substrates (Dagenais et al., 2000a). The *in situ* brain perfusion approach in rats and mice provided similar information regarding BBB penetration for over 20 compounds, suggesting that BBB characteristics are conserved across those two species (Murakami et al., 2000). In addition, with the commercial availability of various genetic knockout mouse models, the *in situ* mouse brain perfusion technique received increasing attention (Dagenais et al., 2001a; Cisternino et al., 2003; Dagenais et al., 2004; Lee et al., 2005). The effect of

plasma protein binding on brain drug uptake also can be determined by changing the composition of perfusion buffer (Mandula et al., 2006; Summerfield et al., 2006; Summerfield et al., 2007). Combined with microdissection, *in situ* brain perfusion also has been used to study the regional cerebral hemodynamics and drug distribution in the brain (Takasato et al., 1984; Suzuki et al., 1998; Youdim et al., 2004; Parepally et al., 2006).

Brain Microdialysis

Intracerebral microdialysis is a sampling technique that allows continuous measurement of brain ECF concentration in rodents, as well as in critically ill patients with severe brain injury (de Lange et al., 1997; Boschi and Scherrmann, 2000; Tunblad et al., 2003; Rambeck et al., 2006). This technique has been used successfully to assess CNS pharmacokinetics of many substrates (Clinckers et al., 2005; Helmy et al., 2007). Simultaneous microdialysis in blood and brain provides information on transport kinetics of unbound drug (Hammarlund-Udenaes et al., 1997; Evrard et al., 1998). Use of recently developed transporter or enzyme gene knockout animal models or chemical inhibitors provides useful information on the mechanisms of *in vivo* brain uptake of various therapeutic agents (Sun et al., 2001b; Potschka et al., 2003). This approach has been used in humans during the anhepatic phase of liver transplantation to study the brain metabolism (Tofteng et al., 2002; Tofteng and Larsen, 2002; Battezzati and Bertoli, 2004). The regional brain ECF concentration is accessible because the microdialysis probe can be implanted virtually in any brain region of interest such as tumors (Apparaju et al., 2007).

The limitations of this technique include extensive surgical preparation and requirement of specialized equipment and expertise. Probe implantation is invasive and may perturb the integrity of the BBB at the implantation site. An extremely sensitive assay for the molecule of interest is required. The difficulties associated with the determination of *in vivo* microdialysis probe efficiency also need to be considered. In the absence of a robust approach to estimating recovery efficiency, microdialysis data can only provide the temporal pattern of changes in concentration, and not actual concentrations per se. The technique also is quite difficult to implement in mice, making use of gene knockout models problematic.

CSF Sampling

In clinical settings, where brain ECF concentrations are not accessible, CSF often is taken as a surrogate measurement under the assumptions that BCSFB shares similar characteristics with BBB with regard to drug transport and that CSF is in equilibrium with brain ECF. The relevance of CSF concentration to unbound brain concentration has been demonstrated for various therapeutic agents (Liu et al., 2006). However, for targets that are distant from CSF passage, the CSF concentration does not necessarily represent the relevant biophase concentration because the underlying assumptions are not universally reasonable (de Lange and Danhof, 2002; Shen et al., 2004). Significantly lower brain ECF concentrations as compared to CSF concentrations have been demonstrated for several antiepileptic drugs (i.e., carbamazepine, topiramate, phenytoin) in patients with intractable epilepsy (Rambeck et al., 2006) and an investigational drug candidate CP-615,003 in rats and dogs (Venkatakrishnan et al., 2007). Active carrier-mediated efflux transport at these two barriers also is different. Inhibition of P-gp with

zosuquidar increased brain penetration by ~ 146-fold, while decreasing CSF penetration by 5-fold (Kaddoumi et al., 2007).

Imaging Techniques

Non-invasive imaging techniques (e.g., positron emission tomography [PET]) have been used in the drug discovery and development process (Gee, 2003; Salvadori, 2007). This approach has been applied successfully in biodistribution studies of drugs both in human and preclinical species, as well as in identification and characterization of pharmacologic targets (Elsinga et al., 2004). The isotopes typically used in PET studies (i.e., ^{11}C, ^{13}N, ^{15}O or ^{18}F) have short half-lives and can be administered to human subjects at sub-pharmacologic doses. The experiments can be repeated in the same subject over a short period of time. Recent studies with the P-gp substrates ^{11}C-carvedilol and ^{11}C-verapamil have demonstrated that PET can be used to assess the functions of P-gp at the BBB (Bart et al., 2005; Ikoma et al., 2006). Studies in *mdr1a(-/-)* mice and rats demonstrated that P-gp function at the BBB is modulated by the P-gp inhibitor cyclosporine A in a concentration-dependent manner (Hendrikse et al., 1998; Bart et al., 2003). A good interspecies correlation has been obtained with imaging techniques between rat and human BBB with regard to P-gp inhibition by cyclosporine A (Hsiao et al., 2006). Additional studies in healthy human subjects or patients provide invaluable information regarding the function of P-gp at the BBB (Takano et al., 2006; Langer et al., 2007; Lubberink et al., 2007).

PET studies are especially useful in investigating the spatial heterogeneity of drug uptake in the brain. The regional blood flow rate and amino acid uptake vary substantially in

gliomas in patients (Wyss et al., 2007). ^{11}C-verapamil uptake in epileptogenic and non-epileptogenic brain regions was studied in medically refractory patients with temporal lobe epilepsy (Langer et al., 2007). The heterogeneous distribution of target receptors and cerebral hemodynamic parameters also can be determined using PET or other noninvasive imaging techniques (e.g., single photon emission tomography [SPECT], magnetic resonance imaging [MRI]) (Rosen et al., 1991; Frankle and Laruelle, 2002; Heiss and Herholz, 2006). Careful experimental design is required because PET imaging measures the total parent and metabolite levels and cannot differentiate between metabolite and parent (Lubberink et al., 2007).

IN VITRO-IN VIVO CORRELATION

A complete understanding of *in vitro*/*in vivo* relationships in preclinical species makes extrapolation to human studies possible. It has been demonstrated that BBB characteristics are conserved between species. Immense effort has been devoted to making predictions of *in vivo* BBB penetration from physicochemical properties (e.g., molecular weight, lipophilicity, pKa, the number of hydrogen bonds) of investigational molecules. Passive permeability at the BBB has been predicted successfully by *in silico* models (Norinder and Haeberlein, 2002; Clark, 2003; Hou and Xu, 2003b; Hou and Xu, 2003a; Liu et al., 2004; Goodwin and Clark, 2005). Nonspecific brain tissue binding, which is related to lipophilicity, and correlated to blood protein binding, also can be predicted using *in silico* models (Wan et al., 2007). However, the prediction of substrates, inducers and/or inhibitors for specific transporter protein or metabolizing enzymes is relatively less successful because the mechanism of action has not been fully understood.

Novel *in vitro* and *in vivo* models have been or need to be developed to study many different aspects of CNS kinetics. Under most situations well-designed experiments with different models can yield consistent results with regard to CNS transport. *In vitro* cell-based models have been used in rank-ordering passive permeability as well as in mechanistic studies of carrier-mediated transport at the BBB (Hansen et al., 2002; Mahar Doan et al., 2002). Quantitative analyses of the P-gp effect on *in vivo* pharmacokinetics and pharmacodynamics have been performed for many clinically important drugs (Summerfield et al., 2006; Kalvass et al., 2007b). *In vitro* models have been used to identify P-gp substrates and/or inhibitors, which has become a key issue in the drug discovery and development process (Polli et al., 2001; Rautio et al., 2006). The *in vitro* P-gp-mediated efflux studies [ratio of apparent permeability in basolateral-to-apical direction to apical-to-basolateral direction] can be quantitatively predictive of *in vivo* P-gp effect at the BBB [ratio of uptake clearance or brain partition coefficient in P-gp deficient mice to P-gp competent mice] (Adachi et al., 2001; Yamazaki et al., 2001; Hochman et al., 2002; Chen et al., 2003b; Summerfield et al., 2006; Kalvass and Pollack, 2007).

Not surprisingly, apparent discrepancies have been observed between *in vitro* and *in vivo* BBB penetration kinetics. There are several limitations associated with *in vitro* models that might explain these discrepancies. The tight junctions of cultured cell monolayers are usually "leakier" than in the intact BBB *in vivo*. It is not known how close the expression level of transporters and metabolizing enzymes in cultured cells is to that *in vivo*. Transporter expression level is a confounding factor in the study of intrinsic transport parameters (Balakrishnan et al., 2007; Korjamo et al., 2007). More importantly, *in vitro*

cellular models are a simplification of the dynamic blood-brain interface, and the three-dimensional architecture, blood flow and protein profiles cannot be reproduced in *in vitro* models. The molecular mechanism of transport of P-gp and other efflux transporters is still unknown (Ambudkar et al., 2003). Development of structure-activity relationships to identify or describe P-gp substrates and inhibitors have been unsuccessful (Pajeva and Wiese, 2002; Wang et al., 2003; Pajeva et al., 2004), in part due to the interplay of passive permeability and P-gp-mediated efflux (Lentz et al., 2000). The emergence of gene knockout animals facilitated the understanding of transport kinetics. However, gene knockout animals have not been fully characterized for potential compensatory mechanisms (Cisternino et al., 2004). Some "specific" chemical inhibitors were found to be not specific (Gupta et al., 2006), so chemical inhibition studies using these inhibitors need to be re-examined. Sex, strain and species differences and pathological conditions might modulate the expression and functional efficiency of transport proteins (Hochman et al., 2002; Merino et al., 2005; Tanaka et al., 2005; Zhang et al., 2005a; Soontornmalai et al., 2006; Vander Borght et al., 2006). The flavonoids chrysin and benzoflavone are potent inhibitors of human BCRP, but only weak inhibitors for rodent Bcrp (Zhang et al., 2005a). In addition, regional heterogeneity of active transport and metabolism in the brain has not been mapped (Reichel, 2006).

PROJECT OVERVIEW

BBB penetration represents an important bottleneck in CNS drug design and development. The rate, extent and regional distribution of drug to the site of action are important aspects of CNS pharmacokinetics. The goal of this dissertation project was to

assess the determinants of brain distribution using *in vitro*, *in situ* and *in vivo* experimental approaches.

First, the *in situ* brain perfusion technique was used to study the BBB permeability of twelve therapeutic compounds with a wide range of physicochemical properties, together with *in vitro* equilibrium dialysis to measure plasma and brain tissue binding. The influence of lipophilicity, intrinsic permeability, and brain tissue binding on the rate of brain:blood equilibration was investigated. The brain distribution equilibrium of alfentanil (high permeability, low brain tissue binding), sufentanil (intermediate permeability, intermediate brain tissue binding) and fexofenadine (low permeability, extensive brain tissue binding) was compared. In addition, the influence of P-gp-mediated efflux at the BBB was assessed using *mdr1a(-/-)* mouse model (Chapter 2).

Fexofenadine and terfenadine are both effective antihistamines. Fexofenadine is an active metabolite of terfenadine, with formation catalyzed by hepatic CYP3A4 in humans. Fexofenadine is poorly permeable at the BBB, while terfenadine readily crosses the BBB. Both antihistamines are P-gp substrates. In the current study, local brain metabolism was evaluated as a potential source of influence on the disposition of terfenadine and fexofenadine. Due to the slow approach to distribution equilibrium, these experiments were performed with subcutaneous osmotic minipump continuous infusion of fexofenadine or terfenadine. The brain metabolism of terfenadine to fexofenadine was studied using *in situ* brain perfusion and whole brain homogenate incubation methods. The time-dependency of fexofenadine brain penetration and P-gp effect at the BBB was examined. A two-compartment pharmacokinetic model was used to simulate the time course of fexofenadine brain uptake (Chapter 3).

The ABC transporters (e.g., P-gp, Bcrp, Mrps) are the major efflux transporters at the BBB. To date, P-gp-mediated efflux at the BBB to extrude the therapeutic agents out of the brain has been widely accepted. However, studies on other efflux transporters remain unclear, and the results have been controversial. Bcrp and P-gp have a similar expression pattern and overlapping substrates. Thus, it was speculated that Bcrp might play as important role as P-gp in defending the brain from exposure to exogenous compounds. Bcrp-overexpressed MDCKII cell line was grown in transwell devices, and many compounds were screened for Bcrp substrate characteristics. Cimetidine, alfuzosin, dipyridamole and LY2228820 were four Bcrp substrates selected based on the *in vitro* cell model. Then, the *in situ* brain perfusion and *in vivo* osmotic minipump administration studies were carried out to test the relevance of Bcrp at the murine BBB using *mdr1a(-/-)* and *Abcg2(-/-)* mouse models (Chapter 4).

There are broad differences in physiology and function in the mammal brain. Therapeutic targets are not homogeneously distributed in the brain. The effectiveness of therapy depends on adequate delivery of drugs to the site of action within specific brain structures. Regional drug exposure is a complex function of local cerebral blood flow rate, brain capillary surface area, transit time in the brain, cerebrospinal fluid (CSF) bulk flow, blood protein binding and nonspecific brain tissue binding, as well as the transport of drugs across the BBB and metabolism in the specific brain region. In the current project, the *in situ* brain perfusion technique was used to study the local cerebral blood flow rate, capillary vascular volume, and the influence of these physiologic parameters on regional drug exposure. In addition, the effect of lipophilicity and P-gp interaction also was investigated using colchicine, quinidine and verapamil as model compounds. The

relevance of this *in situ* brain perfusion technique was evaluated by *in vivo* regional pharmacokinetics of loperamide (Chapter 5).

Reference

Adachi M, Reid G and Schuetz JD (2002a) Therapeutic and biological importance of getting nucleotides out of cells: a case for the ABC transporters, MRP4 and 5. *Adv Drug Deliv Rev* **54:**1333-1342.

Adachi M, Sampath J, Lan LB, Sun D, Hargrove P, Flatley R, Tatum A, Edwards MZ, Wezeman M, Matherly L, Drake R and Schuetz J (2002b) Expression of MRP4 confers resistance to ganciclovir and compromises bystander cell killing. *J Biol Chem* **277:**38998-39004.

Adachi Y, Suzuki H and Sugiyama Y (2001) Comparative studies on in vitro methods for evaluating in vivo function of MDR1 P-glycoprotein. *Pharm Res* **18:**1660-1668.

Ambudkar SV, Kimchi-Sarfaty C, Sauna ZE and Gottesman MM (2003) P-glycoprotein: from genomics to mechanism. *Oncogene* **22:**7468-7485.

Anthonypillai C, Sanderson RN, Gibbs JE and Thomas SA (2004) The distribution of the HIV protease inhibitor, ritonavir, to the brain, cerebrospinal fluid, and choroid plexuses of the guinea pig. *J Pharmacol Exp Ther* **308:**912-920.

Apparaju SK, Gudelsky GA and Desai PB (2007) Pharmacokinetics of gemcitabine in tumor and non-tumor extracellular fluid of brain: an in vivo assessment in rats employing intracerebral microdialysis. *Cancer Chemother Pharmacol*.

Aronica E, Gorter JA, Redeker S, van Vliet EA, Ramkema M, Scheffer GL, Scheper RJ, van der Valk P, Leenstra S, Baayen JC, Spliet WG and Troost D (2005) Localization of breast cancer resistance protein (BCRP) in microvessel endothelium of human control and epileptic brain. *Epilepsia* **46:**849-857.

Assem M, Schuetz EG, Leggas M, Sun D, Yasuda K, Reid G, Zelcer N, Adachi M, Strom S, Evans RM, Moore DD, Borst P and Schuetz JD (2004) Interactions between hepatic Mrp4 and Sult2a as revealed by the constitutive androstane receptor and Mrp4 knockout mice. *J Biol Chem* **279:**22250-22257.

Balakrishnan A, Hussainzada N, Gonzalez P, Bermejo M, Swaan PW and Polli JE (2007) Bias in estimation of transporter kinetic parameters from overexpression systems: Interplay of transporter expression level and substrate affinity. *J Pharmacol Exp Ther* **320:**133-144.

Bart J, Dijkers EC, Wegman TD, de Vries EG, van der Graaf WT, Groen HJ, Vaalburg W, Willemsen AT and Hendrikse NH (2005) New positron emission tomography tracer [(11)C]carvedilol reveals P-glycoprotein modulation kinetics. *Br J Pharmacol* **145:**1045-1051.

Bart J, Willemsen AT, Groen HJ, van der Graaf WT, Wegman TD, Vaalburg W, de Vries EG and Hendrikse NH (2003) Quantitative assessment of P-glycoprotein function in the rat blood-brain barrier by distribution volume of [11C]verapamil measured with PET. *Neuroimage* **20:**1775-1782.

Battezzati A and Bertoli S (2004) Methods of measuring metabolism during surgery in humans: focus on the liver-brain relationship. *Curr Opin Clin Nutr Metab Care* **7:**523-530.

Bauer B, Hartz AM, Fricker G and Miller DS (2005) Modulation of p-glycoprotein transport function at the blood-brain barrier. *Exp Biol Med (Maywood)* **230:**118-127.

Bauer B, Miller DS and Fricker G (2003) Compound profiling for P-glycoprotein at the blood-brain barrier using a microplate screening system. *Pharm Res* **20:**1170-1176.

Bauer B, Yang X, Hartz AM, Olson ER, Zhao R, Kalvass JC, Pollack GM and Miller DS (2006) In vivo activation of human pregnane X receptor tightens the blood-brain barrier to methadone through P-glycoprotein up-regulation. *Mol Pharmacol* **70:**1212-1219.

Begley DJ (2003) Understanding and circumventing the blood-brain barrier. *Acta Paediatr Suppl* **92:**83-91.

Begley DJ (2004) ABC transporters and the blood-brain barrier. *Curr Pharm Des* **10:**1295-1312.

Berezowski V, Landry C, Dehouck MP, Cecchelli R and Fenart L (2004) Contribution of glial cells and pericytes to the mRNA profiles of P-glycoprotein and multidrug resistance-associated proteins in an in vitro model of the blood-brain barrier. *Brain Res* **1018:**1-9.

Bihorel S, Camenisch G, Lemaire M and Scherrmann JM (2007) Influence of breast cancer resistance protein (Abcg2) and p-glycoprotein (Abcb1a) on the transport of

imatinib mesylate (Gleevec((R))) across the mouse blood-brain barrier. *J Neurochem* **102:**1749-1757.

Bonate PL (1995) Animal models for studying transport across the blood-brain barrier. *J Neurosci Methods* **56:**1-15.

Boschi G and Scherrmann J (2000) Microdialysis in mice for drug delivery research. *Adv Drug Deliv Rev* **45:**271-281.

Breedveld P, Beijnen JH and Schellens JH (2006) Use of P-glycoprotein and BCRP inhibitors to improve oral bioavailability and CNS penetration of anticancer drugs. *Trends Pharmacol Sci* **27:**17-24.

Breedveld P, Pluim D, Cipriani G, Wielinga P, van Tellingen O, Schinkel AH and Schellens JH (2005) The effect of Bcrp1 (Abcg2) on the in vivo pharmacokinetics and brain penetration of imatinib mesylate (Gleevec): implications for the use of breast cancer resistance protein and P-glycoprotein inhibitors to enable the brain penetration of imatinib in patients. *Cancer Res* **65:**2577-2582.

Brodie BB, Kurz H and Schanker LS (1960) The importance of dissociaton constant and lipid-solubility in influencing the passage of drugs into the cerebrospinal fluid. *J Pharmacol Exp Ther* **130:**20-25.

Brown RC, Egleton RD and Davis TP (2004) Mannitol opening of the blood-brain barrier: regional variation in the permeability of sucrose, but not 86Rb+ or albumin. *Brain Res* **1014:**221-227.

Carrara S, Reali V, Misiano P, Dondio G and Bigogno C (2007) Evaluation of in vitro brain penetration: Optimized PAMPA and MDCKII-MDR1 assay comparison. *Int J Pharm*.

Cavaglia M, Dombrowski SM, Drazba J, Vasanji A, Bokesch PM and Janigro D (2001) Regional variation in brain capillary density and vascular response to ischemia. *Brain Res* **910:**81-93.

Cecchelli R, Berezowski V, Lundquist S, Culot M, Renftel M, Dehouck MP and Fenart L (2007) Modelling of the blood-brain barrier in drug discovery and development. *Nat Rev Drug Discov* **6:**650-661.

Chen C, Hanson E, Watson JW and Lee JS (2003a) P-glycoprotein limits the brain penetration of nonsedating but not sedating H1-antagonists. *Drug Metab Dispos* **31:**312-318.

Chen C, Liu X and Smith BJ (2003b) Utility of Mdr1-gene deficient mice in assessing the impact of P-glycoprotein on pharmacokinetics and pharmacodynamics in drug discovery and development. *Curr Drug Metab* **4:**272-291.

Chen C and Pollack GM (1997) Blood-brain disposition and antinociceptive effects of -D-penicillamine2,5-enkephalin in the mouse. *J Pharmacol Exp Ther* **283:**1151-1159.

Chen C and Pollack GM (1999) Enhanced antinociception of the model opioid peptide [D-penicillamine] enkephalin by P-glycoprotein modulation. *Pharm Res* **16:**296-301.

Chen ZR, Irvine RJ, Bochner F and Somogyi AA (1990) Morphine formation from codeine in rat brain: a possible mechanism of codeine analgesia. *Life Sci* **46:**1067-1074.

Chiueh CC, Sun CL, Kopin IJ, Fredericks WR and Rapoport SI (1978) Entry of [3H]norepinephrine, [125I]albumin and Evans blue from blood into brain following unilateral osmotic opening of the blood-brain barrier. *Brain Res* **145:**291-301.

Choo EF, Leake B, Wandel C, Imamura H, Wood AJ, Wilkinson GR and Kim RB (2000) Pharmacological inhibition of P-glycoprotein transport enhances the distribution of HIV-1 protease inhibitors into brain and testes. *Drug Metab Dispos* **28:**655-660.

Cisternino S, Mercier C, Bourasset F, Roux F and Scherrmann JM (2004) Expression, up-regulation, and transport activity of the multidrug-resistance protein Abcg2 at the mouse blood-brain barrier. *Cancer Res* **64:**3296-3301.

Cisternino S, Rousselle C, Dagenais C and Scherrmann JM (2001) Screening of multidrug-resistance sensitive drugs by in situ brain perfusion in P-glycoprotein-deficient mice. *Pharm Res* **18:**183-190.

Cisternino S, Rousselle C, Lorico A, Rappa G and Scherrmann JM (2003) Apparent lack of Mrp1-mediated efflux at the luminal side of mouse blood-brain barrier endothelial cells. *Pharm Res* **20:**904-909.

Clark DE (2003) In silico prediction of blood-brain barrier permeation. *Drug Discov Today* **8:**927-933.

Clinckers R, Smolders I, Meurs A, Ebinger G and Michotte Y (2005) Quantitative in vivo microdialysis study on the influence of multidrug transporters on the blood-brain barrier passage of oxcarbazepine: concomitant use of hippocampal monoamines as pharmacodynamic markers for the anticonvulsant activity. *J Pharmacol Exp Ther* **314:**725-731.

Cooray HC, Blackmore CG, Maskell L and Barrand MA (2002) Localisation of breast cancer resistance protein in microvessel endothelium of human brain. *Neuroreport* **13:**2059-2063.

Cvetkovic M, Leake B, Fromm MF, Wilkinson GR and Kim RB (1999) OATP and P-glycoprotein transporters mediate the cellular uptake and excretion of fexofenadine. *Drug Metab Dispos* **27:**866-871.

Dagenais C, Ducharme J and Pollack GM (2001) Uptake and efflux of the peptidic delta-opioid receptor agonist. *Neurosci Lett* **301:**155-158.

Dagenais C, Graff CL and Pollack GM (2004) Variable modulation of opioid brain uptake by P-glycoprotein in mice. *Biochem Pharmacol* **67:**269-276.

Dagenais C, Rousselle C, Pollack GM and Scherrmann JM (2000) Development of an in situ mouse brain perfusion model and its application to mdr1a P-glycoprotein-deficient mice. *J Cereb Blood Flow Metab* **20:**381-386.

de Lange EC (2004) Potential role of ABC transporters as a detoxification system at the blood-CSF barrier. *Adv Drug Deliv Rev* **56:**1793-1809.

de Lange EC and Danhof M (2002) Considerations in the use of cerebrospinal fluid pharmacokinetics to predict brain target concentrations in the clinical setting: implications of the barriers between blood and brain. *Clin Pharmacokinet* **41:**691-703.

de Lange EC, Danhof M, de Boer AG and Breimer DD (1997) Methodological considerations of intracerebral microdialysis in pharmacokinetic studies on drug transport across the blood-brain barrier. *Brain Res Brain Res Rev* **25:**27-49.

Demeule M, Labelle M, Regina A, Berthelet F and Beliveau R (2001) Isolation of endothelial cells from brain, lung, and kidney: expression of the multidrug resistance P-glycoprotein isoforms. *Biochem Biophys Res Commun* **281:**827-834.

Doran A, Obach RS, Smith BJ, Hosea NA, Becker S, Callegari E, Chen C, Chen X, Choo E, Cianfrogna J, Cox LM, Gibbs JP, Gibbs MA, Hatch H, Hop CE, Kasman IN, Laperle J, Liu J, Liu X, Logman M, Maclin D, Nedza FM, Nelson F, Olson E, Rahematpura S, Raunig D, Rogers S, Schmidt K, Spracklin DK, Szewc M, Troutman M, Tseng E, Tu M, Van Deusen JW, Venkatakrishnan K, Walens G, Wang EQ, Wong D, Yasgar AS and Zhang C (2005) The impact of P-glycoprotein on the disposition of drugs targeted for indications of the central nervous system: evaluation using the MDR1A/1B knockout mouse model. *Drug Metab Dispos* **33:**165-174.

Doyle LA, Yang W, Abruzzo LV, Krogmann T, Gao Y, Rishi AK and Ross DD (1998) A multidrug resistance transporter from human MCF-7 breast cancer cells. *Proc Natl Acad Sci U S A* **95:**15665-15670.

Duelli R and Kuschinsky W (1993) Changes in brain capillary diameter during hypocapnia and hypercapnia. *J Cereb Blood Flow Metab* **13:**1025-1028.

Eisenblatter T and Galla HJ (2002) A new multidrug resistance protein at the blood-brain barrier. *Biochem Biophys Res Commun* **293:**1273-1278.

Eisenblatter T, Huwel S and Galla HJ (2003) Characterisation of the brain multidrug resistance protein (BMDP/ABCG2/BCRP) expressed at the blood-brain barrier. *Brain Res* **971:**221-231.

Ejsing TB, Morling N and Linnet K (2007) A review on the relation between the brain-serum concentration ratio of drugs and the influence of P-glycoprotein. *Drug Metabol Drug Interact* **22:**113-129.

Elsinga PH, Hendrikse NH, Bart J, Vaalburg W and van Waarde A (2004) PET Studies on P-glycoprotein function in the blood-brain barrier: how it affects uptake and binding of drugs within the CNS. *Curr Pharm Des* **10:**1493-1503.

Enokizono J, Kusuhara H and Sugiyama Y (2007) Effect of breast cancer resistance protein (Bcrp/Abcg2) on the disposition of phytoestrogens. *Mol Pharmacol* **72:**967-975.

Evrard PA, Ragusi C, Boschi G, Verbeeck RK and Scherrmann JM (1998) Simultaneous microdialysis in brain and blood of the mouse: extracellular and intracellular brain colchicine disposition. *Brain Res* **786:**122-127.

Fenstermacher J, Nakata H, Tajima A, Lin SZ, Otsuka T, Acuff V, Wei L and Bereczki D (1991) Functional variations in parenchymal microvascular systems within the brain. *Magn Reson Med* **19:**217-220.

Fenstermacher JD, Blasberg RG and Patlak CS (1981) Methods for Quantifying the transport of drugs across brain barrier systems. *Pharmacol Ther* **14:**217-248.

Frankle WG and Laruelle M (2002) Neuroreceptor imaging in psychiatric disorders. *Ann Nucl Med* **16:**437-446.

Gee AD (2003) Neuropharmacology and drug development. *Br Med Bull* **65:**169-177.

Ghersi-Egea JF, Leninger-Muller B, Suleman G, Siest G and Minn A (1994) Localization of drug-metabolizing enzyme activities to blood-brain interfaces and circumventricular organs. *J Neurochem* **62:**1089-1096.

Gjedde A and Diemer NH (1985) Double-tracer study of the fine regional blood-brain glucose transfer in the rat by computer-assisted autoradiography. *J Cereb Blood Flow Metab* **5:**282-289.

Golden PL and Pollack GM (1998) Rationale for influx enhancement versus efflux blockade to increase drug exposure to the brain. *Biopharm Drug Dispos* **19:**263-272.

Goldschmidt RB and Steward O (1980) Preferential neurotoxicity of colchicine for granule cells of the dentate gyrus of the adult rat. *Proc Natl Acad Sci U S A* **77:**3047-3051.

Goodwin JT and Clark DE (2005) In silico predictions of blood-brain barrier penetration: considerations to "keep in mind". *J Pharmacol Exp Ther* **315:**477-483.

Graff CL and Pollack GM (2004) Drug transport at the blood-brain barrier and the choroid plexus. *Curr Drug Metab* **5:**95-108.

Graff CL, Zhao R and Pollack GM (2005) Pharmacokinetics of substrate uptake and distribution in murine brain after nasal instillation. *Pharm Res* **22:**235-244.

Gumbleton M and Audus KL (2001) Progress and limitations in the use of in vitro cell cultures to serve as a permeability screen for the blood-brain barrier. *J Pharm Sci* **90:**1681-1698.

Gupta A, Dai Y, Vethanayagam RR, Hebert MF, Thummel KE, Unadkat JD, Ross DD and Mao Q (2006) Cyclosporin A, tacrolimus and sirolimus are potent inhibitors of the human breast cancer resistance protein (ABCG2) and reverse resistance to mitoxantrone and topotecan. *Cancer Chemother Pharmacol* **58:**374-383.

Hagemeyer CE, Rosenbrock H, Ditter M, Knoth R and Volk B (2003) Predominantly neuronal expression of cytochrome P450 isoforms CYP3A11 and CYP3A13 in mouse brain. *Neuroscience* **117:**521-529.

Hammarlund-Udenaes M, Paalzow LK and de Lange EC (1997) Drug equilibration across the blood-brain barrier--pharmacokinetic considerations based on the microdialysis method. *Pharm Res* **14:**128-134.

Hansen DK, Scott DO, Otis KW and Lunte SM (2002) Comparison of in vitro BBMEC permeability and in vivo CNS uptake by microdialysis sampling. *J Pharm Biomed Anal* **27:**945-958.

Heiss WD and Herholz K (2006) Brain receptor imaging. *J Nucl Med* **47:**302-312.

Helmy A, Carpenter KL and Hutchinson PJ (2007) Microdialysis in the human brain and its potential role in the development and clinical assessment of drugs. *Curr Med Chem* **14:**1525-1537.

Hendrikse NH, Schinkel AH, de Vries EG, Fluks E, Van der Graaf WT, Willemsen AT, Vaalburg W and Franssen EJ (1998) Complete in vivo reversal of P-glycoprotein pump function in the blood-brain barrier visualized with positron emission tomography. *Br J Pharmacol* **124:**1413-1418.

Hochman JH, Yamazaki M, Ohe T and Lin JH (2002) Evaluation of drug interactions with P-glycoprotein in drug discovery: in vitro assessment of the potential for drug-drug interactions with P-glycoprotein. *Curr Drug Metab* **3:**257-273.

Hou TJ and Xu XJ (2003a) ADME evaluation in drug discovery. 2. Prediction of partition coefficient by atom-additive approach based on atom-weighted solvent accessible surface areas. *J Chem Inf Comput Sci* **43:**1058-1067.

Hou TJ and Xu XJ (2003b) ADME evaluation in drug discovery. 3. Modeling blood-brain barrier partitioning using simple molecular descriptors. *J Chem Inf Comput Sci* **43:**2137-2152.

Hsiao P, Sasongko L, Link JM, Mankoff DA, Muzi M, Collier AC and Unadkat JD (2006) Verapamil P-glycoprotein transport across the rat blood-brain barrier: cyclosporine, a concentration inhibition analysis, and comparison with human data. *J Pharmacol Exp Ther* **317:**704-710.

Ikoma Y, Takano A, Ito H, Kusuhara H, Sugiyama Y, Arakawa R, Fukumura T, Nakao R, Suzuki K and Suhara T (2006) Quantitative analysis of 11C-verapamil transfer at the human blood-brain barrier for evaluation of P-glycoprotein function. *J Nucl Med* **47:**1531-1537.

Johanson CE, Duncan JA, Stopa EG and Baird A (2005) Enhanced prospects for drug delivery and brain targeting by the choroid plexus-CSF route. *Pharm Res* **22:**1011-1037.

Johnson BM, Zhang P, Schuetz JD and Brouwer KL (2006) Characterization of transport protein expression in multidrug resistance-associated protein (Mrp) 2-deficient rats. *Drug Metab Dispos* **34:**556-562.

Jonker JW, Merino G, Musters S, van Herwaarden AE, Bolscher E, Wagenaar E, Mesman E, Dale TC and Schinkel AH (2005) The breast cancer resistance protein BCRP (ABCG2) concentrates drugs and carcinogenic xenotoxins into milk. *Nat Med* **11:**127-129.

Jonker JW, Smit JW, Brinkhuis RF, Maliepaard M, Beijnen JH, Schellens JH and Schinkel AH (2000) Role of breast cancer resistance protein in the bioavailability and fetal penetration of topotecan. *J Natl Cancer Inst* **92:**1651-1656.

Kaddoumi A, Choi SU, Kinman L, Whittington D, Tsai CC, Ho RJ, Anderson BD and Unadkat JD (2007) Inhibition of P-glycoprotein activity at the primate blood-brain barrier increases the distribution of nelfinavir into the brain but not into the cerebrospinal fluid. *Drug Metab Dispos* **35:**1459-1462.

Kalvass JC, Graff CL and Pollack GM (2004) Use of loperamide as a phenotypic probe of mdr1a status in CF-1 mice. *Pharm Res* **21:**1867-1870.

Kalvass JC and Maurer TS (2002) Influence of nonspecific brain and plasma binding on CNS exposure: implications for rational drug discovery. *Biopharm Drug Dispos* **23:**327-338.

Kalvass JC, Maurer TS and Pollack GM (2007a) Use of plasma and brain unbound fractions to assess the extent of brain distribution of 34 drugs: comparison of unbound concentration ratios to in vivo p-glycoprotein efflux ratios. *Drug Metab Dispos* **35:**660-666.

Kalvass JC, Olson ER, Cassidy MP, Selley DE and Pollack GM (2007b) Pharmacokinetics and Pharmacodynamics of Seven Opioids in P-gp-Competent Mice: Assessment of Unbound Brain EC50 and Correlation of In Vitro, Preclinical, and Clinical Data. *J Pharmacol Exp Ther*.

Kalvass JC and Pollack GM (2007) Kinetic considerations for the quantitative assessment of efflux activity and inhibition: implications for understanding and predicting the effects of efflux inhibition. *Pharm Res* **24:**265-276.

Kartner N, Riordan JR and Ling V (1983) Cell surface P-glycoprotein associated with multidrug resistance in mammalian cell lines. *Science* **221:**1285-1288.

Kassem NA, Deane R, Segal MB, Chen R and Preston JE (2007) Thyroxine (T(4)) transfer from CSF to choroid plexus and ventricular brain regions in rabbit: Contributory role of P-glycoprotein and organic anion transporting polypeptides. *Brain Res*.

Kemper EM, van Zandbergen AE, Cleypool C, Mos HA, Boogerd W, Beijnen JH and van Tellingen O (2003) Increased penetration of paclitaxel into the brain by inhibition of P-Glycoprotein. *Clin Cancer Res* **9:**2849-2855.

Kemper EM, Verheij M, Boogerd W, Beijnen JH and van Tellingen O (2004) Improved penetration of docetaxel into the brain by co-administration of inhibitors of P-glycoprotein. *Eur J Cancer* **40:**1269-1274.

Klein B, Kuschinsky W, Schrock H and Vetterlein F (1986) Interdependency of local capillary density, blood flow, and metabolism in rat brains. *Am J Physiol* **251:**H1333-1340.

Koehler-Stec EM, Simpson IA, Vannucci SJ, Landschulz KT and Landschulz WH (1998) Monocarboxylate transporter expression in mouse brain. *Am J Physiol* **275:**E516-524.

Korjamo T, Kemilainen H, Heikkinen AT and Monkkonen J (2007) Decrease in intracellular concentration causes the shift in Km value of efflux pump substrates. *Drug Metab Dispos* **35:**1574-1579.

Langer O, Bauer M, Hammers A, Karch R, Pataraia E, Koepp MJ, Abrahim A, Luurtsema G, Brunner M, Sunder-Plassmann R, Zimprich F, Joukhadar C, Gentzsch S, Dudczak R, Kletter K, Muller M and Baumgartner C (2007) Pharmacoresistance in Epilepsy: A Pilot PET Study with the P-Glycoprotein Substrate R-[C]verapamil. *Epilepsia*.

Lee YJ, Kusuhara H, Jonker JW, Schinkel AH and Sugiyama Y (2005) Investigation of efflux transport of dehydroepiandrosterone sulfate and mitoxantrone at the mouse blood-brain barrier: a minor role of breast cancer resistance protein. *J Pharmacol Exp Ther* **312:**44-52.

Lentz KA, Polli JW, Wring SA, Humphreys JE and Polli JE (2000) Influence of passive permeability on apparent P-glycoprotein kinetics. *Pharm Res* **17:**1456-1460.

Linnet K and Ejsing TB (2007) A review on the impact of P-glycoprotein on the penetration of drugs into the brain. Focus on psychotropic drugs. *Eur Neuropsychopharmacol*.

Liu X and Chen C (2005) Strategies to optimize brain penetration in drug discovery. *Curr Opin Drug Discov Devel* **8:**505-512.

Liu X, Smith BJ, Chen C, Callegari E, Becker SL, Chen X, Cianfrogna J, Doran AC, Doran SD, Gibbs JP, Hosea N, Liu J, Nelson FR, Szewc MA and Van Deusen J (2005) Use of a physiologically based pharmacokinetic model to study the time to reach brain equilibrium: an experimental analysis of the role of blood-brain barrier permeability, plasma protein binding, and brain tissue binding. *J Pharmacol Exp Ther* **313:**1254-1262.

Liu X, Smith BJ, Chen C, Callegari E, Becker SL, Chen X, Cianfrogna J, Doran AC, Doran SD, Gibbs JP, Hosea N, Liu J, Nelson FR, Szewc MA and Van Deusen J (2006) Evaluation of cerebrospinal fluid concentration and plasma free concentration as a surrogate measurement for brain free concentration. *Drug Metab Dispos* **34:**1443-1447.

Liu X, Tu M, Kelly RS, Chen C and Smith BJ (2004) Development of a computational approach to predict blood-brain barrier permeability. *Drug Metab Dispos* **32:**132-139.

Lubberink M, Luurtsema G, van Berckel BN, Boellaard R, Toornvliet R, Windhorst AD, Franssen EJ and Lammertsma AA (2007) Evaluation of tracer kinetic models for quantification of P-glycoprotein function using (R)-[11C]verapamil and PET. *J Cereb Blood Flow Metab* **27:**424-433.

Mahar Doan KM, Humphreys JE, Webster LO, Wring SA, Shampine LJ, Serabjit-Singh CJ, Adkison KK and Polli JW (2002) Passive permeability and P-glycoprotein-mediated efflux differentiate central nervous system (CNS) and non-CNS marketed drugs. *J Pharmacol Exp Ther* **303:**1029-1037.

Maliepaard M, van Gastelen MA, de Jong LA, Pluim D, van Waardenburg RC, Ruevekamp-Helmers MC, Floot BG and Schellens JH (1999) Overexpression of the BCRP/MXR/ABCP gene in a topotecan-selected ovarian tumor cell line. *Cancer Res* **59:**4559-4563.

Mandula H, Parepally JM, Feng R and Smith QR (2006) Role of site-specific binding to plasma albumin in drug availability to brain. *J Pharmacol Exp Ther* **317:**667-675.

Martin I (2004) Prediction of blood-brain barrier penetration: are we missing the point? *Drug Discov Today* **9:**161-162.

Maurer TS, Debartolo DB, Tess DA and Scott DO (2005) Relationship between exposure and nonspecific binding of thirty-three central nervous system drugs in mice. *Drug Metab Dispos* **33:**175-181.

Merino G, van Herwaarden AE, Wagenaar E, Jonker JW and Schinkel AH (2005) Sex-dependent expression and activity of the ATP-binding cassette transporter breast cancer resistance protein (BCRP/ABCG2) in liver. *Mol Pharmacol* **67:**1765-1771.

Meyer RP, Gehlhaus M, Knoth R and Volk B (2007) Expression and function of cytochrome p450 in brain drug metabolism. *Curr Drug Metab* **8:**297-306.

Meyer RP, Hagemeyer CE, Knoth R, Kaufmann MR and Volk B (2006) Anti-epileptic drug phenytoin enhances androgen metabolism and androgen receptor expression in murine hippocampus. *J Neurochem* **96:**460-472.

Miksys SL and Tyndale RF (2002) Drug-metabolizing cytochrome P450s in the brain. *J Psychiatry Neurosci* **27:**406-415.

Miller DS, Graeff C, Droulle L, Fricker S and Fricker G (2002) Xenobiotic efflux pumps in isolated fish brain capillaries. *Am J Physiol Regul Integr Comp Physiol* **282:**R191-198.

Miller DS, Nobmann SN, Gutmann H, Toeroek M, Drewe J and Fricker G (2000) Xenobiotic transport across isolated brain microvessels studied by confocal microscopy. *Mol Pharmacol* **58:**1357-1367.

Murakami H, Takanaga H, Matsuo H, Ohtani H and Sawada Y (2000) Comparison of blood-brain barrier permeability in mice and rats using in situ brain perfusion technique. *Am J Physiol Heart Circ Physiol* **279:**H1022-1028.

Nies AT, Jedlitschky G, Konig J, Herold-Mende C, Steiner HH, Schmitt HP and Keppler D (2004) Expression and immunolocalization of the multidrug resistance proteins, MRP1-MRP6 (ABCC1-ABCC6), in human brain. *Neuroscience* **129:**349-360.

Norinder U and Haeberlein M (2002) Computational approaches to the prediction of the blood-brain distribution. *Adv Drug Deliv Rev* **54:**291-313.

Ohno K, Pettigrew KD and Rapoport SI (1979) Local cerebral blood flow in the conscious rat as measured with 14C-antipyrine, 14C-iodoantipyrine and 3H-nicotine. *Stroke* **10:**62-67.

Ohtsuki S (2004) New aspects of the blood-brain barrier transporters; its physiological roles in the central nervous system. *Biol Pharm Bull* **27:**1489-1496.

Ohtsuki S and Terasaki T (2007) Contribution of carrier-mediated transport systems to the blood-brain barrier as a supporting and protecting interface for the brain; importance for CNS drug discovery and development. *Pharm Res* **24:**1745-1758.

Oldendorf WH (1970) Measurement of brain uptake of radiolabeled substances using a tritiated water internal standard. *Brain Res* **24:**372-376.

Oldendorf WH (1974) Lipid solubility and drug penetration of the blood brain barrier. *Proc Soc Exp Biol Med* **147:**813-815.

Pajeva IK, Globisch C and Wiese M (2004) Structure-function relationships of multidrug resistance P-glycoprotein. *J Med Chem* **47:**2523-2533.

Pajeva IK and Wiese M (2002) Pharmacophore model of drugs involved in P-glycoprotein multidrug resistance: explanation of structural variety (hypothesis). *J Med Chem* **45:**5671-5686.

Pardridge WM (2004) Log(BB), PS products and in silico models of drug brain penetration. *Drug Discov Today* **9:**392-393.

Parepally JM, Mandula H and Smith QR (2006) Brain uptake of nonsteroidal anti-inflammatory drugs: ibuprofen, flurbiprofen, and indomethacin. *Pharm Res* **23:**873-881.

Polli JW, Baughman TM, Humphreys JE, Jordan KH, Mote AL, Salisbury JA, Tippin TK and Serabjit-Singh CJ (2003) P-glycoprotein influences the brain concentrations of cetirizine (Zyrtec), a second-generation non-sedating antihistamine. *J Pharm Sci* **92:**2082-2089.

Polli JW, Wring SA, Humphreys JE, Huang L, Morgan JB, Webster LO and Serabjit-Singh CS (2001) Rational use of in vitro P-glycoprotein assays in drug discovery. *J Pharmacol Exp Ther* **299:**620-628.

Potschka H, Fedrowitz M and Loscher W (2003) Multidrug resistance protein MRP2 contributes to blood-brain barrier function and restricts antiepileptic drug activity. *J Pharmacol Exp Ther* **306:**124-131.

Rambeck B, Jurgens UH, May TW, Pannek HW, Behne F, Ebner A, Gorji A, Straub H, Speckmann EJ, Pohlmann-Eden B and Loscher W (2006) Comparison of brain extracellular fluid, brain tissue, cerebrospinal fluid, and serum concentrations of antiepileptic drugs measured intraoperatively in patients with intractable epilepsy. *Epilepsia* **47:**681-694.

Rautio J, Humphreys JE, Webster LO, Balakrishnan A, Keogh JP, Kunta JR, Serabjit-Singh CJ and Polli JW (2006) In vitro p-glycoprotein inhibition assays for assessment of clinical drug interaction potential of new drug candidates: a recommendation for probe substrates. *Drug Metab Dispos* **34:**786-792.

Reichel A (2006) The role of blood-brain barrier studies in the pharmaceutical industry. *Curr Drug Metab* **7:**183-203.

Rosen BR, Belliveau JW, Buchbinder BR, McKinstry RC, Porkka LM, Kennedy DN, Neuder MS, Fisel CR, Aronen HJ, Kwong KK and et al. (1991) Contrast agents and cerebral hemodynamics. *Magn Reson Med* **19:**285-292.

Rudick RA, Zirretta DK and Herndon RM (1982) Clearance of albumin from mouse subarachnoid space: a measure of CSF bulk flow. *J Neurosci Methods* **6:**253-259.

Sakurada O, Kennedy C, Jehle J, Brown JD, Carbin GL and Sokoloff L (1978) Measurement of local cerebral blood flow with iodo [14C] antipyrine. *Am J Physiol* **234:**H59-66.

Salvadori P (2007) Positron Emission Tomography Application to Drug Development and Research, in: *Physics for medical imaging applications* (Lemoigne Y, Caner A and Rahal G eds), pp 341-351, Kluwer Academic Publishers Group, Dordrecht.

Sampath J, Adachi M, Hatse S, Naesens L, Balzarini J, Flatley RM, Matherly LH and Schuetz JD (2002) Role of MRP4 and MRP5 in biology and chemotherapy. *AAPS PharmSci* **4:**E14.

Sasabe H, Kato Y, Suzuki T, Itose M, Miyamoto G and Sugiyama Y (2004) Differential involvement of multidrug resistance-associated protein 1 and P-glycoprotein in tissue distribution and excretion of grepafloxacin in mice. *J Pharmacol Exp Ther* **310:**648-655.

Schinkel AH (1999) P-Glycoprotein, a gatekeeper in the blood-brain barrier. *Adv Drug Deliv Rev* **36:**179-194.

Schinkel AH, Smit JJ, van Tellingen O, Beijnen JH, Wagenaar E, van Deemter L, Mol CA, van der Valk MA, Robanus-Maandag EC, te Riele HP and et al. (1994) Disruption of the mouse mdr1a P-glycoprotein gene leads to a deficiency in the blood-brain barrier and to increased sensitivity to drugs. *Cell* **77:**491-502.

Schinkel AH, Wagenaar E, Mol CA and van Deemter L (1996) P-glycoprotein in the blood-brain barrier of mice influences the brain penetration and pharmacological activity of many drugs. *J Clin Invest* **97:**2517-2524.

Seegers U, Potschka H and Loscher W (2002) Transient increase of P-glycoprotein expression in endothelium and parenchyma of limbic brain regions in the kainate model of temporal lobe epilepsy. *Epilepsy Res* **51:**257-268.

Shen DD, Artru AA and Adkison KK (2004) Principles and applicability of CSF sampling for the assessment of CNS drug delivery and pharmacodynamics. *Adv Drug Deliv Rev* **56:**1825-1857.

Sikic BI, Fisher GA, Lum BL, Halsey J, Beketic-Oreskovic L and Chen G (1997) Modulation and prevention of multidrug resistance by inhibitors of P-glycoprotein. *Cancer Chemother Pharmacol* **40 Suppl:**S13-19.

Soontornmalai A, Vlaming ML and Fritschy JM (2006) Differential, strain-specific cellular and subcellular distribution of multidrug transporters in murine choroid plexus and blood-brain barrier. *Neuroscience* **138:**159-169.

Sparreboom A, Loos WJ, Burger H, Sissung TM, Verweij J, Figg WD, Nooter K and Gelderblom H (2005) Effect of ABCG2 genotype on the oral bioavailability of topotecan. *Cancer Biol Ther* **4:**650-658.

Strazielle N and Ghersi-Egea JF (1999) Demonstration of a coupled metabolism-efflux process at the choroid plexus as a mechanism of brain protection toward xenobiotics. *J Neurosci* **19:**6275-6289.

Strazielle N, Khuth ST and Ghersi-Egea JF (2004) Detoxification systems, passive and specific transport for drugs at the blood-CSF barrier in normal and pathological situations. *Adv Drug Deliv Rev* **56:**1717-1740.

Strobel HW, Thompson CM and Antonovic L (2001) Cytochromes P450 in brain: function and significance. *Curr Drug Metab* **2:**199-214.

Sugiyama D, Kusuhara H, Lee YJ and Sugiyama Y (2003) Involvement of multidrug resistance associated protein 1 (Mrp1) in the efflux transport of 17beta estradiol-D-17beta-glucuronide (E217betaG) across the blood-brain barrier. *Pharm Res* **20:**1394-1400.

Summerfield SG, Read K, Begley DJ, Obradovic T, Hidalgo IJ, Coggon S, Lewis AV, Porter RA and Jeffrey P (2007) Central nervous system drug disposition: the relationship between in situ brain permeability and brain free fraction. *J Pharmacol Exp Ther* **322:**205-213.

Summerfield SG, Stevens AJ, Cutler L, del Carmen Osuna M, Hammond B, Tang SP, Hersey A, Spalding DJ and Jeffrey P (2006) Improving the in vitro prediction of in vivo central nervous system penetration: integrating permeability, P-

glycoprotein efflux, and free fractions in blood and brain. *J Pharmacol Exp Ther* **316:**1282-1290.

Sun H, Dai H, Shaik N and Elmquist WF (2003) Drug efflux transporters in the CNS. *Adv Drug Deliv Rev* **55:**83-105.

Sun H, Johnson DR, Finch RA, Sartorelli AC, Miller DW and Elmquist WF (2001a) Transport of fluorescein in MDCKII-MRP1 transfected cells and mrp1-knockout mice. *Biochem Biophys Res Commun* **284:**863-869.

Sun H, Miller DW and Elmquist WF (2001b) Effect of probenecid on fluorescein transport in the central nervous system using in vitro and in vivo models. *Pharm Res* **18:**1542-1549.

Suzuki H, Nagashima T, Tamaki N and Yamadori T (1998) Cerebral ischemia affects glucose transporter kinetics across rat brain microvascular endothelium: quantitative analysis by an in situ brain perfusion method. *Surg Neurol* **49:**67-76.

Syvanen S, Xie R, Sahin S and Hammarlund-Udenaes M (2006) Pharmacokinetic consequences of active drug efflux at the blood-brain barrier. *Pharm Res* **23:**705-717.

Takano A, Kusuhara H, Suhara T, Ieiri I, Morimoto T, Lee YJ, Maeda J, Ikoma Y, Ito H, Suzuki K and Sugiyama Y (2006) Evaluation of in vivo P-glycoprotein function at the blood-brain barrier among MDR1 gene polymorphisms by using 11C-verapamil. *J Nucl Med* **47:**1427-1433.

Takasato Y, Rapoport SI and Smith QR (1984) An in situ brain perfusion technique to study cerebrovascular transport in the rat. *Am J Physiol* **247:**H484-493.

Takenaka K, Morgan JA, Scheffer GL, Adachi M, Stewart CF, Sun D, Leggas M, Ejendal KF, Hrycyna CA and Schuetz JD (2007) Substrate overlap between Mrp4 and Abcg2/Bcrp affects purine analogue drug cytotoxicity and tissue distribution. *Cancer Res* **67:**6965-6972.

Tanaka Y, Slitt AL, Leazer TM, Maher JM and Klaassen CD (2005) Tissue distribution and hormonal regulation of the breast cancer resistance protein (Bcrp/Abcg2) in rats and mice. *Biochem Biophys Res Commun* **326:**181-187.

Taylor EM (2002) The impact of efflux transporters in the brain on the development of drugs for CNS disorders. *Clin Pharmacokinet* **41:**81-92.

Terasaki T and Ohtsuki S (2005) Brain-to-blood transporters for endogenous substrates and xenobiotics at the blood-brain barrier: an overview of biology and methodology. *NeuroRx* **2:**63-72.

Terasaki T, Ohtsuki S, Hori S, Takanaga H, Nakashima E and Hosoya K (2003) New approaches to in vitro models of blood-brain barrier drug transport. *Drug Discov Today* **8:**944-954.

Terasaki T and Pardridge WM (2000) Targeted drug delivery to the brain; (blood-brain barrier, efflux, endothelium, biological transport). *J Drug Target* **8:**353-355.

Tofteng F, Jorgensen L, Hansen BA, Ott P, Kondrup J and Larsen FS (2002) Cerebral microdialysis in patients with fulminant hepatic failure. *Hepatology* **36:**1333-1340.

Tofteng F and Larsen FS (2002) Monitoring extracellular concentrations of lactate, glutamate, and glycerol by in vivo microdialysis in the brain during liver transplantation in acute liver failure. *Liver Transpl* **8:**302-305.

Tohyama K, Kusuhara H and Sugiyama Y (2004) Involvement of multispecific organic anion transporter, Oatp14 (Slc21a14), in the transport of thyroxine across the blood-brain barrier. *Endocrinology* **145:**4384-4391.

Tunblad K, Jonsson EN and Hammarlund-Udenaes M (2003) Morphine blood-brain barrier transport is influenced by probenecid co-administration. *Pharm Res* **20:**618-623.

van Vliet EA, van Schaik R, Edelbroek PM, Voskuyl RA, Redeker S, Aronica E, Wadman WJ and Gorter JA (2007) Region-specific overexpression of P-glycoprotein at the blood-brain barrier affects brain uptake of phenytoin in epileptic rats. *J Pharmacol Exp Ther* **322:**141-147.

Vander Borght S, Libbrecht L, Katoonizadeh A, van Pelt J, Cassiman D, Nevens F, Van Lommel A, Petersen BE, Fevery J, Jansen PL and Roskams TA (2006) Breast cancer resistance protein (BCRP/ABCG2) is expressed by progenitor cells/reactive ductules and hepatocytes and its expression pattern is influenced by

disease etiology and species type: possible functional consequences. *J Histochem Cytochem* **54:**1051-1059.

Venkatakrishnan K, Tseng E, Nelson FR, Rollema H, French JL, Kaplan IV, Horner WE and Gibbs MA (2007) Central nervous system pharmacokinetics of the Mdr1 P-glycoprotein substrate CP-615,003: intersite differences and implications for human receptor occupancy projections from cerebrospinal fluid exposures. *Drug Metab Dispos* **35:**1341-1349.

Villesen HH, Foster DJ, Upton RN, Christrup LL, Somogyi AA, Martinez A and Grant C (2006a) Blood-brain distribution of morphine-6-glucuronide in sheep. *Br J Pharmacol* **149:**754-760.

Villesen HH, Foster DJ, Upton RN, Somogyi AA, Martinez A and Grant C (2006b) Cerebral kinetics of oxycodone in conscious sheep. *J Pharm Sci* **95:**1666-1676.

Vogelgesang S, Warzok RW, Cascorbi I, Kunert-Keil C, Schroeder E, Kroemer HK, Siegmund W, Walker LC and Pahnke J (2004) The role of P-glycoprotein in cerebral amyloid angiopathy; implications for the early pathogenesis of Alzheimer's disease. *Curr Alzheimer Res* **1:**121-125.

Volk HA and Loscher W (2005) Multidrug resistance in epilepsy: rats with drug-resistant seizures exhibit enhanced brain expression of P-glycoprotein compared with rats with drug-responsive seizures. *Brain* **128:**1358-1368.

Wan H, Rehngren M, Giordanetto F, Bergstrom F and Tunek A (2007) High-Throughput Screening of Drug-Brain Tissue Binding and in Silico Prediction for Assessment of Central Nervous System Drug Delivery. *J. Med. Chem.* **50:**4606-4615.

Wang RB, Kuo CL, Lien LL and Lien EJ (2003) Structure-activity relationship: analyses of p-glycoprotein substrates and inhibitors. *J Clin Pharm Ther* **28:**203-228.

Wang Y, Wei Y and Sawchuk RJ (1997) Zidovudine transport within the rabbit brain during intracerebroventricular administration and the effect of probenecid. *J Pharm Sci* **86:**1484-1490.

Wijnholds J, deLange EC, Scheffer GL, van den Berg DJ, Mol CA, van der Valk M, Schinkel AH, Scheper RJ, Breimer DD and Borst P (2000) Multidrug resistance protein 1 protects the choroid plexus epithelium and contributes to the blood-cerebrospinal fluid barrier. *J Clin Invest* **105:**279-285.

Wyss MT, Hofer S, Hefti M, Bartschi E, Uhlmann C, Treyer V and Roelcke U (2007) Spatial heterogeneity of low-grade gliomas at the capillary level: a PET study on tumor blood flow and amino acid uptake. *J Nucl Med* **48:**1047-1052.

Yamazaki M, Neway WE, Ohe T, Chen I, Rowe JF, Hochman JH, Chiba M and Lin JH (2001) In vitro substrate identification studies for p-glycoprotein-mediated transport: species difference and predictability of in vivo results. *J Pharmacol Exp Ther* **296:**723-735.

Youdim KA, Qaiser MZ, Begley DJ, Rice-Evans CA and Abbott NJ (2004) Flavonoid permeability across an in situ model of the blood-brain barrier. *Free Radic Biol Med* **36:**592-604.

Zelcer N, van de Wetering K, Hillebrand M, Sarton E, Kuil A, Wielinga PR, Tephly T, Dahan A, Beijnen JH and Borst P (2005) Mice lacking multidrug resistance protein 3 show altered morphine pharmacokinetics and morphine-6-glucuronide antinociception. *Proc Natl Acad Sci U S A* **102:**7274-7279.

Zhang S, Wang X, Sagawa K and Morris ME (2005) Flavonoids chrysin and benzoflavone, potent breast cancer resistance protein inhibitors, have no significant effect on topotecan pharmacokinetics in rats or mdr1a/1b (-/-) mice. *Drug Metab Dispos* **33:**341-348.

Zhang Y, Han H, Elmquist WF and Miller DW (2000) Expression of various multidrug resistance-associated protein (MRP) homologues in brain microvessel endothelial cells. *Brain Res* **876:**148-153.

Zhang Y, Schuetz JD, Elmquist WF and Miller DW (2004) Plasma membrane localization of multidrug resistance-associated protein homologs in brain capillary endothelial cells. *J Pharmacol Exp Ther* **311:**449-455.

Zlokovic BV (2004) Clearing amyloid through the blood-brain barrier. *J Neurochem* **89:**807-811.

Zlokovic BV, Begley DJ, Djuricic BM and Mitrovic DM (1986) Measurement of solute transport across the blood-brain barrier in the perfused guinea pig brain: method and application to N-methyl-alpha-aminoisobutyric acid. *J Neurochem* **46:**1444-1451.

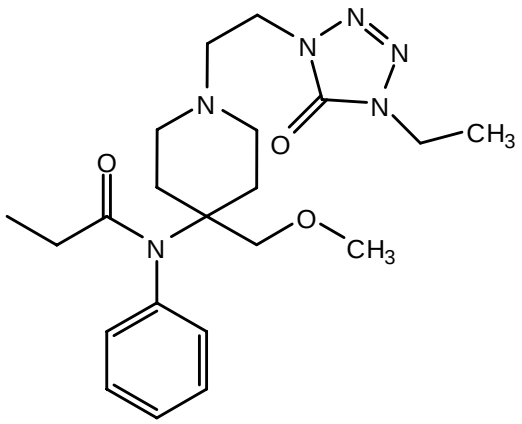

Alfentanil

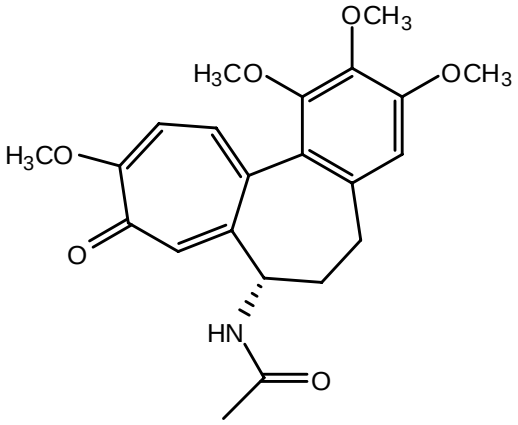

Colchicine

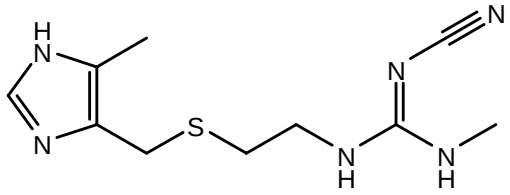

Cimetidine

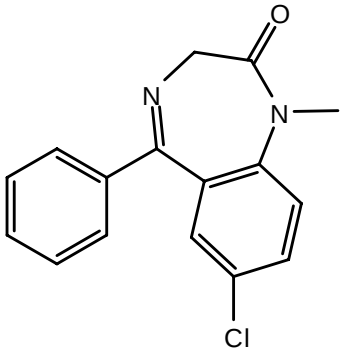

Diazepam

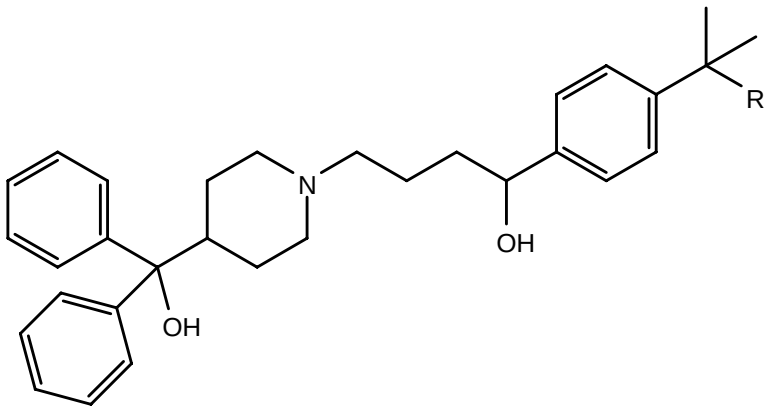

Fexofenadine R=COOH
Terfenadine R=CH_3

Figure 1.1: Chemical structures of selected model compounds.

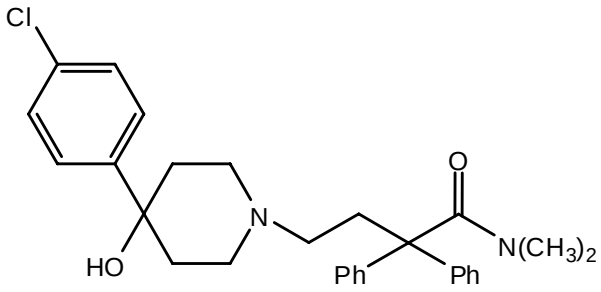

Loperamide

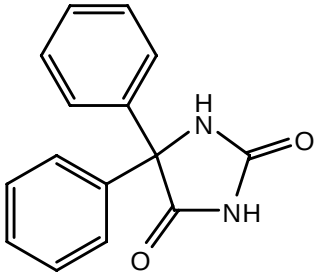

Phenytoin

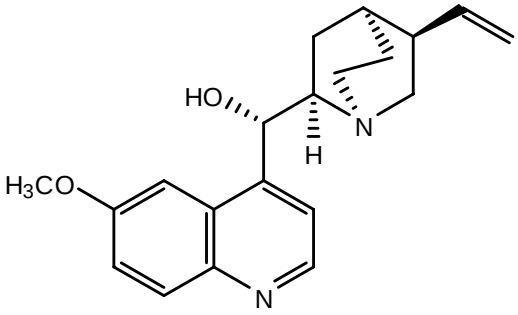

Quinidine

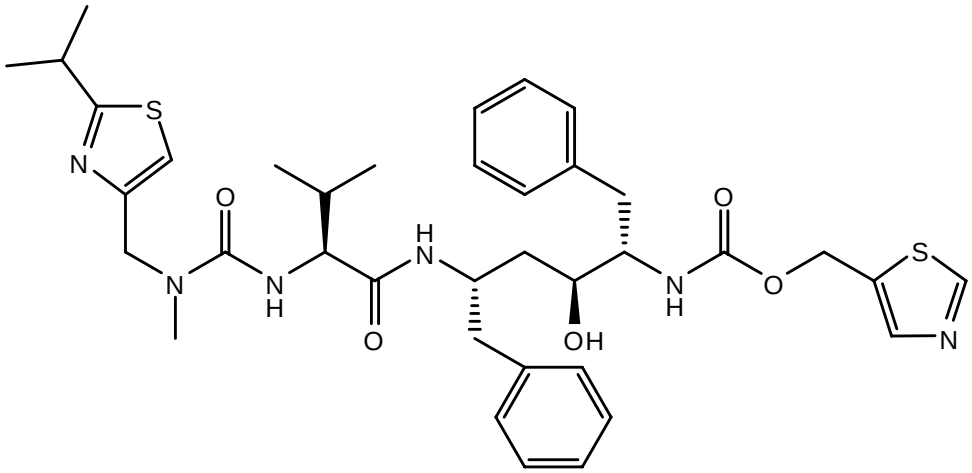

Ritonavir

Figure 1.1: Chemical structures of selected model compounds (continued).

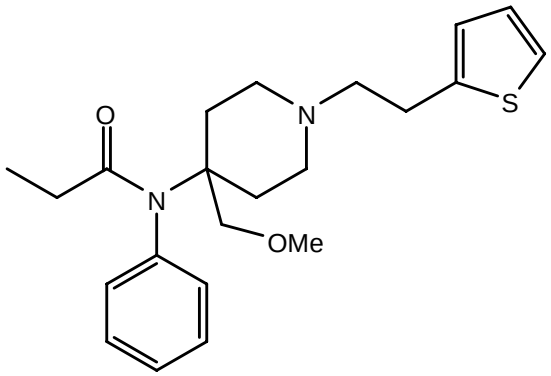

Sufentanil

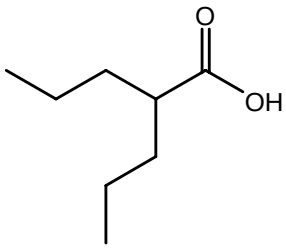

Valproate

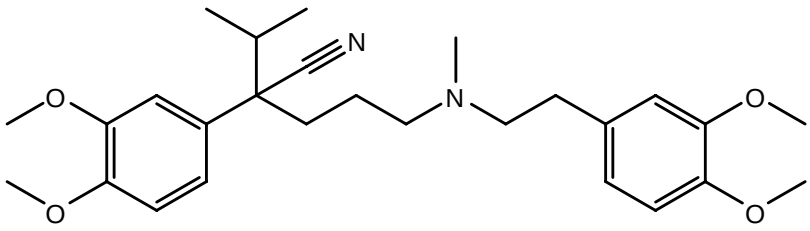

Verapamil

Figure 1.1: Chemical structures of selected model compounds (continued).

CHAPTER 2

ASSESSMENT OF BLOOD-BRAIN BARRIER PERMEABILITY USING THE *IN SITU* MOUSE BRAIN PERFUSION TECHNIQUE

This chapter will be submitted for publication in Pharmaceutical Research and is presented in the style of that journal.

Abstract

Purpose To assess the blood-brain barrier (BBB) permeability of twelve clinically-used drugs in *mdr1a(+/+)* and *mdr1a(-/-)* mice, and investigate the influence of lipophilicity, nonspecific brain tissue binding, and P-gp-mediated efflux in the rate of brain uptake.

Methods The BBB partition coefficient (PS) was determined using the *in situ* mouse brain perfusion technique. The net brain uptake for twelve compounds, and the time course of brain uptake for selected compounds ranging in BBB equilibration kinetics from rapidly-equilibrating (e.g., alfentanil, sufentanil) to slowly-equilibrating (fexofenadine) was determined and compared. The inter-relationship between PS, $f_{u,brain}$, PS×$f_{u,brain}$ and the calculated octanol-water partition coefficient (clogD$_{7.4}$) were examined.

Results There was a sigmoidal relationship in *mdr1a(-/-)* mice between the logPS [logPS(-/-)] and clogD$_{7.4}$ in the range of 0-6. For compounds with clogD$_{7.4}$ less than 1, the initial rate of brain uptake was low and limited by permeability; for compounds with clogD$_{7.4}$ higher than 3, the rate of brain uptake was limited by perfusion rate. In the clogD$_{7.4}$ range of 1-3, the brain uptake clearance was a function of both permeability and blood flow rate. The brain unbound fraction was inversely proportional to the lipophilicity. Alfentanil achieved brain equilibrium approximately 4000-fold faster than fexofenadine, based on the magnitude of PS×*fu,brain*.

Conclusions *In situ* brain perfusion is a useful technique to determine BBB permeability. Lipophilicity, ionization state, molecular weight and polar surface area are all important determinants for brain penetration. The time to blood-to-brain equilibrium varies widely for different compounds, and is determined by a multiplicity of pharmacokinetic factors.

Introduction

The blood-brain barrier (BBB) is a continuous layer of brain capillary endothelial cells, connected by highly-developed tight junctions, that expresses numerous efflux transporters and metabolizing enzymes. The BBB represents a formidable barrier to the access of therapeutic targets for agents intended to have central nervous system (CNS) activity (1-4). Physicochemical properties (e.g., molecular weight, pKa, lipophilicity, polar surface area, and the number of hydrogen bonds) as well as biological factors (e.g., plasma and brain tissue binding, affinity to transporter systems at the BBB) are known determinants of substrate flux across the luminal and abluminal membranes of the brain capillary endothelial cells (5-8). Whereas the role of other efflux transporters at the BBB remains unclear, P-glycoprotein (P-gp)-mediated efflux of many therapeutic agents has been widely accepted (4, 9). P-gp is a 170-kDa membrane protein encoded by multidrug resistance gene *MDR1* in human and *mdr1a* and *mdr1b* in rodents. P-gp-mediated reduction in brain exposure has been linked to the decreased CNS pharmacologic or toxic effects (9, 10).

The logarithm of the brain-to-blood (or brain-to-plasma) concentration ratio (logBB) often is used to characterize and predict brain penetration. However, it is recognized that the unbound brain concentration is the relevant driving force for most pharmacologic events in the CNS. Because logBB is a hybrid parameter that is determined by permeability, plasma and brain tissue binding, and active transport mechanisms, it may provide misleading information regarding potential *in vivo* pharmacologic response, thereby excluding potentially useful drug candidates from further consideration (11, 12). The log of the permeability-surface area coefficient (logPS), in contrast, measures the

ability of a drug to cross the BBB and move into brain tissue over time, and is a more relevant metric of BBB penetration per se. Consequently, logPS has been proposed to replace logBB for assessment and prediction of drug brain penetration (11-13).

PS can be measured using an *in vivo* or *in situ* short-duration vascular perfusion method, e.g., brain uptake index, indicatior dilution, or *in situ* brain perfusion (14). *In situ* brain perfusion was developed to provide a simpler and more accurate method to determine BBB permeability compared to other techniques (15). Furthermore, changes in perfusate composition or use of gene knockout animals enable study of variables such as protein binding and efflux transporter mechanisms, and the resultant influence of these variables on CNS distributional kinetics. This method has been applied to study the CNS uptake of compounds (16-19), and the data generated were used successfully to develop computational models to predict the BBB permeation (13).

Nonspecific brain tissue binding not only influences measures of drug exposure in the brain (7), but also impacts the rate of brain uptake (20). Mathematical modeling of this system showed that the rate to brain equilibrium is determined by the product of PS and $f_{u,brain}$ (PS×$f_{u,brain}$). The equilibrium half-life calculated based on PS×$f_{u,brain}$ was found to be significantly correlated with the experimentally measured distributional half-life (20).

CNS drug discovery and development have been relatively unsuccessful due to the complexity of the BBB and the difficulties associated with the assessment and prediction of CNS penetration (21). Understanding the parameters favorable for CNS penetration is critically important for CNS drug design and optimization, and ultimately for understanding and treating CNS diseases. In the present study, the BBB permeation of 5

compounds with CNS activity, and 7 non-CNS-active drugs, representing a small compound set with substantial structural diversity covering various therapeutic categories and a wide range of physicochemical characteristics, was investigated with the *in situ* mouse brain perfusion technique. The effect of P-gp on net brain uptake, the relationship between the brain permeability coefficient (PS), the unbound drug fraction in mouse brain tissue ($f_{u,brain}$), PS×$f_{u,brain}$ and the calculated octanol-water partition coefficient at pH 7.4 ($clogD_{7.4}$) were examined. In addition, alfentanil and sufentanil are known to reach plasma-biophase equilibration in minutes (22), while fexofenadine is poorly- and slowly-permeable at the BBB (23, 24). The time course of equilibration for these rapidly- and slowly-equilibrating compounds was determined, and the influence of PS and $f_{u,brain}$ on the rate of brain uptake of these compounds was compared.

Materials and Methods

Adult CF-1 *mdr1a(+/+)* and *mdr1a(-/-)* mice (30-40 g, 6-8 weeks of age) were obtained from Charles River Laboratories (Wilmington, MA). All mice were maintained on a 12-h light/dark cycle with access to water and food *ad libitum*. All experimental procedures were performed under full anesthesia induced with ketamine/xylazine (100/10 mg/kg, i.p.), were approved by the Institutional Animal Care and Use Committee at the University of North Carolina at Chapel Hill, and were conducted in accordance with "Principles with Laboratory Animal Care" (NIH publication No. 85-23, revised in 1985).

^{3}H-cimetidine (25.0 Ci/mmol) and ^{14}C-diazepam (56.0 mCi/mmol) were purchased from Amersham Biosciences (Buckinghamshire, UK), ^{14}C-inulin (2.1 mCi/g) from American Radiolabeled Chemical Inc. (St Louis, MO), ^{3}H-inulin (180.0 mCi/g), ^{3}H-colchicine (80.4 Ci/mmol), ^{3}H-verapamil (74.2 Ci/mmol) and ^{3}H-phenytoin (53.1 mCi/mmol) from PerkinElmer (Waltham, MA), ^{3}H-quinidine (20 Ci/mmol) from American Radiolabeled Chemicals Inc (St. Louis, MO), ^{3}H-valproic acid (55 Ci/mmol) from Moravek Biochemicals Inc(Brea, CA). Alfentanil, sufentanil, cimetidine, terfenadine, fexofenadine, loperamide, phenytoin and valproic acid were purchased from Sigma-Aldrich (St. Louis, MO). All other chemicals were commercially available and of reagent grade or better.

In situ Mouse Brain Perfusion

The details of the *in situ* mouse brain perfusion have been described elsewhere (18). Briefly, CF-1 *mdr1a(+/+)* and *mdr1a(-/-)* mice were anesthetized with ketamine/xylazine (100/10 mg/kg, i.p.). The perfusion buffer (Krebs-bicarbonate buffer, with 9 mM of D-glucose, pH 7.4) was oxygenated with 95% O_2 and 5% CO_2 and maintained at 37°C. ^{14}C-

diazepam and ^{3}H- or ^{14}C-inulin were used as blood flow rate and vascular space markers, respectively. Test compounds (2 μM) with or without radiolabeled tracer (0.1-1.6 μCi/mL) were added to the perfusate. The right common carotid artery was cannulated with polyethylene tubing (0.30-mm inner diameter × 0.70-mm outer diameter; Biotrol Diagnostic, Chennevières-les-Louvres, France) following ligation of the external carotid artery. The cardiac ventricles were severed immediately before perfusion at 2.5 mL/min for 60 s (all compounds except alfentanil, sufentanil and fexofenadine) via a syringe pump (Harvard Apparatus, Holliston, MA). Alfentanil and sufentanil (2 μM) were perfused for 10 (alfentanil only), 20, 40 and 60 s, and fexofenadine for 60, 90, and 120 s in *mdr1a(+/+)* and *mdr1a(-/-)* mice, respectively. For additional groups of *mdr1a(+/+)* and *mdr1a(-/-)* mice, fexofenadine was perfused for a single time-point at 60 s, followed by an additional 15-s drug-free saline perfusion to wash out the remaining fexofenadine in the capillary space. All of the experiments were terminated by decapitation, and the right cerebral hemisphere was collected. Aliquots of perfusate were collected through the syringe and tubing for determination of perfusate concentrations. When radiotracers were used, brain samples were digested with 0.7 mL of Solvable® (Packard, Boston, MA) at 50 °C overnight. Five mL of UltimaGold® scintillation cocktail (PerkinElmer, Wellesley, MA) was added and mixed by vortex. Total radioactivity (^{3}H and/or ^{14}C) was determined in a Packard Tri-carb TR 1900 liquid scintillation analyzer (Packard, Boston, MA). For non-radioactive samples, the hemisphere was homogenized with two volumes of distilled water by brief probe sonication. The perfusate and brain samples were stored at -20°C until analysis by HPLC/MS/MS.

Parameters related to the *in situ* brain perfusion, i.e., the cerebral vascular volume (mL/100 g brain), was calculated using equation:

$$V_{vasc} = \frac{X_{inulin}}{C_{inulin}}.$$

At any single time point, the initial brain uptake clearance (Cl_{up}, mL/min/100 g brain) was calculated as:

$$Cl_{up} = \frac{X_{brain}/T}{C_{perf}},$$

and the apparent distributional volume (V_d, mL/100 g brain) was calculated as:

$$V_d = \frac{X_{brain}}{C_{perf}}$$

where the amount of substrate in brain X_{brain} was corrected for blood vessel contamination by subtraction of vascular volume or a final 15-s washout with drug-free saline. For compounds that were perfused for several different times, the V_d values were plotted against perfusion time, the Cl_{up} was calculated as the slope of the initial linear phase (14, 18). The permeability surface product (PS) values were calculated based on Crone-Renkin equation (15):

$$PS = -F_{pf} \times \ln(1 - Cl_{up}/F_{pf}).$$

F_{pf} is the perfusion flow rate measured using ^{14}C-diazepam as the flow rate marker.

Equilibrium Dialysis

Plasma and brain unbound fractions were determined in a 96-well equilibrium dialysis apparatus (HTDialysis, Gales Ferry, CT) using a previously reported method (7). Briefly, fresh CF-1 mouse plasma and brain tissue were obtained the same day of the study. Spectra-Por 2 membranes obtained from Spectrum Laboratories Inc. (Rancho Dominguez, CA) were conditioned in HPLC-grade water for 15 min, followed by 30% ethanol for 15 min, and 100 mM sodium phosphate buffer (pH 7.4) for 15 min. Brain tissue was diluted 3-fold with 100 mM sodium phosphate buffer (pH 7.4) and homogenized with a sonic probe. The drug of interest was added to brain homogenate to achieve a final concentration of 3 and 1 μM, respectively; 150-μl aliquots (n = 6) were loaded into the 96-well equilibrium dialysis apparatus and dialyzed against an equal volume of 100 mM sodium phosphate buffer (pH 7.4). The 96-well equilibrium dialysis apparatus was incubated for 4.5 h in a 155-rpm shaking incubator maintained at 37°C. For non-radioactive samples, after 4.5 h 10 μl of brain homogenate sample and 50 μl of buffer sample were removed from the apparatus and added directly to HPLC vials containing 100 μl of methanol with an appropriate internal standard. A 50-μl aliquot of control buffer was added to the brain homogenate sample, and either a 10-μl aliquot of control brain homogenate was added to the buffer samples to yield identical sample composition between buffer and non-buffer samples. The samples were vortex-mixed, centrifuged, and the supernatant was analyzed by HPLC/MS/MS. For radioactive samples, 5 mL of UltimaGold® scintillation cocktail (PerkinElmer, Wellesley, MA) was added and vortex-mixed. Total radioactivity (^{3}H and/or ^{14}C) was determined in a Packard Tri-carb TR 1900

liquid scintillation analyzer (Packard, Boston, MA). The brain unbound fraction was calculated according to the equation:

$$\text{Undiluted } f_u = \frac{1/D}{((1/f_{u,measured}) - 1) + 1/D}$$

where D represents the -fold dilution of brain tissue, and $f_{u,measured}$ was the ratio of concentrations determined from the buffer and brain homogenate samples.

HPLC/MS/MS Assay

Non-radioactive samples were analyzed by HPLC/MS/MS (API 4000 triple quadrupole with TurboIonSpray interface; Applied Biosystems/MDS Sciex, Concord, ON, Canada). A 25-µL aliquot of the cerebral hemisphere homogenate was transferred to an HPLC vial, and protein was precipitated with 100 µl of methanol containing internal standard (10 ng/mL loperamide), and a 25-µl aliquot of DMSO was added. The sample was vortex-mixed and centrifuged. Standard solutions ranged from 0.5 -5000 nM and were prepared in a similar way, i.e., 25 µl of blank plasma or brain matrix, 100 µl of methanol containing internal standard, and 25 µl of serially-diluted standard solution were mixed and centrifuged. A 3-µl aliquot of supernatant was injected into autosampler (Leap, Carrboro, NC). Test compounds and the internal standard were eluted from an Aquasil C18 column (2.1 x 50 mm, d_p = 5 µm; Thermo Electron Corporation, Waltham, MA) using a mobile phase gradient (A, 0.1% formic acid in water; B, 0.1% formic acid in methanol; 0-0.70-min hold at 0% B, 0.70-3.12-min linear gradient to 90% B, 3.12-4.10 min hold at 90% B, 4.10-4.20-min linear gradient to 0% B, 4.20-4.90-min hold at 0% B; solvent delivery system (Shimadzu, at a flow rate of 0.75 ml/min; from 0.8 ttto 4 min,

flow was directed to the mass spectrometer) and were detected in positive ion mode using multiple reaction monitoring: alfentanil: 417.3 → 268.3 *m*/z, fexofenadine: 502.4 → 466.4 *m*/z, ritonavir: 721.5 → 296.4 *m*/z, sufentanil: 387.2 → 238.4 *m*/z, terfenadine, 472.3 → 436.5 *m*/z, loperamide, 477.4 → 266.0 *m*/z. All analytes were quantified with standard curves (0.05-5000 ng/ml) prepared in the appropriate matrix. The lower limit of detection was 0.5 ng/ml; inter-and intraday CVs were <15% for each of the analytes examined in this study.

Statistical Analysis

Data are reported as mean ± SD for 3 mice per condition. One-way or two-way ANOVA, where appropriate, was used to determine the statistical significance of differences among two or more groups. The level of significance was corrected for multiple comparisons (e.g., Bonferroni test) or adjusted for unequal variance when necessary. In all cases, $p < 0.05$ was considered to be statistically significant.

Results

^{14}C- or ^{3}H-inulin was used as the cerebral capillary space marker (V_{vasc}) to measure BBB physical integrity. V_{vasc} was 1.69±0.10 and 1.68±0.11 mL/100 g in *mdr1a(+/+)* and *mdr1a(-/-)* mice, respectively (two-tailed Student's *t*-test, $p>0.05$). Functional perfusion rate (^{14}C-diazepam Cl_{up}) was 250±41 mL/min/100 g brain in both *mdr1a(+/+)* and *mdr1a(-/-)* mice.

The octanol-water partition coefficients in the unionized state or at pH 7.4 (clogP or $clogD_{7.4}$) for each compound were calculated using Marvin and calculator plugin freeware (www.chemaxon.com, ChemAxon Kft, Budapest, Hungary). The calculated clogP, $clogD_{7.4}$, initial brain uptake clearance Cl_{up} in *mdr1a(+/+)* and *mdr1a(-/-)* mice, PS×$f_{u,brain}$ and the unbound fractions in mouse brain for all compounds determined using equilibrium dialysis or obtained from the literature (25, 26) are summarized in Table 2.1. Based on comparisons of Cl_{up} in *mdr1a(+/+)* and *mdr1a(-/-)* mice, P-gp-mediated efflux decreased the initial rate of brain uptake by up to 14-fold for quinidine in *mdr1a(+/+)* mice. Figure 2.1 demonstrates a sigmoidal relationship between logPS in *mdr1a(-/-)* mice [logPS(-/-)] and $clogD_{7.4}$ in the range of 0-6. Valproic acid and ritonavir were excluded from the regression because the uptake of valproic acid at the BBB is known to be facilitated by a medium-chain fatty acid transporter (27), and ritonavir is extensively bound and sequestrated in the brain capillary endothelium (28). The log of the unbound fraction in mouse brain for these 12 compounds is inversely correlated to $clogD_{7.4}$ (Figure 2.2).

The relationship between PS×$f_{u,brain}$ and clog$D_{7.4}$ is shown in Figure 2.3. The PS×$f_{u,brain}$ was calculated based on the regression in Figures 2.1 and 2.2. This relationship suggests that the rate of blood-to-brain equilibration is not a simple function of lipophilicity, permeability or brain unbound fraction. In addition, the PS×$f_{u,brain}$ varied widely among the compounds studied, with the highest value of 196 for alfentanil and lowest value of 0.05 for colchicine.

The time course of sufentanil and alfentanil brain uptake is presented in Figure 2.4. The apparent distributional volume (V_d) for sufentanil was linear over all of the perfusion times evaluated in both *mdr1a(+/+)* and *mdr1a(-/-)* mice (Figure 2.4A). Alfentanil brain uptake was linear over 20 s in both *mdr1a(+/+)* and *mdr1a(-/-)* mice (Figure 2.4C). The calculated uptake clearance (Cl_{up}) at each time point is shown in Figure 2.4B and 2.4D. Cl_{up} values for sufentanil were constant over the perfusion period and were comparable in *mdr1a(+/+)* and *mdr1a(-/-)* mice (two-way ANOVA, p>0.05). Cl_{up} values for alfentanil were constant for the first 20 s and then decreased significantly at 60 s from ~229 mL/min/100 g to ~102 mL/min/100 g. The Cl_{up} in *mdr1a(-/-)* mice was about 1.4-fold higher than that in *mdr1a(+/+)* mice (two-way ANOVA, p<0.05).

Fexofenadine brain uptake was linear over 120 s in *mdr1a(+/+)* and *mdr1a(-/-)* mice (Figure 2.5A). The initial uptake clearance of fexofenadine, determined with versus without the final washout step, did not differ in either *mdr1a(+/+)* or *mdr1a(-/-)* mice. The brain uptake was 4.4- and 4.6-fold higher in *mdr1a(-/-)* mice than in *mdr1a(+/+)* mice in the absence and presence of final washout step, respectively (Figure 2.5B, two-way ANOVA, p<0.05).

Discussion

Previous studies have suggested that lipophilicity is one of the most important determinants of brain penetration (29, 30), and that logPS in rat brain is related linearly with cLogP (for octanol:water) over 6 orders of magnitude (15, 30). However, the compounds studied previously are, for the most part, non-CNS-therapeutic agents with limited presentation to brain tissue. In the present study, BBB penetration of 12 clinically-used drugs in several therapeutic classes, covering a $clogD_{7.4}$ range of 0-6, was investigated. PS ranged nearly 600-fold, and $f_{u,brain}$ ranged almost 1000-fold, among these compounds. Thus, the selected compound set contained sufficient physicochemical diversity to allow dissection of the contributors to net brain uptake.

The relationship between the logPS in *mdr1a(-/-)* mice [logPS(-/-)] and $clogD_{7.4}$ was generally sigmoidal (Figure 2.1). The logPS for valproic acid fell above this relationship, consistent with the observation that its brain uptake is facilitated by a medium-chain fatty acid transporter (27). Ritonavir brain uptake is slow, although it is highly lipophilic and not ionized at pH 7.4. This slow uptake is explained by the molecular weight of 720.9, and polar surface area of 202 $Å^2$, whereas a molecular weight less than 450 and polar surface area less than 90 $Å^2$ are typically considered to be favorable for brain penetration (31). In addition, capillary depletion techniques have been used to demonstrate that ritonavir is extensively bound to or sequestrated inside the brain capillary endothelium after crossing the luminal membrane, (28). The regression of logPS(-/-) versus clogP showed a similar relationship, with fexofenadine as an outlier. Fexofenadine has a high lipophilicity (logP=5.68) when unionized. However, it is both positively- (due to the tertiary amine group) and negatively- (due to its carboxylic acid group) charged at pH 7.4

($clogD_{7.4}$=0.92), which explains the very low brain penetration of fexofenadine at the BBB, consistent with lipophilicity and ionization state as important factors for brain penetration (29). LogPS(-/-) is limited by permeability for more hydrophilic compounds (cimetidine, fexofenadine and colchicine); and increases with $clogD_{7.4}$ when $clogD_{7.4}$ is in the range of 1-3 (quinidine, sufentanil, quinidine and verapamil). When $clogD_{7.4}$ exceeds a value of 3 (alfentanil, diazepam and terfenadine), BBB permeability does not increase further and becomes limited by capillary perfusion rate.

Interestingly, in the dataset generated for drugs active against CNS targets (CNS^+) in vivo drugs (i.e., diazepam, phenytoin, alfentanil, sufentanil, and valproate), the mean $clogD_{7.4}$ was 2.11, and the mean Cl_{up} values were 93.0 and 101.0 in *mdr1a(+/+)* and *mdr1a(-/-)* mice, respectively. For non-CNS therapeutic (CNS^-) agents (i.e., cimetidine, colchicine, fexofenadine, quinidine, ritonavir, and verapamil), the mean $clogD_{7.4}$ was 1.86, and the mean Cl_{up} values were 6.2 and 34.1 in *mdr1a(+/+)* and *mdr1a(-/-)* mice, respectively. Terfenadine was not included in the CNS^- group because it is known to be a CNS penetrant (23, 32) and it is metabolized rapidly systemically and in the brain (Chapter 3). This comparison clearly shows that CNS^+ drugs tend to have higher Cl_{up} with minimal or no P-gp-mediated efflux. In contrast, CNS^- drugs have lower Cl_{up} in the absence of P-gp, with Cl_{up} decreased further by P-gp-mediated efflux at the BBB. For these P-gp substrates, P-gp-mediated efflux decreased brain uptake by 1.5-, 2.1-, 3.5-, 4.4-, 5.0-, and 13.6-fold for cimetidine, colchicine, ritonavir, fexofenadine, verapamil, and quinidine, respectively. A similar observation, i.e., that the passive permeability and P-gp-mediated efflux could differentiate the CNS and non-CNS drugs, also was observed using *in vitro* cell-based models (33).

No statistical differences were detected between *mdr1a(+/+)* and *mdr1a(-/-)* mice for sufentanil, and alfentanil brain uptake was only 1.4-fold higher in *mdr1a(-/-)* mice than in *mdr1a(+/+)* mice. Sufentanil and alfentanil were reported previously as weak P-gp substrates, with *in vivo* P-gp efflux ratios of 3.0 and 2.8, respectively (34, 35). Previous work also has demonstrated that the P-gp efflux ratio measured *in situ* correlates well with that determined *in vivo*, but with lower apparent P-gp effects at the BBB using the *in situ* brain perfusion technique (19). This result also has been supported by mathematical analysis recently: a smaller ER_B (*in situ* P-gp efflux ratio) compared to ERα (*in vivo* P-gp efflux ratio) is expected for the same experimental system (i.e., same substrate and same animal species) (25). For other P-gp substrates in the present compound set, P-gp-mediated efflux decreased the brain uptake by 1.5- to 13.6-fold; suggesting that the *in situ* brain perfusion technique is a sensitive method to test the efflux transporter kinetics at the BBB.

In the absence of active transport, the rate of brain equilibration is a function of both PS and unbound brain fraction ($f_{u,brain}$), and is directly proportional to the PS×$f_{u,brain}$ product (5, 20). Lipophilic compounds tend to cross the BBB (high PS; Figure 2.1) and bind to brain tissue more extensively (low $f_{u,brain}$; Figure 2.2). The apparent inverse relationship between PS and $f_{u,brain}$ leads to the common assumption that the rate of equilibration across the BBB might be similar for most drugs (36). However, *in vivo* experiments and mathematical modeling indicate that the time to brain equilibrium varied widely among compounds (20). A mathematical simulation based on the sigmoidal relationship between PS and $clogD_{7.4}$ and the linear relationship between $f_{u,brain}$ and $clogD_{7.4}$ showed the trend of the rate to brain equilibrium (PS×$f_{u,brain}$) increases with the lipophilicity of compounds

up to $clogD_{7.4}$ of 3, and then decreases after the compounds become too lipophilic (Figure 2.3). The compounds in the $clogD_{7.4}$ range of 2-3 evidenced the most rapid brain penetration. Alfentanil reached an equilibrium condition about 200-fold faster than sufentanil, and about 2000-fold faster than fexofenadine and ritonavir. This difference is consistent with the clinically-observed onset of alfentanil anaesthetic effect, which is more rapid than that observed for sufentanil (22, 34). In contrast, ritonavir brain uptake has been shown previously to be quite slow, failing to reach equilibrium within 30 min during perfusion in guinea pigs (28).

The *in situ* brain perfusion technique measures the initial rate of brain uptake during a time period when there is no significant back flux from the brain to the perfusate. Care should be taken when a single-time-point method is used with this technique. In many cases, a single time-point at 30- or 60-s can provide an accurate estimate of Cl_{up} (17, 37). However, a curvilinear relationship between net brain uptake and time has been demonstrated for some compounds such as iodoantipyrine (16) that equilibrate rapidly (less than 60 s) across the BBB. In the present study, a similar result was observed for alfentanil, which shares some physicochemical characteristics with iodoantipyrine (high PS and high $f_{u,brain}$). Alfentanil achieved equilibrium in 20 s in both *mdr1a(+/+)* and *mdr1a(-/-)* mice. By 60 s, V_d had reached a plateau due to significant back flux from the brain to the perfusate. The calculated Cl_{up} values therefore decreased about 50-60% at 60 s compared to other time points. Only Cl_{up} calculated based on unidirectional flux from perfusate to brain will reflect the actual rate of alfentanil brain uptake (Figure 2.4C and 2.4D). Sufentanil Cl_{up} was ~8-fold lower than that for alfentanil, corresponding to a lower $clogD_{7.4}$ value. Sufentanil binds to brain tissue ~10-fold more extensively than alfentanil,

limiting the back-flux of sufentanil from the brain to the perfusate during perfusion (essentially creating a sink condition with respect to unbound substrate in brain tissue available for back-diffusion). Sufentanil brain uptake therefore is linear over the entire 60 s perfusion, and Cl_{up} is time-independent.

Fexofenadine brain uptake was unidirectional over 120 s (Figure 2.5). Fexofenadine is a very low-permeability compound and has high nonspecific binding in brain tissue. Combined with a 15-s drug-free saline washout at the end of the perfusion, the single-time-point method for calculating Cl_{up} yielded results similar to those obtained from the three time-point linear phase slope method. Because the variability in vascular volume might appreciably affect the Cl_{up} calculation, particularly for compounds with poor BBB permeability, the washout step increased the accuracy of measurement of the brain permeability when using a single-time-point method (14, 38).

In silico models have become more common in the early phase of the drug discovery process to predict the BBB penetration of new chemical entities and drug candidates. The predictive accuracy of the models depends on the quality of the experimentally measured data and the chemical space covered in the selected molecules. A mechanistic understanding of the generated data, and an expanded high-quality database, are very important for *in silico* model development and validation, and ultimately aid and accelerate the drug design process for the treatment of CNS diseases. The *in situ* brain perfusion technique is a useful method to determine the BBB permeability. However, caution needs to be taken when using a single-time-point method. The time point should sit in the initial linear (unidirectional) phase of brain uptake and a final washout step might increase the accuracy of measuring brain permeability for poorly-permeable

compounds. Brain penetration is a balance between the permeability and nonspecific brain tissue binding. Other variables, i.e., polar surface area, molecular weight, the number of hydrogen bonds, and P-gp-mediated efflux also contribute to measurements of brain penetration. Highly lipophilic compounds tend to have high permeability and high brain tissue binding, which causes the PS×$f_{u,brain}$ product to vary across a wide range. This variability is apparent when comparing a compound such as alfentanil, which reaches equilibrium very quickly, to a compound such as fexofenadine, which reaches equilibrium very slowly.

References

1. R. P. Meyer, M. Gehlhaus, R. Knoth, and B. Volk. Expression and function of cytochrome p450 in brain drug metabolism. *Curr Drug Metab* **8**: 297-306 (2007).

2. D. J. Begley. Understanding and circumventing the blood-brain barrier. *Acta Paediatr Suppl* **92**: 83-91 (2003).

3. G. Miller. Drug targeting. Breaking down barriers. *Science* **297**: 1116-8 (2002).

4. A. H. Schinkel. P-Glycoprotein, a gatekeeper in the blood-brain barrier. *Adv Drug Deliv Rev* **36**: 179-194 (1999).

5. X. Liuand C. Chen. Strategies to optimize brain penetration in drug discovery. *Curr Opin Drug Discov Devel* **8**: 505-12 (2005).

6. J. D. Fenstermacher, R. G. Blasberg, and C. S. Patlak. Methods for Quantifying the transport of drugs across brain barrier systems. *Pharmacol Ther* **14**: 217-48 (1981).

7. J. C. Kalvass and T. S. Maurer. Influence of nonspecific brain and plasma binding on CNS exposure: implications for rational drug discovery. *Biopharm Drug Dispos* **23**: 327-38 (2002).

8. J. C. Kalvass, T. S. Maurer, and G. M. Pollack. Use of plasma and brain unbound fractions to assess the extent of brain distribution of 34 drugs: comparison of unbound concentration ratios to in vivo p-glycoprotein efflux ratios. *Drug Metab Dispos* **35**: 660-6 (2007).

9. J. C. Kalvass, C. L. Graff, and G. M. Pollack. Use of loperamide as a phenotypic probe of mdr1a status in CF-1 mice. *Pharm Res* **21**: 1867-70 (2004).

10. A. H. Schinkel, J. J. Smit, O. van Tellingen, J. H. Beijnen, E. Wagenaar, L. van Deemter, C. A. Mol, M. A. van der Valk, E. C. Robanus-Maandag, H. P. te Riele, and et al. Disruption of the mouse mdr1a P-glycoprotein gene leads to a deficiency in the blood-brain barrier and to increased sensitivity to drugs. *Cell* **77**: 491-502 (1994).

11. W. M. Pardridge. Log(BB), PS products and in silico models of drug brain penetration. *Drug Discov Today* **9**: 392-3 (2004).

12. I. Martin. Prediction of blood-brain barrier penetration: are we missing the point? *Drug Discov Today* **9**: 161-2 (2004).

13. X. Liu, M. Tu, R. S. Kelly, C. Chen, and B. J. Smith. Development of a computational approach to predict blood-brain barrier permeability. *Drug Metab Dispos* **32**: 132-9 (2004).

14. Q. R. Smith. Brain perfusion systems for studies of drug uptake and metabolism in the central nervous system. In Ronald T. Borchardt et al. (ed), *Models for assessing drug absorption and metabolism* (Ronald T. Borchardt et al., ed), Plenum Press, New York, 1996.

15. Y. Takasato, S. I. Rapoport, and Q. R. Smith. An in situ brain perfusion technique to study cerebrovascular transport in the rat. *Am J Physiol* **247**: H484-93 (1984).

16. H. Murakami, H. Takanaga, H. Matsuo, H. Ohtani, and Y. Sawada. Comparison of blood-brain barrier permeability in mice and rats using in situ brain perfusion technique. *Am J Physiol Heart Circ Physiol* **279**: H1022-8 (2000).

17. C. Dagenais, C. L. Graff, and G. M. Pollack. Variable modulation of opioid brain uptake by P-glycoprotein in mice. *Biochem Pharmacol* **67**: 269-76 (2004).

18. C. Dagenais, C. Rousselle, G. M. Pollack, and J. M. Scherrmann. Development of an in situ mouse brain perfusion model and its application to mdr1a P-glycoprotein-deficient mice. *J Cereb Blood Flow Metab* **20**: 381-6 (2000).

19. C. Dagenais, J. Zong, J. Ducharme, and G. M. Pollack. Effect of mdr1a P-glycoprotein gene disruption, gender, and substrate concentration on brain uptake of selected compounds. *Pharm Res* **18**: 957-63 (2001).

20. X. Liu, B. J. Smith, C. Chen, E. Callegari, S. L. Becker, X. Chen, J. Cianfrogna, A. C. Doran, S. D. Doran, J. P. Gibbs, N. Hosea, J. Liu, F. R. Nelson, M. A. Szewc, and J. Van Deusen. Use of a physiologically based pharmacokinetic model to study the time to reach brain equilibrium: an experimental analysis of the role of blood-brain barrier permeability, plasma protein binding, and brain tissue binding. *J Pharmacol Exp Ther* **313**: 1254-62 (2005).

21. W. M. Pardridge. The blood-brain barrier: bottleneck in brain drug development. *NeuroRx* **2**: 3-14 (2005).

22. J. Lotsch. Pharmacokinetic-pharmacodynamic modeling of opioids. *J Pain Symptom Manage* **29**: S90-103 (2005).

23. T. Obradovic, G. G. Dobson, T. Shingaki, T. Kungu, and I. J. Hidalgo. Assessment of the first and second generation antihistamines brain penetration and role of P-glycoprotein. *Pharm Res* **24**: 318-27 (2007).

24. H. Tahara, H. Kusuhara, E. Fuse, and Y. Sugiyama. P-glycoprotein plays a major role in the efflux of fexofenadine in the small intestine and blood-brain barrier, but only a limited role in its biliary excretion. *Drug Metab Dispos* **33**: 963-8 (2005).

25. K. D. Adkisonand D. D. Shen. Uptake of valproic acid into rat brain is mediated by a medium-chain fatty acid transporter. *J Pharmacol Exp Ther* **276**: 1189-200 (1996).

26. C. Anthonypillai, R. N. Sanderson, J. E. Gibbs, and S. A. Thomas. The distribution of the HIV protease inhibitor, ritonavir, to the brain, cerebrospinal fluid, and choroid plexuses of the guinea pig. *J Pharmacol Exp Ther* **308**: 912-20 (2004).

27. J. C. Kalvass and G. M. Pollack. Kinetic considerations for the quantitative assessment of efflux activity and inhibition: implications for understanding and predicting the effects of efflux inhibition. *Pharm Res* **24**: 265-76 (2007).

28. T. S. Maurer, D. B. Debartolo, D. A. Tess, and D. O. Scott. Relationship between exposure and nonspecific binding of thirty-three central nervous system drugs in mice. *Drug Metab Dispos* **33**: 175-81 (2005).

29. B. B. Brodie, H. Kurz, and L. S. Schanker. The importance of dissociaton constant and lipid-solubility in influencing the passage of drugs into the cerebrospinal fluid. *J Pharmacol Exp Ther* **130**: 20-5 (1960).

30. W. H. Oldendorf. Lipid solubility and drug penetration of the blood brain barrier. *Proc Soc Exp Biol Med* **147**: 813-5 (1974).

31. H. van de Waterbeemd, G. Camenisch, G. Folkers, J. R. Chretien, and O. A. Raevsky. Estimation of blood-brain barrier crossing of drugs using molecular size and shape, and H-bonding descriptors. *J Drug Target* **6**: 151-65 (1998).

32. K. M. Mahar Doan, S. A. Wring, L. J. Shampine, K. H. Jordan, J. P. Bishop, J. Kratz, E. Yang, C. J. Serabjit-Singh, K. K. Adkison, and J. W. Polli. Steady-state brain concentrations of antihistamines in rats: interplay of membrane permeability, P-glycoprotein efflux and plasma protein binding. *Pharmacology* **72**: 92-8 (2004).

33. K. M. Mahar Doan, J. E. Humphreys, L. O. Webster, S. A. Wring, L. J. Shampine, C. J. Serabjit-Singh, K. K. Adkison, and J. W. Polli. Passive permeability and P-glycoprotein-mediated efflux differentiate central nervous system (CNS) and non-CNS marketed drugs. *J Pharmacol Exp Ther* **303**: 1029-37 (2002).

34. J. C. Kalvass, E. R. Olson, M. P. Cassidy, D. E. Selley, and G. M. Pollack. Pharmacokinetics and Pharmacodynamics of Seven Opioids in P-gp-Competent Mice: Assessment of Unbound Brain EC50 and Correlation of In Vitro, Preclinical, and Clinical Data. *J Pharmacol Exp Ther* (2007).

35. J. C. Kalvass, E. R. Olson, and G. M. Pollack. Pharmacokinetics and pharmacodynamics of alfentanil in P-glycoprotein-competent and P-glycoprotein-deficient mice: P-glycoprotein efflux alters alfentanil brain disposition and antinociception. *Drug Metab Dispos* **35**: 455-9 (2007).

36. M. Hammarlund-Udenaes, L. K. Paalzow, and E. C. de Lange. Drug equilibration across the blood-brain barrier--pharmacokinetic considerations based on the microdialysis method. *Pharm Res* **14**: 128-34 (1997).

37. S. G. Summerfield, K. Read, D. J. Begley, T. Obradovic, I. J. Hidalgo, S. Coggon, A. V. Lewis, R. A. Porter, and P. Jeffrey. Central nervous system drug disposition: the relationship between in situ brain permeability and brain free fraction. *J Pharmacol Exp Ther* **322**: 205-13 (2007).

38. R. Deaneand M. W. Bradbury. Transport of lead-203 at the blood-brain barrier during short cerebrovascular perfusion with saline in the rat. *J Neurochem* **54**: 905-14 (1990).

Table 2.1: Calculated clogP, $clogD_{7.4}$, uptake clearance in *mdr1a(+/+)* and *mdr1a(-/-)* mice, and brain unbound fraction for selected compounds.

Name	**clogP**	**$clogD_{7.4}$**	**Cl_{up}(+/+)**	**Cl_{up}(-/-)**	**PS× $f_{u,brain}$**	**$f_{u,brain}$ (reference)**
Alfentanil	3.55	3.20	194 ± 38	229 ± 46	196	0.32 (27)
Colchicine	1.08	1.08	0.9 ± 0.1	1.9 ± 0.1	0.05	0.024
Cimetidine	0.24	0.12	0.7 ± 0.2	1.1 ± 0.4	0.6	0.53 (27)
Diazepam	3.01	3.01	250 ± 41	250 ± 41	12.5	0.05 (28)
Fexofenadine	5.68	0.92	0.3 ± 0.1	1.3 ± 0.4	0.1	0.077 (27)
Phenytoin	2.28	2.27	33.4 ± 1.2	34.7 ± 9.9	3.1	0.082
Quinidine	2.32	1.46	3.4 ± 0.4	54.1 ± 12.2	1.6	0.037 (27)
Ritonavir	5.04	5.04	2.3 ± 0.7	8.0 ± 2.7	0.1	0.0106 (27)
Sufentanil	3.17	1.69	34.0 ± 6.6	29.5 ± 9.0	1.1	0.034 (27)
Terfenadine	6.45	4.82	174 ± 52	202 ± 85	0.5	0.0011
Valproate	2.61	0.37	24.3 ± 0.7	18.1 ± 4.5	18.8	1.0
Verapamil	4.30	2.56	31.5 ± 3.0	137 ± 23	7.7	0.033 (27)

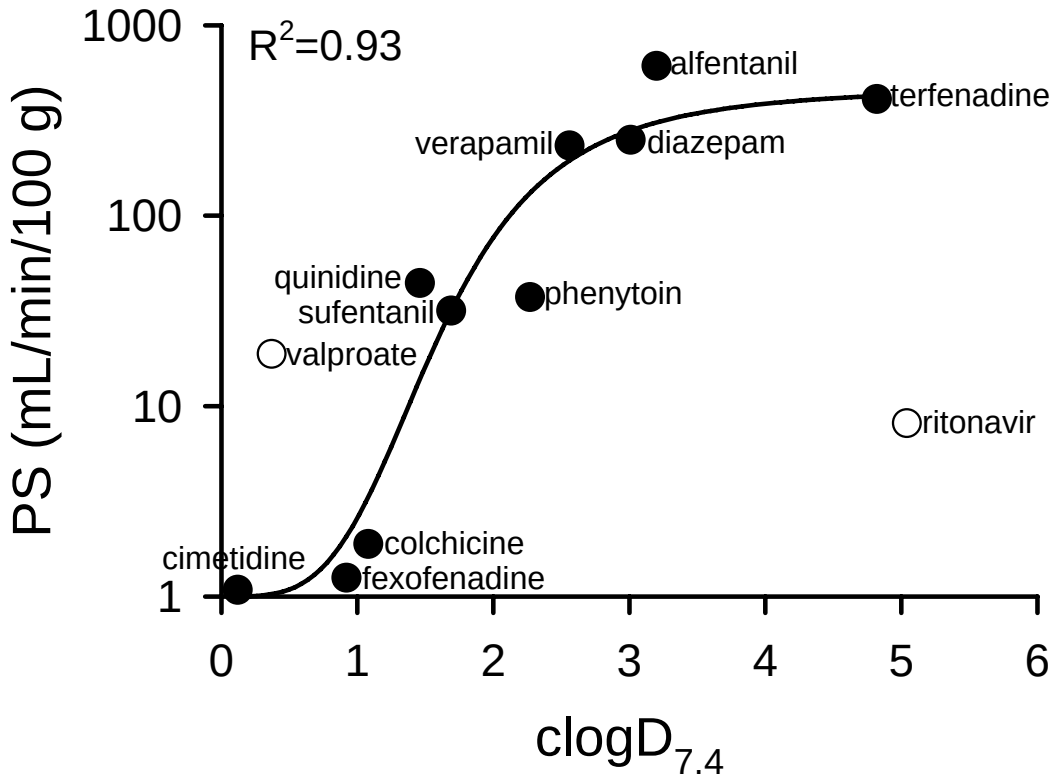

Figure 2.1: Relationship between PS and $clogD_{7.4}$.

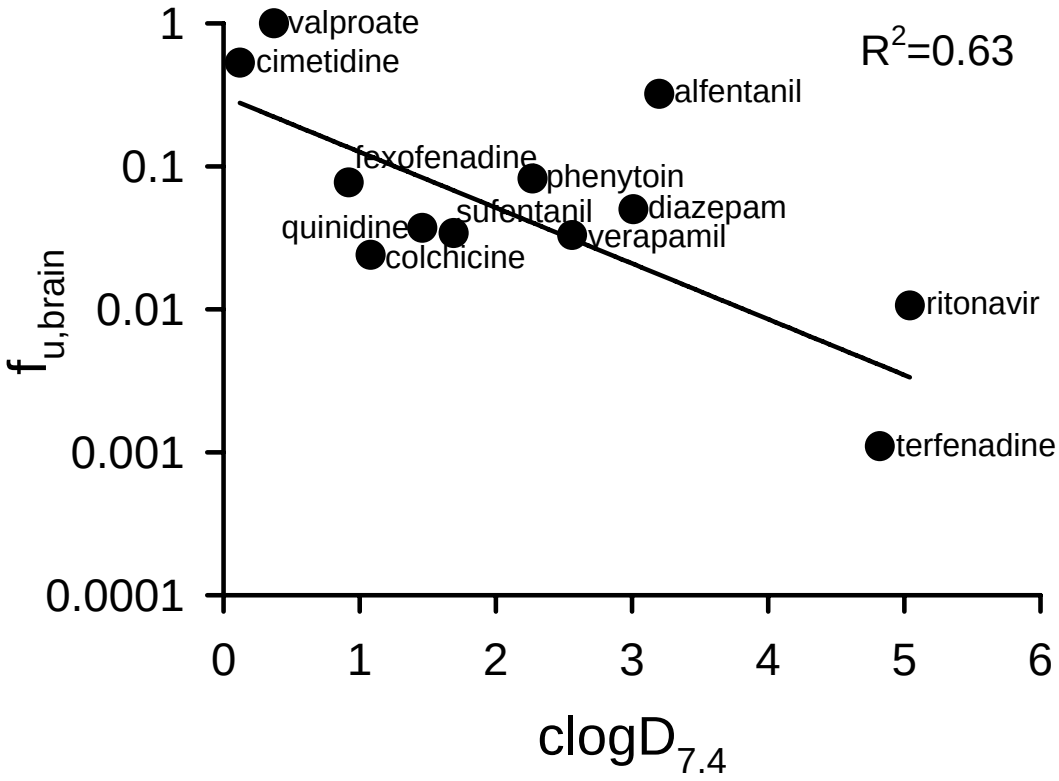

Figure 2.2: Relationship between brain unbound fraction $f_{u,brain}$ and clogD$_{7.4}$.

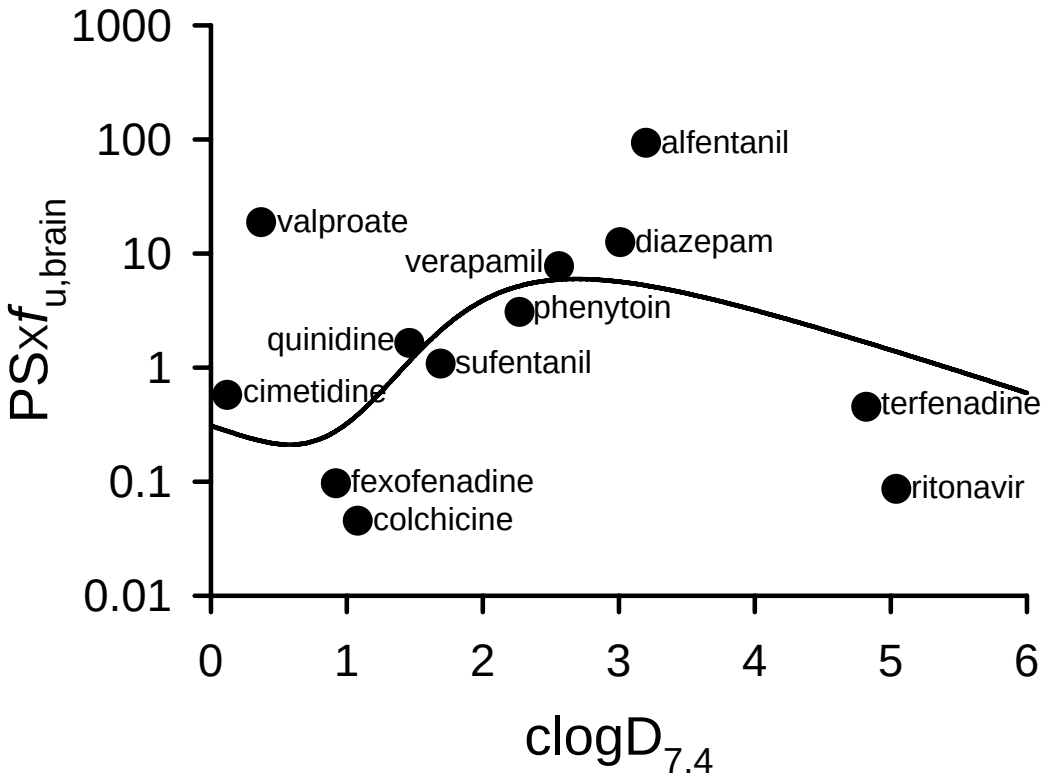

Figure 2.3: Relationship between PS×$f_{u,brain}$ and clogD$_{7.4}$.

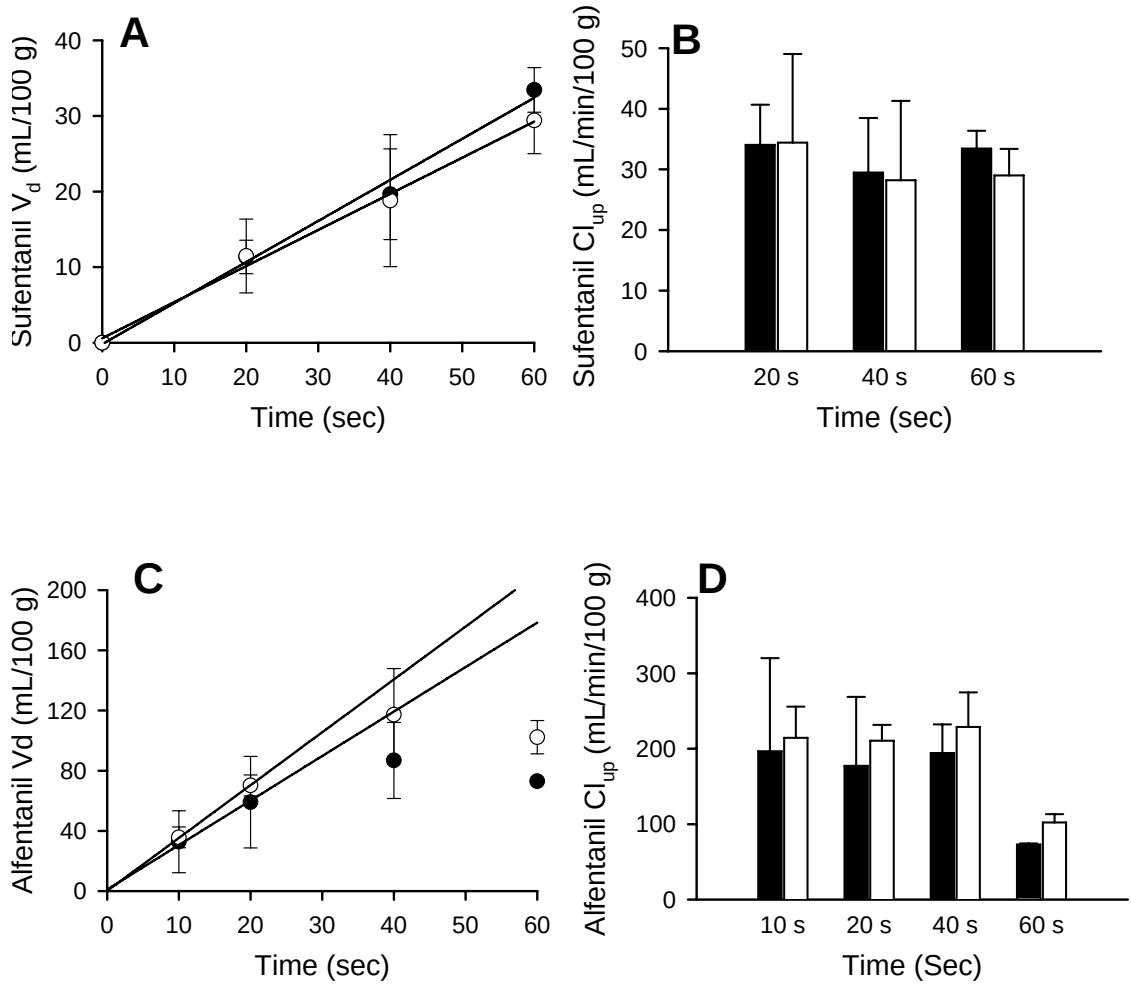

Figure 2.4: The time course of apparent brain distributional volume of (A) sufentanil and (C) alfentanil, and the initial brain uptake clearance of (B) sufentanil and (D) alfentanil, in *mdr1a(+/+)* (solid symbol) and *mdr1a(-/-)* (open symbol) mice following 60 s perfusion at 2.5 mL/min (n=3).

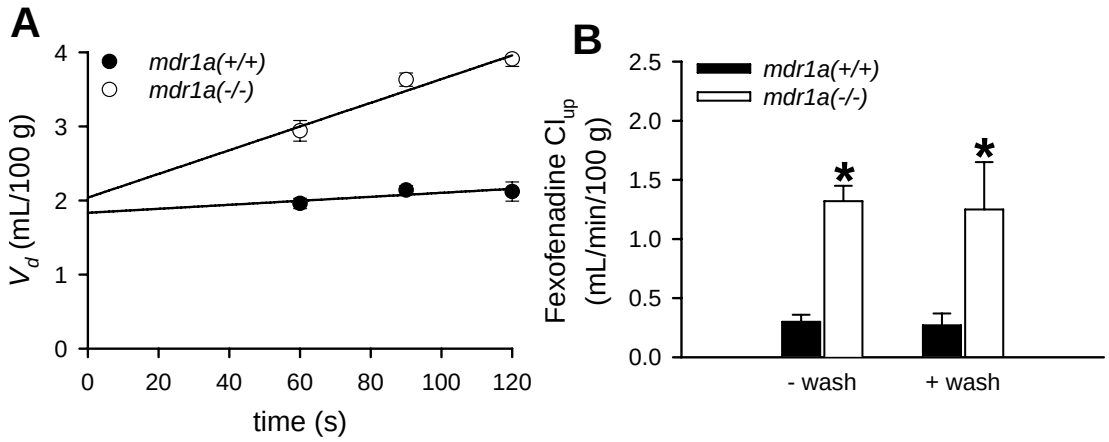

Figure 2.5: (A), The apparent distributional volume at 60-, 90-, and 120-s of perfusion for fexofenadine in *mdr1a(+/+)* (solid circle) and *mdr1a(-/-)* (open circle) mice; and **(B)**, initial brain uptake clearance of fexofenadine in *mdr1a(+/+)* (solid bar) and *mdr1a(-/-)* (open bar) mice in the absence or presence of additional 15-s drug-free saline washout following brain perfusion at 2.5 mL/min for 60 s. Fexofenadine brain uptake increased approximately 5-fold in *mdr1a(-/-)* mice than in *mdr1a(+/+)* mice.

CHAPTER 3

FEXOFENADINE BRAIN EXPOSURE AND THE INFLUENCE OF BLOOD-BRAIN BARRIER P-GLYCOPROTEIN FOLLOWING FEXOFENADINE AND TERFENADINE ADMINISTRATION

This chapter will be submitted for publication in Drug Metabolism and Disposition and is presented in the style of that journal.

Abstract

P-glycoprotein (P-gp) plays an important role in determining net brain uptake of fexofenadine. Initial *in vivo* experiments with 24-hr subcutaneous osmotic minipump administration demonstrated that fexofenadine brain penetration was 48-fold higher in *mdr1a(-/-)* mice than in *mdr1a(+/+)* mice. In constrast, the P-gp efflux ratio at the blood-brain barrier (BBB) for fexofenadine was only ~4 using an *in situ* brain perfusion technique. Pharmacokinetic modeling based on the experimental results indicated that the apparent fexofenadine P-gp efflux ratio is time-dependent due to low passive permeability at the BBB. Fexofenadine brain penetration following terfenadine administration was ~25-27-fold higher than following fexofenadine administration in both *mdr1a(+/+)* and *mdr1a(-/-)* mice, consistent with terfenadine metabolism to fexofenadine in murine brain tissue. Fexofenadine formation rate following terfenadine *in situ* brain perfusion was comparable to that in a 2-hr brain tissue homogenate in vitro incubation. Fexofenadine formation rate increased ~5-fold during a 2-hr brain tissue homogenate incubation with hydroxyl-terfenadine, suggesting that the hydroxylation of terfenadine is the rate-limiting step in fexofenadine formation. Moreover, regional brain metabolism appears to be an important factor in terfenadine brain disposition, and consequently fexofenadine brain exposure. Taken together, these results indicate that the fexofenadine BBB P-gp efflux ratio has been underestimated previously due to lack of complete equilibration of fexofenadine across the blood-brain interface under typical experimental paradigms.

Introduction

The blood-brain barrier (BBB) and blood-cerebrospinal fluid barrier (BCSFB) are the major interfaces and barriers between the central nervous system (CNS) and the peripheral circulation. The BBB and BCSFB are formed by a continuous layer of brain capillary endothelial cells (BBB) or epithelial cells that line the choroid plexus (BCSFB). The highly-developed tight junctions and expression of numerous efflux transporters and metabolizing enzymes limit brain penetration of many endogenous compounds and therapeutic agents (Begley, 2003; Graff and Pollack, 2004).

Brain penetration can be beneficial or detrimental depending on the target site of therapy and the potential for untoward side effects. Adequate exposure in the brain is essential for the treatment of cerebral diseases. However, brain exposure ideally would be minimized for compounds intended to treat peripheral disorders. BBB permeability, a primary determinant of substrate exposure in brain tissue, is influenced by many physicochemical properties such as molecular weight, pKa, lipophilicity, polar surface area, and the number of hydrogen bonds (Brodie et al., 1960; Liu et al., 2004). The extent of brain exposure, and thus the CNS pharmacologic or toxic effect, is determined by passive permeability, plasma and brain tissue binding, uptake or efflux transport activity, CSF bulk flow and biotransformation in the CNS (Fenstermacher et al., 1981; Schinkel et al., 1994; Kalvass and Maurer, 2002; Liu and Chen, 2005; Kalvass et al., 2007a). Accurate prediction of CNS penetration is difficult because of these complex mechanisms and parameters.

Recently, non-specific protein binding (i.e., capacity-limited binding to proteins other than the target receptor) in brain tissue and plasma was first used to predict *in vivo* CNS drug penetration (Kalvass and Maurer, 2002). These predictions were based in part on the assumption that, when compounds distribute between brain and blood solely by passive diffusion, the unbound brain and plasma concentrations are equal at distribution equilibrium. Under these conditions, the brain-to-plasma concentration ratio (brain partition coefficient; $K_{p,brain}$) is simply a function of the relative plasma and tissue unbound fractions $K_{p,brain} = f_{u,plasma} / f_{u,brain}$. For many compounds that are subject to P-gp mediated efflux at the BBB, brain penetration has been predicted successfully based on this approach as modified to account for the P-gp-mediated efflux activity (Summerfield et al., 2006; Kalvass et al., 2007a).

Non-sedating antihistamines represent an interesting class of compounds because the lack of a sedative effect is due primarily to exclusion from the brain at the blood-brain interface. Fexofenadine, for example, has been identified as a substrate of P-gp in Caco-2 cells and MDR1 overexpressing LLC-PK1 cells (Cvetkovic et al., 1999; Petri et al., 2004). P-gp subsequently was demonstrated to decrease intestinal absorption and brain exposure of fexofenadine by comparing wild-type mice to *mdr1a/1b(-/-)* animals (Tahara et al., 2005).

The extent of fexofenadine brain penetration in normal rats and mice is minimal (Mahar Doan et al., 2004; Tahara et al., 2005). In contrast, terfenadine enters the brain rapidly (Mahar Doan et al., 2004; Obradovic et al., 2007). Terfenadine is metabolized to hydroxyl-terfenadine and then to the active metabolite fexofenadine by hepatic CYP3A4

in human (Ling et al., 1995; Markham and Wagstaff, 1998). Metabolic enzymes such as P450s are also expressed in human and rodent brain (Strobel et al., 2001; Miksys and Tyndale, 2002; Meyer et al., 2007). Brain P450s play an important role in local metabolism of endogenous compounds and xenobiotics, though brain P450s is only about 1-10% of liver content and not likely to influence the overall metabolism of the body. Mouse CYP3A11 and CYP3A13, the counterpart of human CYP3A4, were responsible for 6β-hydroxylation of testosterone in the brain and were induced by antiepileptic drug phenytoin treatment (Hagemeyer et al., 2003; Meyer et al., 2006). In the current study, the brain metabolism of terfenadine to fexofenadine was examined.

Despite the ability to predict brain exposure of many compounds, the P-gp effect coupled with relative protein binding in blood and brain tissue can explain only partially the impaired brain penetration of fexofenadine and cetirizine (Kalvass et al., 2007a), two nonsedating antihistamines with poor permeability at the BBB. Fexofenadine brain penetration is ~35-fold overestimated based on the plasma-to-brain unbound fraction ratio assumption; this magnitude of overestimation cannot be explained by the ~3-fold P-gp effect at the BBB that has been reported (Cvetkovic et al., 1999; Tahara et al., 2005). Efflux protein(s) other than P-gp that may serve as barrier transport systems at the blood-brain interface have been proposed (Kalvass et al., 2007a). However, the functional efficiency and biologic significance of other BBB efflux transporters remain unclear, and no evidence is available to suggest an interaction between fexofenadine and other efflux transporters in brain capillary endothelium. The purpose of this study, therefore, was to understand the underlying mechanism(s) governing fexofenadine exposure in brain tissue, and to re-examine P-gp mediated fexofenadine efflux at the BBB. The central hypothesis

underlying this effort is that studies to date have underestimated the actual BBB P-gp effect on fexofenadine brain uptake.

In the current study, the rate and extent of fexofenadine brain uptake and P-gp-mediated efflux activity at the BBB was determined using an *in situ* brain perfusion technique and subcutaneous osmotic minipump containing fexofenadine or terfenadine in *mdr1a(+/+)* and *mdr1a(-/-)* mice, continuously release drug over 24 to 168 hours. A pharmacokinetic model was used to simulate the time-dependence of P-gp efflux ratio for fexofenadine and other compounds that have different passive permeability at the BBB. In addition, the influence of local metabolism on terfenadine brain disposition and consequent fexofenadine brain exposure was investigated.

Materials and Methods

Adult CF-1 *mdr1a(+/+)* mice and their natural mutant *mdr1a (-/-)* counterparts (30-40 g, 6-8 weeks of age) were purchased from Charles River Laboratories (Wilmington, MA). All mice were maintained on a 12-h light/dark cycle with access to water and food *ad libitum*. All experimental procedures were performed under full anesthesia induced with ketamine/xylazine (100/10 mg/kg, i.p.). All procedures were approved by the Institutional Animal Care and Use Committee at the University of North Carolina at Chapel Hill and were conducted in accordance with "Principles with Laboratory Animal Care" (NIH publication No. 85-23, revised in 1985).

^{14}C-diazepam (56.0 mCi/mmol) was purchased from Amersham Biosciences (Buckinghamshire, UK). ^{3}H-inulin (180.0 mCi/g) was purchased from PerkinElmer (Waltham, MA). Terfenadine, fexofenadine hydrochloride and loperamide were purchased from Sigma-Aldrich (St. Louis, MO). All of the other chemicals were commercially available and of reagent grade.

In Situ Mouse Brain Perfusion

The details of the *in situ* mouse brain perfusion have been described elsewhere (Dagenais et al., 2000a). Briefly, mice were anesthetized with ketamine/xylazine (100/10 mg/kg, i.p.). The perfusion buffer (Krebs-bicarbonate buffer, with 9 mM of D-glucose, pH 7.4) was oxygenated with 95% O_2 and 5% CO_2 and maintained at 37°C. ^{14}C-diazepam and ^{3}H-inulin were used as blood flow rate and vascular space markers, respectively. Fexofenadine or terfenadine at a final concentration of 2 μM was added to the perfusate. The right common carotid artery was cannulated with PE-10 tubing (Braintree Scientific

Inc., Braintree, MA) following ligation of the external carotid artery. The cardiac ventricles were severed immediately before perfusion at 2.5 mL/min for 60 s via a syringe pump (Harvard Apparatus, Holliston, MA). The experiment was terminated by decapitation And the right cerebral hemisphere was collected. Aliquots of perfusate were collected through the syringe and tubing for determination of substrate concentrations in perfusate. The perfusate and brain samples were stored at -20°C until analysis by HPLC/MS/MS. The radioactive brain samples were digested with 0.7 mL of Solvable® ((Packard, Boston, MA) at 50°C overnight. Five mL of UltimaGold® scintillation cocktail (PerkinElmer, Wellesley, MA) was added and vortex-mixed. Total radioactivity (^{3}H and/or ^{14}C) was determined in a Packard Tri-carb TR 1900 liquid scintillation analyzer (Packard, Boston, MA).

Parameters related to the *in situ* brain perfusion, i.e., the cerebral vascular volume (mL/100 g brain), was calculated using equation:

$$V_{vasc} = \frac{X_{inulin}}{C_{inulin}}.$$

the initial brain uptake clearance (Cl_{up}, mL/min/100 g brain) was calculated as:

$$Cl_{up} = \frac{X_{brain}/T}{C_{perf}},$$

and the apparent distributional volume (V_d, mL/100 g brain) was calculated as:

$$V_d = \frac{X_{brain}}{C_{perf}}$$

where the amount of substrate in brain X_{brain} was corrected for blood vessel contamination by subtraction of vascular volume or a final 15-s washout with drug-free saline. The permeability surface product (PS) values were calculated based on Crone-Renkin equation (Takasato et al., 1984):

$$PS = -F_{pf} \times \ln(1 - Cl_{up}/F_{pf}) .$$

F_{pf} is the perfusion flow rate measured using ^{14}C-diazepam as the flow rate marker.

Mathematical Modeling and Simulations

The time to equilibrium of brain penetration is dependent on the passive permeability, brain unbound fraction and BBB P-gp-mediated efflux (Liu et al., 2005; Kalvass et al., 2007b). The time course of P-gp efflux ratio following continuous infusion was simulated based on a similar model structure with additional P-gp-mediated efflux activity. As the structure shown in Figure 3.1, the model contains one central (blood) compartment and one brain compartment; V_c and V_{br} are the physiologic blood and brain volumes, respectively. Cl_d represents the passive permeability between blood and brain compartments, Cl_{eff} is the P-gp-mediated efflux clearance, Cl is the systemic clearance, and $f_{u,p}$ and $f_{u,br}$ are plasma and brain unbound fraction, respectively. Modeling was based in part on the assumption that only unbound drug is able to cross the BBB. The passive permeability Cl_d for fexofenadine is very low relative to the blood flow rate, and therefore was assumed to be equal to the permeability coefficient PS determined by the *in situ* brain perfusion technique. Numerical values for these parameters were assigned as follows: V_p=49 mL/kg, V_{br}=17 mL/kg (Brown et al., 1997), Cl=30 mL/min/kg (Tahara et al., 2005), $f_{u,p}$ =0.35 and $f_{u,br}$ =0.077 (Kalvass et al., 2007a), The infusion rate k0 was set

to a value of 1 (unit dose). Fexofenadine PS=0.22 mL/min/100 g brain based on the *in situ* brain perfusion data. Three pairs of Cl_d and Cl_{eff} were assigned: Cl_{d1}=0.022, Cl_{d2}=0.22, Cl_{d3}=2.22 mL/min/kg; the corresponding Cl_{eff1}=0.54; Cl_{eff2}=5.39, Cl_{eff3}=53.90 mL/min/kg for P-gp-competent mice assuming a steady-state P-gp efflux ratio of 25. Cl_{eff}=0 for all P-gp deficient mice. The P-gp efflux ratio was calculated as the ratio of brain partition coefficient in P-gp deficient mice to P-gp competent mice. The differential equations used for simulations were:

$$V_c \times \frac{dC}{dt} = k0 - (Cl + Cld) \times C \times f_{u,p} + (Cld + Cleff) \times C_{br} \times f_{u,br}$$

$$V_{br} \times \frac{dC_{br}}{dt} = Cld \times C \times f_{u,p} - (Cld + Cleff) \times C_{br} \times f_{u,br}$$

where C and C_{br} are the total plasma and brain concentrations, respectively.

In vivo Osmotic Minipump Studies

CF-1 mice (n=3 per group) were anesthetized with ketamine/xylazine (100/10 mg/kg, i.p.). Alzet® model # 2001 osmotic minipump (release rate 1 µl/h over one week, Alza Corporation, Palo Alto, CA) was selected. Initial experiments were directed at determining fexofenadine brain penetration and P-gp efflux ratio following fexofenadine and terfenadine administration. To produce similar plasma concentrations of fexofenadine for comparison, pumps were filled with fexofenadine hydrochloride (80 µg/pump) or terfenadine (900 µg/pump) dissolved in 50% DMSO (200 µl/pump) and placed subcutaneously in the back of *mdr1a(+/+)* and *mdr1a(-/-)* mice. The experiment was terminated by decapitation 24 hr following implantation. Additional experiments were performed to study the time course of fexofenadine P-gp efflux ratio at the BBB. To

accomplish this goal, additional groups of *mdr1a(+/+)* and *mdr1a(-/-)* mice received fexofenadine hydrochloride (872 μg/pump) to produce plasma concentrations similar to those reported by Tahara et al. (2005). The mice were sacrificed at 24, 72 and 168 hr post-implantation. Trunk blood was collected in heparinized 1.5-mL microcentrifuge tubes, and plasma was harvested following centrifugation at 3,000 rpm for 5 min. The plasma and brain samples were stored at -20°C until analysis by HPLC/MS/MS. The contribution of residual blood in the brain tissue to the brain partition coefficient was corrected by subtracting 1.8% from the calculated brain-to-plasma concentration ratio (Brown et al., 1997; Dagenais et al., 2000a).

Mouse Brain Metabolism

Terfenadine brain metabolism was determined under two different experimental conditions. First, *mdr1a(+/+)* and *mdr1a(-/-)* mouse brain hemispheres were perfused with 2 μM terfenadine for 1 min (n=3, with a procedure identical to that described in "*In situ* Mouse Brain Perfusion"). The concentrations of fexofenadine formed in the perfused brain hemisphere were determined by HPLC/MS/MS. Second, fresh *mdr1a(+/+)* mouse brains were harvested, washed with 0.15 M KCl, and homogenized in two volumes of phosphate buffer (pH 7.4, 1.15% KCl). Terfenadine or hydroxyl-terfenadine at a final concentration of 200 nM was incubated with brain homogenate (10 mg/mL) in the presence of potassium phosphate buffer (0.1 M, pH 7.4) and magnesium chloride (5 mM). The reaction was initiated by addition of freshly prepared NADPH (2 mM) (Ling et al., 1995; Holleran et al., 2004). After 2 hr incubation at 37 ^{o}C in shaking water bath, the reaction was terminated by addition of ice-cold methanol to precipitate protein. The samples were centrifuged at 10,000 g for 10 min. The supernatant was transferred to a

fresh tube and evaporated under a stream of dry nitrogen. The residue was reconstituted with 50% methanol in water, and an internal standard was added. The formation of fexofenadine from terfenadine or hydroxyl-terfenadine was determined by HPLC/MS/MS.

Sample Preparation and Quantitation

The brain tissue was homogenized with addition of two volumes of distilled water following brief probe sonication. The perfusate was diluted with two volumes of methanol. A 25-µl aliquot of plasma or brain homogenate was transferred to an HPLC vial, and protein was precipitated with 100 µl of methanol containing internal standard (10 ng/mL loperamide) followed by a 25-µl aliquot of DMSO. The sample was vortex-mixed and centrifuged. Standard solutions ranging from 0.5 to 5000 nM were prepared in a similar manner. Briefly, 25 µl of blank plasma or brain homogenate, 100 µl of methanol containing internal standard, and 25 µl of serially-diluted standard solution were mixed and centrifuged. The supernatant was analyzed by HPLC-tandem mass spectrometry (API 4000 triple quadrupole with TurboIonSpray interface; Applied Biosystems/MDS Sciex, Concord, ON, Canada). Three microliters of sample solutions were injected via an autosampler (Leap, Carrboro, NC). Fexofenadine, terfenadine, terfenadine-OH, and the internal standard loperamide were eluted from an Aquasil C18 column (2.1 x 50 mm, d_p = 5 µm; Thermo Electron Corporation, Waltham, MA) using a mobile phase gradient (A, 0.1% formic acid in water; B, 0.1% formic acid in methanol; 0-0.70-min hold at 0% B, 0.70-3.12-min linear gradient to 90% B, 3.12-4.10 min hold at 90% B, 4.10-4.20-min linear gradient to 0% B, 4.20-4.90-min hold at 0% B; solvent delivery system [Shimadzu]; flow rate = 0.75 ml/min; 0.8-4 min directed to mass spectrometer) and were detected in positive ion mode using multiple reaction monitoring: fexofenadine: 502.4→466.4 *m*/*z*,

terfenadine, 472.3→436.5 *m*/*z*; terfenadine-OH, 488.3→452.5 *m*/*z*; loperamide, 477.4→266.0 *m*/*z*. All analytes were quantified with standard curves in the linear range of the relationship between detector response and analyte concentration prepared in the appropriate matrix. The lower limit of detection was 0.5 ng/ml; inter-and intraday CVs were <15%.

Statistical Analysis

Data are reported as mean ± standard deviation (SD) for 3 mice per condition. A two-tailed student's t-test, or either a one-way or two-way ANOVA, where appropriate, was used to determine the statistical significance of differences among two or more groups. The level of significance was corrected for multiple comparisons (e.g., Bonferroni test) or adjusted for unequal variance when necessary. In all cases, $p < 0.05$ was considered to be statistically significant.

Results

In Situ Mouse Brain Perfusion

^{3}H-inulin was used as the brain capillary space marker to measure the BBB physical integrity. ^{14}C-diazepam was perfused as a marker of functional perfusate flow rate. The vascular volume was 1.69±0.10 mL/100 g and functional flow rate was 250±41 mL/min/100 g brain. P-gp gene deficiency had no influence on the vascular volume or functional perfusion rate. The initial brain uptake clearance (Cl_{up}, mL/min/100 g brain tissue) of fexofenadine and terfenadine in *mdr1a(+/+)* and *mdr1a(-/-)* mice is shown in Figure 3.2. The P-gp efflux ratio, calculated as the ratio of Cl_{up} in *mdr1a(-/-)* mice to *mdr1a(+/+)* mice, was 4.4 and 1.1 for fexofenadine and terfenadine, respectively.

Mathematical Modeling and Simulation

Simulations were conducted with three different sets of values for the passive permeability (Cl_d) and P-gp-mediated efflux clearance (Cl_{eff}) (Figure 3.3). The time course of the apparent fexofenadine P-gp efflux ratio was simulated when Cl_d was equal to the actual value determined from the *in situ* brain perfusion experiment (1×PS). All of the other variables were physiologic or biologic parameters (i.e., V_c, V_{br}, $f_{u,p}$, and $f_{u,br}$) or estimates of fexofenadine pharmacokinetic parameters (i.e., Cl) obtained from the literature (Brown et al., 1997; Tahara et al., 2005; Kalvass et al., 2007a). The simulations predicted that 12 hr and 36 hr would be required for fexofenadine to achieve 50% and 90% of the steady-state P-gp efflux ratio, respectively. When Cl_d was increased 10-fold, the time to achieve the maximum P-gp efflux ratio shortened. In contrast, when Cl_d was

10-fold lower than the actual experimental value obtained for fexofenadine, the P-gp efflux ratio did not plateau during the time frame of the simulation.

In Vivo Osmotic Minipump Studies

Fexofenadine brain-to-plasma concentration ratios at 24 hr following administration of either fexofenadine or terfenadine in *mdr1a(+/+)* and *mdr1a(-/-)* mice are displayed in Figure 3.4. Steady-state fexofenadine plasma concentrations were 28.5 ± 8.3 and 45.5 ± 3.1 nM in *mdr1a(+/+)* and *mdr1a(-/-)* mice during fexofenadine administration, respectively. During terfenadine administration, concentrations of terfenadine in plasma and brain tissue were below the limit of quantitation. However, plasma concentrations of fexofenadine derived from terfenadine were identical in *mdr1a(+/+)* (7.1±2.8 nM) and *mdr1a(-/-)* (7.1±1.7 nM) mice. Fexofenadine brain-to-plasma concentration ratios after 24 hr of fexofenadine administration were 0.0056 ± 0.010 and 0.27 ± 0.08 in *mdr1a(+/+)* and *mdr1a(-/-)* mice, respectively. In contrast, the fexofenadine brain-to-plasma concentration ratio after 24 hr of terfenadine administration were 0.14 ± 0.03 and 7.44 ± 2.12 in *mdr1a(+/+)* and *mdr1a(-/-)* mice, respectively. The fexofenadine brain-to-plasma ratios therefore were ~25- and 27-fold higher in *mdr1a(+/+)* and *mdr1a(-/-)* mice, respectively, after terfenadine administration as compared to after fexofenadine administration. The calculated fexofenadine P-gp efflux ratios following fexofenadine and terfenadine administration are 48 and 55, respectively.

Fexofenadine hydrochloride at dose of 872 μg/pump, selected to produce plasma concentrations (380-480 nM) similar to those in a previous study by Tahara et al. (2005), was administered in *mdr1a(+/+)* and *mdr1a(-/-)* mice for 24, 72 and 168 hr. Plasma

concentrations of fexofenadine achieved with this approach were 305 ± 74 and 836 ± 138 nM in *mdr1a(+/+)* and *mdr1a(-/-)* mice, respectively, and did not vary with time during this period. The brain-to-plasma concentration ratios of fexofenadine during prolonged continuous infusion by subcutaneous osmotic minipumps are shown in Figure 3.5. The P-gp efflux ratios were 17, 23 and 25, at 24, 72, and168 hr, respectively. The calculated P-gp efflux ratio values, together with the P-gp efflux ratio at 2.5 hr from Tahara et al. (2005), are shown in Figure 3.3. These experimentally-derived values correspond closely with the predicted values based on the mathematical simulation.

Mouse Brain Metabolism

Fexofenadine formation rate in brain tissue during *in situ* brain perfusion with 2 μM of terfenadine for 1 min in *mdr1a(+/+)* and *mdr1a(-/-)* mice; and after 2-hr incubation of 200 nM of terfenadine or hydroxyl-terfenadine with whole brain tissue homogenate, is displayed in Figure 3.6. The fexofenadine formation rate during 1-min terfenadine brain perfusion was 17.0 ± 3.1 and 12.0 ± 5.4 nmole/min/kg brain tissue in *mdr1a(+/+)* and *mdr1a(-/-)* mice, respectively. Fexofenadine formation rate during a 2-hr incubation of whole brain homogenate with terfenadine or hydroxyl-terfenadine was 12.9 ± 3.5 or 74.9 ± 11.8 nmole/min/kg brain tissue, respectively.

Discussion

Lipophilicity and ionization at physiologic pH are important determinants of brain penetration (Brodie et al., 1960). Fexofenadine is ionized at physiologic pH and crosses the BBB to only a minimal extent. In contrast to pre-formed fexofenadine, the fexofenadine prodrug terfenadine, a very lipophilic molecule, evidenced a brain uptake that approximated perfusate flow. This very high uptake clearance was similar between *mdr1a(+/+)* and *mdr1a(-/-)* mice, even though terfenadine has been reported to be a P-gp substrate (Mahar Doan et al., 2004; Obradovic et al., 2007). The lack of a discernible P-gp effect for this substrate was consistent with the efficient unidirectional uptake of terfenadine during short-term brain perfusion.

P-gp has been reported to be involved in fexofenadine intestinal secretion, and thus in the systemic disposition of this compound. [^{14}C]-fexofenadine plasma concentrations in *mdr1a* knockout mice were ~4.6-fold higher than that in wild-type mice after intravenous administration (Cvetkovic et al., 1999). In the current study, fexofenadine plasma concentrations in *mdr1a(-/-)* mice were approximately 60-206% higher than in *mdr1a(+/+)* mice. These observations are in contrast to a previous report by Tahara et al (2005), which indicated that plasma concentrations of fexofenadine were similar in P-gp-competent and P-gp-deficient bile duct cannulated mice..

P-gp also is involved in fexofenadine penetration of the BBB. The influence of P-gp on brain uptake of fexofenadine was demonstrated for the first time with the *in situ* brain perfusion technique, using the *mdr1a(-/-)* mouse model of P-gp deficiency. The P-gp effect during short-term brain perfusion (4.4-fold) was modest. *In vivo* administration

under conditions that produce steady-state provides a more sensitive approach to quantitating the BBB P-gp effect than short-term brain perfusion when substrate equilibration across the blood-brain interface is slow. Continuous infusion with a subcutaneous osmotic minipump provides useful steady-state information from a simple experimental system. This approach was used in the current study. As anticipated, the *in vivo* P-gp efflux ratio exceeded that determined by the *in situ* brain perfusion, which has been demonstrated experimentally in the present study and previously (Dagenais et al., 2001). The present results also are consistent with previous mathematical predictions based on a simple three-compartment model (representing plasma, endothelial cell layer, and brain) that showed ERα (*in vivo* P-gp efflux ratio) must be higher than ER_B (*in situ* P-gp efflux ratio) for the same substrate and efflux transporter system (Kalvass and Pollack, 2007).

Fexofenadine brain-to-plasma concentration ratio at 24 hr (i.e., during continuous minipump administration) was 25- to 27-fold higher following terfenadine administration than fexofenadine administration in both *mdr1a(+/+)* and *mdr1a(-/-)* mice. This difference might be due to the low permeability of fexofenadine. In the presence of such a low uptake clearance, a significantly longer period of time would be required to reach distribution equilibrium across the BBB, and so the apparent brain-to-plasma ratio at 24 hr may be an underprediction of the true equilibrium value. Indeed, this situation has been demonstrated previously by Liu et al. (2005) using a simulation approach. Alternatively, the precursor of fexofenadine, terfenadine, is permeable at the BBB. If terfenadine is metabolized in the brain after crossing the BBB, an increase in

fexofenadine brain exposure, relative to administration of preformed fexofenadine, would be predicted.

To test the first possible mechanism, simulation studies were conducted in parallel with animal experiments. Mathematical modeling demonstrated that the P-gp efflux ratio must be time-dependent. Moreover, these simulations successfully predicted the P-gp efflux ratios measured at the selected experimental time points. The interpretation of the simulation results is both straightforward and logical: because it takes longer for slowly-permeable compounds to equilibrate across the BBB, the experimentally-determined P-gp efflux ratio also will take a longer time to reach its equilibrium (theoretically maximum) condition. Experimentally, fexofenadine was administered for a prolonged time period up to 168 hr. The present results demonstrate a clear time-dependence of fexofenadine P-gp efflux ratio during this time range of 24 to 168 hr. The determined P-gp efflux ratio values, together with the P-gp efflux ratio of ~3.3 at 2.5 hr taken from Tahara et. al. (2005), were almost superimposable with the predicted values based on the model simulation.

In order to assess the influence of P-gp on fexofenadine brain exposure when fexofenadine is formed from terfenadine, versus when fexofenadine is administered directly, fexofenadine plasma concentrations must be similar between the two administration modalities. To achieve similar fexofenadine concentrations from pre-formed fexofenadine as compared to fexofenadine concentrations following terfenadine administration, fexofenadine hydrochloride was administered via osmotic minipump at a continuous rate of 1.5 nmoles/hr. The fexofenadine P-gp efflux ratios determined *in vivo* at distribution equilibrium were similar (55 vs. 48) regardless of whether fexofenadine

was formed from terfenadine or administered directly. The P-gp efflux ratio decreased when fexofenadine plasma concentration was ~10-fold higher (305 nM) in the time-course studies, consistent with at least partial saturation of the transport process.

Based on the impaired brain penetration of fexofenadine in both *mdr1a(+/+)* and *mdr1a(-/-)* mice at all time points following fexofenadine administration, the 25-27-fold increase of fexofenadine brain penetration following terfenadine administration could not be explained by simply attaining distribution equilibrium more rapidly with the prodrug. Thus, it was important to address the possibility that local metabolism of terfenadine to fexofenadine in the brain was responsible for the observed difference. Terfenadine is metabolized to hydroxyl-terfenadine, then to the carboxylic acid metabolite fexofenadine, by hepatic CYP3A4 in humans. CYP3A11 and 3A13 are the murine counterparts of human 3A4, and are expressed in mouse liver and brain (Hagemeyer et al., 2003; Meyer et al., 2006). Following terfenadine administration, terfenadine plasma and brain concentrations were below the limit of quantitation, although fexofenadine concentrations in plasma and brain were substantial. These observations confirm efficient metabolism of terfenadine in the mouse. Fexofenadine plasma concentrations were identical in *mdr1a(+/+)* and *mdr1a(-/-)* mice, indicating that the formation rate of fexofenadine from terfenadine did not differ between mouse strains. Terfenadine appeared to be metabolized to fexofenadine in mouse brain during a short (1-min) brain perfusion, as well as during a 2-hr *in vitro* incubation with brain tissue homogenate (Figure 3.6).

Fexofenadine formation rate in the brain during terfenadine brain perfusion was comparable between *mdr1a(+/+)* and *mdr1a(-/-)* mice, suggesting that the correspondent enzyme(s) activity in brain was not modulated by P-gp. These novel observations

provided supporting evidence, consistent with the pharmacokinetic arguments, that terfenadine must be metabolized to fexofenadine both systemically and regionally in the brain. The local metabolism significantly increased fexofenadine brain exposure compared to what would be expected if fexofenadine was simply formed from terfenadine systemically.

The enzyme(s) responsible for terfenadine-to-fexofenadine biotransformation in murine brain is unknown, although it is reasonable to speculate that CYP3A11 and/or CYP3A13 may be responsible. This metabolic situation may have pharmacologic consequences. Fexofenadine is a non-sedating antihistamine, at least in part because it does not penetrate the BBB efficiently. In contrast, high-dose terfenadine administration has been associated with sedative effects (Mattila and Paakkari, 1999). It is possible that terfenadine itself is the causative agent for sedation. Alternatively, terfenadine may be inert, but provide sufficient fexofenadine to the brain, via local metabolism, to allow fexofenadine to cause sedation.

Antihistamines represent an interesting pharmacologic class from the standpoint of BBB permeation and central nervous system responsivity. Fexofenadine and cetirizine are both non-sedating antihistamines due to poor BBB permeability secondary to P-gp-mediated efflux at the BBB (Polli et al., 2003). Hydroxyzine is sedating, as is terfenadine at high doses (Mattila and Paakkari, 1999). A comprehensive pharmacokinetic study of cetirizine following intravenous administration of cetirizine and hydroxyzine has been conducted (Chen et al., 2003a). Re-examination of these published results demonstrated that the cetirizine P-gp efflux ratio was ~4.4 after administration of preformed cetirizine. However, the cetirizine P-gp efflux ratio following administration of hydroxyzine, the

more permeable precursor of cetirizine, was ≥125 at 240 min. This experimentally-determined efflux ratio is remarkably similar to the predicted value of 111 based on the unbound fraction of cetirizine in plasma versus brain and the intrinsic transport activity of cetirizine by P-gp (Kalvass et al., 2007a). Thus, the overall prediction of antihistamine brain penetration could be substantially improved by using accurately determined P-gp efflux ratios (that is, the efflux ratios determined after complete equilibration across the BBB). Such an approach would effectively address the two outliers – fexofenadine and cetirizine - identified in a previous compound set (Kalvass et al., 2007a).

An additional consideration for these compounds is that the cetirizine brain-to-plasma concentration ratio at 240 min was ~7-fold higher following hydroxyzine administration as compared to ceterizine administration. This situation is analogous to that for the terfenadine-fexofenadine precursor-metabolite pair as shown in the present series of experiments.. The specific enzyme(s) responsible for hydroxyzine metabolism are unknown. However, it is conceivable that hydroxyzine enters the brain and subsequently is metabolized to cetirizine, thus increasing cetirizine local exposure following hydroxyzine administration. Clearly, additional experimentation would be required to confirm this speculation.

Based on the current study with the terfenadine/fexofenadine pair, together with published results for the hydroxyzine/cetirizine pair, administration of a permeable prodrug seems to provide useful information about the true P-gp efflux ratio for a poorly permeable metabolite. For many slow-equilibrating compounds, partitioning through the BBB is the rate-limiting step in brain uptake. In this situation, the assumption that simple diffusion of unbound substrate across the BBB leads to equivalent unbound

concentrations in brain and plasma is violated because distribution equilibrium might not be achieved within the confines of a given experiment, thus result in a lower extent of brain penetration than predicted based on the equilibrium assumption. Such a situation has been demonstrated for NFPS (N[3-(4'-fluorophenyl)-3-(4'-phenylphenoxy)propyl]sarcosine), which failed to reach equilibrium within a 24-hr experiment (Liu et al., 2005).

Following prodrug administration, a poorly-permeable metabolite formed in the brain (i.e., in capillary endothelial cells, neurons, or glial cells) might evidence access to the P-gp binding site that is different from access that could be achieved from the luminal side (i.e., after systemic formation of the metabolite or direct administration of the pre-formed compound). The relative rate of metabolite formation in systemic circulation versus brain certainly would influence brain exposure, apparent brain-to-blood partitioning, and calculated P-gp efflux ratios. These experimental aspects warrant further investigation. Taken together, brain exposure is an integrative effect of passive permeability, protein binding in plasma and brain, interaction with active transporters at the BBB, and, in the special case of poorly permeable metabolites, the systemic and regional brain metabolism. Finally, brain exposure for poorly permeable compounds is complicated further by CSF bulk flow, which in the mouse is ~0.071 mL/min/100 g (Rudick et al., 1982). CSF bulk flow also poses a significant influence on the brain exposure of low-permeability compounds (Liu and Chen, 2005).

In conclusion, the current study investigated fexofenadine brain penetration and P-gp efflux ratio following fexofenadine and terfenadine administration. The results demonstrated that P-gp is an important determinant of fexofenadine efflux at the BBB

and, consequently, the presentation of fexofenadine to brain tissue. Studies to date have underestimated the actual P-gp efflux ratio of fexofenadine at the BBB because the P-gp efflux ratio is time-sensitive, and previous experiments were not sufficiently long to uncover the true efflux ratio. The present experiments also demonstrated for the first time the metabolism of terfenadine to fexofenadine in murine brain. The enzyme(s) responsible for terfenadine metabolism in the brain require further investigation. These latter results underscore the fact that enzymes in the brain or the BBB not only represent a metabolic barrier for substrate presentation to the brain, but also might activate some drugs to cause CNS responses (either therapeutic or toxic). Modulation of brain metabolic enzymes by co-administered drugs might represent a source of drug-drug interaction.

References

Begley DJ (2003) Understanding and circumventing the blood-brain barrier. *Acta Paediatr Suppl* **92:**83-91.

Brodie BB, Kurz H and Schanker LS (1960) The importance of dissociaton constant and lipid-solubility in influencing the passage of drugs into the cerebrospinal fluid. *J Pharmacol Exp Ther* **130:**20-25.

Brown RP, Delp MD, Lindstedt SL, Rhomberg LR and Beliles RP (1997) Physiological parameter values for physiologically based pharmacokinetic models. *Toxicol Ind Health* **13:**407-484.

Chen C, Hanson E, Watson JW and Lee JS (2003) P-glycoprotein limits the brain penetration of nonsedating but not sedating H1-antagonists. *Drug Metab Dispos* **31:**312-318.

Cvetkovic M, Leake B, Fromm MF, Wilkinson GR and Kim RB (1999) OATP and P-glycoprotein transporters mediate the cellular uptake and excretion of fexofenadine. *Drug Metab Dispos* **27:**866-871.

Dagenais C, Rousselle C, Pollack GM and Scherrmann JM (2000) Development of an in situ mouse brain perfusion model and its application to mdr1a P-glycoprotein-deficient mice. *J Cereb Blood Flow Metab* **20:**381-386.

Dagenais C, Zong J, Ducharme J and Pollack GM (2001) Effect of mdr1a P-glycoprotein gene disruption, gender, and substrate concentration on brain uptake of selected compounds. *Pharm Res* **18:**957-963.

Fenstermacher JD, Blasberg RG and Patlak CS (1981) Methods for Quantifying the transport of drugs across brain barrier systems. *Pharmacol Ther* **14:**217-248.

Graff CL and Pollack GM (2004) Drug transport at the blood-brain barrier and the choroid plexus. *Curr Drug Metab* **5:**95-108.

Hagemeyer CE, Rosenbrock H, Ditter M, Knoth R and Volk B (2003) Predominantly neuronal expression of cytochrome P450 isoforms CYP3A11 and CYP3A13 in mouse brain. *Neuroscience* **117:**521-529.

Holleran JL, Fourcade J, Egorin MJ, Eiseman JL, Parise RA, Musser SM, White KD, Covey JM, Forrest GL and Pan SS (2004) In vitro metabolism of the phosphatidylinositol 3-kinase inhibitor, wortmannin, by carbonyl reductase. *Drug Metab Dispos* **32:**490-496.

Kalvass JC and Maurer TS (2002) Influence of nonspecific brain and plasma binding on CNS exposure: implications for rational drug discovery. *Biopharm Drug Dispos* **23:**327-338.

Kalvass JC, Maurer TS and Pollack GM (2007a) Use of plasma and brain unbound fractions to assess the extent of brain distribution of 34 drugs: comparison of unbound concentration ratios to in vivo p-glycoprotein efflux ratios. *Drug Metab Dispos* **35:**660-666.

Kalvass JC, Olson ER, Cassidy MP, Selley DE and Pollack GM (2007b) Pharmacokinetics and Pharmacodynamics of Seven Opioids in P-gp-Competent Mice: Assessment of Unbound Brain EC50 and Correlation of In Vitro, Preclinical, and Clinical Data. *J Pharmacol Exp Ther*.

Kalvass JC and Pollack GM (2007) Kinetic considerations for the quantitative assessment of efflux activity and inhibition: implications for understanding and predicting the effects of efflux inhibition. *Pharm Res* **24:**265-276.

Ling KH, Leeson GA, Burmaster SD, Hook RH, Reith MK and Cheng LK (1995) Metabolism of terfenadine associated with CYP3A(4) activity in human hepatic microsomes. *Drug Metab Dispos* **23:**631-636.

Liu X and Chen C (2005) Strategies to optimize brain penetration in drug discovery. *Curr Opin Drug Discov Devel* **8:**505-512.

Liu X, Smith BJ, Chen C, Callegari E, Becker SL, Chen X, Cianfrogna J, Doran AC, Doran SD, Gibbs JP, Hosea N, Liu J, Nelson FR, Szewc MA and Van Deusen J (2005) Use of a physiologically based pharmacokinetic model to study the time to reach brain equilibrium: an experimental analysis of the role of blood-brain barrier permeability, plasma protein binding, and brain tissue binding. *J Pharmacol Exp Ther* **313:**1254-1262.

Liu X, Tu M, Kelly RS, Chen C and Smith BJ (2004) Development of a computational approach to predict blood-brain barrier permeability. *Drug Metab Dispos* **32:**132-139.

Mahar Doan KM, Wring SA, Shampine LJ, Jordan KH, Bishop JP, Kratz J, Yang E, Serabjit-Singh CJ, Adkison KK and Polli JW (2004) Steady-state brain concentrations of antihistamines in rats: interplay of membrane permeability, P-glycoprotein efflux and plasma protein binding. *Pharmacology* **72:**92-98.

Markham A and Wagstaff AJ (1998) Fexofenadine. *Drugs* **55:**269-274; discussion 275-266.

Mattila MJ and Paakkari I (1999) Variations among non-sedating antihistamines: are there real differences? *Eur J Clin Pharmacol* **55:**85-93.

Meyer RP, Gehlhaus M, Knoth R and Volk B (2007) Expression and function of cytochrome p450 in brain drug metabolism. *Curr Drug Metab* **8:**297-306.

Meyer RP, Hagemeyer CE, Knoth R, Kaufmann MR and Volk B (2006) Anti-epileptic drug phenytoin enhances androgen metabolism and androgen receptor expression in murine hippocampus. *J Neurochem* **96:**460-472.

Miksys SL and Tyndale RF (2002) Drug-metabolizing cytochrome P450s in the brain. *J Psychiatry Neurosci* **27:**406-415.

Obradovic T, Dobson GG, Shingaki T, Kungu T and Hidalgo IJ (2007) Assessment of the first and second generation antihistamines brain penetration and role of P-glycoprotein. *Pharm Res* **24:**318-327.

Petri N, Tannergren C, Rungstad D and Lennernas H (2004) Transport characteristics of fexofenadine in the Caco-2 cell model. *Pharm Res* **21:**1398-1404.

Polli JW, Baughman TM, Humphreys JE, Jordan KH, Mote AL, Salisbury JA, Tippin TK and Serabjit-Singh CJ (2003) P-glycoprotein influences the brain concentrations of cetirizine (Zyrtec), a second-generation non-sedating antihistamine. *J Pharm Sci* **92:**2082-2089.

Rudick RA, Zirretta DK and Herndon RM (1982) Clearance of albumin from mouse subarachnoid space: a measure of CSF bulk flow. *J Neurosci Methods* **6:**253-259.

Schinkel AH, Smit JJ, van Tellingen O, Beijnen JH, Wagenaar E, van Deemter L, Mol CA, van der Valk MA, Robanus-Maandag EC, te Riele HP and et al. (1994)

Disruption of the mouse mdr1a P-glycoprotein gene leads to a deficiency in the blood-brain barrier and to increased sensitivity to drugs. *Cell* **77:**491-502.

Strobel HW, Thompson CM and Antonovic L (2001) Cytochromes P450 in brain: function and significance. *Curr Drug Metab* **2:**199-214.

Summerfield SG, Stevens AJ, Cutler L, del Carmen Osuna M, Hammond B, Tang SP, Hersey A, Spalding DJ and Jeffrey P (2006) Improving the in vitro prediction of in vivo central nervous system penetration: integrating permeability, P-glycoprotein efflux, and free fractions in blood and brain. *J Pharmacol Exp Ther* **316:**1282-1290.

Tahara H, Kusuhara H, Fuse E and Sugiyama Y (2005) P-glycoprotein plays a major role in the efflux of fexofenadine in the small intestine and blood-brain barrier, but only a limited role in its biliary excretion. *Drug Metab Dispos* **33:**963-968.

Takasato Y, Rapoport SI and Smith QR (1984) An in situ brain perfusion technique to study cerebrovascular transport in the rat. *Am J Physiol* **247:**H484-493.

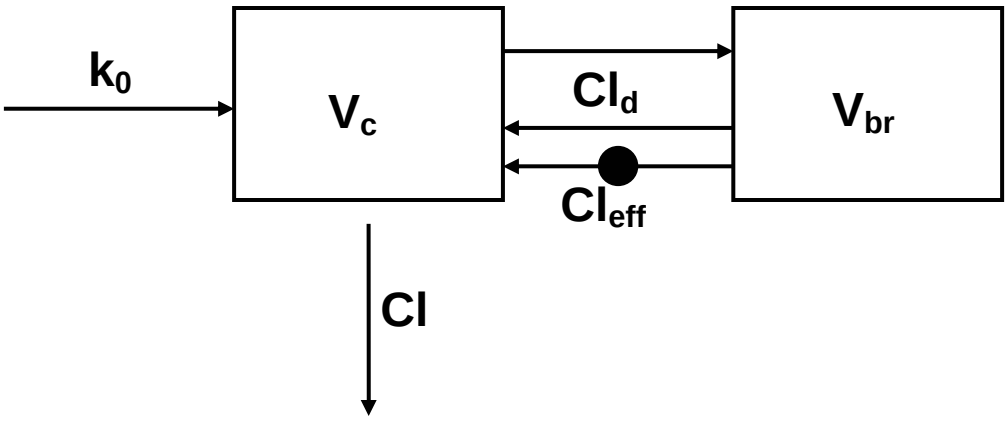

Figure 3.1: Scheme for the mathematical model used to simulate the P-gp efflux ratio over time. Parameter definitions are included in the Materials and Methods section.

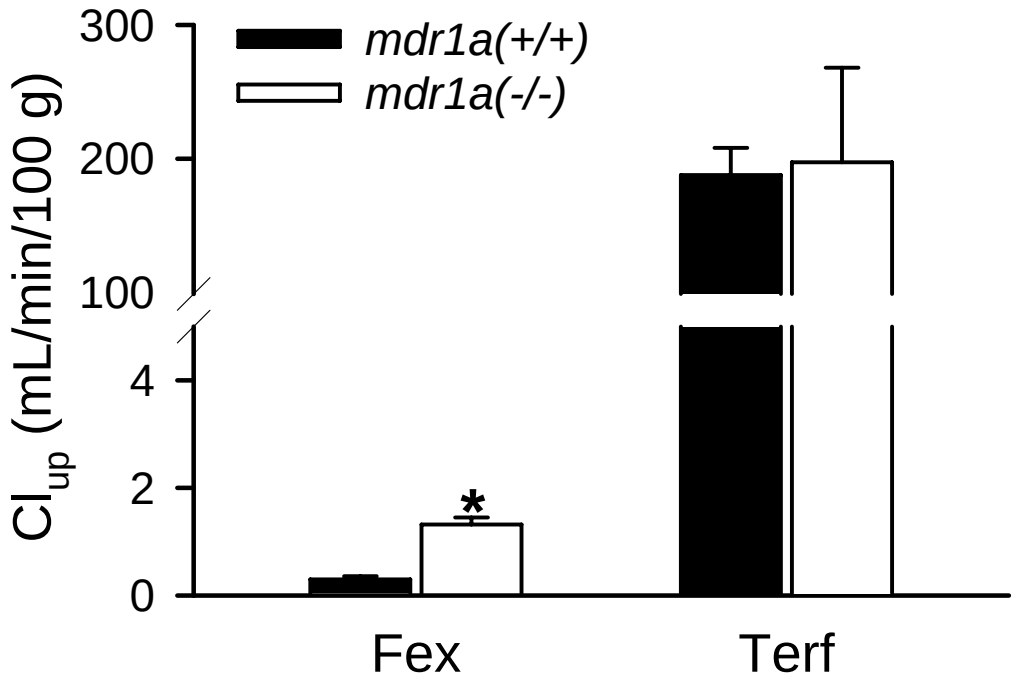

Figure 3.2: Initial brain uptake clearance (Cl_{up}, mL/min/100 g) for fexofenadine and terfenadine in *mdr1a(+/+)* (solid bar) and *mdr1a(-/-)* (open bar) mice. The mouse brain hemisphere was perfused via the common carotid artery at 2.5 mL/min for 60 s. Data are presented as mean ± SD (n=3). Student's *t*-test was used to determine the statistical significance of P-gp effect between *mdr1a(+/+)* and *mdr1a(-/-)* mice. Asterisk (*) represents a statistical difference ($p<0.05$) between *mdr1a(+/+)* and *mdr1a(-/-)* mice.

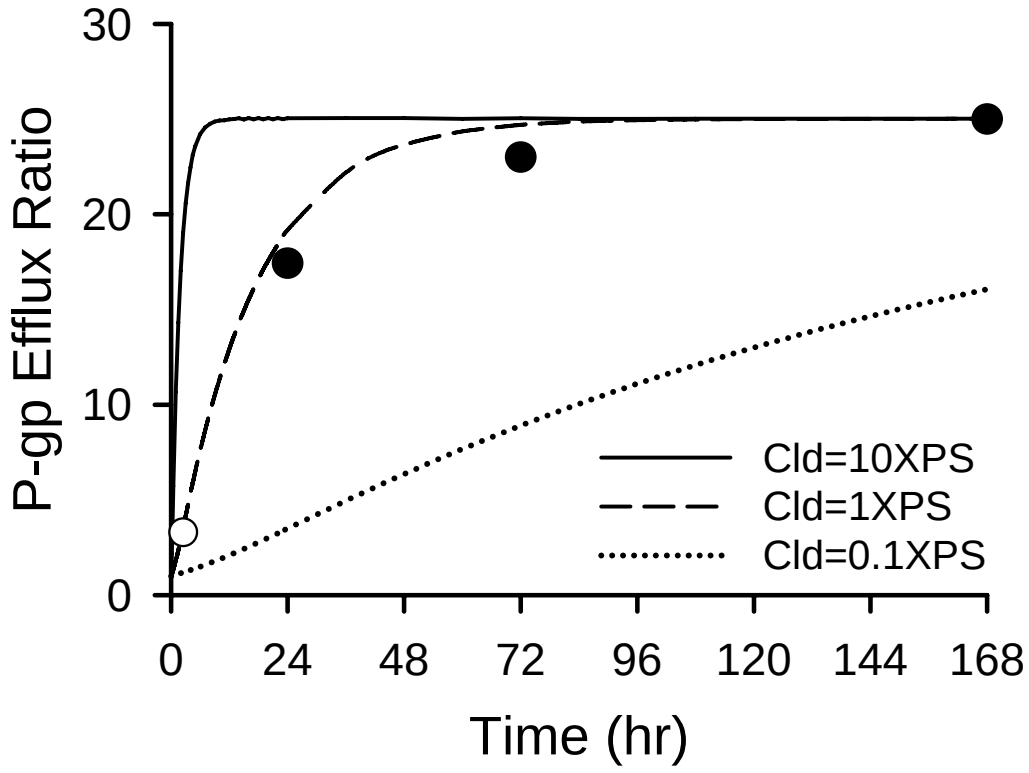

Figure 3.3: Simulated P-gp efflux ratios over time for varying passive permeability (Cl_d) and P-gp-mediated efflux clearance (Cl_{eff}) (—, Cl_d=2.24, Cl_{eff}=53.90; ----, Cl_d=0.22, Cl_{eff}=5.39; ·····, Cl_d=0.022, Cl_{eff}=0.54; Cl_{eff}=0 for P-gp-deficient mice). The P-gp efflux ratio was calculated as the ratio of brain-to-plasma concentration ratio in *mdr1a(-/-)* mice to *mdr1a(+/+)* mice. The solid circles (●) represent fexofenadine P-gp efflux ratios determined at 24, 72, and 168 hr during subcutaneous osmotic minipump administration. The open circle (○) is the P-gp efflux ratio determined at 2.5 hr in Tahara et al., (2005).

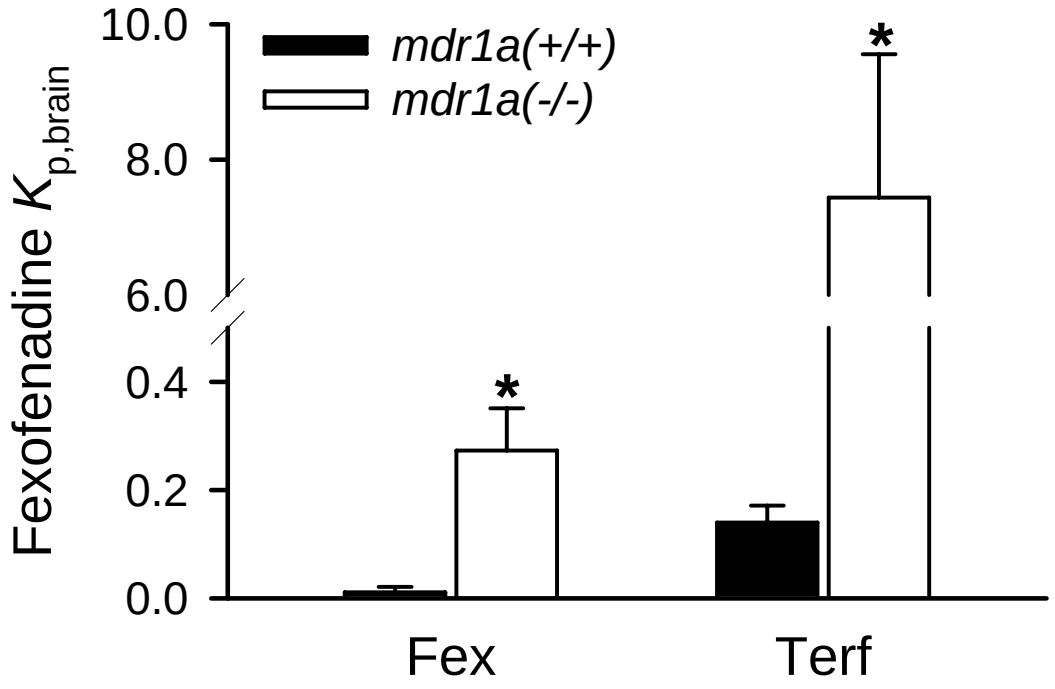

Figure 3.4: Fexofenadine brain-to-plasma concentration ratio at 24 hr in *mdr1a(+/+)* (solid bar) and *mdr1a(-/-)* (open bar) mice following subcutaneous osmotic minipump administration of fexofenadine or terfenadine. Data are presented as mean ± SD (n=3). Student's t-tests were used to compare brain-to-plasma concentration ratios between *mdr1a(+/+)* and *mdr1a(-/-)* mice. Asterisk (*) represents a statistical difference ($p<0.05$) between *mdr1a(+/+)* and *mdr1a(-/-)* mice.

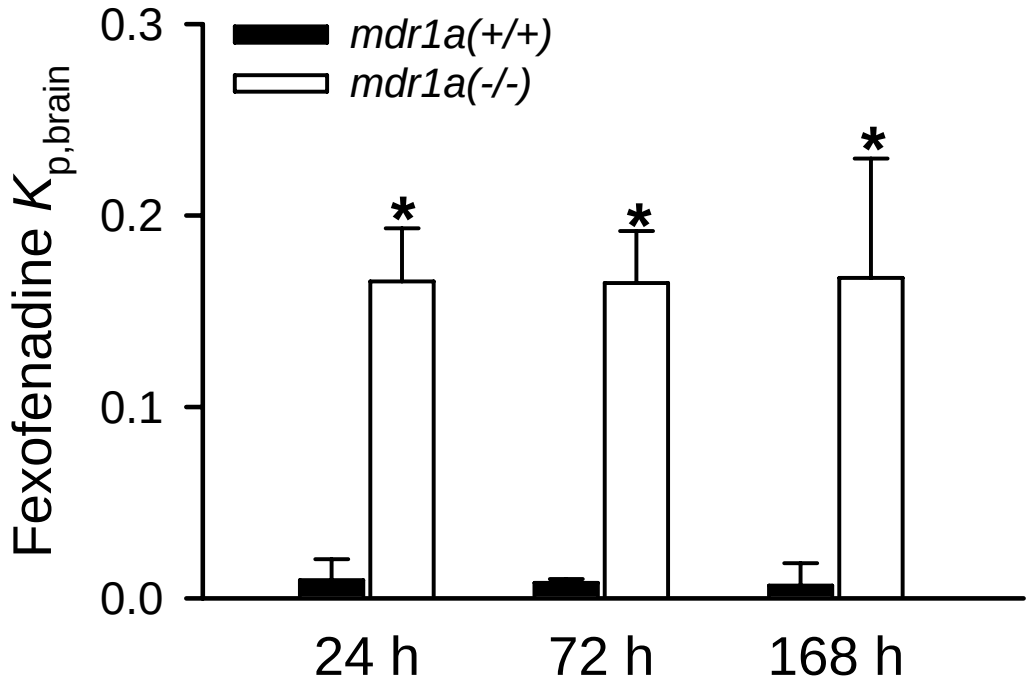

Figure 3.5: Fexofenadine brain-to-plasma concentration ratio in *mdr1a(+/+)* (solid bar) and *mdr1a(-/-)* (opne bar) mice at 24, 72 and 168 hr following subcutaneous osmotic minipump administration of fexofenadine. Data are presented as mean ± SD (n=3). Two-way ANOVA was used to compare brain-to-plasma concentration ratios between *mdr1a(+/+)* and *mdr1a(-/-)* mice; and among the time points, respectively. Asterisk (*) represents a statistical difference ($p<0.05$) between *mdr1a(+/+)* and *mdr1a(-/-)* mice. There was no differences for fexofenadine brain partition coefficients at different time points.

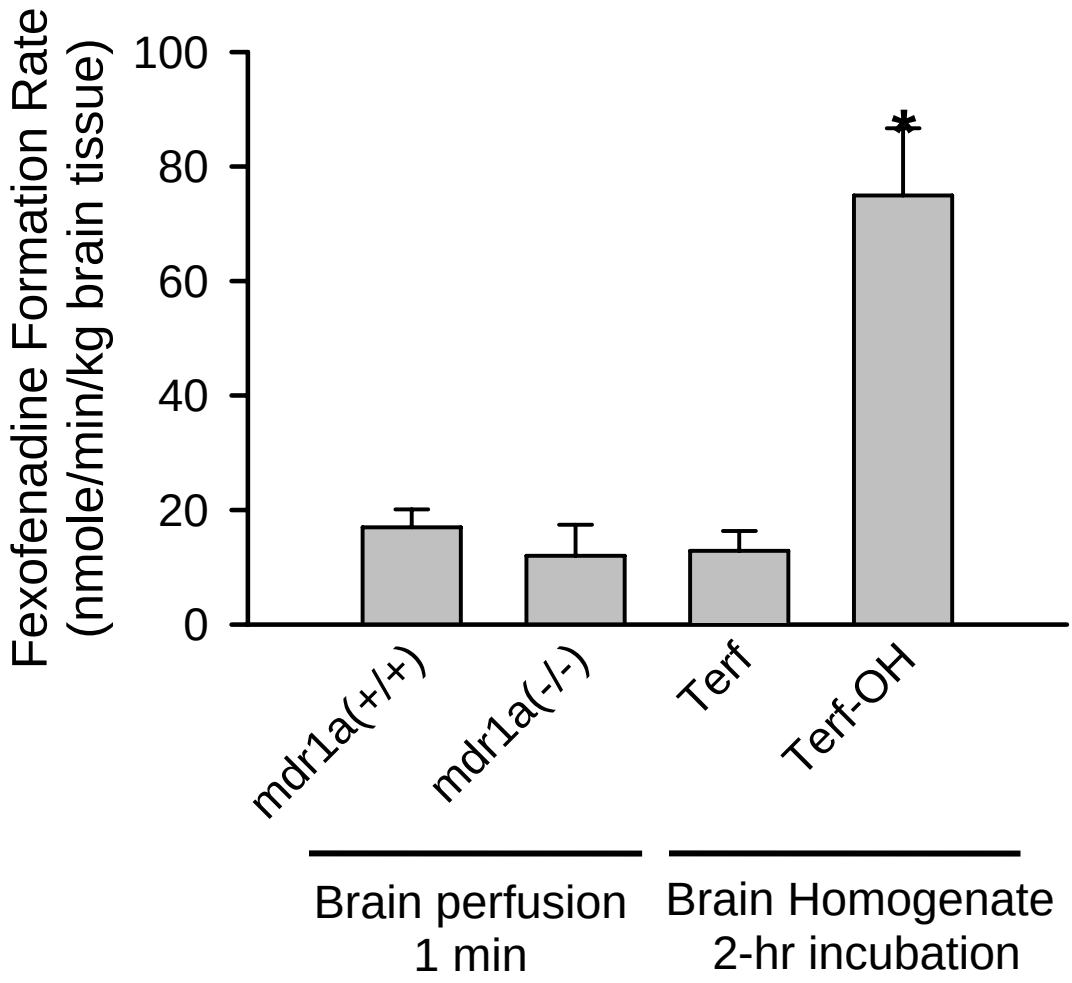

Figure 3.6: Fexofenadine formation rate in the brain hemisphere following 60 s terfenadine *in situ* mouse brain perfusion in *mdr1a(+/+)* and *mdr1a(-/-)* mice, or a 2-hr incubation of terfenadine (Terf) or terfenadine-OH (Terf-OH) with whole brain tissue homogenate. Data are presented as mean ± SD (n=3). One-way ANOVA statistical analysis corrected for multiple comparisons (Bonferroni test) demonstrated that fexofenadine formation rate in the brain was significantly higher when incubated with terfenadine-OH than incubation with terfenadine or one-minute terfenadine brain perfusion (*, $p<0.05$).

CHAPTER 4

BREAST CANCER RESISTANCE PROTEIN INTERACTS WITH VARIOUS COMPOUNDS *IN VITRO*, BUT PLAYS A MINOR ROLE IN SUBSTRATE EFFLUX AT THE BLOOD-BRAIN BARRIER

This chapter will be submitted for publication in Drug Metabolism and Disposition and is presented in the style of that journal.

Abstract

Expression of breast cancer resistance protein (Bcrp) at the blood-brain barrier (BBB) has been revealed recently. In order to investigate comprehensively the potential role of Bcrp at the murine BBB, a chemically-diverse set of model compounds (cimetidine, alfuzosin, dipyridamole and LY2228820) was evaluated utilizing a multiexperimental design. Bcrp1 stably-transfected MDCKII cell monolayer transport studies demonstrated that each compound had affinity for Bcrp, and that polarized transport by Bcrp was abolished completely by the Bcrp inhibitor chrysin. However, none of the compounds differed in brain uptake between Bcrp wild-type and knockout *Abcg2*(-/-) mice under either an *in situ* brain perfusion or a 24-hr subcutaneous osmotic minipump continuous infusion experimental paradigm. In addition, alfuzosin and dipyridamole were shown to undergo transport by P-gp in an MDCKII-MDR1 cell monolayer model. Alfuzosin brain uptake was four-fold higher in *mdr1a(-/-)* mice than in *mdr1a(+/+)* mice in *in situ* and *in vivo* studies, demonstrating for the first time that it undergoes P-gp-mediated efflux at the BBB. In contrast, P-gp had no effect on dipyridamole brain penetration *in situ* or *in vivo*. Dipyridamole brain penetration was appreciable, with brain concentrations that approximated plasma concentrations. In summary, Bcrp mediates *in vitro* transport of various compounds, but appears to play a minimal role at the BBB *in vivo*. Correlation analyses indicate that *in situ* brain permeability is dependent on the lipophilicity of compounds in the absence of efflux transport. In addition, *in situ* brain uptake clearance correlates with the apparent passive permeability in *in vitro* transport and cellular accumulation studies.

Introduction

The blood-brain barrier (BBB) is composed of brain capillary endothelial cells, which are characterized by highly-developed tight junctions, lack of fenestrations and paucity of pinocytic and transcytotic activities. Expression of metabolic enzymes and efflux transporters in these and associated glial cells provide additional limiting factors at the BBB. Insufficient drug exposure at the pharmacologic target within the brain, as a consequence of limited flux from blood to brain, represents a major obstacle for effective treatment of CNS disorders (Begley, 2004b; Pardridge, 2005). It is widely accepted that P-glycoprotein (P-gp) is expressed abundantly at the BBB and functions as an efflux pump thay extrude toxic substances and therapeutic agents in the brain-to-blood direction, representing a functional barrier to brain uptake (Schinkel, 1999). The potential role of other members of ATP-binding cassette (ABC) efflux transporters, such as multidrug resistance-associated proteins (Mrps) and breast cancer resistance protein (Bcrp), at the BBB is less clear, although the proteins appear to be expressed at the BBB in various species (Soontornmalai et al., 2006; Yousif et al., 2007).

Bcrp is a recently-identified member of ABC efflux transporter encoded by gene *Abcg2* (Doyle et al., 1998). Bcrp is widely expressed in the intestine, liver, mammary gland, and placenta. The functional efficiency of Bcrp in these organs, such as intestinal secretion, fetal penetration and breast milk secretion of various compounds (e.g., topotecan, nitrofurantoin and cimetidine), has been documented clearly (Jonker et al., 2000; Jonker et al., 2005). In addition, Bcrp is expressed on the luminal side of brain capillary endothelial cells in mice, rats, pig and human, with localization similar to that of P-gp; mRNA expression level for Bcrp also is similar to that of P-gp (Maliepaard et al., 1999;

Cooray et al., 2002; Eisenblatter and Galla, 2002; Eisenblatter et al., 2003; Cisternino et al., 2004; Aronica et al., 2005; Lee et al., 2005; Tanaka et al., 2005).

Bcrp mediates the transport of a wide variety of substrates, from sulfoconjugated organic anions to various organic cations. The extensive overlap of Bcrp with P-gp in expression pattern and substrate specificity leads to the hypothesis that Bcrp, like P-gp, might have an important role in the handling of substrate drugs, with subsequent regulation of pharmacologic response, in animals and humans (Tanaka et al., 2005). However, studies to date have not clarified Bcrp function at the BBB, which remains very controversial. Brain penetration of imatinib mesylate was 2.5-fold higher in Bcrp-deficient mice as compared to wild-type animals, suggesting that Bcrp represents a functional barrier to brain uptake of this compound (Breedveld et al., 2005). In contrast, the initial rate of brain uptake of imatinib mesylate did not differ between wild-type and *Bcrp1(-/-)* mice during *in situ* brain perfusion, and GF120918 (elacridar), an inhibitor of P-gp and Bcrp, did not alter brain uptake of imatinib in *mdr1a/1b(-/-)* mice, suggesting that Bcrp was not involved in imatinib brain uptake (Bihorel et al., 2007).

Exploring the role of Bcrp at the BBB may provide important information on the design of efficient drug delivery to CNS, and may add to the understanding CNS toxicity, for Bcrp substrates. In the present study, four compounds with different physicochemical properties, cimetidine, alfuzosin, dipyridamole, and LY2228820, four compounds were selected as model substrates based on the *in vitro* screening in an MDCKII-Bcrp cell monolayer transport assay to evaluate comprehensively the role of Bcrp at the murine BBB. Cimetidine, a prototypical histamine H2 receptor antagonist, recently was demonstrated to possess anti-tumor activity against a variety of cancers and malignant

brain glioma (Lefranc et al., 2006). Cimetidine is a hydrophilic compound that has poor brain penetration (Hough et al., 1986) and is actively secreted from rat mammary gland and placenta by Bcrp (Jonker et al., 2005; Staud et al., 2006). Alfuzosin is a clinical uroselective *alpha*1-adrenergic receptor antagonist with proven efficacy and safety in the treatment of benign prostatic hyperplasia (BPH). Alfuzosin is a structural analog of prazosin, which is a prototypical Bcrp substrate (Marbury et al., 2002; Guay, 2004; Staud et al., 2006). Dipyridamole is a platelet inhibitor used for treatment of stroke. It is a P-gp inhibitor and was identified recently as a human BCRP substrate (Hervey and Goa, 1999; Verstuyft et al., 2003; Zhang et al., 2005b). LY2228820 is a P38 mitogen-activated protein kinase (MAPK) inhibitor discovered by Eli Lilly and Company. In the present study, bidirectional transport of these model compounds across the MDCKII-Bcrp and MDCKII-MDR1 cell monolayers was evaluated. The initial brain uptake clearance (Cl_{up}) was determined using *in situ* brain perfusion with Bcrp-competent [C57BL/6, *Abcg2(+/-)*] and Bcrp -deficient [*Abcg2(-/-)*], P-gp-competent [*mdr1a(+/+)*] and P-gp -deficient [*mdr1a(-/-)*] mouse models. In addition, the P-gp and Bcrp inhibitor GF120918 was co-perfused with test compounds in the brain perfusion paradigm to generate a chemical knockout model. Finally, *in vivo* brain penetration of substrates was measured at 24 hr during continuous subcutaneous infusion with an osmotic minipump.

Materials and Methods

Animals

Adult *mdr1a(+/+)* mice and its natural mutant *mdr1a* (-/-) mice (30-40 g, 6-8 weeks of age) were obtained from Charles River Laboratories. Male C57BL/6 wild-type [*Abcg2(+/-)*], *Abcg2(+/+)* and *Abcg2*(-/-) mice (25-35 g) were a gift from Eli Lilly and Company. Details regarding the background, generation, and breeding of these mice have been described elsewhere (Zamek-Gliszczynski et al., 2006). All mice were maintained on a 12-h light/dark cycle with access to water and food *ad libitum*. All experimental procedures were performed under full anesthesia induced with ketamine/xylazine (100/10 mg/kg, i.p.). All procedures were approved by the Institutional Animal Care and Use Committee at the University of North Carolina at Chapel Hill and were conducted in accordance with "Principles with Laboratory Animal Care" (NIH publication No. 85-23, revised in 1985).

Materials

Cimetidine and dipyridamole were purchased from Sigma-Aldrich (St. Louis, MO). Alfuzosin was obtained from Toronto Research Chemicals Inc (New York, ON, Canada). LY2228820 and ^{14}C-LY2228820 were kind gifts from Eli Lilly and Company (Indianapolis, IN). GF120918 [N-(4-[2-(1,2,3,4-tetrahydro-6,7-dimethoxy-2-isoquinolinyl)ethyl]-phenyl)-9,10-dihydro-5-methoxy-9-oxo-4-acridine carboxamide] was a kind gift from GlaxoSmithKline (Research Triangle Park, NC). ^{3}H-cimetidine (25.0 Ci/mmol) and ^{14}C-diazepam (56.0 mCi/mmol) were purchased from Amersham Biosciences (Buckinghamshire, UK). ^{14}C-inulin (2.1 mCi/g) was purchased from

American Radiolabeled Chemical Inc. (St Louis, MO). ^{3}H-inulin (180.0 mCi/g) and ^{3}H-colchicine (80.4 Ci/mmol) were purchased from PerkinElmer (Waltham, MA). All of the other chemicals were commercially available and of reagent grade.

Cell Culture

Madin-Darby canine kidney (MDCKII) cells stably expressing either murine wild-type *Abcg2* (Bcrp1) or human wild-type *ABCB1* (P-gp) were obtained from the Netherlands Cancer Institute under a Materials Transfer Agreement. MDCK cells were maintained at 37^{o}C in humidified 5% CO_2/95% air using Eagle's MEM culture medium supplemented with 10% (v/v) fetal bovine serum, penicillin, and streptomycin. A 1:10 split was done twice per week and cells at passage 7-10 (Bcrp) or 20-30 (P-gp) were plated at 50,000 cells/cm^2 in 12-well Transwell filter inserts (1.13 cm^2 surface area). Medium was changed on days 3 and 5 and the cell monolayers used on day 6.

Bi-directional Flux Experiments *In vitro*

Cells were rinsed twice with Dulbecco's phosphate-buffered saline (PBS) containing 10 mM Hepes, pH 7.4. Some cells were pretreated twice for 15 min each with PBS containing either 2.5 μM of LSN335984, a close structural analog to zosuquidar (LY335979), to potently and selectively inhibit P-gp, or 20 μM chrysin, to specifically inhibit Bcrp. Transport was measured in both directions across uninhibited and inhibited cell monolayers using a substrate concentration of 5 μM diluted from a 10 mM DMSO stock solution (final DMSO concentration of 0.05%) and a single 60-min time interval (screening mode). The upper chamber (A) contained 0.5 mL PBS and the lower chamber (B) contained 1.0 mL PBS without and with inhibitor. The system was mixed using a

Clay-Adams Nutator® and kept at 37 C in room atmosphere. Solute concentration was determined for the donor and receiver solutions, and mass balance was achieved by extracting the cells with methanol. The apparent permeability coefficients (P_{app}) were estimated as the slope of the mass transported per 60 min relative to the total recovered mass according to Ho et al. (2000). BA/AB P_{app} ratios were calculated for each cell line. Cell monolayer integrity was monitored with percent leakage of ^{14}C-mannitol in the absence and presence of solute and DMSO. Positive controls run periodically included amprenavir for P-gp and prazosin for Bcrp with triamterene as control for a non-substrate. Experiments were done in duplicate at least twice. All test solutes were quantified by reverse-phase high performance liquid chromatography with detection by tandem mass spectrometry (HPLC/MS/MS) as detailed below.

In situ Mouse Brain Perfusion

The details of the *in situ* mouse brain perfusion have been described elsewhere (Dagenais et al., 2000a). Briefly, mice were anesthetized with ketamine/xylazine (100/10 mg/kg, i.p.). The right common carotid artery was cannulated with polyethylene tubing (0.30-mm inner diameter × 0.70-mm outer diameter; Biotrol Diagnostic, Chennevières-les-Louvres, France) following ligation of the external carotid artery. The cardiac ventricles were severed immediately before perfusion at 2.5 mL/min for 60 s via a syringe pump (Harvard Apparatus, Holliston, MA). The perfusion buffer (Krebs-bicarbonate buffer, with 9 mM of D-glucose, pH 7.4) was oxygenated with 95% O_2 and 5% CO_2 and maintained at 37°C. ^{14}C-diazepam and ^{3}H- or ^{14}C-inulin were used as blood flow rate and vascular space markers, respectively. The test compounds, ^{3}H-cimetidine (1.6 μCi/mL), ^{14}C-LY2228820 (0.1 μCi/mL), alfuzosin (2 μM) or dipyridamole (1, 2, 5 μM) was added

to the perfusate to achieve appropriate concentrations. GF120918 and dipyridamole were dissolved in DMSO. The final concentration of DMSO in the perfusate was less than 2%. GF120918 (2 μM) was co-perfused with alfuzosin and dipyridamole to inhibit P-gp and Bcrp. The experiment was terminated by decapitation. The brain was carefully removed from the skull, cleaned of meninges and choroids plexus, the cerebellum was excised and the right brain hemisphere was collected. Aliquots of perfusate were collected from the catheter and weighed for determination of perfusate concentration.

All non-radioactive samples were analyzed by HPLC/MS/MS. Radioactive brain samples were digested in 0.7 mL Solvable® (Packard, Boston, MA) at 50 °C overnight. Five mL of UltimaGold® scintillation cocktail (PerkinElmer, Wellesley, MA) was added and vortex-mixed. Total radioactivity (^{3}H and/or ^{14}C) was determined in a Packard Tri-carb TR 1900 liquid scintillation analyzer (Packard, Boston, MA). Parameters related to the *in situ* mice brain perfusion, i.e., the cerebral vascular volume (mL/100 g brain) was calculated using equation: $V_{vasc} = \frac{X_{inulin}}{C_{inulin}}$; the initial brain uptake clearance (Cl_{up}, mL/min/100 g brain) were calculated as: $Cl_{up} = \frac{X_{brain}/T}{C_{perf}}$, where the amount of substrate in brain X_{brain} was corrected for residual blood contamination (Dagenais et al., 2000a).

Osmotic Minipump Studies

Mdr1a(+/+), *mdr1a(-/-)*, C57BL/6, and *Abcg2(-/-)* mice (n=3) were anesthetized with ketamine/xylazine (100/10 mg/kg, i.p.). An Alzet 2001D® osmotic minipump (Alza Corporation, Palo Alto, CA) was selected to release the drug continuously over 24 hr at a flow rate of 8 μl/h. The concentration of dosing solution was adjusted to the average

animal body weight and mean pump rate to deliver an appropriate dose. Cimetidine, alfuzosin and dipyridamole were dissolved in 50% DMSO and loaded into the minipumps. Cimetidine (200 μg/pump, approximately 6.4 mg/kg/day) was implanted subcutaneously in the back of C57BL/6 and *Abcg2*(-/-) mice. Alfuzosin (200 μg/pump, approximately 6.4 mg/kg/day) and two doses of dipyridamole (40 and 400 μg/pump, approximately 1.28 and 12.8 mg/kg/day, respectively, with the higher dose dissolved in 80% DMSO to ensure adequate solubility) were implanted subcutaneously in *mdr1a(+/+)*, *mdr1a(-/-)*, C57BL/6, and *Abcg2(-/-)* mice. The experiments were terminated at 24 hr by decapitation. The brain was removed carefully from the skull and weighed. Trunk blood was collected in heparinized 1.5-mL microcentrifuge tubes. Plasma was harvested following centrifugation at 3,000 rpm for 5 minutes. The plasma and brain samples were stored at -20°C until analysis by HPLC/MS/MS. To ensure a reliable drug release during the dosing period, the minipump was removed from the body and the residual volume was measured.

HPLC/MS/MS Assay

Two volumes of distilled water were added to brain samples and homogenized with brief probe sonication. Plasma, brain homogenate and perfusate samples were analyzed by HPLC/MS/MS (API 4000 triple quadrupole with TurboIonSpray interface; Applied Biosystems/MDS Sciex, Concord, ON, Canada). A 25-μL aliquot of brain hemisphere homogenate or plasma was transferred to an HPLC vial, and protein was precipitated with 100 μl of methanol containing internal standard (10 ng/mL loperamide), followed by a 25-μl aliquot of DMSO. The sample was vortex-mixed and centrifuged. Three microliters of sample solutions were injected via an autosampler (Leap, Carrboro, NC).

Cimetidine, alfuzosin, dipyridamole and the internal standard, loperamide, were eluted from an Aquasil C18 column (2.1 x 50 mm, d_p = 5 μm; Thermo Electron Corporation, Waltham, MA) using a mobile phase gradient (A, 0.1% formic acid in water; B, 0.1% formic acid in methanol; 0-0.70-min hold at 0% B, 0.70-3.12-min linear gradient to 90% B, 3.12-4.10 min hold at 90% B, 4.10-4.20-min linear gradient to 0% B, 4.20-4.90-min hold at 0% B; solvent delivery system (Shimadzu); flow rate = 0.75 ml/min; 0.8-4 min directed to mass spectrometer) and were detected in positive ion mode using multiple reaction monitoring: cimetidine: 253.1→117.0 *m*/*z*, alfuzosin, 390.2→235.2 *m*/*z*; dipyridamole, 505.5→429.3 *m*/*z*. All analytes were quantified with standard curves (0.05-5000 ng/ml) prepared in the appropriate matrix. The lower limit of detection was 0.1 ng/ml for all analytes; inter-and intraday CVs were <15%.

Statistical Analysis

Data are reported as mean ± SD for 3 mice per condition. Two-tailed student's t-test, one-way or two-way ANOVA, where appropriate, was used to determine the statistical significance of differences among two or more groups. The level of significance was corrected for multiple comparisons (e.g., Bonferroni test) or adjusted for unequal variance when necessary. In all cases, $p < 0.05$ was considered to be statistically significant.

Results

In vitro Transport

The basolateral-to-apical / apical-to-basolateral (B-A / A-B) P_{app} ratios for each of the four compounds tested ranged from 16 to 37, suggesting that each compound underwent carrier-mediated efflux across MDCKII-Bcrp cell monolayers. The positive control prazosin had a ratio of 27, which compared favorably to historical data (mean ± standard deviation) of 22 ± 7 (n=17). In addition, the B-A / A-B P_{app} ratios were decreased substantially (to 1.1 ~ 2.0) in the presence of the Bcrp inhibitor chrysin (Table 4.1). Prazosin efflux by MDCKII-Bcrp was not inhibited by the specific P-gp inhibitor LSN335984 (data not shown). Cellular substrate concentrations at equilibrium, estimated by methanol wash, of alfuzosin, dipyridamole, and ^{14}C-LY2228820, were decreased ~4 fold in Bcrp-expressing cells because of active efflux, whereas cellular cimetidine concentrations were very low and unaffected by Bcrp. Alfuzosin and dipyridamole also were identified as P-gp substrates when substrate flux was evaluated in the MDCK-MDR1 cell monolayer model, with P-gp-mediated transport inhibited by the P-gp inhibitor LSN335984 (Figure 4.1). In these cases, cellular concentrations at equilibrium were decreased 4- to 6-fold in the presence of Bcrp-mediated efflux. Amprenavir efflux by MDCKII-MDR1 wans not inhibited by the Bcrp inhibitor chrysin (data not shown).

In situ Brain Perfusion

^{14}C-inulin was used as a brain capillary space marker to assess BBB physical integrity. BBB integrity was not changed by knockout of the *mdr1a* or *Abcg2* gene or by co-perfusion with 2 μM GF120918. In addition, the brain capillary volumes in C57BL/6 and

Abcg2(-/-) mice were comparable to those in CF-1 mice. The cerebral blood flow rates in C57BL/6 and *Abcg2(-/-)* mice also were similar to that in CF-1 mice, measured using ^{14}C-diazepam as the marker (data not shown).

The values of initial brain uptake clearance of ^{3}H-cimetidine and ^{14}C-LY2228820 in all four mouse strains, i.e., C57BL/6 and *Abcg2(-/-)*, *mdr1a(+/+)* and *mdr1a(-/-)* mice, are presented in Table 4.2. Cimetidine does not cross the BBB to an appreciable extent. Cimetidine Cl_{up} increased by 33%, but did not reach statistical difference (1.1 ± 0.4 vs. 0.8 ± 0.3 mL/min/100 g, p>0.05) when co-perfused with 2 μM GF120918 in C57BL/6 mice. ^{14}C-LY2228820 is very permeable at the BBB. The initial rate of brain uptake in *mdr1a(-/-)* mice was close to the functional perfusate flow rate (250 ± 41 mL/min/100 g), and was 2.3-fold higher than that in *mdr1a(+/+)* mice (p<0.05). ^{14}C-LY2228820 was also perfused in *Abcg2(+/+)* mice and the Cl_{up} was 120 ± 9 mL/min/100g brain, which did not differ significantly from that in C57BL/6 and *Abcg2(-/-)* mice (136 ± 3 and 131 ± 26 mL/min/100 g, one-way ANOVA, p>0.05).

Alfuzosin brain uptake was moderate in all mouse strains. The inhibitory effect of GF120918 on P-gp- and/or Bcrp-mediated alfuzosin efflux is illustrated in Figure 4.3. Figure 4.3A showed alfuzosin brain uptake is comparable in C57BL/6 and *Abcg2(-/-)* mice in the absence of GF120918 (p>0.05). Co-perfusion with GF120918 significantly increased alfuzosin brain uptake in both C57BL/6 and *Abcg2(-/-)* mice (p<0.05, inhibitory effect), but to a greater extent in *Abcg2 (-/-)* mice (p<0.05, strain difference). The increased alfuzosin brain uptake can be ascribed to P-gp inhibition in the BBB by GF120918. Figure 4.3B demonstrates that alfuzosin brain uptake increased ~3.7-fold in *mdr1a(-/-)* mice compared to *mdr1a(+/+)* mice (p<0.05). Consistently, alfuzosin brain

uptake increased about 4.4-fold with GF120918 co-perfusion in *mdr1a(+/+)* mice (p<0.05). GF120918 had no effect on alfuzosin brain uptake in *mdr1a(-/-)* mice.

Three concentrations (1, 2, and 5 μM) of dipyridamole were perfused in C57BL/6 and *Abcg2(-/-)* mice, respectively (Figure 4.4). Two-way ANOVA analysis indicated that there was no statistical differences between these two mouse strains at any of the concentrations tested, or among concentrations in any mouse strain (p>0.05).

Figure 4.5 depicts dipyridamole brain uptake when perfused at 2 μM in the absence or presence of 2 μM GF120918 in all four mouse strains. Dipyridamole brain uptake did not differ between C57BL/6 and *Abcg2(-/-)* mice, or between *mdr1a(+/+)* and *mdr1a(-/-)* mice. Figure 4.5A illustrates dipyridamole brain uptake was increased by 2.2-fold in the presence of 2 μM GF120918 co-perfusion in both C57BL/6 and *Abcg2(-/-)*, respectively (two-way ANOVA, p<0.05). Co-perfusion of GF120918 increased dipyridamole brain uptake by 1.4-fold in *mdr1a(+/+)* and *mdr1a(-/-)* mice, although the differences were not statistically significant (p>0.05; two-way ANOVA, Figure 4.5B).

Osmotic Minipump Studies

The vehicle, DMSO, up to 50% in water has been reported to be compatible with the minipump (www.alzet.com). The osmotic minipumps provided reliable delivery of cimetidine, alfuzosin, and dipyridamole (at dose of 1.28 mg/kg/day). However, with the dipyridamole administration rate of 12.8 mg/kg/day, precipitation was visible around the exit hole of the device at the end of the experiment. Cimetidine brain-to-plasma concentration ratios were 0.024 ± 0.005 and 0.020 ± 0.017 in C57BL/6 and *Abcg2*(-/-) mice, respectively (Student's *t*-test, p>0.05). The plasma and brain concentrations were

highly variable with dipyridamole dose of 12.8 mg/kg/day, so only the brain-to-plasma concentration ratios of alfuzosin and dipyridamole (1.28 mg/kg/day) are shown in Figure 4.6. Alfuzosin brain penetration was significantly higher (4.1-fold) in *mdr1a(-/-)* mice compared to *mdr1a(+/+)* mice (Student's *t*-test, $p<0.05$). Alfuzosin and dipyridamole brain penetration was ~3.5-fold higher in *Abcg2(-/-)* mice compared to C57BL/6 mice, although these differences did not achieve statistical significance. In addition, dipyridamole brain penetration at 1.28 mg/kg/day was comparable between *mdr1a(+/+)* and *mdr1a(-/-)* mice (Student's *t*-test, $p>0.05$). Although dipyridamole plasma and brain concentrations at a dose rate of 12.8 mg/kg/day were highly variable (no statistical analysis was conducted for these data), the trend suggested that brain concentrations exceeded plasma concentrations in all mouse strains. Overall, brain penetration of dipyridamole appeared to be higher at 12.8 mg/kg/day than at 1.28 mg/kg/day (data not shown).

Discussion

Bcrp mediates intestinal and biliary secretion, substrate extrusion at mammary epithelia and in the placenta, and plays an important pharmacologic and toxicologic role in the absorption and disposition of xenobiotics and xenotoxins (Jonker et al., 2000; Jonker et al., 2005). However, the extent to which Bcrp might influence brain distribution of known Bcrp substrates has been unclear. The current study investigated the functional efficiency of Bcrp *in vitro*, *in situ* and *in vivo* using four model compounds: cimetidine, alfuzosin, dipyridamole and ^{14}C-LY2228820.

Asymmetric transport of cimetidine was mediated by Bcrp in transfected MDCK cell lines (Table 4.1), as evidenced by a B-A / A-B P_{app} ratio of 16. Under similar experimental conditions, a B-A / A-B P_{app} ratio of ~9 has been reported (Pavek et al., 2005). Cimetidine was transported actively by Bcrp in an MDCKII-Bcrp1 cell line as well as in rat and mouse liver and rat placenta (McNamara et al., 1996; Merino et al., 2005; Staud et al., 2006). However, in the current study *Abcg2* gene knockout did not change the initial rate of brain uptake or steady-state brain distribution using *in situ* brain perfusion and *in vivo* brain penetration paradigms. In addition, cimetidine brain uptake was independent of P-gp and Bcrp inhibition by GF120918. Furthermore, cimetidine brain penetration was minimal during a 24-hr continuous subcutaneous infusion, and steady-state brain-to-plasma concentration ratios in C57BL/6 and *Abcg2*(-/-) mice were similar to a previously published value of 0.017 after i.p. injection of cimetidine (100 mg/kg) in rats (Hough et al., 1986). The present results indicate that Bcrp does not pose a substantial barrier for cimetidine brain uptake, and that the poor brain penetration of cimetidine is primarily due to low passive permeability.

This study constitutes the first investigation of alfuzosin interaction with ABC efflux transporters. Alfuzosin Cl_{up} and brain-to-plasma concentration ratio in *mdr1a(-/-)* mice were 4.4- and 4.1-fold higher than those in *mdr1a(+/+)* mice, respectively. In addition, P-gp-mediated alfuzosin efflux was inhibited by GF120918 in *mdr1a(+/+)*, C57BL/6 and *Abcg2(-/-)* mice, but not in *mdr1a(-/-)* mice, which confirmed that alfuzosin is a P-gp substrate at the BBB. In contrast, alfuzosin appears to be transported efficiently by Bcrp only when Bcrp is overexpressed *in vitro*. Alfuzosin Cl_{up} and brain-to-plasma concentration ratio was comparable between C57BL/6 and *Abcg2(-/-)* mice and co-perfusion with GF120918 did not increase alfuzosin Cl_{up} in *mdr1a(-/-)* mice. Taken together, these data indicate that alfuzosin is not transported by Bcrp at the BBB. In all mouse strains, alfuzosin did not cross the BBB substantially, and brain concentrations were much lower than plasma concentrations.

Dipyridamole has been reported to be a substrate of human Bcrp in both HEK and MDCK cell lines stably-transfected with human BCRP (Zhang et al., 2005b). The current study confirms that dipyridamole interacts with murine Bcrp and human P-gp *in vitro* (Table 4.1 and Figure 4.1). Brain uptake of dipyridamole was not concentration-dependent in the range of 1-5 μM (a range selected based on a reported mean dipyridamole clinical plasma concentration of 3.5 μM (1.77 μg/mL; (Hervey and Goa, 1999). In addition, brain penetration did not vary between mouse strains (C57BL/6 versus *Abcg2(-/-)* mice). Co-perfusion with GF120918 did not increase brain uptake in *mdr1a(-/-)* mice, animals that express Bcrp, but not P-gp, at the BBB. Thus, Bcrp cannot be an important factor in determining dipyaridamole brain uptake. In addition, the initial rate of

dipyridamole brain uptake did not differ between *mdr1a(+/+)* and *mdr1a(-/-)* mice, suggesting that dipyridamole is not transported by P-gp at the mouse BBB.

Co-perfusion with GF120918 caused a modest but significant increase in dipyridamole Cl_{up} in C57BL/6 and *Abcg2(-/-)* mice, suggesting the possibility of an unknown GF120918-sensitive mechanism other than P-gp- or Bcrp-mediated transport, that influences dipyridamole flux across the BBB. Interestingly, brain penetration of dipyridamole following a 24-hr continuous subcutaneous infusion was dose-dependent (data not shown), while a tendency towards concentration-dependent uptake in Bcrp-competent, but not Bcrp-deficient, mice during brain perfusion was not statistically significant (Figure 4.4). Under the current osmotic minipump experimental paradigm, dipyridamole plasma concentration at 24 hr was about 28.2 ng/ml (~56 nM), which was significantly lower than clinically-relevant concentrations ~3.5 μM (Hervey and Goa, 1999) or the concentrations (1-5 μM) evaluated in the current brain perfusion study. Brain penetration increased when dipyridamole dose was increased from 1.28 mg/kg/day to 12.8 mg/kg/day, suggesting that dipyridamole brain penetration may be mediated by unknown saturable and high-affinity efflux transport mechanism(s), which likely is the same mechanism inhibited by GF120918 *in situ*.

Efflux of ^{14}C-LY2228820 was mediated by Bcrp *in vitro*. ^{14}C-LY2228820 transport across the BBB was highly permeable, consistent with the rapid passive diffusion observed in *in vitro* cell monolayers. Brain uptake of ^{14}C-LY2228820 was almost perfusion flow rate-limited in *mdr1a(-/-)* mice. In *mdr1a(+/+)* mice, ^{14}C-LY2228820 brain uptake decreased about almost 60%. ^{14}C-LY2228820 brain uptake in *Abcg2(+/+)*

mice was comparable to C57BL/6 and *Abcg2(-/-)* mice, indicating that ^{14}C-LY2228820 brain uptake is not limited by Bcrp.

Taken together, all four model compounds appeared to interact with Bcrp in the MDCK-Bcrp cell line *in vitro*. However, none was transported by Bcrp at the mouse BBB, using the genetic knockout models, i.e., Bcrp-competent [C57BL/6, *Abcg2(+/-)*] and Bcrp-deficient [*Abcg2(-/-)*], as well as P-gp-competent [*mdr1a(+/+)*] and P-gp-deficient [*mdr1a(-/-)*] mouse models for comparison, or chemical inhibition with GF120918, an inhibitor of P-gp and Bcrp. It is widely accepted that genetic knockout models are equivalent and essentially interchangeable with specific chemical knockout models, especially for cases in which the desired genetic knockout models are not available, as is most common in rat studies. However, the compensatory regulation of other transporter proteins following knockout of specific gene, as well as the specificity of inhibitors, are always fundamental concerns in the functional studies. Bcrp mRNA has been reported to be upregulated in *mdr1a(-/-)* mice, and was 3-fold higher than that in *mdr1a(+/+)* mice (Cisternino et al., 2004). Other evidence suggested that mRNA levels of *mdr1a*, *Mrp1*, *Mrp4* and *oatp2* were not changed in Bcrp knockout mice (Lee et al., 2005). Similarly, chemical inhibitors such as PSC833 for P-gp, probenecid for Mrps, and GF120918 for both P-gp and Bcrp are widely used in the literature. Cyclosporine A which has long been regarded as a specific P-gp inhibitor, has recently been demonstrated to inhibit Bcrp and OATPs (Xia et al., 2007). In a quercetin *in situ* rat brain perfusion study, co-perfusion with the P-gp inhibitor PSC833 did not change Cl_{up} of quercetin, while co-perfusion of P-gp/Bcrp inhibitor GF120918 significantly enhanced brain uptake of quercetin (Youdim et al., 2004). The authors concluded that Bcrp was involved in quercetin brain uptake. In the

absence of appropriate comparisons with a genetic knockout model, or information regarding the specificity of a given inhibitor for a transporter, such a conclusion is potentially erroneous.

In situ brain perfusion has been used efficiently to measure BBB permeability, which has been demonstrated to be dependent on the lipophilicity and protein binding in brain tissue for compounds that undergo solely passive diffusion at the BBB (Takasato et al., 1984; Summerfield et al., 2007). Figure 4.7A demonstrates that in the absence of P-gp, the Cl_{up} values for cimetidine, alfuzosin, dipyridamole and LY2228820 in *mdr1a(-/-)* mice were correlated (R^2=0.956) with $clogD_{7.4}$, the calculated logarithm of octanol water partition coefficient at pH 7.4 (the values of $clogD_{7.4}$ are 0.12, 0.56, 3, 6.3 for cimetidine, alfuzosin, dipyridamole and LY2228820, respectively), which were obtained using Marvin and calculator plugin freeware (www.chemaxon.com, ChemAxon Kft, Budapest, Hungary). In addition, the *in situ* brain permeability has been found to be correlated with *in vitro* apparent permeability (Summerfield et al., 2007). There is a good correlation between the Cl_{up} values and the $P_{app,AB}$ or $P_{app,BA}$ in MDCKII-Bcrp cell line when Bcrp was completely inhibited by chrysin (Figure 4.7B). In addition, Cl_{up} is correlated with the cellular accumulation (R^2=0.952, Figure 4.7C). These correlation analyses indicated that the cell line model may serve as a high-throughput *in vitro* system to predict passive permeability and contribute to improved compound selection in CNS drug discovery and development.

A recent observation demonstrated that the protein expression of Bcrp in human and rat brain microvessel endothelial cells is much lower than in the *in vitro* overexpressed system (Lee et al., 2007). This difference in protein expression might explain the

discrepancies between the *in vitro* cell line model and *in situ* or *in vivo* animal models. As an overexpressed cell line model, good *in vitro-in vivo* correlation has been identified for P-gp efflux ratio in the brain (Adachi et al., 2001), in which P-gp is abundantly expressed.

In summary, the results of the present study suggest that Bcrp plays a minor role in brain distribution of cimetidine, alfuzosin, dipyridamole and LY2228820, although each of these compounds interacted with Bcrp in transfected cell line models. Together with previously published data on prazosin, DHEAS and mitoxantrone (Cisternino et al., 2004; Lee et al., 2005), these results strongly suggest that Bcrp does not contribute significantly to murine BBB function. The present results also raise the related question of the specific role of organic anion transporters (Mrp1, Mrp2 and Mrp4) in the overall barrier function at the blood-brain interface. It has been shown that inhibition of Mrp2 and Mrp4 significantly enhanced brain exposure of antiepileptic drugs, topotecan and nucleotides; however, the efflux effects observed were modest and all less than 2-fold (Potschka et al., 2003; Leggas et al., 2004; Belinsky et al., 2007). The spectrum of reports to date suggest that is likely that P-gp, but not other ABC efflux transporters, provides the primary transport-mediated attenuation of brain uptake in the intact BBB. Caution must be taken in the design and interpretation of *in vitro* and *in situ* experiments prior to assigning specific functional importance to a given efflux transport system in the *in vivo* situation. In this regard, the current results with alfuzosin may serve as a useful template. These experiments demonstrated that alfuzosin is a P-gp substrate, with a 4-fold P-gp effect at the BBB. This P-gp effect was observed consistently among *in vitro*, *in situ* and *in vivo* experiments. This type of information set should be available for a given

substrate/transport protein pair prior to ascribing functional *in vivo*, and potential pharmacologic/toxicologic importance, to that transport protein *in vivo*.

References

Adachi Y, Suzuki H and Sugiyama Y (2001) Comparative studies on in vitro methods for evaluating in vivo function of MDR1 P-glycoprotein. *Pharm Res* **18:**1660-1668.

Aronica E, Gorter JA, Redeker S, van Vliet EA, Ramkema M, Scheffer GL, Scheper RJ, van der Valk P, Leenstra S, Baayen JC, Spliet WG and Troost D (2005) Localization of breast cancer resistance protein (BCRP) in microvessel endothelium of human control and epileptic brain. *Epilepsia* **46:**849-857.

Begley DJ (2004) Delivery of therapeutic agents to the central nervous system: the problems and the possibilities. *Pharmacol Ther* **104:**29-45.

Belinsky MG, Guo P, Lee K, Zhou F, Kotova E, Grinberg A, Westphal H, Shchaveleva I, Klein-Szanto A, Gallo JM and Kruh GD (2007) Multidrug resistance protein 4 protects bone marrow, thymus, spleen, and intestine from nucleotide analogue-induced damage. *Cancer Res* **67:**262-268.

Bihorel S, Camenisch G, Lemaire M and Scherrmann JM (2007) Influence of breast cancer resistance protein (Abcg2) and p-glycoprotein (Abcb1a) on the transport of imatinib mesylate (Gleevec((R))) across the mouse blood-brain barrier. *J Neurochem* **102:**1749-1757.

Breedveld P, Pluim D, Cipriani G, Wielinga P, van Tellingen O, Schinkel AH and Schellens JH (2005) The effect of Bcrp1 (Abcg2) on the in vivo pharmacokinetics and brain penetration of imatinib mesylate (Gleevec): implications for the use of breast cancer resistance protein and P-glycoprotein inhibitors to enable the brain penetration of imatinib in patients. *Cancer Res* **65:**2577-2582.

Cisternino S, Mercier C, Bourasset F, Roux F and Scherrmann JM (2004) Expression, up-regulation, and transport activity of the multidrug-resistance protein Abcg2 at the mouse blood-brain barrier. *Cancer Res* **64:**3296-3301.

Cooray HC, Blackmore CG, Maskell L and Barrand MA (2002) Localisation of breast cancer resistance protein in microvessel endothelium of human brain. *Neuroreport* **13:**2059-2063.

Dagenais C, Rousselle C, Pollack GM and Scherrmann JM (2000) Development of an in situ mouse brain perfusion model and its application to mdr1a P-glycoprotein-deficient mice. *J Cereb Blood Flow Metab* **20:**381-386.

Doyle LA, Yang W, Abruzzo LV, Krogmann T, Gao Y, Rishi AK and Ross DD (1998) A multidrug resistance transporter from human MCF-7 breast cancer cells. *Proc Natl Acad Sci U S A* **95:**15665-15670.

Eisenblatter T and Galla HJ (2002) A new multidrug resistance protein at the blood-brain barrier. *Biochem Biophys Res Commun* **293:**1273-1278.

Eisenblatter T, Huwel S and Galla HJ (2003) Characterisation of the brain multidrug resistance protein (BMDP/ABCG2/BCRP) expressed at the blood-brain barrier. *Brain Res* **971:**221-231.

Guay DR (2004) Extended-release alfuzosin hydrochloride: a new alpha-adrenergic receptor antagonist for symptomatic benign prostatic hyperplasia. *Am J Geriatr Pharmacother* **2:**14-23.

Hervey PS and Goa KL (1999) Extended-release dipyridamole/aspirin. *Drugs* **58:**469-475; discussion 476-467.

Hough LB, Glick SD and Su K (1986) Cimetidine penetrates brain and inhibits non-opiate footshock-induced analgesia. *Pharmacol Biochem Behav* **24:**1257-1261.

Jonker JW, Merino G, Musters S, van Herwaarden AE, Bolscher E, Wagenaar E, Mesman E, Dale TC and Schinkel AH (2005) The breast cancer resistance protein BCRP (ABCG2) concentrates drugs and carcinogenic xenotoxins into milk. *Nat Med* **11:**127-129.

Jonker JW, Smit JW, Brinkhuis RF, Maliepaard M, Beijnen JH, Schellens JH and Schinkel AH (2000) Role of breast cancer resistance protein in the bioavailability and fetal penetration of topotecan. *J Natl Cancer Inst* **92:**1651-1656.

Lee G, Babakhanian K, Ramaswamy M, Prat A, Wosik K and Bendayan R (2007) Expression of the ATP-binding Cassette Membrane Transporter, ABCG2, in Human and Rodent Brain Microvessel Endothelial and Glial Cell Culture Systems. *Pharm Res*.

Lee YJ, Kusuhara H, Jonker JW, Schinkel AH and Sugiyama Y (2005) Investigation of efflux transport of dehydroepiandrosterone sulfate and mitoxantrone at the mouse blood-brain barrier: a minor role of breast cancer resistance protein. *J Pharmacol Exp Ther* **312:**44-52.

Lefranc F, Yeaton P, Brotchi J and Kiss R (2006) Cimetidine, an unexpected anti-tumor agent, and its potential for the treatment of glioblastoma (review). *Int J Oncol* **28:**1021-1030.

Leggas M, Adachi M, Scheffer GL, Sun D, Wielinga P, Du G, Mercer KE, Zhuang Y, Panetta JC, Johnston B, Scheper RJ, Stewart CF and Schuetz JD (2004) Mrp4 confers resistance to topotecan and protects the brain from chemotherapy. *Mol Cell Biol* **24:**7612-7621.

Maliepaard M, van Gastelen MA, de Jong LA, Pluim D, van Waardenburg RC, Ruevekamp-Helmers MC, Floot BG and Schellens JH (1999) Overexpression of the BCRP/MXR/ABCP gene in a topotecan-selected ovarian tumor cell line. *Cancer Res* **59:**4559-4563.

Marbury TC, Blum RA, Rauch C and Pinquier JL (2002) Pharmacokinetics and safety of a single oral dose of once-daily alfuzosin, 10 mg, in male subjects with mild to severe renal impairment. *J Clin Pharmacol* **42:**1311-1317.

McNamara PJ, Meece JA and Paxton E (1996) Active transport of cimetidine and ranitidine into the milk of Sprague Dawley rats. *J Pharmacol Exp Ther* **277:**1615-1621.

Merino G, van Herwaarden AE, Wagenaar E, Jonker JW and Schinkel AH (2005) Sex-dependent expression and activity of the ATP-binding cassette transporter breast cancer resistance protein (BCRP/ABCG2) in liver. *Mol Pharmacol* **67:**1765-1771.

Pardridge WM (2005) The blood-brain barrier: bottleneck in brain drug development. *NeuroRx* **2:**3-14.

Pavek P, Merino G, Wagenaar E, Bolscher E, Novotna M, Jonker JW and Schinkel AH (2005) Human breast cancer resistance protein: interactions with steroid drugs, hormones, the dietary carcinogen 2-amino-1-methyl-6-phenylimidazo(4,5-b)pyridine, and transport of cimetidine. *J Pharmacol Exp Ther* **312:**144-152.

Potschka H, Fedrowitz M and Loscher W (2003) Multidrug resistance protein MRP2 contributes to blood-brain barrier function and restricts antiepileptic drug activity. *J Pharmacol Exp Ther* **306:**124-131.

Schinkel AH (1999) P-Glycoprotein, a gatekeeper in the blood-brain barrier. *Adv Drug Deliv Rev* **36:**179-194.

Soontornmalai A, Vlaming ML and Fritschy JM (2006) Differential, strain-specific cellular and subcellular distribution of multidrug transporters in murine choroid plexus and blood-brain barrier. *Neuroscience* **138:**159-169.

Staud F, Vackova Z, Pospechova K, Pavek P, Ceckova M, Libra A, Cygalova L, Nachtigal P and Fendrich Z (2006) Expression and transport activity of breast cancer resistance protein (Bcrp/Abcg2) in dually perfused rat placenta and HRP-1 cell line. *J Pharmacol Exp Ther* **319:**53-62.

Summerfield SG, Read K, Begley DJ, Obradovic T, Hidalgo IJ, Coggon S, Lewis AV, Porter RA and Jeffrey P (2007) Central nervous system drug disposition: the relationship between in situ brain permeability and brain free fraction. *J Pharmacol Exp Ther* **322:**205-213.

Takasato Y, Rapoport SI and Smith QR (1984) An in situ brain perfusion technique to study cerebrovascular transport in the rat. *Am J Physiol* **247:**H484-493.

Tanaka Y, Slitt AL, Leazer TM, Maher JM and Klaassen CD (2005) Tissue distribution and hormonal regulation of the breast cancer resistance protein (Bcrp/Abcg2) in rats and mice. *Biochem Biophys Res Commun* **326:**181-187.

Verstuyft C, Strabach S, El-Morabet H, Kerb R, Brinkmann U, Dubert L, Jaillon P, Funck-Brentano C, Trugnan G and Becquemont L (2003) Dipyridamole enhances digoxin bioavailability via P-glycoprotein inhibition. *Clin Pharmacol Ther* **73:**51-60.

Xia CQ, Liu N, Miwa GT and Gan LS (2007) Interactions of cyclosporin a with breast cancer resistance protein. *Drug Metab Dispos* **35:**576-582.

Youdim KA, Qaiser MZ, Begley DJ, Rice-Evans CA and Abbott NJ (2004) Flavonoid permeability across an in situ model of the blood-brain barrier. *Free Radic Biol Med* **36:**592-604.

Yousif S, Marie-Claire C, Roux F, Scherrmann JM and Decleves X (2007) Expression of drug transporters at the blood-brain barrier using an optimized isolated rat brain microvessel strategy. *Brain Res* **1134:**1-11.

Zamek-Gliszczynski MJ, Nezasa K, Tian X, Kalvass JC, Patel NJ, Raub TJ and Brouwer KL (2006) The important role of Bcrp (Abcg2) in the biliary excretion of sulfate

and glucuronide metabolites of acetaminophen, 4-methylumbelliferone, and harmol in mice. *Mol Pharmacol* **70:**2127-2133.

Zhang Y, Gupta A, Wang H, Zhou L, Vethanayagam RR, Unadkat JD and Mao Q (2005) BCRP transports dipyridamole and is inhibited by calcium channel blockers. *Pharm Res* **22:**2023-2034.

Table 4.1: Transport of ^{3}H-cimetidine, alfuzosin, dipyridamole and ^{14}C-LY2228820 (all at 5 μM) across MDCKII-Bcrp cell monolayer in the absence (-) or presence (+) of Bcrp inhibitor chrysin (20 μM). Mass recoveries were 92 to 112%.

Compound Name	Inhibitor	P_{app} ± SD ($\times 10^{-6}$ cm/s)		B-A/A-B P_{app} ratio
		A-B	B-A	
Cimetidine	-	1.4 ± 0.2	23 ± 2	16
	+	1.8 ± 0.2	3.6 ± 0.3	2.0
Alfuzosin	-	1.9 ± 0.002	60 ± 1	31
	+	25 ± 1	30 ± 2	1.2
Dipyridamole	-	2.6 ±1 .0	90 ± 0.3	34
	+	48 ± 1	70 ± 3	1.5
LY2228820	-	3.9 ± 0.2	143 ± 1	37
	+	44 ± 3	50 ± 8	1.1

Table 4.2: Initial brain uptake clearance (Cl_{up}, mL/min/100 g) for ^{3}H-cimetidine and ^{14}C-LY2228820 in C57BL/6, *Abcg2(-/-)* mice, *mdr1a(+/+)* and *mdr1a(-/-)* mice. Data are presented as mean ± SD (n=3). Two-tailed student's *t*-tests were used to determine the statistical significance of the Bcrp effect between C57BL/6 and *Abcg2*(-/-) mice, and P-gp effect between *mdr1a(+/+)* and *mdr1a(-/-)* mice. Asterisk (*) represents a statistical difference ($p<0.05$) between *mdr1a(+/+)* and *mdr1a(-/-)* mice for ^{14}C-LY2228820 initial brain uptake.

Cl_{up} (mL/min/100g)	C57BL/6	*Bcrp(-/-)*	*mdr1a(+/+)*	*mdr1a(-/-)*
Cimetdine	0.8 ± 0.3	0.5 ± 0.1	0.7 ± 0.2	1.1 ± 0.4
LY2228820	136 ± 33	131 ± 26	104 ± 8	239 ± 24 *

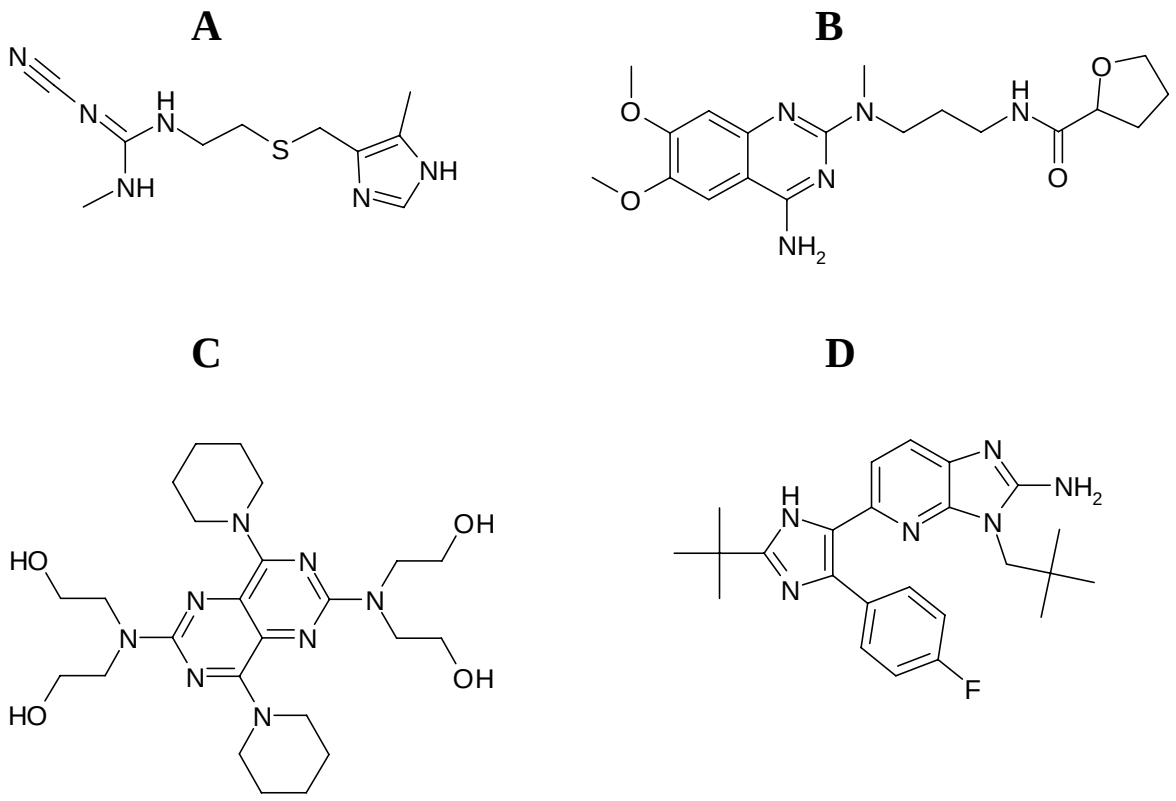

Figure 4.1: Chemical structures of cimetidine (A), alfuzosin (B), dipyridamole (C) and LY2228820 (D).

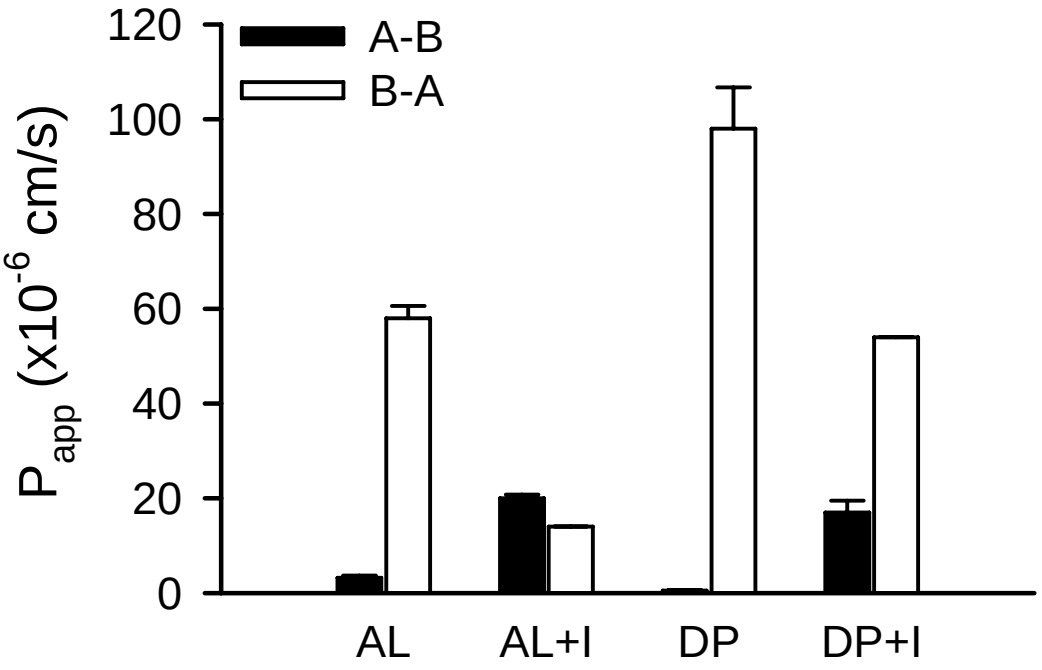

Figure 4.2: Apparent permeability (P_{app}, $\times 10^{-6}$ cm/s) of alfuzosin (AL) and dipyridamole (DP) across the MDCKII-MDR1 cell monolayer in apical-to-basolateral (A-B, solid bar) and basolateral-to-apical (B-A, open bar) directions in the absence (AL, DP) or presence (AL+I, DP+I) of P-gp inhibitor LSN335984 (2.5 μM).

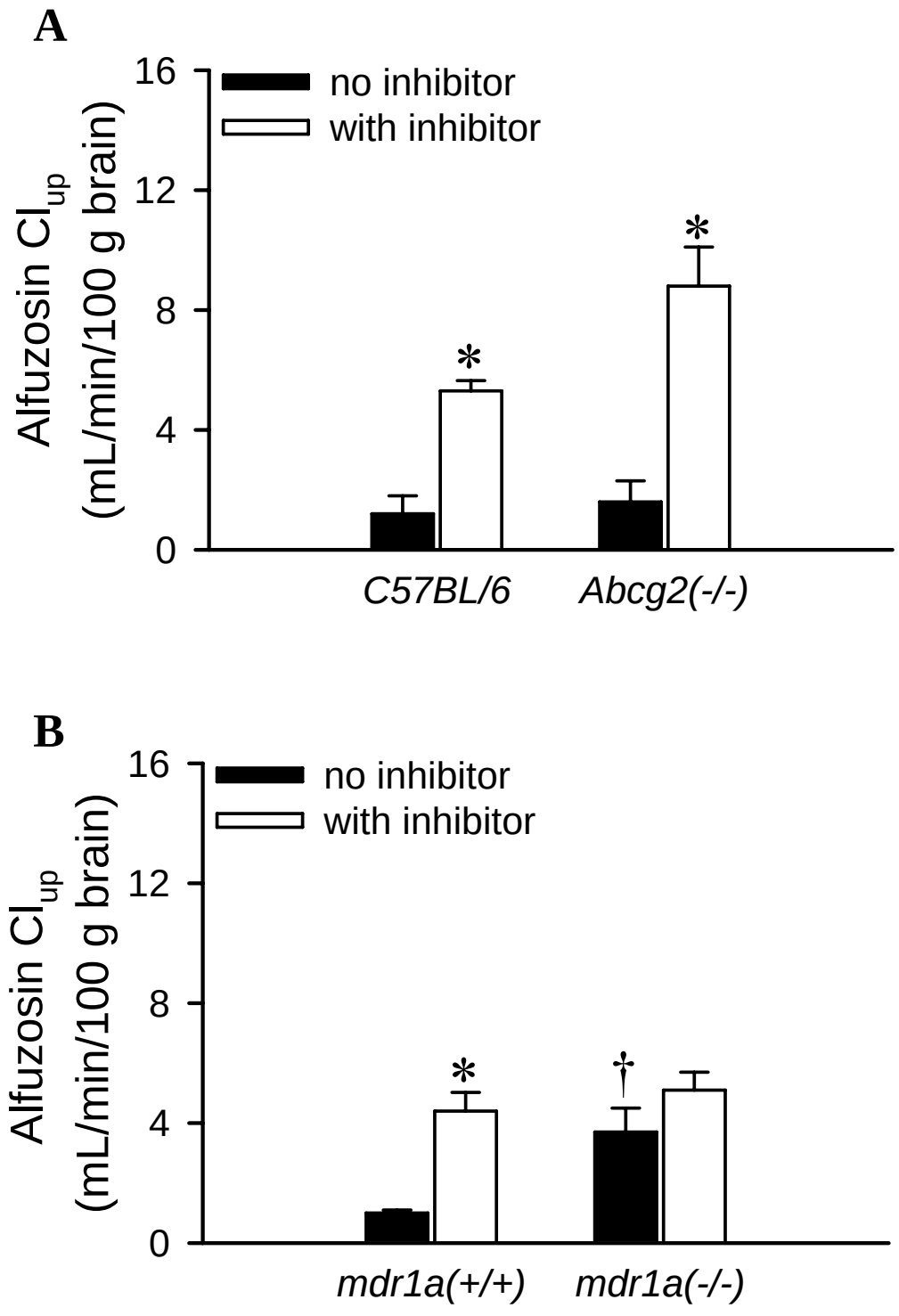

Figure 4.3: Initial brain uptake clearance (Cl_{up}, mL/min/100 g brain) of alfuzosin in the absence (solid bar) and presence (open bar) of co-perfusion with P-gp and Bcrp inhibitor

GF120918 in (A) C57BL/6 and *Abcg2(-/-)* mice, (B) *mdr1a(+/+)* and *mdr1a(-/-)* mice. Two-way ANOVA analysis was used to determine the statistical significance of GF120918 inhibitory effect and Bcrp effect [C57BL/6 vs. *Abcg2(-/-)*] or P-gp effect [*mdr1a(+/+)* vs. *mdr1a(-/-)*]. Asterisk (*) represents a statistical difference ($p<0.05$) with GF120918 inhibition ; dagger (†) represents a statistical difference ($p<0.05$) in the initial rate of alfuzosin brain uptake between *mdr1a(+/+)* and *mdr1a(-/-)* mice.

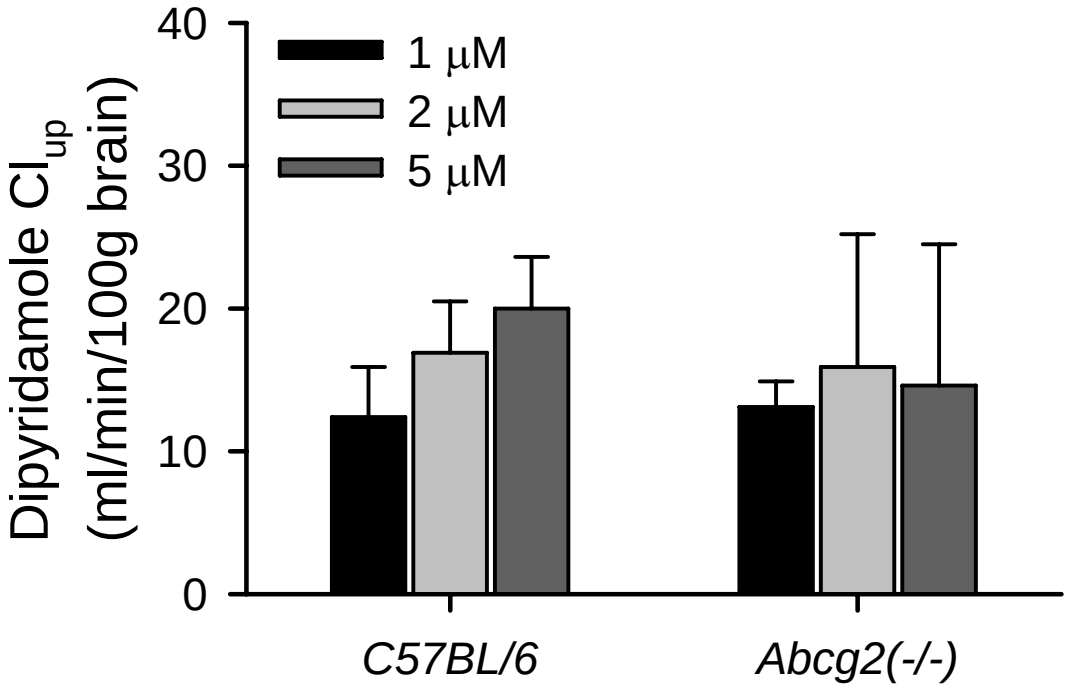

Figure 4.4: Initial brain uptake clearance (Cl_{up}, mL/min/100 g) for dipyridamole at different concentrations (1, 2, and 5 μM) in C57BL/6 and *Abcg2(-/-)* mice. Two-way ANOVA analysis was used to determine the statistical significance of concentration-dependence and Bcrp effect (p>0.05).

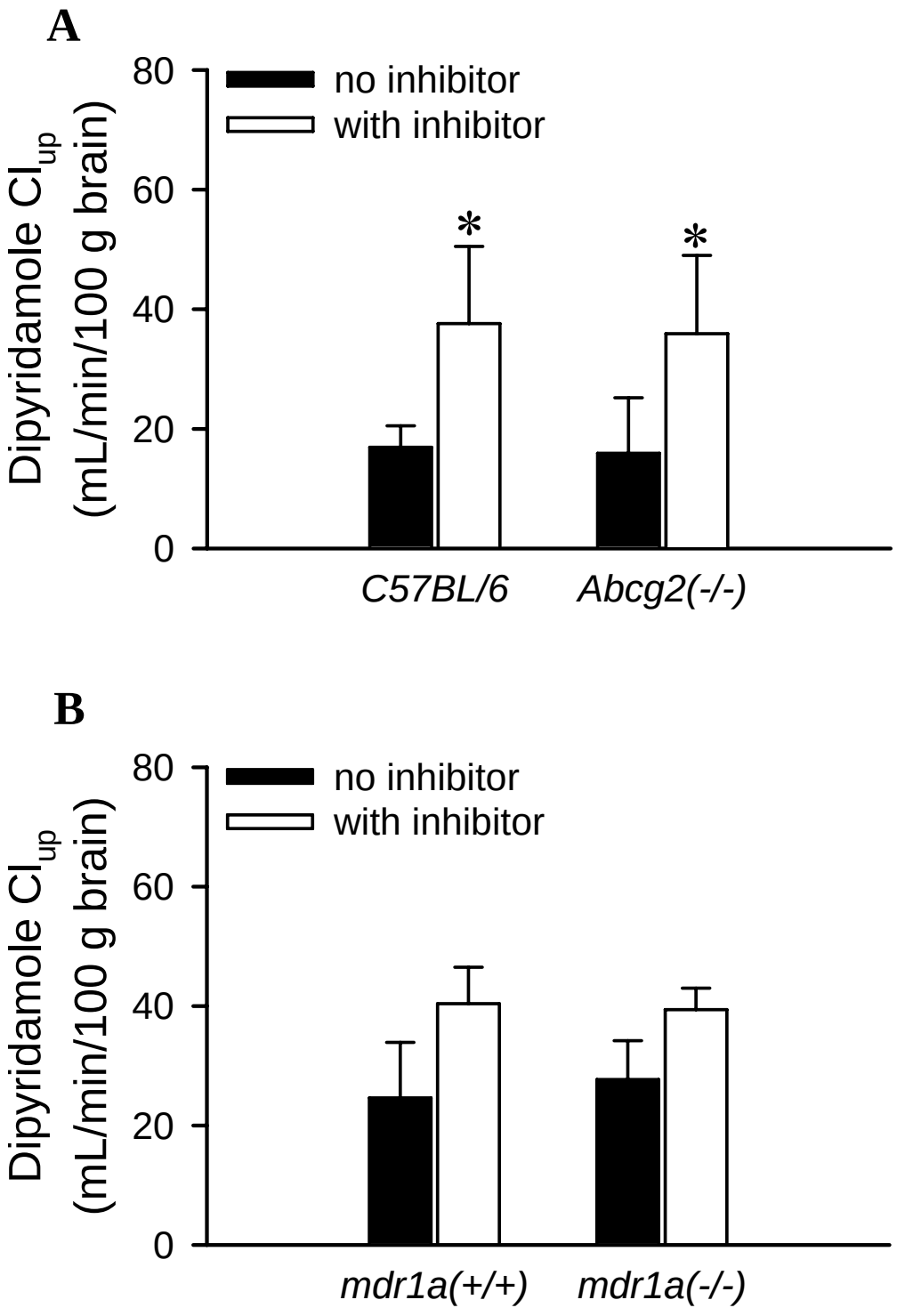

Figure 4.5: Initial brain uptake clearance (Cl_{up}, mL/min/100 g brain) of dipyridamole in the absence (solid bar) and presence (open bar) of co-perfusion with P-gp and Bcrp

inhibitor GF120918 in (A) C57BL/6 and *Abcg2(-/-)* mice, (B) *mdr1a(+/+)* and *mdr1a(-/-)* mice. Two-way ANOVA analysis was used to determine the statistical significance of GF120918 inhibitory effect and Bcrp effect [C57BL/6 vs. *Abcg2(-/-)*] or P-gp effect [*mdr1a(+/+)* vs. *mdr1a(-/-)*]. Asterisk (*) represents a statistical difference ($p<0.05$) with GF120918 inhibition.

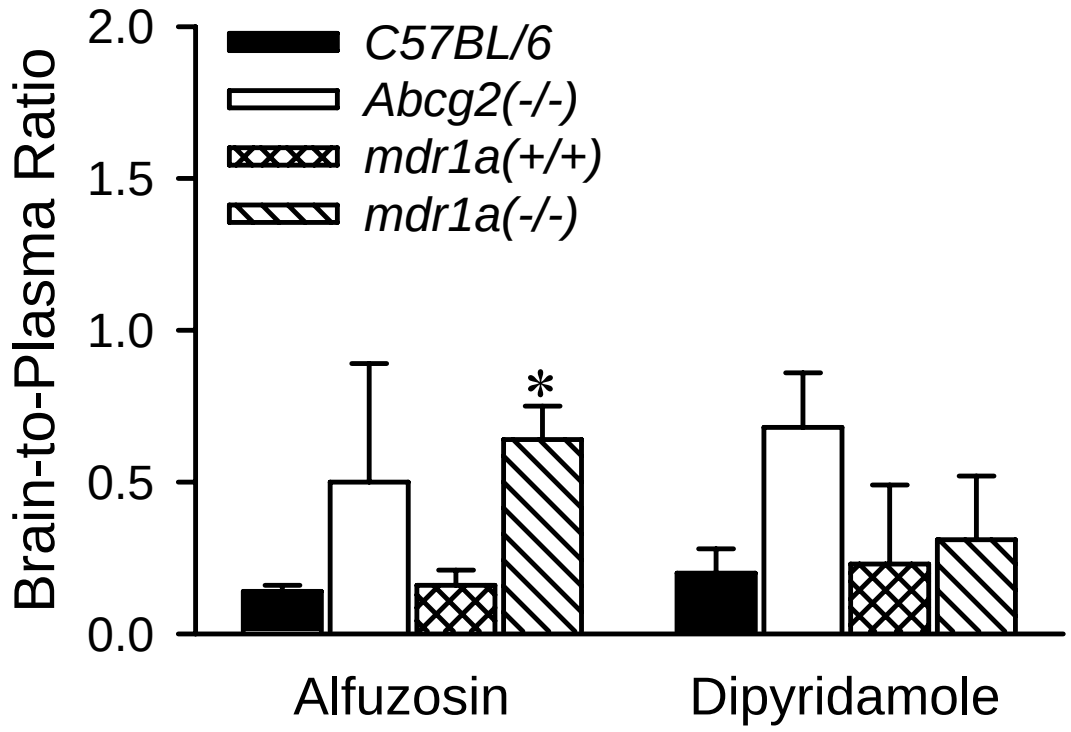

Figure 4.6: Brain-to-plasma concentration ratios for alfuzosin and dipyridamole in C57BL/6 and *Abcg2(-/-)* mice, *mdr1a(+/+)* and *mdr1a(-/-)* mice following 24 hr of osmotic minipump administration. Data are presented as mean ± SD (n=3). Two tailed student's *t*-tests were used to compare brain-to-plasma concentration ratios between C57BL/6 and *Abcg2(-/-)* mice, and between *mdr1a(+/+)* and *mdr1a(-/-)* mice. Asterisk (*) represents a statistical difference ($p<0.05$) between *mdr1a(+/+)* and *mdr1a(-/-)* mice for alfuzosin brain penetration.

A

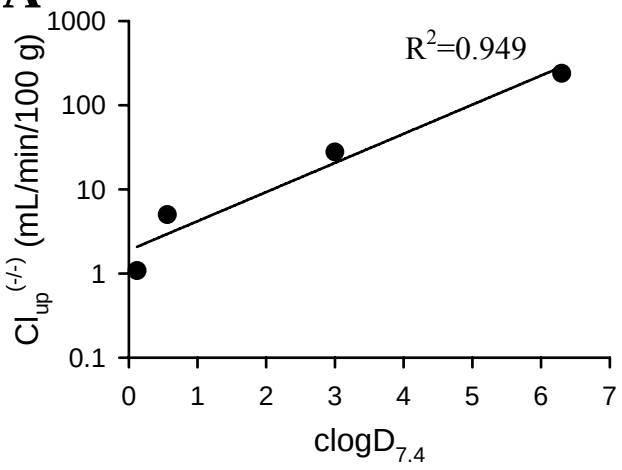
R2=0.949
1000
100
10
1
0.1
Clup(-/-) (mL/min/100 g)
0
1
2
3
4
5
6
7
clogD7.4

B

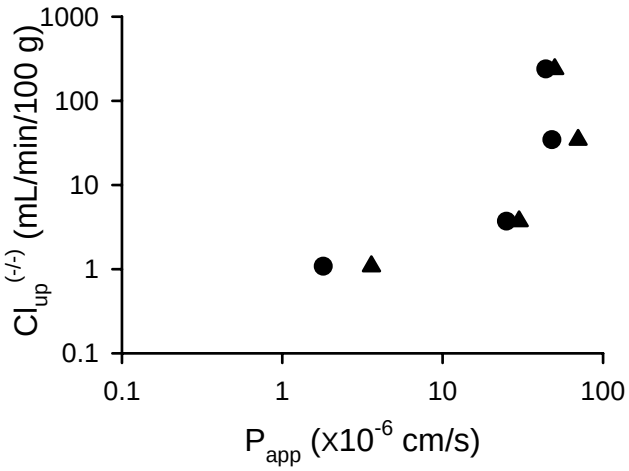
1000
100
10
1
0.1
Clup(-/-) (mL/min/100 g)
0.1
1
10
100
Papp (x10-6 cm/s)

C

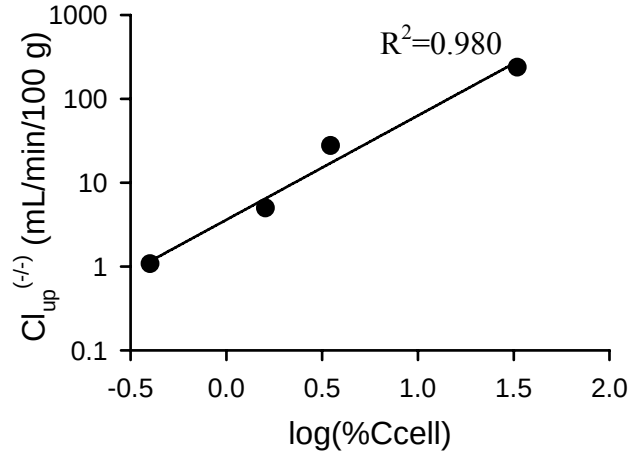
R2=0.980
1000
100
10
1
0.1
Clup(-/-) (mL/min/100 g)
-0.5
0.0
0.5
1.0
1.5
2.0
log(%Ccell)

Figure 4.7: Relationship between the initial uptake clearance of substrates in *mdr1a(-/-)* mice [$Cl_{up}^{(-/-)}$], and (A) calculated octanol-water partition coefficient at pH 7.4 ($clogD_{7.4}$); and (B) the *in vitro* P_{app} in A-B (circles) or in B-A (triangles) direction; and (C) the percent dose of cellular accumulation [log(%Ccell)] in MDCKII-Bcrp cells incubated with 20 μM of chrysin.

CHAPTER 5

REGIONAL DIFFERENCES IN CAPILLARY DENSITY, PERFUSION RATE, AND P-GLYCOPROTEIN ACTIVITY: A QUANTITATIVE ANALYSIS OF REGIONAL DRUG EXPOSURE IN THE BRAIN

This chapter will be submitted for publication in Journal of Cerebral Blood Flow and Metabolism and is presented in the style of that journal.

Abstract

An adequate exposure of therapeutic agents to the relevant pharmacologic target within the brain is essential for the effective treatment of many central nervous system (CNS) disorders. Previous studies have indicated that the rate of regional blood flow, local cerebral vascular volume, regional blood-brain barrier (BBB) permeability and P-glycoprotein (P-gp)-mediated efflux can influence regional drug exposure. In the current study, an *in situ* brain perfusion technique was used to assess the impact of local capillary density, blood flow rate and P-gp activity on regional drug exposure for the P-gp substrates colchicine, quinidine, verapamil, and loperamide, and the perfusion flow rate marker diazepam, and the vascular volume marker inulin, in *mdr1a(+/+)* and *mdr1a(-/-)* mice. Regional perfusion flow rate varied 7.5-fold, and capillary density (based on vascular volume) varied 3.7-fold, across the thirteen brain regions examined. The rate of regional flow, as well as P-gp-mediated colchicine efflux activity, was directly proportional to local capillary density. A decrease in perfusion rate attenuated verapamil brain uptake and had significant effect on P-gp-mediated efflux activity for this substrate in brain regions with lower capillary density. Regional brain uptake and calculated logD at pH7.4 were well-related in P-gp-deficient mice, suggesting that in the absence of P-gp-mediated efflux, physicochemical properties of the compound (i.e., lipophilicity) serve as the primary determinant of regional brain uptake. Loperamide regional brain uptake during a 60-s brain perfusion or at 30 min after subcutaneous administration was significantly correlated with local capillary density. The highest P-gp-mediated efflux activity was consistently observed in cerebral cortex and midbrain regions for loperamide following short-term brain perfusion and at all time points following subcutaneous

administration. These results emphasize the complexity of factors that determine regional substrate exposure in brain, which may have pharmacologic consequences when the target receptor evidences regional expression.

Introduction

For many cerebral disorders, such as brain tumors, Parkinson's disease, stroke, and ischemia, the disease focus or the therapeutic target is localized in specific regions of the brain. In such cases, the efficacy of therapy will depend on adequate delivery of drugs to the brain region that contains the pharmacologically-relevant target. Regional drug exposure in the CNS is a function of many drug- and region-specific factors, including physicochemical characteristics (lipophilicity and ionization state), protein binding in blood and brain tissue, drug concentration in blood, local cerebral blood flow rate, brain capillary surface area, regional capillary transit time, cerebrospinal fluid (CSF) bulk flow, and the flux of drugs across the blood-brain barrier (BBB) that may include both passive and active (transport-mediated) components (Klein et al., 1986; Kalvass and Maurer, 2002; Norinder and Haeberlein, 2002; Liu and Chen, 2005). For example, previous studies in this laboratory demonstrated that P-glycoprotein (P-gp)-mediated efflux at the BBB influences the distribution of ^{3}H-verapamil within the brain following intranasal administration to P-gp-competent and P-gp-deficient mice (Graff et al., 2005; Appendix). Pharmacokinetic modeling of these data revealed that the apparent P-gp effect on verapamil exposure was negligible in some regions, and produced nearly a 100-fold attenuation of exposure in others. Knowledge of the regional cerebral vascular volume and blood flow rate, as well as regional P-gp activity, is of particular interest with regard to targeted treatment for cerebral diseases.

The BBB and blood-cerebrospinal fluid barrier (BCSFB) are major interfaces between the CNS and peripheral circulation. The BBB is composed of brain capillary endothelial

cells, which are characterized by highly-developed tight junctions and a paucity of fenestrae and pinocytotic vesicles. In addition to this physical barrier to substrate flux, expression of efflux transport proteins and metabolic enzymes at the blood-brain interface further limit the penetration of substances into the CNS. P-gp, the most extensively studied BBB efflux transporter, is expressed at the luminal side of the brain capillary endothelium and mediates the flux of various endogenous compounds and xenobiotics in the brain-to-blood direction (Schinkel et al., 1994), thereby serving as an important barrier to the entry of P-gp substrates into brain. P-gp, a member of the ATP-binding cassette (ABC) superfamily of transport proteins, is a 170-kDa membrane protein encoded by multidrug resistance gene (*ABCB1* in human, *Abcb1a* and *Abcb1b* in rodents). Impaired BBB penetration represents the primary obstacle in CNS drug development since more than 98% of all new drugs evaluated for CNS applications do not cross the BBB (Terasaki and Pardridge, 2000). P-gp appears to be a significant factor in poor brain uptake of many agents.

The mammalian brain is a highly specialized organ from both the structural and functional perspective. There are broad regional differences in neurophysiologic functions such as local neuronal activity, neurotransmitter distribution, and oxygen and glucose utilization. The rate of local cerebral blood flow under physiologic conditions varies about 18-fold among brain areas in the rat (Fenstermacher et al., 1991). In addition, the capillary blood volume and surface area of the BBB differ between brain regions; these differences may result in regional variations in drug exposure (Duelli and Kuschinsky, 1993).

Clinical practice has shown variations in sensitivity to the therapeutic effect or CNS side effects of drugs associated with different brain regions. For example, the hippocampus is especially vulnerable to ischemia and colchicine cytotoxicity (Goldschmidt and Steward, 1980; Cavaglia et al., 2001). The administration of chemotherapeutic agents in combination with transient, reversible hyperosmotic opening of the BBB has been explored as an approach in the treatment of brain tumors; *in vivo* experiments and data generated with *in situ* rat brain perfusion techniques have demonstrated the variations in BBB disruption in different brain regions following hyperosmotic treatment, suggesting that the clinical efficacy of hyperosmolar disruption therapy may be affected by the location of the tumor within the brain (Chiueh et al., 1978; Brown et al., 2004). Region-specific overexpression of P-gp has been reported to decrease phenytoin concentrations in the temporal hippocampus and parahippocampal cortex region in chronic epileptic rats (van Vliet et al., 2007).

Brain uptake index, brain microdialysis, single-pass indicator-dilution, and PET imaging techniques have been used to study the impact of local cerebral blood flow rate and capillary density on the regional brain exposure of nutrients or therapeutic agents (Sokoloff et al., 1977; Fenstermacher et al., 1991; Rosen et al., 1991; Suzuki et al., 1998; Gee, 2003; Brown et al., 2004; Tohyama et al., 2004; Rambeck et al., 2006; Wyss et al., 2007). For example, a close correspondence between local cerebral glucose utilization, local cerebral blood flow, and density of perfused capillaries has been identified in rat brain (Klein et al., 1986; Schrock and Kuschinsky, 1988). During *in situ* brain perfusion, uptake of the Oatp14 substrate thyroid hormone T4 into brain is 3-fold higher in the cerebral cortex than in the cerebellum (Tohyama et al., 2004).

In situ brain perfusion was first developed to evaluate BBB permeability in rats (Takasato et al., 1984), and was modified for use in mice (Dagenais et al., 2000a). This technique allows examination of single-pass permeability of molecules at the BBB without systemic contamination, with complete control of the composition and flow of perfusion buffer, and without other pharmacokinetic events (e.g., hepatic metabolism) confounding the experimental results. In the present study, the *in situ* brain perfusion technique was utilized to study the impact of local cerebral perfusion flow rate, vascular volume, and P-gp activity on regional drug exposure. ^{14}C-diazepam and ^{3}H-inulin, selected as markers of functional perfusion flow rate and vascular volume, respectively, were perfused simultaneously, followed by microdissection of the brain to assess regional flow and capillary density. Subsequent experiments were directed towards examining regional brain exposure of the P-gp substrates colchicine, quinidine, loperamide and verapamil during perfusion in P-gp-competent and P-gp-deficient mice, allowing assessment of regional P-gp activity in P-gp-expressing animals. The *in situ* perfusion experiments were complemented by an *in vivo* evaluation of P-gp-mediated efflux activity over 12 hr following subcutaneous administration of loperamide to assess the potential time-dependency of efflux activity estimates.

Materials and Methods

Adult CF-1 [*mdr1a(+/+)* and *mdr1a* (-/-)] mice (30-40 g, 6-8 weeks of age) were obtained from Charles River Laboratories (Wilmington, MA). All mice were maintained on a 12-h light/dark cycle with access to water and food *ad libitum*. All experimental

procedures were performed under full anesthesia induced with ketamine/xylazine (100/10 mg/kg, i.p.). All procedures were approved by the Institutional Animal Care and Use Committee at the University of North Carolina at Chapel Hill and were conducted in accordance with "Principles with Laboratory Animal Care" (NIH publication No. 85-23, revised in 1985).

^{14}C-diazepam (56.0 mCi/mmol) was purchased from Amersham Biosciences (Buckinghamshire, UK). ^{14}C-inulin (2.1 mCi/g) and ^{3}H-quinidine (20 Ci/mmol) were obtained from American Radiolabeled Chemical Inc. (St Louis, MO). ^{3}H-inulin (180.0 mCi/g), ^{3}H-colchicine (80.4 Ci/mmol) and ^{3}H-verapamil (74.2 Ci/mmol) were purchased from PerkinElmer (Waltham, MA). Loperamide and fexofenadine were purchased from Sigma-Aldrich (St. Louis, MO). All of the other chemicals were commercially available and of reagent grade.

In Situ Mouse Brain Perfusion Procedure

In situ mouse brain perfusions were conducted as described by (Dagenais et al., 2000a). Briefly, P-gp competent- [*mdr1a(+/+)*] and -deficient [*mdr1a(-/-)*] mice (n=3) were anesthetized with ketamine/xylazine (100/10 mg/kg, i.p.). The perfusion buffer (Krebs-bicarbonate buffer, with 9 mM of D-glucose, pH 7.4) was oxygenated with 95% O_2 and 5% CO_2 and maintained at 37°C. The right common carotid artery was cannulated with PE-10 tubing (Braintree Scientific Inc., Braintree, MA) following ligation of the external carotid artery. The cardiac ventricles were severed immediately before starting perfusion for 60 s at 2.5 mL/min via a syringe pump (Harvard Apparatus, Holliston, MA). The experiment was terminated by decapitation immediately following perfusion. The right

cerebral hemisphere was removed carefully and placed on cold saline-soaked filter paper and dissected on ice. Approximately 150 mg of perfusate was collected through the syringe and tubing.

Brain Perfusion Experimental Design

In order to determine the regional cerebral capillary volume and functional perfusion flow rate, ^{14}C-inulin (at 1.6 μCi/mL) and ^{14}C-diazepam at (0.4 μCi/mL) as vascular volume and blood flow rate markers, respectively, were perfused simultaneously for 60 s in *mdr1a(+/+)* and *mdr1a(-/-)* mice (n=3). In separate studies, ^{3}H-colchicine (at 1.6 μCi/mL), ^{3}H-verapamil (at 0.4 μCi/mL), ^{3}H-quinidine (at 1 μCi/mL), or unlabeled loperamide (at 2 μM) was perfused for 60 s, followed by 15 s of cold saline washout to remove remaining perfusate in the vasculature. Additional groups of *mdr1a(+/+)* and *mdr1a(-/-)* mice (n=3) were perfused with ^{3}H-verapamil at 1 mL/min to investigate the potential influence of changes in flow rate on apparent regional P-gp activity.

Loperamide Subcutaneous Administration

Loperamide was administered to *mdr1a(+/+)* mice (30 mg/kg, s.c.) and *mdr1a(-/-)* mice (1 mg/kg, s.c.), and animals (n=3 per group) were sacrificed by decapitation at 0.5, 1, 2, 4, 6 and 12 hr post-dose. The doses were selected to produce approximately equivalent brain tissue concentrations in the two mouse strains. Trunk blood was collected and centrifuged at 3,000 rpm for 5 min. The plasma was transferred to a fresh microcentrifuge tube and stored at -20 °C until analysis by HPLC/MS/MS. The brain was carefully removed from skull, cleaned of meninges and choroid plexus, dissected on ice, and stored at -20 °C pending analysis.

Mouse Brain Microdissection

To ensure the reproducibility of the dissection technique, bregma coordinates and anatomic boundaries defining each region were established based on the Franklin and Paxinos mouse brain atlas (Franklin and Paxinos, 1996). The microdissection procedure was conducted according to photographs and step-by-step instructions downloaded from a publicly-accessible relational database (www.barlow-lockhartbrainmapnimhgrant.org). For studies involving radiolabeled substrate, the perfused brain hemisphere was dissected into 13 regions (olfactory bulb, striatum, hippocampus, frontal cortex, parietal cortex, occipital cortex, superior and inferior colliculi, hypothalamus, thalamus, midbrain, pons, medulla, and cerebellum). Larger brain regions were required for accurate loperamide analysis. Accordingly, the perfused hemisphere for loperamide *in situ* studies, or brain tissue after in vivo administration of loperamide, was dissected into seven regions [olfactory bulb, striatum, hippocampus, cortex, midbrain (including midbrain, thalamus and hypothalamus), brainstem (including pons and medulla) and cerebellum].

Radioactive Sample Quantitation

Samples containing radiolabeled substrate were digested with 0.3 mL of Solvable® (Packard, Boston, MA) at 50 °C for 4 hr. UltimaGold® scintillation cocktail (PerkinElmer, Wellesley, MA) was added (5 mL) and vortex-mixed. Total radioactivity (^{3}H and/or ^{14}C) was determined in a Packard Tri-carb TR 1900 liquid scintillation analyzer (Packard, Boston, MA).

Loperamide Sample Preparation and HPLC/MS/MS Assay

Distilled water was added to brain samples (2:1 v/w) and homogenized with brief probe sonication. Plasma (for *in vivo* studies), brain homogenate, and perfusate (for *in situ* studies) samples were analyzed by HPLC/MS/MS (API 4000 triple quadrupole with TurboIonSpray interface; Applied Biosystems/MDS Sciex, Concord, ON, Canada). A 25-µL aliquot of brain hemisphere homogenate or plasma was transferred to an HPLC vial, and protein was precipitated with 100 µl of methanol containing internal standard (10 ng/mL fexofenadine), followed by a 25-µl aliquot of DMSO. The sample was vortex-mixed and centrifuged. Standard solutions, ranging from 0.5-5000 nM were prepared similarly, i.e., 25 µl of blank plasma or brain matrix, 100 µl of methanol containing internal standard, and 25 µl of serially-diluted standard solution was mixed and centrifuged. Supernatant (3 µl) was injected by autosampler (Leap, Carrboro, NC). Loperamide and the internal standard, fexofenadine, were eluted from an Aquasil C18 column (2.1 x 50 mm, d_p = 5 µm; Thermo Electron Corporation, Waltham, MA) using a mobile phase gradient (A, 0.1% formic acid in water; B, 0.1% formic acid in methanol; 0-0.70-min hold at 0% B, 0.70-3.12-min linear gradient to 90% B, 3.12-4.10 min hold at 90% B, 4.10-4.20-min linear gradient to 0% B, 4.20-4.90-min hold at 0% B; solvent delivery system (Shimadzu); flow rate = 0.75 ml/min; 0.8-4 min directed to mass spectrometer) and were detected in positive ion mode using multiple reaction monitoring: fexofenadine: 502.4→466.4 *m*/z, loperamide, 477.4→266.0 *m*/z. The lower limit of detection was 0.5 ng/ml; inter-and intraday CVs were <15%.

Parameter Calculation

The regional vasculature volume was calculated using the equation:

$$V_{vasc} = \frac{X_{inulin}}{C_{inulin}}$$

where X_{inulin} and C_{inulin} are the amount of ^{3}H-inulin radioactivity in the brain region and concentration in the perfusate, respectively. Regional ^{14}C-diazepam brain uptake clearance (Cl_{up}), which is flow rate-limited and therefore serves as a surrogate marker of functional perfusate flow, was calculated using the equation:

$$Cl_{up} = \frac{(X_{brain} - X_{vasc})/T}{C_{perf}}$$

for each brain region (Dagenais et al., 2000a). For each of the test compounds, regional Cl_{up} was calculated using

$$Cl_{up} = \frac{X_{brain}/T}{C_{perf}}$$

No correction for substrate mass contained in residual was made as the vasculature substrate content was cleared via the 15-s cold saline washout at the end of the perfusion period.

Statistical Analysis

Data are reported as mean ± SD for 3 mice per condition. One-way or two-way ANOVA, where appropriate, was used to determine the statistical significance of differences among

two or more groups. The level of significance was corrected for multiple comparisons (e.g., Bonferroni test) or adjusted for unequal variance when necessary. In all cases, $p < 0.05$ was considered to be statistically significant.

Results

Regional Cerebral Vascular Volume and Flow Rate

During *in situ* mouse brain perfusion, the regional vascular volume and perfusion flow rate in *mdr1a(+/+)* and *mdr1a(-/-)* mice were comparable, so the data were pooled for each structure, as summarized in Table 5.1 (n=6, mean±SD). The regional vascular volume ranged from 0.62 mL/100 g in pons and medulla to 2.21 mL/100 g in colliculi. The perfusion flow rate ranged from 38.1 mL/min/100 g in medulla to 285 mL/min/100 g in colliculi. An orthogonal linear least-squares regression analysis between the local blood flow rate and vascular volume, with a correlation coefficient of 0.955, is illustrated in Figure 5.1.

Regional P-gp Activity in Mouse Brain

The regionality of brain uptake of ^{3}H-colchicine, ^{3}H-quinidine and ^{3}H-verapamil in *mdr1a(+/+)* and *mdr1a(-/-)* mice is shown in Figure 5.2. Colchicine, quinidine and verapamil brain uptake were significantly higher in most of the brain regions studied in *mdr1a(-/-)* mice compared to wild-type animals, consistent with P-gp-associated impairment of brain uptake. In addition, a stronger relationship between Cl_{up} and regional vascular volume was observed in *mdr1a(-/-)* vs. *mdr1a(+/+)* mice. The actual regional P-

gp efflux ratios were calculated as the ratios of Cl_{up} values in *mdr1a(-/-)* mice to wild-type mice for each compound, and plotted against regional cerebral vascular volume (Figure 5.3). Approximately 67.9% of the variance in colchicine regional P-gp efflux ratio can be explained by the local cerebral vascular volume (Figure 5.3A). However, there is essentially no relationship between regional P-gp activity and vascular volume for quinidine or verapamil (Figure 5.3B and 5.3C, less than 1% of the variance in P-gp efflux ratio can be explained by the local vascular volume). The regression excluding pons, medulla and cerebellum (triangles in Figure 5.3C) for verapamil evidences a reasonable correlation between regional P-gp efflux ratio and vascular volume (R^2=0.656).

Effect of Flow Rate Perturbation on Brain Distribution

To investigate the influence of regional cerebral perfusion flow rate on regional P-gp efflux of verapamil, mouse brain perfusions were performed at a lower flow rate (1 mL/min). The resulting change in P-gp efflux ratio is plotted against the P-gp efflux ratio at the standard flow rate (Figure 5.4). Pons, medulla and cerebellum were excluded from the regression because in these areas the brain uptake was essentially flow rate-limited. A linear relationship (R^2=0.861) was observed between the flow-related change in P-gp effect and local P-gp activity. In the brain regions that showed significant P-gp activity (such as parietal cortex and colliculi), changes in perfusion flow had little influence on P-gp activity. In regions with limited P-gp activity, a change in perfusion flow rate had a more substantial impact on P-gp activity. A similar regression analysis also demonstrated a relationship between regional vascular volume and P-gp activity (R^2=0.622, data not shown).

Regional P-gp Transport of Loperamide

Loperamide samples were analyzed by HPLC/MS/MS. Seven larger brain regions were dissected to satisfy the requirement of sample preparation reproducibility and analytical sensitivity. Regional P-gp-mediated efflux of loperamide correlated well with regional vascular volume during *in situ* brain perfusion for 60 s in mice (R^2=0.639; data not shown). Figure 5.5 illustrates the regional P-gp effect following subcutaneous administration of loperamide, with the P-gp efflux ratio at 0.5, 1, 2, 4, 6, 12 hr plotted for each region. The regional P-gp efflux ratio was statistically (R^2=0.775) related to the regional vascular volume only at the earliest time point (0.5 hr). P-gp efflux ratios were always the highest in cerebral cortex and the midbrain regions at all time points (data not shown).

Effect of Lipophilicity on Regional Brain Distribution

Three-dimensional illustrations of the brain distribution of colchicine, quinidine, verapamil and diazepam in each brain region vs. $clogD_{7.4}$ (the logarithm of the octanol water partition coefficient at pH7.4) are provided in Figure 5.6. The value of $clogD_{7.4}$ for each compound was estimated using Marvin and calculator plugin freeware (www.chemaxon.com, ChemAxon Kft, Budapest, Hungary). The initial rate of brain uptake in *mdr1a(-/-)* mice [Cl_{up}(-/-), mL/min/100 g] was a function of lipophilicity. $LogCl_{up}$(-/-) increased with increasing $clogD_{7.4}$ until Cl_{up}(-/-) approached the regional perfusion flow rate (for verapamil and diazepam). In pons, medulla and cerebellum, the functional perfusion flow rates were lower than in other brain structures (Figure 5.6A). In the presence of P-gp, the initial rate of colchicine, quinidine and verapamil brain uptake

was mitigated by P-gp-mediated efflux (Figure 5.6B). The P-gp efflux ratio was not a function of lipophilicity (Figure 5.6C).

Discussion

The BBB is a tightly regulated barrier that serves to maintain homeostasis of the microenvironment in the brain. BBB penetration is the first step in the access of CNS targets for therapeutic agents and toxicants in the brain. Most of the targets for treatment of brain disorders, e.g., neurodegenative disorders (dopamine receptors), epilepsy (e.g., GABA receptors) and neuropathic pain (μ-opioid receptors) are not homogeneously distributed in the brain (Heiss and Herholz, 2006). To achieve optimal therapeutic effect, adequate drug exposure at the site of action is important. Regional drug exposure in the brain is influenced not only by regional BBB permeability, but also by hemodynamic parameters such as local blood flow and capillary density.

In situ brain perfusion has become an important technique for measuring BBB permeability (Takasato et al., 1984; Dagenais et al., 2000a). The advantages of the *in situ* brain perfusion technique include elimination of the confounding factors of systemic disposition (such as hepatic metabolism and plasma protein binding) and maintenance of the intact physiologic condition of the brain. ^{14}C-diazepam and ^{3}H-inulin were used as functional perfusion flow rate and capillary volume markers, respectively (Dagenais et al., 2000a). In the current study, these two markers were used to study the local perfusion flow rate and capillary density in different brain structures.

A good relationship between local cerebral vascular volume and blood flow rate has been identified using various experimental techniques in conscious or anesthetized animals and humans (Klein et al., 1986; Suzuki et al., 1998; Wyss et al., 2007). In addition, heterogeneous cerebral vascular volume and blood flow have been found to be correlated with the local rate of neurophysiologic activity as expressed by glucose utilization. Structures with high glucose utilization, e.g., inferior colliculus, tend to have a high capillary density (Klein et al., 1986; Schrock and Kuschinsky, 1988). The current study demonstrated that brain structures such as colliculi, thalamus and parietal cortex have the highest vascular volume and functional flow rate, while the brainstem (pons and medulla) and cerebellum have the lowest vascular volume and functional flow rate. A significant correlation between local cerebral vascular volume (inulin volume) and local perfusion flow rate (diazepam Cl_{up}) was demonstrated (Figure 5.1). The mean transit time, calculated as the ratio of vascular volume to blood flow rate in each brain structure, was 0.4-0.6 s among most of the regions. A notable exception was medulla, where the mean transit time was 1.0 s. These values are similar to the transit times (0.3-0.6 s) reported for various rat brain areas, as determined by an autoradiography technique following intravenous administration of ^{14}C-iodoantipyrine (Fenstermacher et al., 1991).

Brain capillary diameters are influenced by many factors such as CO_2, O_2 and electrolyte concentrations in blood. However, capillary diameters do not vary between different brain structures (Gjedde and Diemer, 1985; Duelli and Kuschinsky, 1993). Gjedde et al (Gjedde and Diemer, 1985) demonstrated that in brain regions with higher blood flow, there is a correspondingly larger capillary vascular volume, i.e., larger capillary density and total surface area. Thus the cerebral capillary is considered standard across the brain.

For example, the number of glucose transporters per unit capillary surface area is the same in all regions, and the apparent glucose permeability in all brain capillary beds are the same. Regional differences in the rates of blood flow and glucose uptake are the result of different capillary densities or the length of capillaries in the regions of the brain (Gjedde and Diemer, 1985). In the current study, the uptake clearance in *mdr1a(-/-)* mice [Cl_{up}(-/-)] for colchicine, quinidine, verapamil and diazepam correlated well with the local capillary density, with R^2 values of 0.708, 0.862, 0.856, and 0.955, respectively, suggesting that the surface area in the regional BBB is very important for brain uptake (Figure 5.1 and 5.2). However, there was practically no such relationship in wild-type mice for colchicine (R^2=0.019) and quinidine (R^2=0.191). Both compounds are P-gp substrates, with brain uptake impaired by P-gp-mediated efflux. For verapamil, also a P-gp substrate, brain uptake was correlated with capillary density (R^2=0.726). This discrepancy can be explained by the fact that verapamil is quite permeable at the BBB. As its rate of brain uptake approaches the flow rate, verapamil uptake is influenced more significantly by flow than by P-gp activity. In addition, verapamil is a weaker P-gp substrate than quinidine, as reflected by the magnitude of P-gp efflux ratios (4.7 and 16.7, respectively). Thus, all other factors being equal, P-gp would be expected to have less of an effect on verapamil uptake than on quinidine uptake across the BBB.

Figure 5.3A illustrates that the colchicine P-gp efflux ratio correlated with capillary density. The P-gp efflux ratio determined using *in situ* brain perfusion technique (ER_B) has been shown to be directly proportional to P-gp efflux activity, using a mathematical three-compartment model in which P-gp efflux activity was directly proportional to functional protein expression level (Kalvass and Pollack, 2007). The present results with

colchicine suggest that the expression level of P-gp, a membrane-bound protein expressed in the brain capillary endothelium, is related to local capillary density. Thus, it is likely that the amount of P-gp per unit capillary surface area is the same in all regions and functions similarly. This is also consistent with the observations that P-gp is expressed in endothelial cells, with little or no expression in other brain cells (i.e., astrocytes and neurons) under normal conditions (Schinkel, 1999; Yousif et al., 2007). Surprisingly, there was not such a strong correlation between P-gp effect and capillary density for verapamil or quinidine. Verapamil P-gp efflux ratios were high in the pons and cerebellum. The pons, medulla and cerebellum are perfused by vertebral arteries under normal conditions, so are not perfused well with carotid artery perfusion under the current experimental technique (Takasato et al., 1984). Verapamil brain uptake in these areas is perfusion-limited. Regression analyses excluding these regions demonstrated a good correlation between the P-gp efflux ratio and capillary volume (R^2=0.656, Figure 5.3C). Regional P-gp efflux ratios following intranasal administration of verapamil also showed that the most substantial regional P-gp effects were in parietal cortex and the thalamas (Graff et al., 2005; Appendix), corresponding to the areas that have the highest capillary density and, by analogy, P-gp expression level. Other variables might contribute to quinidine brain uptake and its interaction with P-gp, such as more than one P-gp binding site for this substrate (unpublished data), and the interplay of passive permeability at the BBB with perfusion flow rate.

In earlier studies, the apparent distributional volume (V_d) for colchicine, quinidine, verapamil and diazepam has been demonstrated to be a linear function of perfusion time over 60 s (Dagenais et al., 2000a; Dagenais et al., 2004). In the current study, all of the

perfusions were conducted for 60 s to maximize the brain exposure and analytical sensitivity while maintaining time-linear conditions. In addition, a final 15-s drug-free saline perfusion was utilized to wash out the residual perfusate remaining in the vascular space. This washout step is especially useful for poorly-permeable compounds such as colchicine, for which subtraction of vascular contamination might lead to appreciable variability in the estimated mass of substrate in brain. The V_d for colchicine in seven regions of rat brain ranged from 0.18 µl/g in cerebellum to 10.7 µl/g in the hippocampus, and was increased significantly upon pretreatment with P-gp inhibitor PSC833 and GF120918 in all regions (Youdim et al., 2004). In the present study, Cl_{up} (equivalent to V_d) ranged from 0.57 to 2.07 mL/min/100 g, with the lowest exposure in pons and medulla, and the highest exposure in hippocampus, olfactory bulb and colliculi, areas that have been reported to be selectively vulnerable to colchicine toxicity (Goldschmidt and Steward, 1982; Mundy and Tilson, 1990). One previous study using a perfusion procedure showed no regional differences (Drion et al., 1996). This discrepancy can be explained by the differences in the brain perfusion procedure, and in particular the presence or absence of a washout step in the perfusion protocol. Other experimental differences (e.g., the structures selected for evaluation) may have contributed to differences in results between the two studies.

Among the P-gp substrates evaluated, verapamil is the most permeable at the BBB, with a brain uptake clearance in most brain regions approaching perfusion flow rate in *mdr1a(-/-)* mice. Verapamil brain uptake is expected to be sensitive to changes in perfusion flow rate. For this reason, verapamil was selected as a model compound to study the impact of blood flow on brain uptake and P-gp effect. A lower perfusion rate (1

mL/min) was selected for comparison to the standard flow rate (2.5 mL/min). Changes in blood flow cause capillary diameters to change, thus altering the surface area for regional uptake (Duelli and Kuschinsky, 1993). At a lower perfusion rate, a vasoconstricting effect occurs, and capillary diameter and surface area decrease. As expected, lower brain uptake was observed for verapamil at 1 mL/min compared to 2.5 mL/min. The P-gp efflux ratios also decreased, but to differing extents based on brain region, at the lower perfusion rate. The change in P-gp efflux ratio in response to a decrease in perfusion flow was found to be correlated with the basal (i.e., at 2.5 mL/min) regional P-gp effect. Changes in flow appeared to have a more substantial impact in areas that had a weaker P-gp activity, but little or no effect in areas with stronger P-gp activity (i.e., areas that have larger capillary beds). A good correlation existed between the change in P-gp efflux ratio and the P-gp efflux ratio determined at 2.5 mL/min or regional cerebral volumes, when excluding pons, medulla and cerebellum regions for reasons described above.

The *in situ* brain perfusion is an oversimplified system that only approximates intact systems. In the *in vivo* situation, factors such as plasma protein binding and non-specific binding in brain tissue, hemodynamic parameters such as pCO2, pO2, pH, and electrolyte concentrations influence the vascular volume, blood flow rate, and BBB permeability. At the earliest time point (0.5 hr) following subcutaneous administration, loperamide P-gp efflux ratio correlated with local capillary density, a result anticipated based upon the preceding *in situ* perfusion experiments. At all later time points, the apparent P-gp effect lost regionality, most likely due to inter-area diffusion and exchange, including distribution across the regional BBB. This explanation is kinetically sound because it is expected that the short-term perfusion in mouse brain represents *in vivo* situation prior to

attainment of distribution equilibrium (i.e., the initial phase of brain uptake, when the brain behaves as an approximate sink for substrate uptake). In contrast, later time points during *in vivo* distribution (i.e., when no net flux occurs between blood and brain tissue) brain-to-blood partitioning is determined primarily by relative protein binding in blood and brain tissue, not BBB permeability in isolation. A previous study resulted in a similar observation: short-term (up to 30 s) intravenous infusion of ^{3}H-nicotine might be used to estimate local cerebral blood flow rate (initial rate of brain uptake determined by flow rate) and long-term (up to 4 min) infusion could be used to estimate density of cells and nerve endings, which was determined by the tissue binding of nicotine (Ohno et al., 1979).

Lipophilicity has been demonstrated to be one of the most important factors in determining brain exposure (Brodie et al., 1960). Experimental and modeling approaches demonstrated that the regional brain exposure of various compounds (antipyrine, verapamil, and diazepam) in dissected coronal brain slices is determined by lipophilicity, with the diffusivity factors directly proportional to logP values (Graff et al., 2005; Appendix). In the current study, the regional brain exposure of colchicine, quinidine, verapamil and diazepam in *mdr1a(-/-)* mice was a function of $clogD_{7.4}$ in all brain regions. However, in the regions (pons, medulla and cerebellum) that were not well-perfused, brain uptake was limited by flow rate even with compounds with lower lipophilicity. This situation caused Cl_{up} to plateau for compounds with increasing lipophilicity. The regional brain exposure of colchicine, quinidine and verapamil (all P-gp substrates) in wild-type mice was impaired by P-gp-mediated efflux to different extents depending on the efficiency of P-gp effect. No correlation was observed between regional P-gp efflux ratio

and clog$D_{7.4}$. Other variables such as the number of binding sites, or affinity towards the binding sites influence the nature of substrate interaction with P-gp.

In conclusion, the current study used an *in situ* mouse brain perfusion technique to illustrate the interplay between regional brain capillary volume, blood flow, and P-gp activity, and the impact of these factors on regional drug exposure in mouse brain. The *in vivo* studies with loperamide confirmed that this *in situ* brain perfusion technique is an approximation to *in vivo* situation and is helpful in understanding the underlying mechanisms of regional brain exposure in the more complicated intact system.

References

Brodie BB, Kurz H, Schanker LS. (1960) The importance of dissociaton constant and lipid-solubility in influencing the passage of drugs into the cerebrospinal fluid. *J Pharmacol Exp Ther* 130:20-25

Brown RC, Egleton RD, Davis TP. (2004) Mannitol opening of the blood-brain barrier: regional variation in the permeability of sucrose, but not 86Rb+ or albumin. *Brain Res* 1014:221-227

Cavaglia M, Dombrowski SM, Drazba J, Vasanji A, Bokesch PM, Janigro D. (2001) Regional variation in brain capillary density and vascular response to ischemia. *Brain Res* 910:81-93

Chiueh CC, Sun CL, Kopin IJ, Fredericks WR, Rapoport SI. (1978) Entry of [3H]norepinephrine, [125I]albumin and Evans blue from blood into brain following unilateral osmotic opening of the blood-brain barrier. *Brain Res* 145:291-301

Dagenais C, Graff CL, Pollack GM. (2004) Variable modulation of opioid brain uptake by P-glycoprotein in mice. *Biochem Pharmacol* 67:269-276

Dagenais C, Rousselle C, Pollack GM, Scherrmann JM. (2000) Development of an in situ mouse brain perfusion model and its application to mdr1a P-glycoprotein-deficient mice. *J Cereb Blood Flow Metab* 20:381-386

Drion N, Lemaire M, Lefauconnier JM, Scherrmann JM. (1996) Role of P-glycoprotein in the blood-brain transport of colchicine and vinblastine. *J Neurochem* 67:1688-1693

Duelli R, Kuschinsky W. (1993) Changes in brain capillary diameter during hypocapnia and hypercapnia. *J Cereb Blood Flow Metab* 13:1025-1028

Fenstermacher J, Nakata H, Tajima A, Lin SZ, Otsuka T, Acuff V, Wei L, Bereczki D. (1991) Functional variations in parenchymal microvascular systems within the brain. *Magn Reson Med* 19:217-220

Franklin KB, Paxinos G. (1996) *The mouse brain in stereotaxic coordinates*. San Diego: Academic Press, Inc.

Gee AD. (2003) Neuropharmacology and drug development. *Br Med Bull* 65:169-177

Gjedde A, Diemer NH. (1985) Double-tracer study of the fine regional blood-brain glucose transfer in the rat by computer-assisted autoradiography. *J Cereb Blood Flow Metab* 5:282-289

Goldschmidt RB, Steward O. (1980) Preferential neurotoxicity of colchicine for granule cells of the dentate gyrus of the adult rat. *Proc Natl Acad Sci U S A* 77:3047-3051

Goldschmidt RB, Steward O. (1982) Neurotoxic effects of colchicine: differential susceptibility of CNS neuronal populations. *Neuroscience* 7:695-714

Graff CL, Zhao R, Pollack GM. (2005) Pharmacokinetics of substrate uptake and distribution in murine brain after nasal instillation. *Pharm Res* 22:235-244

Heiss WD, Herholz K. (2006) Brain receptor imaging. *J Nucl Med* 47:302-312

Kalvass JC, Maurer TS. (2002) Influence of nonspecific brain and plasma binding on CNS exposure: implications for rational drug discovery. *Biopharm Drug Dispos* 23:327-338

Kalvass JC, Pollack GM. (2007) Kinetic considerations for the quantitative assessment of efflux activity and inhibition: implications for understanding and predicting the effects of efflux inhibition. *Pharm Res* 24:265-276

Klein B, Kuschinsky W, Schrock H, Vetterlein F. (1986) Interdependency of local capillary density, blood flow, and metabolism in rat brains. *Am J Physiol* 251:H1333-1340

Liu X, Chen C. (2005) Strategies to optimize brain penetration in drug discovery. *Curr Opin Drug Discov Devel* 8:505-512

Mundy WR, Tilson HA. (1990) Neurotoxic effects of colchicine. *Neurotoxicology* 11:539-547

Norinder U, Haeberlein M. (2002) Computational approaches to the prediction of the blood-brain distribution. *Adv Drug Deliv Rev* 54:291-313

Ohno K, Pettigrew KD, Rapoport SI. (1979) Local cerebral blood flow in the conscious rat as measured with 14C-antipyrine, 14C-iodoantipyrine and 3H-nicotine. *Stroke* 10:62-67

Rambeck B, Jurgens UH, May TW, Pannek HW, Behne F, Ebner A, Gorji A, Straub H, Speckmann EJ, Pohlmann-Eden B, Loscher W. (2006) Comparison of brain extracellular fluid, brain tissue, cerebrospinal fluid, and serum concentrations of antiepileptic drugs measured intraoperatively in patients with intractable epilepsy. *Epilepsia* 47:681-694

Rosen BR, Belliveau JW, Buchbinder BR, McKinstry RC, Porkka LM, Kennedy DN, Neuder MS, Fisel CR, Aronen HJ, Kwong KK, et al. (1991) Contrast agents and cerebral hemodynamics. *Magn Reson Med* 19:285-292

Schinkel AH. (1999) P-Glycoprotein, a gatekeeper in the blood-brain barrier. *Adv Drug Deliv Rev* 36:179-194

Schinkel AH, Smit JJ, van Tellingen O, Beijnen JH, Wagenaar E, van Deemter L, Mol CA, van der Valk MA, Robanus-Maandag EC, te Riele HP, et al. (1994) Disruption of the mouse mdr1a P-glycoprotein gene leads to a deficiency in the blood-brain barrier and to increased sensitivity to drugs. *Cell* 77:491-502

Schrock H, Kuschinsky W. (1988) Cerebral blood flow, glucose use, and CSF ionic regulation in potassium-depleted rats. *Am J Physiol* 254:H250-257

Sokoloff L, Reivich M, Kennedy C, Des Rosiers MH, Patlak CS, Pettigrew KD, Sakurada O, Shinohara M. (1977) The [14C]deoxyglucose method for the measurement of local cerebral glucose utilization: theory, procedure, and normal values in the conscious and anesthetized albino rat. *J Neurochem* 28:897-916

Suzuki H, Nagashima T, Tamaki N, Yamadori T. (1998) Cerebral ischemia affects glucose transporter kinetics across rat brain microvascular endothelium: quantitative analysis by an in situ brain perfusion method. *Surg Neurol* 49:67-76

Takasato Y, Rapoport SI, Smith QR. (1984) An in situ brain perfusion technique to study cerebrovascular transport in the rat. *Am J Physiol* 247:H484-493

Terasaki T, Pardridge WM. (2000) Targeted drug delivery to the brain; (blood-brain barrier, efflux, endothelium, biological transport). *J Drug Target* 8:353-355

Tohyama K, Kusuhara H, Sugiyama Y. (2004) Involvement of multispecific organic anion transporter, Oatp14 (Slc21a14), in the transport of thyroxine across the blood-brain barrier. *Endocrinology* 145:4384-4391

van Vliet EA, van Schaik R, Edelbroek PM, Voskuyl RA, Redeker S, Aronica E, Wadman WJ, Gorter JA. (2007) Region-specific overexpression of P-glycoprotein at the blood-brain barrier affects brain uptake of phenytoin in epileptic rats. *J Pharmacol Exp Ther* 322:141-147

Wyss MT, Hofer S, Hefti M, Bartschi E, Uhlmann C, Treyer V, Roelcke U. (2007) Spatial heterogeneity of low-grade gliomas at the capillary level: a PET study on tumor blood flow and amino acid uptake. *J Nucl Med* 48:1047-1052

Youdim KA, Qaiser MZ, Begley DJ, Rice-Evans CA, Abbott NJ. (2004) Flavonoid permeability across an in situ model of the blood-brain barrier. *Free Radic Biol Med* 36:592-604

Yousif S, Marie-Claire C, Roux F, Scherrmann JM, Decleves X. (2007) Expression of drug transporters at the blood-brain barrier using an optimized isolated rat brain microvessel strategy. *Brain Res* 1134:1-11

Table 5.1: Regional cerebral vascular volume (V_{vasc}) and perfusion flow rate determined by *in situ* brain perfusion at 2.5 mL/min for 60 s in *mdr1a(+/+)* and *mdr1a(-/-)* mice (n=3 per strain). There is no statistical difference between these two strains (one-way ANOVA, $p>0.05$ for each brain region). The data in *mdr1a(+/+)* and *mdr1a(-/-)* mice are pooled and presented below (n=6). The V_{vasc} and flow rate in different brain regions are statistically different (one-way ANOVA, $p<0.05$)

Region	**V_{vasc} (mL/100 g)**	**Flow Rate (mL/min/100 g)**
olfactory bulb	1.1±0.3	155±52
striatum	1.5±0.5	180±20
hippocampus	1.6±0.3	200±4
frontal cortex	1.5±0.3	167±21
parietal cortex	1.7±0.3	223±11
occipital cortex	1.7±0.4	215±24
colliculi	2.2±0.5	285±49
hypothalamus	1.5±0.4	214±21
thalamus	1.9±0.4	238±39
midbrain	1.6±0.3	198±20
pons	0.6±0.1	65±45
medulla	0.6±0.2	38±32
cerebellum	1.1±0.2	122±40

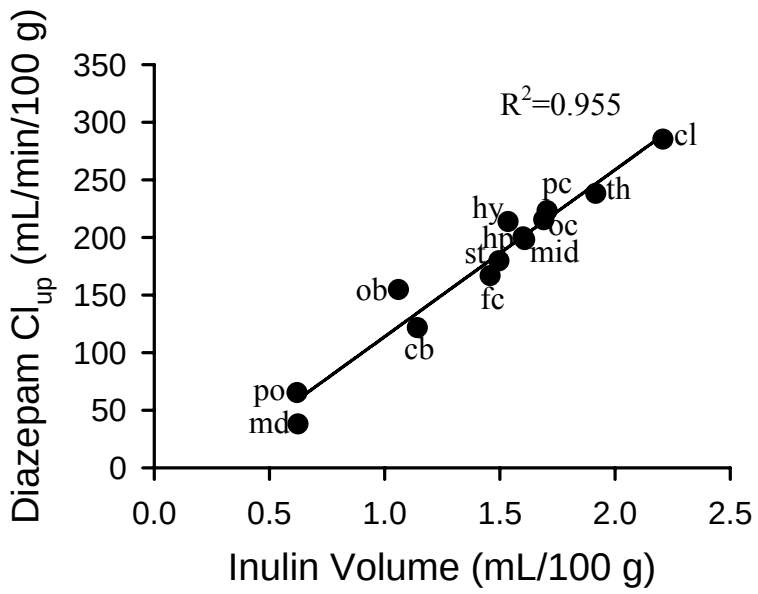

Figure 5.1: The relationship between regional flow rate (^{14}C-diazepam Cl_{up}, mL/min/100 g brain tissue) and regional cerebral vascular volume (^{3}H-inulin volume, mL/100 g brain tissue). Orthoganol linear least-squares regression (r^2=0.955). ob, olfactory bulb; st, striatum; hp, hippocampus; fc, frontal cortex; pc, parietal cortex; oc, occipital cortex; cl, colliculi; hy, hypothalamus; th, thalamus; mid, midbrain; po, pons; md, medulla; cb, cerebellum.

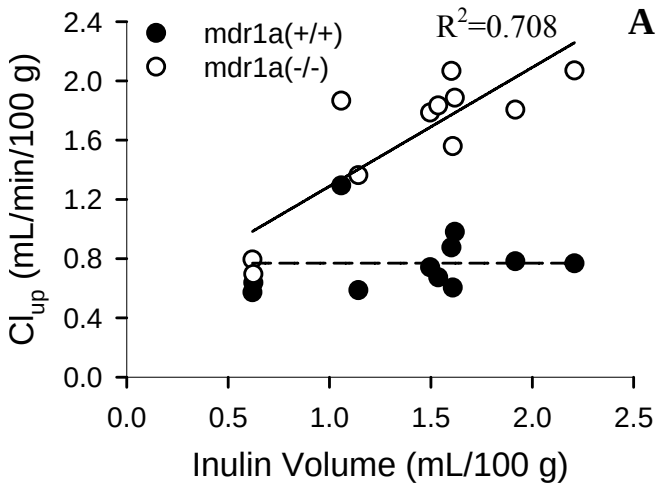
A
mdr1a(+/+)
mdr1a(-/-)
R^2=0.708
Cl_{up} (mL/min/100 g)
Inulin Volume (mL/100 g)
0.0
0.4
0.8
1.2
1.6
2.0
2.4
0.0
0.5
1.0
1.5
2.0
2.5

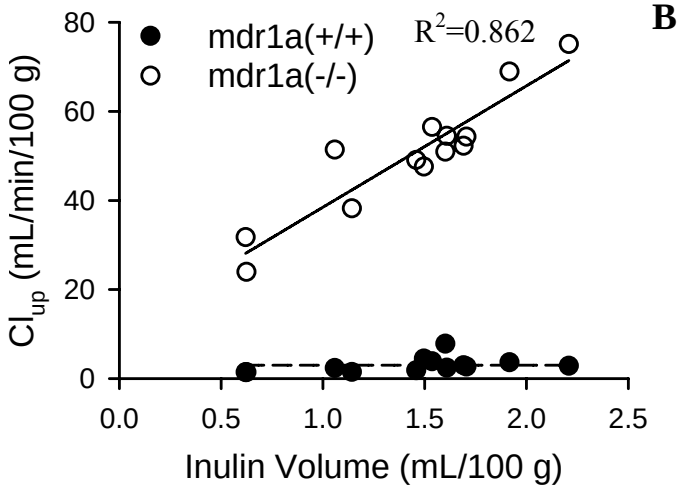
B
mdr1a(+/+)
mdr1a(-/-)
R^2=0.862
Cl_{up} (mL/min/100 g)
Inulin Volume (mL/100 g)
0
20
40
60
80
0.0
0.5
1.0
1.5
2.0
2.5

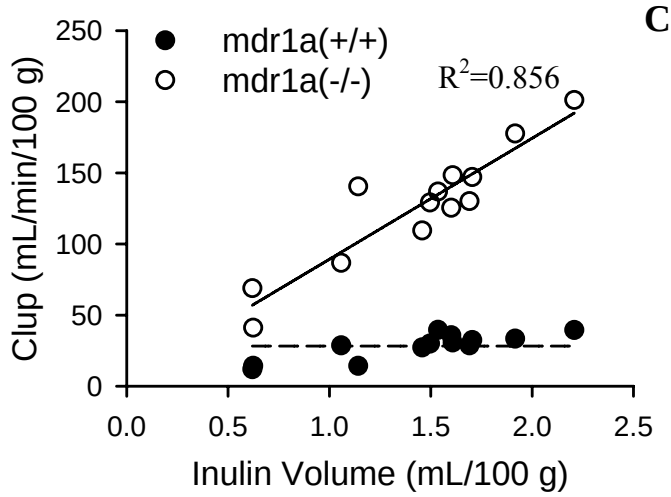
C
mdr1a(+/+)
mdr1a(-/-)
R^2=0.856
Clup (mL/min/100 g)
Inulin Volume (mL/100 g)
0
50
100
150
200
250
0.0
0.5
1.0
1.5
2.0
2.5

Figure 5.2: The regional Cl_{up} (mL/min/100 g brain tissue) in *mdr1a(+/+)* (solid symbol) and *mdr1a(-/-)* (open symbol) mice versus regional cerebral vascular volume (inulin volume, mL/100 g brain tissue) for (A) colchicine, (B) quinidine, and (C) verapamil. The solid lines are orthogonal linear regression line in *mdr1a(-/-)* mice, the dashed lines are the arithmatic mean of Cl_{up} in *mdr1a(+/+)* mice.

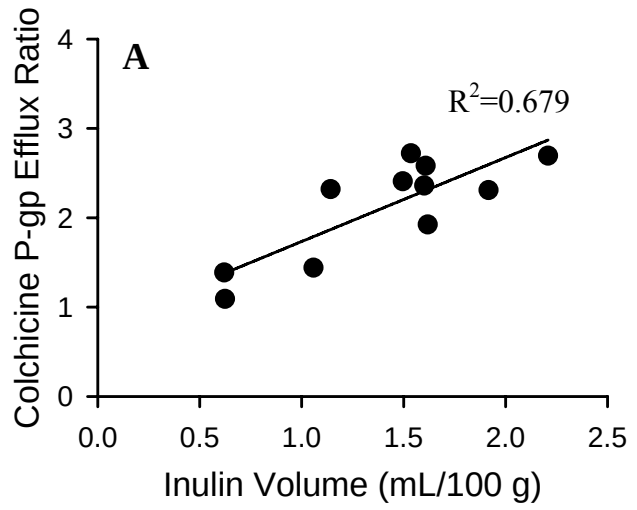
A
R^2=0.679
Colchicine P-gp Efflux Ratio
Inulin Volume (mL/100 g)
0
1
2
3
4
0.0
0.5
1.0
1.5
2.0
2.5

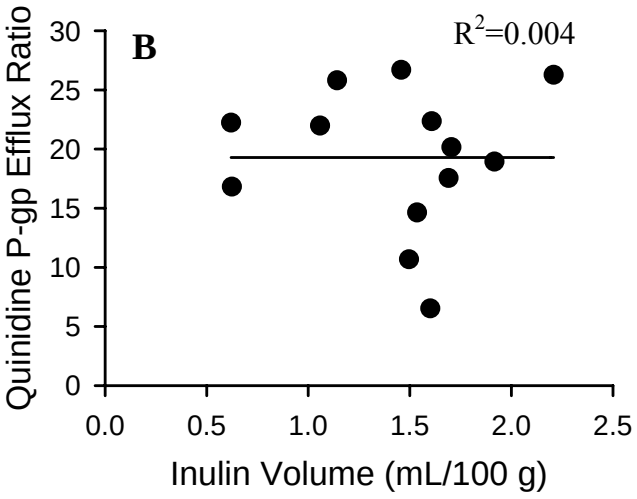
B
R^2=0.004
Quinidine P-gp Efflux Ratio
Inulin Volume (mL/100 g)
0
5
10
15
20
25
30
0.0
0.5
1.0
1.5
2.0
2.5

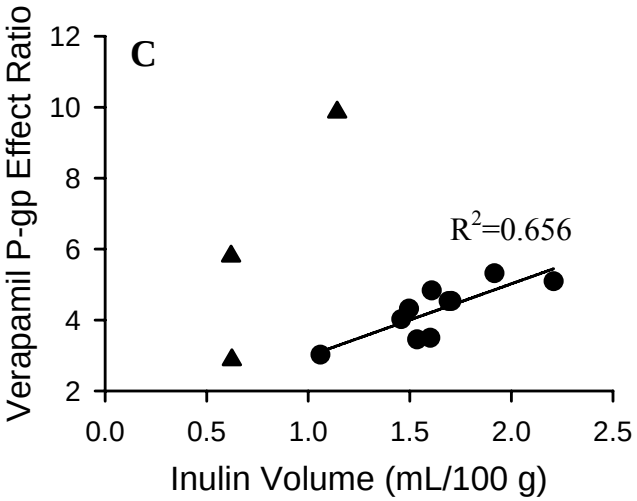
C
R^2=0.656
Verapamil P-gp Effect Ratio
Inulin Volume (mL/100 g)
2
4
6
8
10
12
0.0
0.5
1.0
1.5
2.0
2.5

Figure 5.3: The observed relationship of regional P-gp efflux ratio and cerebral vascular volume (inulin volume, mL/100 g brain tissue) determined by *in situ* brain perfusion at 2.5 mL/min for 60 s in *mdr1a(+/+)* and *mdr1a(-/-)* mice for (A) colchicine, (B) quinidine, and (C) verapamil. The orthogonal regression was carried out for colchicine and quinidine using all thirteen brain regions examined, and for verapamil using all brain regions (circles) excluding pons, medulla and cerebellum (triangles).

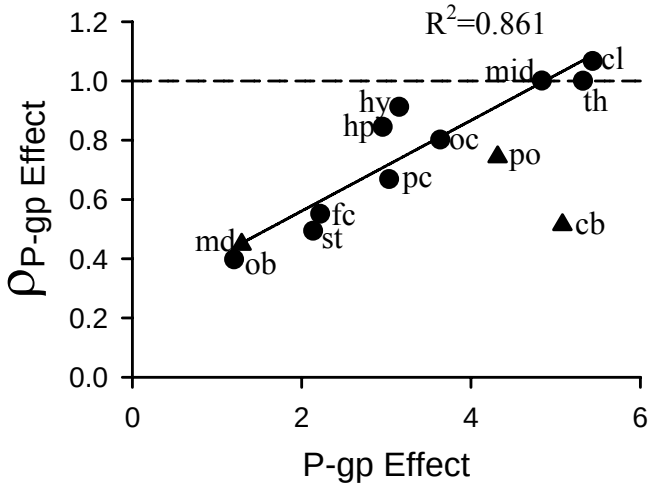

Figure 5.4: The influence of perfusion flow rate perturbation in the regional verapamil P-gp efflux ratio. The Y-axis is the percent change of P-gp efflux ratio at 1 mL/min to 2.5 mL/min; the abscissa is the regional P-gp efflux ratio at perfusion flow rate of 2.5 mL/min. The orthogonal least-squares linear regression was conducted with all brain regions (circles) (R^2=0.861). The triangles (pons, medulla and cerebellum) was not included into regression. ob, olfactory bulb; st, striatum; hp, hippocampus; fc, frontal cortex; pc, parietal cortex; oc, occipital cortex; cl, colliculi; hy, hypothalamus; th, thalamus; mid, midbrain; po, pons; md, medulla; cb, cerebellum.

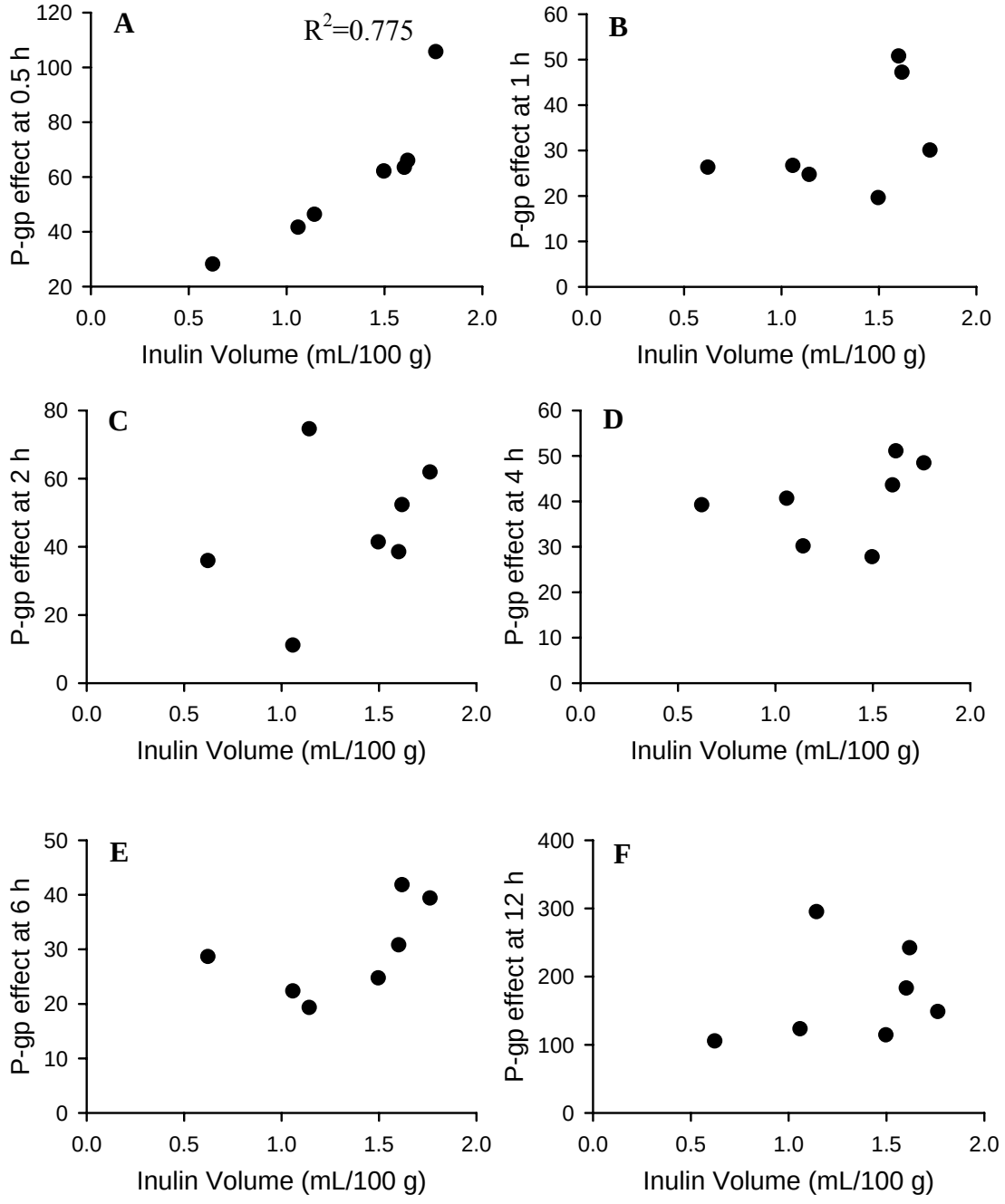

Figure 5.5: The relationship of regional P-gp efflux ratio of loperamide and regional cerebral vascular volume at (A) 0.5 h, (B) 1 h, (C) 2 h, (D) 4 h, (E) 6 h, and (F) 12 h following subcutaneous administration of 30 and 1 mg/kg of loperamide in *mdr1a(+/+)* and *mdr1a(-/-)* mice, respectively.

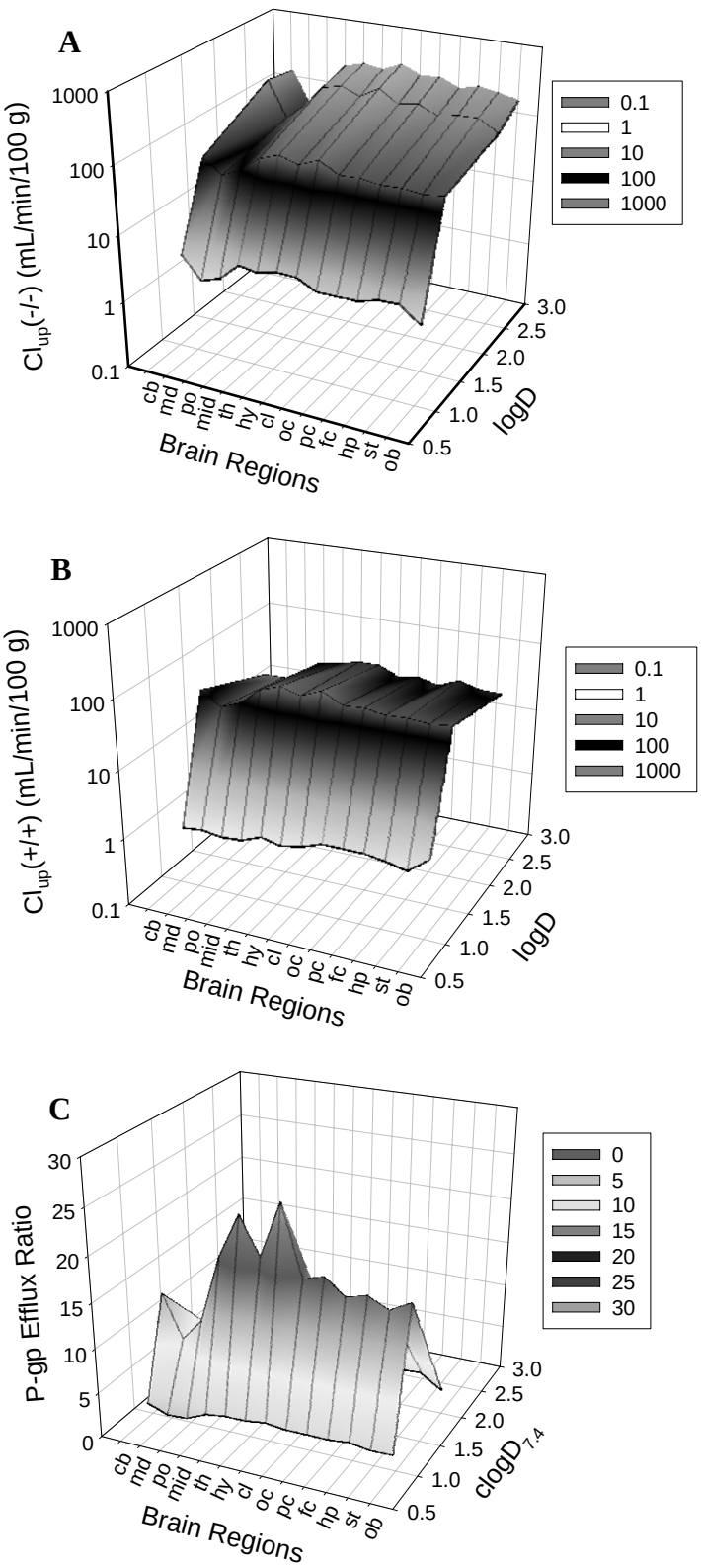
A
1000
100
10
1
0.1
Cl_{up}(-/-) (mL/min/100 g)
cb md po mid th hy cl oc pc fc hp st ob
Brain Regions
3.0
2.5
2.0
1.5
1.0
0.5
logD
0.1
1
10
100
1000
B
1000
100
10
1
0.1
Cl_{up}(+/+) (mL/min/100 g)
cb md po mid th hy cl oc pc fc hp st ob
Brain Regions
3.0
2.5
2.0
1.5
1.0
0.5
logD
0.1
1
10
100
1000
C
30
25
20
15
10
5
0
P-gp Efflux Ratio
cb md po mid th hy cl oc pc fc hp st ob
Brain Regions
3.0
2.5
2.0
1.5
1.0
0.5
$clogD_{7.4}$
0
5
10
15
20
25
30

Figure 5.6: The relationship of brain uptake of colchicine, quinidine and verapamil and diazepam (A) in *mdr1a(-/-)* mice [$Cl_{up}^{(-/-)}$], (B) *mdr1a(+/+)* mice and (C) P-gp efflux ratios and the logarithm of octanol water patition coefficient at pH 7.4 ($clogD_{7.4}$) in each brain region. ob, olfactory bulb; st, striatum; hp, hippocampus; fc, frontal cortex; pc, parietal cortex; oc, occipital cortex; cl, colliculi; hy, hypothalamus; th, thalamus; mid, midbrain; po, pons; md, medulla; cb, cerebellum.

CHAPTER 6

CONCLUSIONS

The blood-brain barrier (BBB) and blood-cerebrospinal fluid barrier (BCSFB) are the major interfaces between the central nervous system (CNS) and the peripheral circulation. The BBB and BCSFB are formed by the brain capillary endothelial cells and epithelial cells lining the choroid plexus, respectively. Highly-developed tight junctions, lack of fenestrae, limited pinocytotic or transcytotic activities, and expression of numerous efflux transporters and metabolizing enzymes at both barriers limit brain penetration of many endogenous compounds and therapeutic agents (Begley 2003; Graff and Pollack 2004). The surface area of the BBB is approximately 3,000-times that of BCSFB, and consequently is the primary obstacle for CNS drug penetration. CNS pharmacologic or toxic response is determined by the rate and/or extent of drug presentation to the site of action, and the intrinsic ability of the agent to elicit a biologic effect.

CNS exposure is determined by complex processes as illustrated in Figure 6.1. The CNS can be viewed as compartmentalized with respect to target localization. Depending on that localization, it is the unbound extracellular fluid (ECF), unbound intracellular, or, in limited cases, cerebrospinal fluid (CSF) concentration that drives the biologic response. Passive and active flux processes at the BBB and BCSFB, nonspecific binding (i.e., to non-receptor proteins) in plasma and brain tissue, metabolism at the BBB or BCSFB, and CSF turnover rate all can influence significantly the net brain exposure to therapeutic or toxic compounds (Brodie et al. 1960; Fenstermacher et al. 1981; Kalvass and Maurer 2002; Kalvass et al. 2007a; Liu and Chen 2005; Liu et al. 2004; Schinkel et al. 1994). An additional complication is that therapeutic targets are not homogeneously distributed throughout the brain, but rather are region-specific. Regional physiologic factors such as

blood flow rate, brain capillary density, capillary residence time, and expression of transport proteins and metabolic enzymes will determine regional drug exposure.

Studies focused on how various pathological conditions may influence the physical and functional aspects of the BBB have been somewhat limited in scope. Understanding the kinetics of drug uptake into brain (whether or not the compound cross the BBB and, if so, how fast and to what extent compound reaches the brain; the extent of drug exposure at the specific site of action; the relationship between dose, target site exposure, receptor occupancy and the pharmacologic response) is crucial to providing direction for drug design and development in the treatment of CNS disorders. However, the current understanding of many of these aspects is limited due to the complexity of the organ system and the techniques used to characterize brain distribution. For example, the functional efficiency of efflux transporters other than P-glycoprotein (P-gp) is mostly unknown and largely controversial. Similarly, the functional role of metabolizing enzymes expressed in the brain or at the blood-brain interface is only beginning to be appreciated. In the current dissertation project, a variety of experimental approaches, including *in vitro*, *in situ* and *in vivo* models were used to study: (1) the factors determining the BBB permeability; (2) the impact of P-gp and brain metabolism on brain exposure to a poorly permeable model compound, fexofenadine; (3) the potential role of breast cancer resistance protein (Bcrp) as a barrier transporter at the blood-brain interface; and (4) the mechanisms that dictate regional distribution of compounds within the brain.

The Rate of Brain Penetration

The *in situ* brain perfusion technique was developed in 1984, and represents a powerful experimental tool for examining brain uptake kinetics under near-sink conditions. This model has many advantages over several older techniques (i.e., brain uptake index, systemic administration *in vivo*) in measuring the initial rate of brain uptake and BBB permeability (Takasato et al. 1984). The intact architecture of the BBB is maintained during perfusion, but confounding factors such as protein binding or systemic metabolism are avoided. The complete control of the composition of perfusion buffer and perfusate flow make this method applicable to studying several different aspects of CNS kinetics, such as the ability of compounds to cross the BBB, the potential modulation of transporter kinetics at the BBB, and regionality of substrate distribution. By adapting the perfusion technique for use in mice (Dagenais et al. 2000), the use of genetic knockout animal models became possible, providing invaluable information on the impact of efflux transport by P-gp on brain exposure (Dagenais et al. 2001a; Dagenais et al. 2004; Dagenais et al. 2001b; Graff and Pollack 2005; Zong and Pollack 2003).

Lipophilicity has been recognized as one of the most important determinants for brain penetration due to the diffusion barrier presented by the plasma membrane of brain capillary endothelial cells. In previous studies (Smith 2003; Takasato et al. 1984), it has been demonstrated that the rate of brain uptake is proportional to lipophilicity at physiologic pH ($clogD_{7.4}$). However, the compounds were mostly non-therapeutic agents with limited lipophilicity ($clogD_{7.4}<1$). In Chapter 2, a sigmoidal relationship was demonstrated for twelve compounds with $clogD_{7.4}$ in the range of 0-6. Compounds with low lipid solubility cannot penetrate the plasma membrane of the BBB endothelium, and

uptake is limited by permeability (i.e., the rate of uptake under approximate sink conditions in the brain is limited by the rate of diffusion through the membrane). For compounds with $clogD_{7.4}$ higher than 3, the rate of brain uptake is limited by the blood flow (or, in the case of *in situ* perfusion, the perfusate flow rate) and therefore is not sensitive to passive permeability. For compounds with a $clogD_{7.4}$ between 1 and 3, the rate of brain uptake is a function of permeability and flow rate.

It is interesting to note that, for the 5 CNS-active drugs investigated in this study, the mean passive permeability was approximately 3-fold higher than the non-CNS active drugs in the compound set. Furthermore, none of the CNS-active drugs were subject to P-gp-mediated efflux at the BBB, whereas the mean P-gp efflux ratio for the non-CNS active drugs was approximately 5.5. These results suggested that passive permeability and P-gp-mediated efflux activity at the BBB can differentiate the CNS and non-CNS drugs. From the drug design standpoint, a potential strategy for enhancing the probability of success in drug development is to design lipophilic agents that are not substrates of efflux transporters at the BBB. In addition, similar to the overall brain exposure, the regional distribution of drugs in different brain structures also was determined by lipophilicity and P-gp-mediated efflux (Chapter 5).

The rate of brain equilibration with blood (i.e., the time to distribution equilibrium across the blood-brain interface) is an important aspect of CNS kinetics because it can influence the onset and offset of CNS activity. Some therapeutic indications, such as brain infections, stroke, epilepsy, neuropathic pain, and trauma, require a rapid onset of action, whereas other indications, such as Alzheimer's disease (AD), Parkinson's disease (PD) and depression, can be treated effectively with drugs with a slow onset of action. The rate

of brain penetration is not only a function of permeability, but also of nonspecific binding in brain tissue. It is the difference in apparent brain distributional volume that contributes to the difference between the onset time of alfentanil and fentanil. Both compounds have similar systemic pharmacokinetics. Generally, BBB permeability increases with lipophilicity, whereas the brain tissue unbound fraction has an inverse relationship with lipophilicity. The apparent inverse relationship between PS and $f_{u,brain}$ makes the equilibration half-life a complex function of lipophilicity, with the most rapid equilibration for compounds with a $clogD_{7.4}$ in the range of 1-3 (Figure 2.3). In the twelve compounds investigated in this portion of the dissertation project, alfentanil evidenced the most rapid equilibration. Both alfentanil and diazepam brain uptake were rapid and limited by perfusion flow rate. Alfentanil brain equilibrium was reached in 20 s, whereas diazepam brain uptake was still unidirectional after 60 s of brain perfusion. Diazepam binds more extensively than alfentanil to proteins in brain tissue, resulting in a larger apparent brain volume for diazepam than alfentanil, with a consequent longer time required to establish distribution equilibrium. Mathematical modeling and simulation, coupled with experimental results, demonstrated that the intrinsic equilibration half-life is an inverse function of product of permeability and brain tissue unbound fraction ($PS \times f_{u,brain}$) (Liu and Chen 2005; Liu et al. 2005). Colchicine, ritonavir, and fexofenadine demonstrated very slow equilibration across the BBB. The equilibration half-life varied widely among the different compounds studied. This result also can be inferred, and therefore supported at least indirectly, by *in vivo* pharmacodynamic studies that indicated a 70-fold difference in brain equilibration half-life ($t_{1/2eq,brain}$) between alfentanil and morphine (Kalvass et al. 2007b).

The Extent of Brain Penetration

For compounds that distribute between blood and brain solely by passive diffusion, the plasma-to-brain unbound fraction ratio has been used successfully to predict *in vivo* brain-to-plasma concentration ratio at distribution equilibrium, under the assumption that unbound brain and plasma concentrations will be equal at steady-state or post-distributional equilibrium. P-gp attenuates the extent of brain exposure by 2- to 65-fold for many therapeutic agents (Chen et al. 2003b; Kalvass et al. 2004). Previous efforts to predict brain penetration of P-gp substrates have demonstrated that this assumption still holds for most compounds. The brain partition coefficient $K_{p,brain}$ is determined by the plasma and brain unbound fraction ratio and the magnitude of the P-gp efflux ratio at the BBB (Kalvass et al. 2007a; Summerfield et al. 2006).

Sedative side effects are common for first-generation antihistamines, most of which have high passive permeability and are not subject to P-gp-mediated efflux at the BBB. Consequently, the unbound brain concentration is as high as the unbound plasma concentration. In contrast, brain penetration of the second-generation antihistamines fexofenadine and cetirizine is minimal, and these compounds do not cause sedation. In Chapter 3, fexofenadine brain penetration was almost completly restricted by P-gp-mediated efflux at the BBB, and increased ~50-fold in P-gp-deficient mice. Following a continuous infusion with a subcutaneously-implanted osmotic minipump, not only fexofenadine brain penetration, but also P-gp efflux ratio, was found to increase over time. This temporal pattern was predicted by a two-compartment model with the passive diffusion and P-gp-mediated efflux mediating substrate flux between the systemic circulation and the brain compartment. In addition, following administration of the

permeable prodrug terfenadine, fexofenadine brain exposure increased ~25-fold compared to fexofenadine administration due to the conversion of terfenadine to fexofenadine in the brain tissue.

In addition to P-gp, which significantly decreases the rate and extent of brain penetration, Bcrp is another important efflux transporter expressed at the BBB. However, even though cimetidine, alfuzosin, dipyridamole and LY2228820 have been demonstrated to be transported by Bcrp in the MDCKII-Bcrp cell line, none of these compounds showed impaired BBB penetration in wild-type mice compared to the genetic knockout *Abcg2(-/-)* mouse model or to animals treated with co-perfusion of the chemical inhibitor GF120918 (Chapter 4). Bcrp might only play a minor role, and P-gp is the predominant efflux transporter at the BBB in limiting drug brain exposure.

Taken together, these results suggested that the extent of brain exposure, and ultimately the pharmacologic or toxicologic profile, might be influenced by passive diffusion, active transport, nonspecific binding in plasma and brain tissue, and metabolic deactivation or activation at the blood brain interface and/or inside the brain tissue.

Regional Distribution Among Brain Structures

Effective neurotherapeutics depend on the ability to achieve adequate drug exposure at the site of action. The brain is a highly structurally- and functionally-specialized organ, and therapeutic targets are not distributed homogeneously throughout the brain (Heiss and Herholz 2006). For example, regional blood flow rate in rat brain spans an approximate 18-fold range, and has been shown to correlate with regional brain capillary density (Fenstermacher et al. 1991; Klein et al. 1986). These local physiologic parameters

determine the surface area for substrate exchange between blood and brain, the rate of mass delivery to serve as the driving force for such exchange, and the residence time in different brain structures allowing substrate diffusion across the capillary endothelium of interaction with transport protein or enzymes expressed at the blood-brain interface. Each of the factors will potentially contribute to the consequent regional drug exposure. In regions such as cerebellum and brain stem, the blood supply comes from vertebral arteries, whereas the remainder of the brain is supplied by the carotid arteries under normal physiologic conditions. Drug exposure typically is low in cerebellum and brain stem, which causes problems in the treatment of diseases reside in these brain regions.

In Chapter 5, the regional brain capillary vascular volume and blood flow rate were determined with *in situ* brain perfusion and microdissection techniques, using ^{3}H-inulin and ^{14}C-diazepam as the brain capillary vascular volume and blood flow rate markers, respectively. The results of this study demonstrated that brain capillary density (inferred from vascular volume) and perfusion rate range approximately 3.7- and 7.5-fold, respectively, in thirteen dissected brain structures (olfactory bulb, striatum, hippocampus, frontal cortex, parietal cortex, occipital cortex, colliculi, hypothalamus, thalamus, midbrain, pons, medulla and cerebellum). Regional functional perfusate flow rate, as inferred from the uptake clearance of diazepam, which is known to be flow rate-limited (Dagenais et al. 2000; Takasato et al. 1984), strongly correlated with local capillary density. In general, brain structures with a more dense capillary bed and richer blood flow (e.g., inferior and superior colliculi, parietal cortex and thalamus) have more available surface area for drug uptake into brain. However, an increase in available surface area does not necessarily lead to a proportionate increase in uptake clearance. It would be

reasonable to hypothesize that regions with more dense capillaries also would have a higher level of expression of barrier transporters such as P-gp. Indeed, brain perfusion with structurally-diverse drugs (P-gp substrates colchicine, quinidine, and verapamil and non-P-gp substrate diazepam) indicated that regional drug exposure varied about 3.0- to 5.5-fold in P-gp-deficient mice. Colchicine demonstrated the highest exposure in inferior colliculus and olfactory bulb, consistent with the earlier report that these regions in experimental animals and human were most vulnerable to colchicine-induced CNS toxicity (Goldschmidt and Steward 1982; Mundy and Tilson 1990).

The regionality of P-gp-mediated efflux at the BBB has been demonstrated in murine brain following intranasal verapamil administration (Graff et al. 2005; Appendix I). Although the conclusions were based on rather sophisticated mathematical modeling of the data, the results clearly suggest a marked regionality in the influence of P-gp on distribution of verapamil within the brain. P-gp is principally expressed in the brain capillary endothelial cells, and therefore the regional P-gp expression level is determined by regional brain capillary density. In Chapter 5, during brain perfusion, P-gp-mediated efflux decreased brain penetration by 2- to 20-fold for different P-gp substrates (colchicine, verapamil and quinidine) in *mdr1a(+/+)* mice compared to *mdr1a(-/-)* mice. Brain exposure was attenuated by P-gp to differing extents based on both substrate and brain region; regional P-gp efflux ratios varied ~ 2.5- to 4.0-fold in different brain structures for colchicine, verapamil and quinidine. The P-gp-mediated colchicine and verapamil efflux activity was directly proportional to local capillary density (Figure 5.3). In addition, verapamil brain uptake was determined in part by the perfusate flow rate, and decreased with decreasing flow. Changes or differences in perfusate flow did not only

affect verapamil brain uptake by altering the rate of substrate presentation to the brain vasculature, but also by modulating P-gp-mediated efflux activity in brain regions with lower capillary density (i.e., regions with weaker P-gp activities). In contrast, virtually no effect of alterations in flow were noted in regions with the highest capillary densities (i.e., regions with stronger P-gp activities). For poorly-permeable compounds such as colchicine, the change in flow rate had no effect on BBB permeability. This is understandable because flow is not the rate-limiting step in either permeation across the endothelial cell membrane or access to the efflux transport site (presumable a binding domain on P-gp that resides within the endothelial cell membrane) (Begley 2004; Raub 2006; Sharom et al. 2005).

Drug Metabolism in the Brain

Drug metabolizing Phase I enzymes (cytochromes P450) and Phase II conjugating enzymes are expressed in the CNS (Ghersi-Egea et al. 1994; Strobel et al. 2001). The blood-brain and blood-CSF interfaces provide a metabolic barrier, in addition to the physical and transport barriers often considered, for penetrating lipophilic compounds. The expression of metabolic enzymes within the brain is cell- and region-specific (Meyer et al. 2007). In some brain regions, the expression level can be as high as, or even higher than, that in the liver. Biotransformation machinery is present in the brain in part to detoxify or decrease xenobiotic exposure, thereby protecting the organ from chemical insult. However, as with the liver, xenobiotic metabolism in brain also can result in bioactivation of compounds, resulting in the possible formation of pharmacologically active or neurotoxic products. Experiments performed as part of this dissertation project (Chapter 3) demonstrated that terfenadine was metabolized to fexofenadine in murine

brain. Administration of terfenadine caused a 25-fold higher fexofenadine brain exposure as compared to exposure following administration of pre-formed fexofenadine.

As discussed earlier in this dissertation, most models of CNS pharmacokinetics and pharmacodynamics are based on the assumption that unbound substrate concentrations are equivalent at distribution equilibrium. This equivalence of unbound concentration (i.e., driving force) is a hallmark characteristic of substrate distribution by passive processes across a blood:tissue interface. When asymmetrical transport is present (i.e., when flux is dominated by protein-mediated transport in either the uptake or the efflux direction) the unbound concentration of substrate on either side of a diffusional barrier, such as the BBB in the case of fexofenadine, may not be equal even at presumed distribution equilibrium. Because fexofenadine flux from the systemic circulation into brain is limited by both poor permeation and efflux transport, it would be reasonable to hypothesize that unbound concentrations in brain would be less than or equal to, but certainly would not exceed, unbound concentrations in blood. However, when fexofenadine is formed from terfenadine within the brain, the situation changes quite significantly; the unbound brain concentration of fexofenadine was approximately 1.6-fold higher that the unbound concentration in plasma. Earlier studies demonstrated that codeine was metabolized by brain CYP2D6 to morphine, leading to a consequent analgesic effect (Chen et al. 1990; Pai et al. 2004). Similarly, ceterizine brain exposure increased ~7-fold following hydroxyzine administration as compared to direct administration of the pre-formed substrate (Chen et al. 2003a). Thus, local metabolism clearly can play an important role in drug exposure in brain, and might be the most

important causative factor in pharmacologic or toxicologic events in the CNS for certain substances.

In addition to the foregoing observations, mounting evidence has shown that brain P450s are inducible by therapeutic agents, also in a region- and cell-specific manner (Volk et al. 1991). For example, phenytoin induces expression of CYP3A11 and CYP19 in murine brain, which leads to increased testosterone metabolism in the brain (Meyer et al. 2006). Thus, drug-drug interactions may lead to altered CNS pharmacodynamics via a variety of mechanisms: substrate displacement from protein binding sites in plasma and/or brain, inhibition of protein-mediated transport in either the uptake or the efflux direction, inhibition of deactivation or activation biotransformation processes in the brain, and potential induction of either transport or local metabolism. It is imperative to understand the prevailing mechanism or mechanisms of interaction in any given case in order to develop appropriate therapeutic guidelines for the management of such interactions.

Furthermore, several P450 isoforms are responsible for the endogenous biochemical pathways, such as the local synthesis and regulation of steroid hormones, arachidonic acid metabolism (whose metabolites are cerebrovascular regulator, and in turn, pharmacological intervention of blood flow rate) and neurotransmitters synthesis and metabolism. These represent additional sites and mechanisms of potential unanticipated outcomes of drug therapy.

Experimental Models to Study BBB Kinetics

For CNS drug discovery and development, choosing the best experimental models of the BBB depends on many factors, including cost, time, and how closely a model needs to resemble *in vivo* conditions. *In vitro* modeling of the BBB is a simplification of the *in vivo* situation. While cell-based BBB assays are more cost- and time-efficient experimental tools than *in situ* and *in vivo* methods, they lack three-dimensional architecture, blood flow, and sometimes lose the morphology and functional efficiencies of physical and transport barriers as they are elaborated in the intact organism. *In situ* brain perfusion offers a very accurate method to studying the rate of BBB penetration, although it requires technical expertise and raises the issue of interspecies comparisons of distributional events. *In vivo* disposition studies also provide direct measurement of BBB penetration, but are labor-intensive and animal-consumptive. *In situ* and *in vivo* methods have become especially useful for the study of transporter kinetics due to the emergence of various gene knockout animal models and the availability of, in some cases, selective or specific chemical inhibitors.

All experimental models have specific advantages and limitations. It is not possible to develop an ideal model that represents all aspects of BBB penetration. An alternative approach is the combined use of several models to study different aspects of BBB kinetics, including both mechanistic and quantitative information domains. MDCK cells have been used successfully to rank order the ability of compounds to cross the BBB based on passive permeability across the cell membrane. Passive permeability determined in this cell-based models correlated well with the *in situ* brain permeability (Summerfield et al. 2007). Experiments performed in this dissertation project also demonstrated good

correlation between passive membrane permeability in MDCK cells and BBB permeability in mouse brain (Figure 4.7B and 4.7C, Chapter 4). Recently, primary brain capillary endothelial cell culture and immortalized cell lines have been developed as the alternative *in vitro* BBB model. For example, permeability in cultured bovine brain microvessel endothelial cells is predictive of *in vivo* BBB permeability based on *in vivo* brain microdialysis (Hansen et al. 2002). Furthermore, P-gp-mediated efflux kinetics also have been studied using cell lines that express endogenous P-gp (i.e., Caco-2) or stably transfected P-gp (MDCK and LLC-PK1 cells). The *in vitro* P-gp effect determined in these models was correlated among the different cell lines, and all cell lines correlated with the P-gp effect determined using *in situ* and *in vivo* methods (Adachi et al. 2001; Hochman et al. 2002; Yamazaki et al. 2001). Marketed CNS and non-CNS drugs can be differentiated by membrane permeability and P-gp-mediated efflux in P-gp-transfected MDCK cells, indicating that the drug candidates with passive permeability > 150 nm/s and non-P-gp substrates are more likely to be successful CNS therapeutics (Mahar Doan et al. 2002). The passive permeability and P-gp-mediated efflux at the BBB also differentiated the CNS- and non-CNS drugs in the present studies (Chapter 2).

In addition to observational experimentation, the theoretical relationship between *in vitro*, *in situ* and *in vivo* transport kinetics has been quantitatively evaluated using a three-compartment modeling and simulation approach. The different model systems can be characterized equivalently by the parameter "efflux ratio" which is a function of efflux activity and passive membrane permeability (Kalvass and Pollack 2007). A good correlation between *in vitro* (regardless the cell origins or P-gp expression levels) and *in vivo* ($K_{p,brain}$ ratio in P-gp-deficient mice to wild-type mice) P-gp efflux ratios was

observed for 55-member compound set (Chen et al. 2003b). These studies suggested that under certain conditions *in vitro* models are predictive, quantitatively and mechanistically, of some elements of *in vivo* transporter kinetics at the BBB.

Various experimental models have established P-gp as a gatekeeper at the BBB to maintain the homeostasis of the neuronal environment. However, discrepancies between different model systems are observed frequently, which cast doubt on the validity and to what extent the *in vitro* model can resemble *in vivo* situation. The differences can be many fold, although the underlying reasons for these differences have not been fully explained. One likely contributor is blood flow, which is an important characteristic of the *in vivo* BBB that is absent in cell-based models. Lipophilic compounds cross the BBB readily, and are limited in uptake by blood flow. In addition, the molecular mechanisms of P-gp-mediated efflux, and even the substrate interaction site(s) of P-gp, are still unknown. Access to the binding site that resides inside the plasma membrane can be the rate-limiting step for hydrophilic compounds, and transport efficiency might be influenced by residence time at or near the binding site. This residence time is, in turn, influenced by the rate of blood flow through the vessel, at least for substrates of intermediate permeability.

An additional experimental complexity is that the expression level, localization, and functional efficiency of P-gp at the BBB all may vary among different animal species, including human (Ohtsuki and Terasaki 2007; Yamazaki et al. 2001). P-gp in rodents was reported to be principally expressed in the luminal side of the brain capillary endothelial cells, whereas P-gp is expressed in brain capillary endothelial cells, astrocytes, and neurons in human (Bendayan et al. 2006; Golden and Pardridge 1999). The inhibitory

effect of P-gp inhibitors showed significant species differences with different affinity toward P-gp in different species (Katoh et al. 2006; Suzuyama et al. 2007). Such differences make the extrapolation from *in vitro* and animal research to clinical studies quite difficult. Previous studies have demonstrated that other efflux transport proteins expressed at the BBB might be upregulated when P-gp was knocked out. For example, Bcrp mRNA level increased 3-fold in *mdr1a/1b*(-/-) mice (Cisternino et al. 2004). However, the functional efficiency of this compensatory mechanism at the BBB is still unknown. In addition, some presumably "specific" P-gp inhibitors have been found to be non-specific in studies of transport kinetics, e.g., cyclosporin A has been found to inhibit Bcrp and Oatp (Gupta et al. 2006; Xia et al. 2007).

With P-gp as the most extensively-studied efflux transporter at the BBB, increasing attention has been paid to the potential role of Bcrp at the BBB due to the immense similarity of expression pattern and substrate specificity between these two proteins. However, while Bcrp mRNA and protein have been reported to be expressed at the BBB, the functional efficiency of Bcrp at the blood-brain interface remains controversial. Some studies have suggested that Bcrp is functional at the BBB (Breedveld et al. 2005; Enokizono et al. 2007), while others indicate a minor role of this transporter at the BBB (Cisternino et al. 2004; Lee et al. 2005). In the present studies (Chapter 4), Bcrp substrates (cimetidine, alfuzosin, dipyridamole and LY2228820) were identified in MDCKII-Bcrp transwell transport screening assays. None of these substrates evidenced increased brain penetration following knockout of Bcrp gene or chemical (GF120918) inhibition.

As with many other aspects of BBB function, the reasons underling the discrepancies between *in vitro* (MDCKII-Bcrp in this case) and *in vivo* (brain perfusion in Bcrp-competent versus Bcrp-deficient mice; brain perfusion in Bcrp-competent mice with and without a chemical inhibitor) models are unknown. Such discrepancies also have been observed in previous studies (Cisternino et al. 2004; Lee et al. 2005). A recent observation demonstrated that Bcrp protein in human and rat brain capillary endothelial cells is expressed at a much lower level than in *in vitro* overexpressed system (Lee et al. 2007). In addition, the compensatory mechanism (e.g., increased Mrp4 protein expression in spleen and thymus) has also been demonstrated for Bcrp knockout mice (Takenaka et al. 2007).

Other efflux transporters such as multidrug resistance associated proteins (Mrps) have been reported to be expressed at the BBB, and the functional efficiency in effluxing organic anions out of the brain has been speculated. However, organic anions and nucleotide drugs are mostly hydrophilic compounds and ionized at physiologic pH. *In vivo* BBB penetration was primarily restricted by passive permeability of such compounds. Even though some evidence has demonstrated that *in vivo* BBB penetration of these compounds (e.g., PMEA, AZT) was further impaired by Mrps, brain penetration is not significant even in Mrp-knockout animals (Belinsky et al. 2007).

BBB Characteristics under Pathological Conditions

Potentially interrupted BBB integrity under pathological conditions such as HIV infection, meningitis, traumatic brain injury, Alzheimer's disease, multiple sclerosis, gliomas and metastatic brain tumors, epileptic seizures, hypertension, and stroke has been implicated.

The compromised BBB might lead to increased brain penetration of therapeutic agents (e.g., increased morphine concentrations in injured brain) and even macromolecules such as albumin (Ederoth et al. 2004). This potential has been exploited for presumed therapeutic gain with the hyperosmotic disruption of the BBB in the case of CNS cancer chemotherapy (Hsieh et al. 2005).

Several physiologic parameters may be influenced by disease states or by the untoward effects of therapeutic agents. Ischemia affects the BBB integrity and decreases cerebral glucose uptake even in the presence of increased glucose transporter GLUT1 mRNA level (Cavaglia et al. 2001; Suzuki et al. 1998). Changes in arterial pCO_2 influence the diameter of brain capillaries, thus modulating the surface area for exchange at the blood-brain interface (Duelli and Kuschinsky 1993). A high fat diet alters the cerebral blood flow rate and/or brain capillary density (Hasselbalch et al. 1996; Puchowicz et al. 2007). Cerebral blood flow rate may be increased pharmacologically, as is the case with nicotine administration or consumption (Hans et al. 1993).

In addition, overexpression of efflux transporters has been reported in epileptic brain. For patients with refractory epilepsy, MDR1, MRP2 and MRP5 were upregulated in epileptic tissue. P-gp was induced in glial cells and neurons in epilepticus region, whereas P-gp is majorly expressed at the endothelial cells under normal conditions. The overexpression is also region- and cell-specific (van Vliet et al. 2007).

Prediction of BBB Distribution Kinetics for Investigational Molecules

CNS drug discovery and development is especially important due to the large unmet needs in clinical therapeutics, and in large part due to an increasing aging population.

Most of the drug candidates for CNS therapeutics that have good *in vitro* efficacy cannot cross the BBB to reach the intended target in concentrations sufficient to exert a meaningful pharmacologic effect. Lipophilicity is the most important determinant of BBB penetration. *In silico* models are usually the only option for compound screening in terms of BBB permeability during the early phase of drug discovery process. *In silico* models can only characterize and predict passive permeability of the BBB based on the parameters determined in *in vitro, in situ* and *in vivo* models using the physicochemical properties (lipophilicity, pKa, polar surface areas, etc) of investigational molecules. Significant recent progress has been made towards rational CNS drug discovery (Feng 2002; Goodwin and Clark 2005; Liu and Chen 2005). As generally-accepted "rules of thumb", compounds with molecular weight less than 450 Da, polar surface area less than 80 $Å^2$, octanol-water partition coefficient 1-3 are favorable to cross the BBB (Clark 2003; Norinder and Haeberlein 2002).

The extent of brain exposure ($K_{p,brain}$) of compounds that undergo passive diffusion at the BBB was successfully predicted by *in vitro* plasma-to-brain unbound fraction ratio determined with the equilibrium dialysis method (Kalvass et al. 2007a), and was used most often as the index parameter in BBB *in silico* model development and prediction. An *in silico* model also has been developed to predict brain tissue unbound fraction based on the chemical structures of compounds. The degree of protein binding was found to be related to compound lipophilicity (Wan et al. 2007). However, it is frequently stated that unbound drug concentration is more relevant for the pharmacologic and toxic effects in the CNS. Using $K_{p,brain}$ to predict and screen drug candidates therefore might be potentially erroneous and misleading.

A recent trend is to use passive permeability as a surrogate in model development. However, passive permeability is a parameter that describes the rate, but not necessarily the extent, of brain penetration. An index parameter that characterizes the extent of brain exposure $K_{p,free}$ has been proposed (Liu and Chen 2005). An additional complication is the fact that the therapeutic targets within the brain are not homogeneously distributed. Because the brain is a compartmentalized organ, drug exposure at the site of action is the most relevant parameter to assess and predict the pharmacologic effect. Compartmentalization, as shown in Figure 6.1, is a simple illustration of this characteristic. The therapeutic targets for most of CNS acting drugs are accessible from the brain extracellular fluid. Only for some diseases, such as brain tumor and HIV infection, will the effect site be inside the cell. The regional drug distribution in different brain structures is influenced by the local cerebral blood flow rate, capillary density, nonspecific binding and P-gp efficiency. It is very difficult to determine and predict the unbound brain concentration at the site of action. Combined use of different models has been employed to understand the underlying mechanisms and complex processes of brain distribution (Venkatakrishnan et al. 2007; Zhuang et al. 2006). Brain microdialysis, *in vitro* nonspecific protein binding assay, brain slices and CSF sampling are the most prevalent methods to determine the unbound brain concentration (Becker and Liu 2006; de Lange et al. 1997; Kalvass and Maurer 2002; Shen et al. 2004).

However, it is important to bear in mind that the BBB is not only a physical barrier. Lipophilic compounds which in theory will be effective permeants of the lipoidal BBB also tend to be P-gp substrates. Thus, compounds that would otherwise be able to cross the BBB are subject to the efflux and/or metabolism at the BBB and BCSFB interfaces

and associated brain parenchymal cells. Uptake transporters also are present in the BBB. While these proteins in theory can be exploited for therapeutic gain, it has been difficult to design drugs as substrates of these proteins because of their high specificity for endogenous compounds and nutrients (Ohtsuki and Terasaki 2007).

From a practical standpoint, the most effective strategy is to design compounds with adequate lipid solubility that do not interact with efflux transporters at the BBB. However, the effort to predict P-gp substrates based on physicochemical properties or chemical structure alone has been frustrating, and the attempt to establish structure-activity relationships to identify P-pg substrates and inhibitors has been unsuccessful. So, P-gp substrates still need to be identified via screening with selected *in vitro* and *in vivo* methods. The non-cerebral origin, P-gp transfected MDCK or LLC-PK1 cell lines, are relatively high-throughput screening methods. Together with *in situ* brain perfusion technique and *in vivo* brain distribution method, *in vivo* P-gp effect at the BBB can be revealed.

The BBB is also a metabolic barrier, although limited knowledge has been gained in this area (Meyer et al. 2007; Strobel et al. 2001). Lipophilc compounds that permeate the BBB and escape efflux transport may be metabolized by enzymes expressed at the blood-brain and blood-CSF interfaces, astrocytes and neurons. Specific experimental models need to be developed to investigate brain metabolic enzyme function and regulation, especially the region- and cell-specific aspects of this phenomenon. Cell culture systems from distinct neuronal populations and *in vivo* animal models with microdissected regions have to be developed. In addition, *in silico* models need to be developed to predict the substrates, inhibitors and inducers of specific enzyme isoforms, and the

consequences of brain metabolism on the pharmacologic and toxic effects need to be considered.

The predictive accuracy of *in silico* model, in the present context whether they are developed to address issues of distribution, transport, or metabolism, is directly determined by the quality of the experimental data used for model development and validation. The recent shift from logBB to logPS or $K_{p,free}$ have made model development even more difficult because of the limited available database in the existing literature due to technical challenges, cost, time and labor-intensity associated with the relevant experimental paradigms. In general, the current models can produce reasonable prediction of *in vivo* passive brain uptake. More components, such as active transport and metabolic activity, nonspecific binding in blood and brain tissue, and factors that dictate regional distribution within the brain areas need to be added to the modeling strategy in order to predict effectively the multiplicity of aspects that ultimately determine CNS drug response.

Summary

Ideally, a comprehensive understanding of the primary mechanisms underlying and determining CNS pharmacokinetics and pharmacodynamics will be gained to facilitate description and prediction of the time-course of drug concentrations at the site of action in specific brain structures, as well as in specific compartments of the brain such as the extracellular fluid, intracellular fluid, and CSF. Ultimately, the kinetics of substrate flux through these various compartments of the brain will be important determinants of the magnitude and time-course of the pharmacologic/toxic effects in the CNS. Immense

progress has been made in the understanding of CNS kinetics at the level of BBB permeability. However, understanding substrate kinetics within the brain, that is, after the substrate has penetrated the BBB, represents an important frontier for CNS pharmacology research. Regional distribution in different brain anatomical structures, drug exposure at the target site, elimination by local metabolism and active transport from the brain are critical issues that have been understudied, and must be understood with some degree of precision if the development of new neurotherapeutic compounds is to become an efficient enterprise. The creation of new experimental BBB models, new and innovative methods of data analysis, novel use of simulation experiments based on known elements of system behavior, and integration of new data with the current knowledge base from *in vitro*, animal and human studies. all will be required to achieve this important goal.

Additional aspects such as the change of BBB characteristics under pathological conditions, the potential contribution of polymorphisms of BBB transporters and metabolic enzymes to interpatient variability, metabolic enzymes as therapeutic targets, extrapolation of *in vitro* and animal data to human clinical studies, and *in vivo* therapeutic target efficacy all are important topics that require further investigation.

Reference

Adachi Y, Suzuki H, Sugiyama Y. (2001) Comparative studies on in vitro methods for evaluating in vivo function of MDR1 P-glycoprotein. *Pharm Res* 18:1660-1668

Becker S, Liu X. (2006) Evaluation of the utility of brain slice methods to study brain penetration. *Drug Metab Dispos* 34:855-861

Begley DJ. (2003) Understanding and circumventing the blood-brain barrier. *Acta Paediatr Suppl* 92:83-91

Begley DJ. (2004) ABC transporters and the blood-brain barrier. *Curr Pharm Des* 10:1295-1312

Belinsky MG, Guo P, Lee K, Zhou F, Kotova E, Grinberg A, Westphal H, Shchaveleva I, Klein-Szanto A, Gallo JM, Kruh GD. (2007) Multidrug resistance protein 4 protects bone marrow, thymus, spleen, and intestine from nucleotide analogue-induced damage. *Cancer Res* 67:262-268

Bendayan R, Ronaldson PT, Gingras D, Bendayan M. (2006) In situ localization of P-glycoprotein (ABCB1) in human and rat brain. *J Histochem Cytochem* 54:1159-1167

Breedveld P, Pluim D, Cipriani G, Wielinga P, van Tellingen O, Schinkel AH, Schellens JH. (2005) The effect of Bcrp1 (Abcg2) on the in vivo pharmacokinetics and brain penetration of imatinib mesylate (Gleevec): implications for the use of breast cancer resistance protein and P-glycoprotein inhibitors to enable the brain penetration of imatinib in patients. *Cancer Res* 65:2577-2582

Brodie BB, Kurz H, Schanker LS. (1960) The importance of dissociaton constant and lipid-solubility in influencing the passage of drugs into the cerebrospinal fluid. *J Pharmacol Exp Ther* 130:20-25

Cavaglia M, Dombrowski SM, Drazba J, Vasanji A, Bokesch PM, Janigro D. (2001) Regional variation in brain capillary density and vascular response to ischemia. *Brain Res* 910:81-93

Chen C, Hanson E, Watson JW, Lee JS. (2003a) P-glycoprotein limits the brain penetration of nonsedating but not sedating H1-antagonists. *Drug Metab Dispos* 31:312-318

Chen C, Liu X, Smith BJ. (2003b) Utility of Mdr1-gene deficient mice in assessing the impact of P-glycoprotein on pharmacokinetics and pharmacodynamics in drug discovery and development. *Curr Drug Metab* 4:272-291

Chen ZR, Irvine RJ, Bochner F, Somogyi AA. (1990) Morphine formation from codeine in rat brain: a possible mechanism of codeine analgesia. *Life Sci* 46:1067-1074

Cisternino S, Mercier C, Bourasset F, Roux F, Scherrmann JM. (2004) Expression, up-regulation, and transport activity of the multidrug-resistance protein Abcg2 at the mouse blood-brain barrier. *Cancer Res* 64:3296-3301

Clark DE. (2003) In silico prediction of blood-brain barrier permeation. *Drug Discov Today* 8:927-933

Dagenais C, Ducharme J, Pollack GM. (2001a) Uptake and efflux of the peptidic delta-opioid receptor agonist. *Neurosci Lett* 301:155-158

Dagenais C, Graff CL, Pollack GM. (2004) Variable modulation of opioid brain uptake by P-glycoprotein in mice. *Biochem Pharmacol* 67:269-276

Dagenais C, Rousselle C, Pollack GM, Scherrmann JM. (2000) Development of an in situ mouse brain perfusion model and its application to mdr1a P-glycoprotein-deficient mice. *J Cereb Blood Flow Metab* 20:381-386

Dagenais C, Zong J, Ducharme J, Pollack GM. (2001b) Effect of mdr1a P-glycoprotein gene disruption, gender, and substrate concentration on brain uptake of selected compounds. *Pharm Res* 18:957-963

de Lange EC, Danhof M, de Boer AG, Breimer DD. (1997) Methodological considerations of intracerebral microdialysis in pharmacokinetic studies on drug transport across the blood-brain barrier. *Brain Res Brain Res Rev* 25:27-49

Duelli R, Kuschinsky W. (1993) Changes in brain capillary diameter during hypocapnia and hypercapnia. *J Cereb Blood Flow Metab* 13:1025-1028

Ederoth P, Tunblad K, Bouw R, Lundberg CJ, Ungerstedt U, Nordstrom CH, Hammarlund-Udenaes M. (2004) Blood-brain barrier transport of morphine in patients with severe brain trauma. *Br J Clin Pharmacol* 57:427-435

Enokizono J, Kusuhara H, Sugiyama Y. (2007) Effect of breast cancer resistance protein (Bcrp/Abcg2) on the disposition of phytoestrogens. *Mol Pharmacol* 72:967-975

Feng MR. (2002) Assessment of blood-brain barrier penetration: in silico, in vitro and in vivo. *Curr Drug Metab* 3:647-657

Fenstermacher J, Nakata H, Tajima A, Lin SZ, Otsuka T, Acuff V, Wei L, Bereczki D. (1991) Functional variations in parenchymal microvascular systems within the brain. *Magn Reson Med* 19:217-220

Fenstermacher JD, Blasberg RG, Patlak CS. (1981) Methods for Quantifying the transport of drugs across brain barrier systems. *Pharmacol Ther* 14:217-248

Ghersi-Egea JF, Leninger-Muller B, Suleman G, Siest G, Minn A. (1994) Localization of drug-metabolizing enzyme activities to blood-brain interfaces and circumventricular organs. *J Neurochem* 62:1089-1096

Golden PL, Pardridge WM. (1999) P-Glycoprotein on astrocyte foot processes of unfixed isolated human brain capillaries. *Brain Res* 819:143-146

Goldschmidt RB, Steward O. (1982) Neurotoxic effects of colchicine: differential susceptibility of CNS neuronal populations. *Neuroscience* 7:695-714

Goodwin JT, Clark DE. (2005) In silico predictions of blood-brain barrier penetration: considerations to "keep in mind". *J Pharmacol Exp Ther* 315:477-483

Graff CL, Pollack GM. (2004) Drug transport at the blood-brain barrier and the choroid plexus. *Curr Drug Metab* 5:95-108

Graff CL, Pollack GM. (2005) Functional evidence for P-glycoprotein at the nose-brain barrier. *Pharm Res* 22:86-93

Graff CL, Zhao R, Pollack GM. (2005) Pharmacokinetics of substrate uptake and distribution in murine brain after nasal instillation. *Pharm Res* 22:235-244

Gupta A, Dai Y, Vethanayagam RR, Hebert MF, Thummel KE, Unadkat JD, Ross DD, Mao Q. (2006) Cyclosporin A, tacrolimus and sirolimus are potent inhibitors of the human breast cancer resistance protein (ABCG2) and reverse resistance to mitoxantrone and topotecan. *Cancer Chemother Pharmacol* 58:374-383

Hans FJ, Wei L, Bereczki D, Acuff V, Demaro J, Chen JL, Otsuka T, Patlak C, Fenstermacher J. (1993) Nicotine increases microvascular blood flow and flow velocity in three groups of brain areas. *Am J Physiol* 265:H2142-2150

Hansen DK, Scott DO, Otis KW, Lunte SM. (2002) Comparison of in vitro BBMEC permeability and in vivo CNS uptake by microdialysis sampling. *J Pharm Biomed Anal* 27:945-958

Hasselbalch SG, Madsen PL, Hageman LP, Olsen KS, Justesen N, Holm S, Paulson OB. (1996) Changes in cerebral blood flow and carbohydrate metabolism during acute hyperketonemia. *Am J Physiol* 270:E746-751

Heiss WD, Herholz K. (2006) Brain receptor imaging. *J Nucl Med* 47:302-312

Hochman JH, Yamazaki M, Ohe T, Lin JH. (2002) Evaluation of drug interactions with P-glycoprotein in drug discovery: in vitro assessment of the potential for drug-drug interactions with P-glycoprotein. *Curr Drug Metab* 3:257-273

Hsieh CH, Chen YF, Chen FD, Hwang JJ, Chen JC, Liu RS, Kai JJ, Chang CW, Wang HE. (2005) Evaluation of pharmacokinetics of 4-borono-2-(18)F-fluoro-L-phenylalanine for boron neutron capture therapy in a glioma-bearing rat model with hyperosmolar blood-brain barrier disruption. *J Nucl Med* 46:1858-1865

Kalvass JC, Graff CL, Pollack GM. (2004) Use of loperamide as a phenotypic probe of mdr1a status in CF-1 mice. *Pharm Res* 21:1867-1870

Kalvass JC, Maurer TS. (2002) Influence of nonspecific brain and plasma binding on CNS exposure: implications for rational drug discovery. *Biopharm Drug Dispos* 23:327-338

Kalvass JC, Maurer TS, Pollack GM. (2007a) Use of plasma and brain unbound fractions to assess the extent of brain distribution of 34 drugs: comparison of unbound concentration ratios to in vivo p-glycoprotein efflux ratios. *Drug Metab Dispos* 35:660-666

Kalvass JC, Olson ER, Cassidy MP, Selley DE, Pollack GM. (2007b) Pharmacokinetics and Pharmacodynamics of Seven Opioids in P-gp-Competent Mice: Assessment of Unbound Brain EC50 and Correlation of In Vitro, Preclinical, and Clinical Data. *J Pharmacol Exp Ther*

Kalvass JC, Pollack GM. (2007) Kinetic considerations for the quantitative assessment of efflux activity and inhibition: implications for understanding and predicting the effects of efflux inhibition. *Pharm Res* 24:265-276

Katoh M, Suzuyama N, Takeuchi T, Yoshitomi S, Asahi S, Yokoi T. (2006) Kinetic analyses for species differences in P-glycoprotein-mediated drug transport. *J Pharm Sci* 95:2673-2683

Klein B, Kuschinsky W, Schrock H, Vetterlein F. (1986) Interdependency of local capillary density, blood flow, and metabolism in rat brains. *Am J Physiol* 251:H1333-1340

Lee G, Babakhanian K, Ramaswamy M, Prat A, Wosik K, Bendayan R. (2007) Expression of the ATP-binding Cassette Membrane Transporter, ABCG2, in Human and Rodent Brain Microvessel Endothelial and Glial Cell Culture Systems. *Pharm Res*

Lee YJ, Kusuhara H, Jonker JW, Schinkel AH, Sugiyama Y. (2005) Investigation of efflux transport of dehydroepiandrosterone sulfate and mitoxantrone at the mouse blood-brain barrier: a minor role of breast cancer resistance protein. *J Pharmacol Exp Ther* 312:44-52

Liu X, Chen C. (2005) Strategies to optimize brain penetration in drug discovery. *Curr Opin Drug Discov Devel* 8:505-512

Liu X, Smith BJ, Chen C, Callegari E, Becker SL, Chen X, Cianfrogna J, Doran AC, Doran SD, Gibbs JP, Hosea N, Liu J, Nelson FR, Szewc MA, Van Deusen J. (2005) Use of a physiologically based pharmacokinetic model to study the time to reach brain equilibrium: an experimental analysis of the role of blood-brain barrier permeability, plasma protein binding, and brain tissue binding. *J Pharmacol Exp Ther* 313:1254-1262

Liu X, Tu M, Kelly RS, Chen C, Smith BJ. (2004) Development of a computational approach to predict blood-brain barrier permeability. *Drug Metab Dispos* 32:132-139

Mahar Doan KM, Humphreys JE, Webster LO, Wring SA, Shampine LJ, Serabjit-Singh CJ, Adkison KK, Polli JW. (2002) Passive permeability and P-glycoprotein-mediated efflux differentiate central nervous system (CNS) and non-CNS marketed drugs. *J Pharmacol Exp Ther* 303:1029-1037

Meyer RP, Gehlhaus M, Knoth R, Volk B. (2007) Expression and function of cytochrome p450 in brain drug metabolism. *Curr Drug Metab* 8:297-306

Meyer RP, Hagemeyer CE, Knoth R, Kaufmann MR, Volk B. (2006) Anti-epileptic drug phenytoin enhances androgen metabolism and androgen receptor expression in murine hippocampus. *J Neurochem* 96:460-472

Mundy WR, Tilson HA. (1990) Neurotoxic effects of colchicine. *Neurotoxicology* 11:539-547

Norinder U, Haeberlein M. (2002) Computational approaches to the prediction of the blood-brain distribution. *Adv Drug Deliv Rev* 54:291-313

Ohtsuki S, Terasaki T. (2007) Contribution of carrier-mediated transport systems to the blood-brain barrier as a supporting and protecting interface for the brain; importance for CNS drug discovery and development. *Pharm Res* 24:1745-1758

Pai HV, Kommaddi RP, Chinta SJ, Mori T, Boyd MR, Ravindranath V. (2004) A frameshift mutation and alternate splicing in human brain generate a functional form of the pseudogene cytochrome P4502D7 that demethylates codeine to morphine. *J Biol Chem* 279:27383-27389

Puchowicz MA, Xu K, Sun X, Ivy A, Emancipator D, LaManna JC. (2007) Diet-induced ketosis increases capillary density without altered blood flow in rat brain. *Am J Physiol Endocrinol Metab* 292:E1607-1615

Raub TJ. (2006) P-glycoprotein recognition of substrates and circumvention through rational drug design. *Mol Pharm* 3:3-25

Schinkel AH, Smit JJ, van Tellingen O, Beijnen JH, Wagenaar E, van Deemter L, Mol CA, van der Valk MA, Robanus-Maandag EC, te Riele HP, et al. (1994) Disruption of the mouse mdr1a P-glycoprotein gene leads to a deficiency in the blood-brain barrier and to increased sensitivity to drugs. *Cell* 77:491-502

Sharom FJ, Lugo MR, Eckford PD. (2005) New insights into the drug binding, transport and lipid flippase activities of the p-glycoprotein multidrug transporter. *J Bioenerg Biomembr* 37:481-487

Shen DD, Artru AA, Adkison KK. (2004) Principles and applicability of CSF sampling for the assessment of CNS drug delivery and pharmacodynamics. *Adv Drug Deliv Rev* 56:1825-1857

Smith QR. (2003) A review of blood-brain barrier transport techniques. *Methods Mol Med* 89:193-208

Strobel HW, Thompson CM, Antonovic L. (2001) Cytochromes P450 in brain: function and significance. *Curr Drug Metab* 2:199-214

Summerfield SG, Read K, Begley DJ, Obradovic T, Hidalgo IJ, Coggon S, Lewis AV, Porter RA, Jeffrey P. (2007) Central nervous system drug disposition: the relationship between in situ brain permeability and brain free fraction. *J Pharmacol Exp Ther* 322:205-213

Summerfield SG, Stevens AJ, Cutler L, del Carmen Osuna M, Hammond B, Tang SP, Hersey A, Spalding DJ, Jeffrey P. (2006) Improving the in vitro prediction of in vivo central nervous system penetration: integrating permeability, P-glycoprotein efflux, and free fractions in blood and brain. *J Pharmacol Exp Ther* 316:1282-1290

Suzuki H, Nagashima T, Tamaki N, Yamadori T. (1998) Cerebral ischemia affects glucose transporter kinetics across rat brain microvascular endothelium: quantitative analysis by an in situ brain perfusion method. *Surg Neurol* 49:67-76

Suzuyama N, Katoh M, Takeuchi T, Yoshitomi S, Higuchi T, Asashi S, Yokoi T. (2007) Species differences of inhibitory effects on P-glycoprotein-mediated drug transport. *J Pharm Sci* 96:1609-1618

Takasato Y, Rapoport SI, Smith QR. (1984) An in situ brain perfusion technique to study cerebrovascular transport in the rat. *Am J Physiol* 247:H484-493

Takenaka K, Morgan JA, Scheffer GL, Adachi M, Stewart CF, Sun D, Leggas M, Ejendal KF, Hrycyna CA, Schuetz JD. (2007) Substrate overlap between Mrp4 and Abcg2/Bcrp affects purine analogue drug cytotoxicity and tissue distribution. *Cancer Res* 67:6965-6972

van Vliet EA, van Schaik R, Edelbroek PM, Voskuyl RA, Redeker S, Aronica E, Wadman WJ, Gorter JA. (2007) Region-specific overexpression of P-glycoprotein at the blood-brain barrier affects brain uptake of phenytoin in epileptic rats. *J Pharmacol Exp Ther* 322:141-147

Venkatakrishnan K, Tseng E, Nelson FR, Rollema H, French JL, Kaplan IV, Horner WE, Gibbs MA. (2007) Central nervous system pharmacokinetics of the Mdr1 P-glycoprotein substrate CP-615,003: intersite differences and implications for human receptor occupancy projections from cerebrospinal fluid exposures. *Drug Metab Dispos* 35:1341-1349

Volk B, Hettmannsperger U, Papp T, Amelizad Z, Oesch F, Knoth R. (1991) Mapping of phenytoin-inducible cytochrome P450 immunoreactivity in the mouse central nervous system. *Neuroscience* 42:215-235

Wan H, Rehngren M, Giordanetto F, Bergstrom F, Tunek A. (2007) High-Throughput Screening of Drug-Brain Tissue Binding and in Silico Prediction for Assessment of Central Nervous System Drug Delivery. *J. Med. Chem.* 50:4606-4615

Xia CQ, Liu N, Miwa GT, Gan LS. (2007) Interactions of cyclosporin a with breast cancer resistance protein. *Drug Metab Dispos* 35:576-582

Yamazaki M, Neway WE, Ohe T, Chen I, Rowe JF, Hochman JH, Chiba M, Lin JH. (2001) In vitro substrate identification studies for p-glycoprotein-mediated transport: species difference and predictability of in vivo results. *J Pharmacol Exp Ther* 296:723-735

Zhuang Y, Fraga CH, Hubbard KE, Hagedorn N, Panetta JC, Waters CM, Stewart CF. (2006) Topotecan central nervous system penetration is altered by a tyrosine kinase inhibitor. *Cancer Res* 66:11305-11313

Zong J, Pollack GM. (2003) Modulation of P-glycoprotein transport activity in the mouse blood-brain barrier by rifampin. *J Pharmacol Exp Ther* 306:556-562

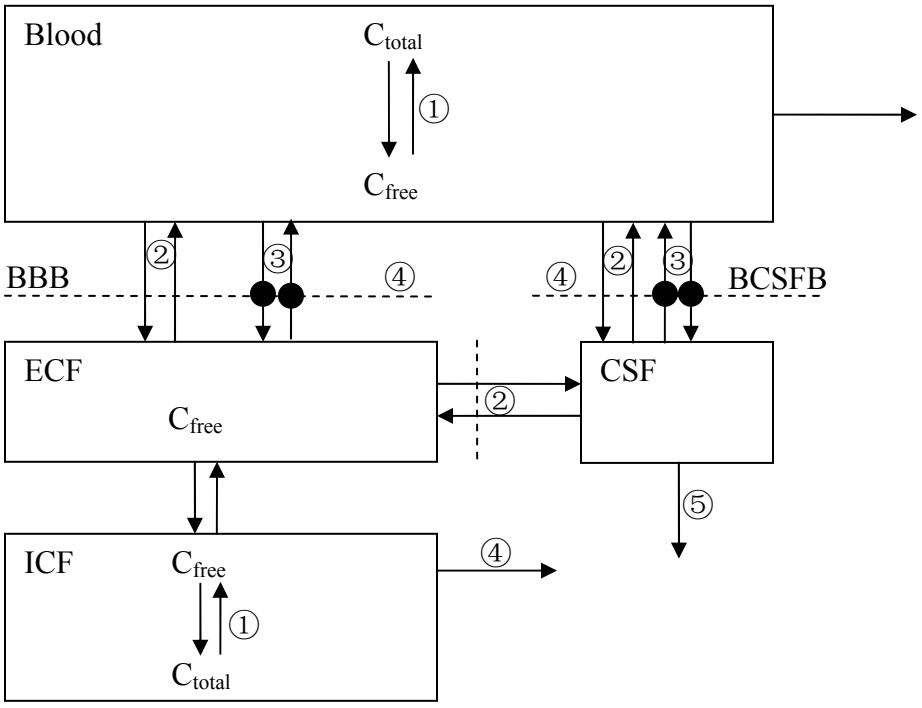

Figure 6.1: A simplified illustration of central nervous system compartmentalization. ①, protein binding; ②, passive diffusion; ③, active transport; ④, metabolism; ⑤, CSF turnover.

Abbreviations: BBB, blood-brain barrer; BCSFB, blood-cerebrospinal fluid barrer; CSF, cerebrospinal fluid; ECF, extracellular fluid; ICF, intracellular fluid.

APPENDIX

PHARMACOKINETICS OF SUBSTRATE UPTAKE AND DISTRIBUTION IN MURINE BRAIN AFTER NASAL INSTILLATION

This chapter has been published in Pharmaceutical Research and is presented in the style of that journal.

ABSTRACT

Purpose: This study was conducted to develop a physiologically-relevant mathematical model for describing brain uptake and disposition of nasally-administered substrates.

Methods: [^{14}C]-antipyrine, [^{14}C]-diazepam, [^{3}H]-sucrose or [^{3}H]-verapamil was administered nasally to CF-1 mice. P-gp-deficient mice also received [^{3}H]-verapamil to probe the influence of P-gp on uptake/distribution. Mice were sacrificed at selected intervals, and 20 serial 300-μm coronal brain sections were obtained to determine radioactivity. A series of compartmental pharmacokinetic models was developed and fit to concentration vs. time/distance data.

Results: After nasal instillation, substrate concentration was highest in the olfactory bulb and decreased with distance. In the absence of transport-mediated flux, peak brain exposure occurred at 6 hr. A catenary pharmacokinetic model with slice-specific brain-to-blood efflux rate constants and slice-to-slice diffusivity factors was capable of fitting the data. P-gp limited fractional absorption of [^{3}H]-verapamil via efflux from the nasal cavity and olfactory epithelium. P-gp also increased the rate constants associated with [^{3}H]-verapamil efflux 1.5 – to –190-fold, depending on brain region. P-gp limited [^{3}H]-verapamil uptake from the nasal cavity into brain, and facilitated removal of [^{3}H]-verapamil from brain during rostral-to-caudal distribution.

Conclusions: Taken together, the data and associated modeling provide a comprehensive assessment of the influence of P-gp on brain uptake and disposition of nasally-administered substrates.

Key Words: P-glycoprotein, Nasal administration, Blood-brain barrier, Pharmacokinetics, Brain Slices

INTRODUCTION

Treatment of central nervous system (CNS) disorders remains challenging, primarily due to the inability of potential therapeutic agents to reach the relevant pharmacologic target. The blood-brain barrier (BBB) forms a nearly impenetrable barrier that excludes compounds based on their physicochemical properties and affinity for active efflux transport (1). P-glycoprotein (P-gp) is a barrier transporter that limits brain uptake of substrates from a variety of therapeutic classes, including protease inhibitors, anti-epileptics and anti-cancer agents (2-4). P-gp is considered a prototypical multidrug resistance (MDR) transport protein, originally identified based on its ability to render cancer cells resistant to chemotherapy (5), and is the most well-characterized of the BBB efflux transport systems. P-gp is a 170-kDa plasma membrane, energy-dependent efflux protein that is a member of the ABC superfamily of transport systems (6, 7), and is expressed on the luminal side of the brain capillary endothelium (8). P-gp expels a wide range of functionality and structurally unrelated compounds from the endothelial cell. In general, P-gp substrates are hydrophobic, amphipathic molecules with a planar ring system, a molecular weight >400 kDa, and a positive charge at pH 7.4 (9). However, due to the complexities involved with multiple substrate and ATP binding sites and conformational changes secondary to substrate binding, no comprehensive structure-activity relationships have been established for P-gp (10).

Due to the formidable obstacle imposed by the BBB, there has been increased interest in developing strategies to overcome this barrier. It has been a widely held view that nasal delivery provides a means to circumvent the BBB and thus may allow increased CNS penetration of compounds that otherwise display limited CNS exposure (11). In general, there are three pathways that a drug administered into the nasal cavity may travel. These routes include entry

into the systemic circulation directly from the nasal mucosa (12), entry into the olfactory bulb via axonal transport along neurons (13), and direct entry into the brain via the olfactory epithelium (14). A drug that enters into the systemic circulation must be absorbed through the nasal mucosa. Administration via this route avoids hepatic/GI first-pass effects and therefore may provide more extensive systemic exposure for substrates that have poor oral bioavailability (15). However, this particular route does not represent an advantage for the delivery of agents to the CNS (as the substrate must traverse the BBB from the systemic circulation), and is thus not a focus of this paper. A drug also may be carried along the olfactory neuron by intracellular axonal transport to the olfactory bulb. This olfactory nerve pathway would allow the drug to be taken up into the neuronal cell (located in the olfactory epithelium) by endocytosis and subsequently transported into the CNS. This pathway is utilized by some metals, viruses, and proteins (13, 16, 17) and represents a path by which the BBB may be bypassed. Despite the ability of this pathway to deliver agents to the olfactory bulb, transport to CNS sites beyond the olfactory system is unclear. Furthermore, this route is slow (requiring hours to days to reach certain brain regions), and thus cannot account for the immediate appearance (within minutes) of some solutes in the brain and/or CSF following nasal administration. The mechanisms governing direct delivery of substrate to the brain via the olfactory epithelium are not well understood. This pathway purportedly involves delivery of the substrate directly to the brain parenchymal tissue, to the cerebrospinal fluid (CSF), or to both (18). While the BBB does not exist at the olfactory epithelium, P-gp (and likely other BBB transporters) is functional at this barrier (19). The experiments reported in this communication were designed to explore the kinetics of brain uptake and distribution via this direct olfactory epithelial pathway.

There is increasing evidence that a direct nose-to-brain pathway (resulting in rapid brain uptake)

exists and can be accessed by a variety of compounds, in both rodent models and humans (14, 20, 21). To exploit this direct olfactory epithelial route of delivery, a compound must cross the olfactory membrane via the transcellular pathway or via the paracellular pathway. The former route is utilized by small lipophilic (primarily by diffusion) or large molecules (primarily by receptor-mediated endocytosis), while the latter route is utilized by small hydrophilic molecules (22). There are a variety of factors that will affect the permeability of nasally-delivered drugs, including the biology of the system (i.e., structural features, pH, mucociliary clearance, and biochemical factors such as enzymes) and formulation factors [i.e., physicochemical properties of the drug and formulation (23)]. For instance, it has been shown that the uptake of drugs into the CSF and brain parenchyma is dependent on molecular weight and lipophilicity. It is clear that a comprehensive understanding of the mechanisms governing this pathway is necessary in order to investigate the use of nasal administration as a practical means of delivering agents to the brain.

Many of the studies examining brain uptake after nasal administration have utilized CSF concentrations as a surrogate for brain exposure. This may not be an accurate representation of pharmacologically relevant CNS penetration since CSF is not necessarily in equilibrium with brain tissue. Other experimental protocols have determined substrate in whole brain, which provides an estimate of overall brain exposure but gives no information regarding localization within the brain. Although regional exposure has been addressed with microdialysis, this method provides information for only one discrete location per animal. Previous studies in this laboratory utilized whole brain homogenate (24), and thus the potential distribution of substrate within the brain, and the pharmacologic implications associated with this distribution, were unclear (19). Therefore, the purpose of the present study was to examine the kinetics of rostral-

to-caudal distribution of nasally-administered compounds (in the absence of transporter-mediated flux) and to develop a mathematical model to explain the disposition of these model compounds. In addition, the impact of P-gp-mediated efflux on brain uptake and distribution was considered with the standard P-gp substrate verapamil.

METHODS

Materials

Probe substrates were obtained from the following sources: [^{3}H]-(±)-verapamil (85 Ci/mmol), [^{14}C]-diazepam (56 mCi/mmol), and [^{3}H]-sucrose (10.2 Ci/mmol) [NEN Life Science Products, Boston, MA]; [^{14}C]-antipyrine (55 mCi/mmol) [American Radiolabeled Chemicals, St. Louis, MO]. All other reagents used in this study were of the highest grade available from commercial sources.

Animals

Adult CF-1 mice [*mdr1a(+/+)* and *mdr1a(-/-)*, 30-40 g, 8-12 weeks of age] were purchased from Charles River Laboratories (Wilmington, MA) and maintained in a breeding colony in the School of Pharmacy, The University of North Carolina. Male and female mice were housed separately (maximum of 4 animals per cage) in wire-mesh cages in a temperature- and humidity-controlled room with a 12-h-dark/12-h-light cycle, and had unrestricted access to food and water. The Institutional Animal Care and Use Committee of the University of North Carolina approved the experimental protocols, and all procedures were conducted according to the "Principles of Laboratory Animal Care" (NIH publication #85-23, revised in 1985).

Nasal Administration

Nasal administration was performed as previously reported (19). Briefly, mice (n=4/group) were anesthetized by intraperitoneal injection of ketamine and xylazine (140 and 8 mg/kg, respectively). The mice were placed in a supine position on a 37°C heating pad to maintain body temperature with the head held back and a dowel (~7 mm) under the neck to limit liquid flow down the trachea. Solutions containing test compounds (pH 7) were warmed to 37°C in a water bath prior to instillation. Tracers were added at a concentration of 0.5 mCi/mL. The solutions (5 μM, 5 μL/nostril) were administered via separate 10-μL gas-tight syringes (2 inch, 23 gauge needle) to each nostril. Timing for the purpose of determining substrate uptake was initiated following completion of instillation. The animals were allowed free mobility upon awakening from the anesthesia. Brain uptake was terminated by decapitation at pre-determined time points (2, 4, 6, 8, 10, 12, 18 hr post-dose). The brain was removed rapidly from the skull, blotted dry, and mounted on a platform with cyanoacrylate to allow coronal slicing.

Systemic Administration

Mice (n=4/group) were anesthetized as described above. Substrates (5 mg/kg in 50% Methanol) with appropriate tracers (0.5 mCi/mL) were administered via tail vein injection (<0.01 mL/g). Brain uptake was terminated by decapitation at 2, 6, or 10 hr post-dose. Following the experiment, the brain was removed and prepared for slicing as described above.

Fresh Tissue Slicing

After allowing the tissue to set for approximately 2 min, the platform was submersed in 2°C phosphate buffered saline (PBS) for slicing (Vibratome 3000, St. Louis, MO). Coronal sections

(300 μm) were cut with a 35º-blade angle using Vibratome feather blades [low speed (setting 1), high amplitude (setting 8)]. Sequential slices were obtained in the rostral to caudal direction. Slices were removed from the buffer and placed in tared 8-mL glass scintillation vials and weighed. The tissue was digested with 0.3 mL Solvable® (Packard, Boston, MA) at 50°C overnight. After cooling, samples were mixed with 5 mL scintillation cocktail (Ultimate Gold XR®; Packard) and total radioactivity was determined. Scintillation counting (referenced to appropriate quench curves for single- or dual-label counting, depending on the experiment) was performed in a Packard Tri-Carb model 1900 TR (Packard). Brain samples obtained from naïve mice were analyzed, and these blanks were subtracted from all samples to correct for apparent background.

Data Analysis

Data are expressed as mean ± SD (n=4) unless otherwise noted. Where appropriate, a two-tailed Student's *t*-test was used to evaluate the statistical significance of differences between experimental groups. In all cases, $P<0.05$ was used as the criterion of statistical significance.

The total fraction of radioactivity in the whole brain at each time point was calculated as the percentage of the total amount of radioactivity in the administered dose:

$$\text{fraction (\%)} = \frac{\text{amount (dpm/mg, brain)} * \text{brain weight (mg)}}{\text{total dose administered (dpm)}} \times 100$$

The area under the slice concentration-time curve ($AUC_{0\rightarrow 18}$ for nasal administration, $AUC_{0\rightarrow 10}$ for systemic administration) was calculated to assess the regional exposure from time zero to 18 hr following nasal administration (and time zero to 10 hr following systemic administration) according to the linear trapezoidal method.

Pharmacokinetic Modeling

Mean data for substrate concentration in each slice at each time point were fit simultaneously with the scheme depicted in Figure A.1A. Because the substrate dose used in these experiments was low, linear conditions were assumed. The model incorporated first-order absorption from the nasal cavity into brain (k_a), with subsequent passive diffusion in the rostral-to-caudal direction between adjacent slices (k_{12}). It was assumed that the slice-to-slice diffusion rate constant was independent of brain region. Flux from the nasal cavity (k_n), as well as from each individual slice (k_{oi}) was included. To account for the different physicochemical properties of the substrates (i.e., lipophilicity), diffusivity factors (Df_j for each compound j) were utilized as a modulator of the absorption rate constant (k_a) and the rate constant for slice-to-slice diffusion (k_{12}).

The amount of [^{14}C]-diazepam or [^{14}C]-antipyrine in wild-type mice, and [^{3}H]-verapamil in *mdr1a(-/-)* animals, in each brain slice was modeled vs. time with the following differential equations:

In the nasal cavity, $\frac{dX_{nasal}}{dt} = -(Df_j \bullet k_a \bullet X_{nasal}) - (k_n \bullet X_{nasal})$

For the first slice, $\frac{dX_1}{dt} = (Df_j \bullet k_a \bullet X_{nasal}) - (Df_j \bullet k_{12} \bullet X_1) - (k_{o1} \bullet X_1)$

For all subsequent slices, $\frac{dX_i}{dt} = (Df_j \bullet k_{12} \bullet X_{(i-1)}) - (k_{oi} \bullet X_i) - (Df_j \bullet k_{12} \bullet X_i)$

For the last slice, $\frac{dX_{20}}{dt} = (Df_j \bullet k_{12} \bullet X_{19}) - (k_{o20} \bullet X_{20})$

where at t=0, $X_{nasal} = F_{abs}*X_0$ (X_0 was the dose administered); for all subsequent slices, the initial value X_i (i=2→20) was equal to zero at time zero.

To account for the impact of P-gp on [^{3}H]-verapamil disposition, additional flux parameters were incorporated from the brain (k_{1p}) and the nasal cavity (k_{np}). In order to determine the value of k_{np}, k_n was fixed at 1.87 hr^{-1}, the value determined in the absence of P-gp-mediated efflux (i.e., from [^{3}H]-verapamil disposition in *mdr1a(-/-)* mice).

The amount of [^{3}H]-verapamil in each brain slice of *mdr1a(+/+)* animals was modeled vs. time with the following differential equations:

In the nasal cavity, $\frac{dX_{nasal}}{dt} = -[(k_{np} + k_n) \bullet X_{nasal}] - (Df_j \bullet k_a \bullet X_{nasal}) + (k_{1p} \bullet X_1)$

For the first slice, $\frac{dX_1}{dt} = (Df_j \bullet k_a \bullet X_{nasal}) - (k_{1p} \bullet X_1) - (k_{o1} \bullet X_1) - (Df_j \bullet k_{12} \bullet X_1)$

For all subsequent slices, $\frac{dX_i}{dt} = (Df_j \bullet k_{12} \bullet X_{(i-1)}) - (k_{oi} \bullet X_i) - (Df_j \bullet k_{12} \bullet X_i)$

For the last slice, $\frac{dX_{20}}{dt} = (Df_j \bullet k_{12} \bullet X_{19}) - (k_{o20} \bullet X_{20})$

where the initial conditions for each slice were as defined above for mdr1a(-/-) animals.

A model based on the scheme depicted in Figure A.1B was utilized to determine whether systemic concentrations contributed significantly to the brain uptake and disposition of model substrates. This model was similar to Model A, but incorporated a first-order absorption into

blood from the nasal cavity (k_b) and bi-directional flux from blood into the sequential slices (k_{pci}, k_{cpi}). It also allowed for elimination of substrate from the blood compartment (k_{ob}).

Model differential equations were fit to the mean data by nonlinear least-squares regression with WinNonlin Software (Pharsight, Palo Alto, CA, USA). Assessment of the goodness of fit of the model to the observed data was based on coefficients of variation (CV%) and distribution of residual error. Akaike's Information Criteria (AIC) was used to compare the appropriateness of alternative model structures.

RESULTS

Brain Uptake Following Nasal Instillation

For all of the compounds studied, the total amount present in the brain (expressed as % dose) following nasal instillation peaked at 6 hr post-dose (Figure A.2). [^{14}C]-diazepam had the highest amount in brain at 6 hr (3.58±0.28%), followed by [^{3}H]-verapamil in the *mdr1a(-/-)* mice (3.16±0.74%) and [^{14}C]-antipyrine (2.84±0.34%). In general, the temporal profiles of these compounds were similar. In contrast, [^{3}H]-sucrose showed very limited uptake (0.91±0.22%), and although the amount in brain peaked at 6 hr, the profile evidenced little relationship with time. The *mdr1a(+/+)* mice exhibited much lower brain uptake of [^{3}H]-verapamil compared to *mdr1a(-/-)* animals (1.2±0.31% at 6 hr; $p<0.001$), consistent with P-gp-mediated efflux. The total amount delivered to the brain (expressed as $AUC_{0\rightarrow18}$) varied among the substrates examined, with [^{14}C]-diazepam displaying the highest exposure (32.8±6.3 %dose*hr/mg), followed by [^{3}H]-verapamil in the *mdr1a(-/-)* mice (29.5±5.3 %dose*hr/mg) and [^{14}C]-antipyrine

(26.2±4.8 %dose*hr/mg). [^{3}H]-sucrose and [^{3}H]-verapamil in the *mdr1a(+/+)* mice both displayed markedly lower brain exposure (8.3±2.3 and 10.2±2.1 %dose*hr/mg, respectively; $p<0.01$ for [^{3}H]-verapamil compared to *mdr1a(-/-)* animals). In the absence of an influence of P-gp, the amount delivered to the brain correlated significantly ($r^2=0.95$) with the log P values of the model substrates (Figure A.3).

Brain Distribution Following Nasal Instillation

Regional exposure (i.e., exposure in each brain tissue slice; dose-normalized and expressed as $AUC_{0\rightarrow18}$) differed among the model substrates (Figure A.4). As was the case with total brain content, [^{14}C]-diazepam exhibited the highest exposure in each slice, followed by [^{3}H]-verapamil in *mdr1a(-/-)* animals, [^{14}C]-antipyrine, [^{3}H]-sucrose and [^{3}H]-verapamil in *mdr1a(+/+)* animals. Exposure was highest in the olfactory region (slices #1-3) and decreased towards the more rostral portions of the brain. In addition, [^{3}H]-sucrose evidenced virtually no substrate exposure beyond slice #5.

Brain Uptake and Distribution Following Systemic Administration

To assess the difference in brain distribution following nasal administration compared to systemic administration, the model compounds also were administered systemically (i.v.) to mice, and both total amount delivered (% dose) and total exposure ($AUC_{0\rightarrow10}$) were determined. Systemic administration resulted in a larger fraction of the dose being delivered to the brain for each of the compounds, and the peak amount in brain occurred at 2 hr (compared to 6 hr for nasal administration). The peak brain content was 11.7±2.6, 8.7±2.3, 5.9±1.8 and 1.3±0.4% for [^{14}C]-diazepam, [^{3}H]-verapamil in *mdr1a(-/-)* mice, [^{14}C]-antipyrine and [^{3}H]-verapamil in

mdr1a(+/+) mice, respectively. There was no [^{3}H]-sucrose detectable in the brain following systemic administration.

The regional exposure also differed between systemic administration compared to nasal administration (Figure A.5). Substrate content following systemic administration was relatively constant across the slices; certainly, preferential accumulation in specific slices was not evident. However, the amount of substrate in slices #7-10 was lower than in other areas of the brain. These slices correspond anatomically with regions containing the striatum, parietal cortex and thalamus, structures that have relatively low blood volumes (25).

Pharmacokinetic Modeling

Serial coronal tissue slicing was used in the present investigation to examine the distribution of substrates in the brain. The primary objective of this study was to determine the effect of lipophilicity and P-gp-mediated efflux on substrate uptake into and distribution within the brain. Thus, a compartmental modeling approach was selected to analyze the data comprehensively. A model based on the scheme depicted in Figure A.1A was fit simultaneously to the substrate concentration vs. slice and time data. Representative descriptions of the data for individual slices are shown in Figure A.6. These panels illustrate the difference in [^{3}H]-verapamil distribution between P-gp-competent and P-gp-deficient mice. Final parameter estimates describing the brain distribution of substrates following nasal instillation in the presence and absence of P-gp are shown in Table A.1. In the presence as compared to absence of P-gp, the efflux rate constants for [^{3}H]-verapamil in each individual slice increased (1.4 to190-fold, depending on brain region), indicative of increased efflux mediated by P-gp within the brain. The presence of P-gp also necessitated the inclusion of two additional flux components, one from the nasal cavity

(k_{np}) and one at the olfactory epithelium (k_{1p}). These localizations are supported anatomically, given that P-gp has been identified in the nasal mucosa (26) and work in this laboratory has demonstrated the presence of P-gp in the olfactory epithelium (unpublished data). The P-gp-mediated efflux from the nasal cavity was larger than at the olfactory epithelium (8.92 vs. 4.32 hr^{-1}, respectively), consistent with the larger surface area of the nasal cavity compared to the olfactory epithelium. The absorption of substrate (from nasal cavity to brain, k_a) was decreased in the presence of P-gp (0.126 vs. 0.0835 hr^{-1}), consistent with P-gp-mediated efflux at this barrier resulting in a reduced rate of absorption. The slice-to-slice diffusional component of the model (k_{12}) remained essentially the same regardless of the presence of P-gp, indicating that the difference in disposition was due primarily to the transporter mediating egress from the brain. It is interesting to note that the diffusivity factors recovered correlated quite well with the reported log P values (and peak % dose absorbed) of these compounds (r^2=0.98).

Three-dimensional representations (comparing amount of substrate vs. time vs. slice number) of the model fit for the distribution of [^{14}C]-diazepam, [^{14}C]-antipyrine and [^{3}H]-verapamil (in *mdr1a(-/-)* and *mdr1a(+/+)* mice) are shown in Figures A.7-A.10, respectively. These profiles clearly demonstrate that substrate exposure is dependent on time after administration, slice number (i.e., specific brain region), lipophilicity (by comparing different substrates), and transporter specificity. In addition, each of these profiles evidenced a consistent plateau in slices obtained from the mid-brain.

To consider the impact of P-gp beyond the olfactory epithelium, the [^{3}H]-verapamil efflux parameters for individual slices in the presence vs. the absence of P-gp were compared, yielding slice-specific P-gp effects (Figure A.11). The influence of P-gp on [^{3}H]-verapamil efflux from brain was dependent on brain region, with the highest P-gp effects observed in slices #6-10.

Alternative models that included various combinations of rate constants and altered compartmental structure were evaluated. For instance, the addition of a blood compartment for only slices #1-3 (corresponding to the olfactory region) was included with bi-directional flux to account for multiple routes of substrate input at this site (from nasal cavity and the systemic circulation). In order to assess the potential for brain uptake occurring via the systemic circulation (following rapid absorption through the nasal mucosa), the model structure shown in Figure A.1B was considered. The data did not support these alternative models, as evidenced by a poor distribution of residual error, increased coefficients of variation for model parameters, and increased AIC. In addition, adjacent slices with similar substrate concentrations and common anatomical structures were grouped and included as lumped compartments. Bi-directional passive diffusion between adjacent slices also was considered, as were various feedback loops. Ultimately, the model structure and data analysis approach (Figure A.1A) chosen were superior and provided the best description of the observed data.

DISCUSSION

The compounds selected for this study were chosen based on physicochemical properties (lipophilicity, molecular weight) and to probe the influence of P-gp on brain uptake from the nasal cavity and subsequent distribution in the organ. Sucrose was selected to assess the feasibility of utilizing the nasal route to deliver a bulky hydrophilic compound that is unable to cross the BBB. Diazepam was chosen as a highly lipophilic model compound, the brain uptake of which has been shown to be blood flow-limited (25). Antipyrine was included in the

compound set due to its intermediate lipophilicity. Finally, verapamil was chosen as a model P-gp substrate to study the effects of P-gp-mediated efflux on brain uptake and distribution.

In the absence of transporter-mediated flux ([^{3}H]-verapamil in *mdr1a(-/-)* mice; all other compounds in wild-type animals) the peak fraction of the dose in brain correlated well with the log P values for this compound set (Figure A.3). This observation suggests that brain uptake from the nasal cavity was mediated by the direct olfactory route, and is consistent with literature for nasal delivery of small molecules. It has been shown previously that uptake of low molecular weight molecules across the olfactory epithelium is dependent on the physicochemical properties of the compound, and that CNS uptake by this pathway correlates with lipophilicity (21).

Serial sectioning of the brain revealed that tissue exposure (i.e., AUC in discrete slices) following nasal delivery was dependent on the specific brain region. Regardless of the substrate examined, nasal delivery resulted in preferential exposure in the rostral portions of the brain; exposure decreased consistently as the compound distributed caudally. The profile for [^{3}H]-sucrose supports the premise that the direct olfactory epithelial pathway was being probed. Although [^{3}H]-sucrose appeared in brain following nasal administration, it did not distribute beyond the olfactory region. Furthermore, no [^{3}H]-sucrose was detectable in the brain following systemic administration (Figure A.5). Thus, the amount observed in brain following nasal administration was the result of a direct nose-to-brain transport. The most lipophilic compound tested, [^{14}C]-diazepam, had the highest total exposure, likely due to efficient diffusion through the olfactory epithelium into the brain. The shape of the profiles for nasally-administered [^{14}C]-antipyrine and [^{3}H]-verapamil (in the *mdr1a(-/-)* animals) were similar to that for [^{14}C]-diazepam, although these compounds had a somewhat lower total exposure, consistent with a lower lipophilicity.

Compared to nasal administration, systemic administration resulted in a more homogenous distribution of substrate in brain. The total exposure for the compounds was slightly increased (<1.5-fold) compared to nasal administration (43.8±8.9, 35.4±7.8 and 25.9±6.2 %dose*hr/mg for [^{14}C]-diazepam, [^{3}H]-verapamil (in *mdr1a(-/-)* mice) and [^{14}C]-antipyrine, respectively). Interestingly, substrate persistence in brain appeared to be lower after systemic compared to nasal administration (data not shown), consistent with previous observations that nasal delivery results in increased residence time in the brain (27). In addition, a distinctly lower exposure was noted for all compounds (except sucrose) between slices #7-10. Anatomically, these slices are comprised of the parietal cortex, striatum and thalamus, which are brain regions with relatively low blood volume (25). If resident blood volumes and blood flow are related, one would anticipate decreased exposure in regions with low blood volume prior to attainment of complete distribution equilibrium. The ability to detect regional differences in substrate exposure that have a known physiologic correlate suggests that the coronal slicing method is sufficiently sensitive to reveal nuances in brain distribution.

The presence of P-gp-mediated efflux resulted in significantly reduced net [^{3}H]-verapamil delivered to the brain (Figure A.2). Also, the profile for [^{3}H]-verapamil distribution in *mdr1a(+/+)* brain compared to *mdr1a(-/-)* animals (Figure A.4) differed somewhat in shape with significantly reduced total exposure, suggesting that P-gp-mediated efflux influenced both initial brain uptake and overall brain distribution following nasal administration.

Since it appeared that serial sectioning was sufficiently sensitive to explore compound distribution within the brain, rigorous mathematical modeling of the data was conducted to further explore and clarify this direct route of delivery. The optimized model (Figure A.1A) was able to describe substrate distribution across time and brain region. Given that [^{3}H]-sucrose

failed to distribute significantly past the olfactory region, it was excluded from the modeling exercise. The data from each slice at each time point was modeled simultaneously to generate a comprehensive 3-dimensional representation of distribution within the brain as a function of time, distance and, in the case of [^{3}H]-verapamil, interactions with an efflux transporter (Figures A.7-A.10). Attempts to consolidate the model by grouping adjacent slices provided inferior results, perhaps due to subtle differences in distribution kinetics between discrete brain regions. The model recovered a single slice-to-slice distributional rate constant for all test compounds, which was modulated by a compound-specific diffusivity factor related to lipophilicity. This result indicates that, in the absence of transporter-mediated flux, physicochemical properties of the compound (i.e., lipophilicity) serve as the primary determinant of brain uptake and distribution.

The results of the modeling for [^{3}H]-verapamil were consistent with earlier work indicating that P-gp is functional at the olfactory epithelium and serves to attenuate brain uptake after nasal administration (19). These results also clearly show that P-gp operates throughout the brain to efflux substrates during rostral-to-caudal distribution. However, the magnitude of the influence of P-gp on substrate residence in brain evidenced distinct regionality. In contrast to compounds such as diazepam that rely solely on diffusional translocation, the brain distribution of substrates of efflux transporters (in this case, P-gp) is dominated by the transporter-mediated process.

Incorporation of P-gp-mediated efflux into the model led to several interesting quantitative results. P-gp was modeled at the nasal mucosa and the olfactory epithelium (represented by the rate constants k_{np} and k_{1p}, respectively); both sites of expression influenced net uptake of [^{3}H]-verapamil into brain from the nasal cavity. P-gp also was modeled throughout the brain (presumably at the BBB), facilitating loss of substrate from each slice. However, the impact of P-gp on substrate distribution varied significantly among brain regions. The k_{oi} ratio between P-

gp-competent and P-gp-deficient animals defined the P-gp effect on substrate persistence in each slice. Between slices #6-10 (anatomically corresponding to the thalamus, striatum and parietal cortex regions; Figure A.11), the P-gp effect was significantly higher than in other regions of the brain. This regionality in P-gp-mediated flux is consistent with recent literature suggesting preferential P-gp induction in the striatum and frontal cortex in a rat seizure model (28), and may suggest an increased basal expression of P-gp in this region. The significance of this observation is not entirely clear, but the pharmacologic implications are apparent. In order to be an effective CNS agent, a compound must be able to access its pharmacologic target. Opioid receptors are concentrated in the thalamus and cortex (29), and the increased P-gp function in these regions suggests that this may serve a protective mechanism for these and perhaps other key receptors. Further studies are needed to elucidate the significance of the apparent regionality in P-gp function within the brain regions.

Both the data and modeling support the direct pathway of delivery via the olfactory epithelium as the primary route of brain uptake for these compounds. Although the present experiments cannot rule out the contribution of the olfactory nerve pathway, the modeling and time frame of the experiments suggest that the primary pathway of delivery being explored is likely direct. It is possible that the direct pathway and the olfactory nerve pathway work coordinately, although such coordination has not been documented. Alternatively, it is possible that exposure via the systemic circulation contributes to rapid substrate appearance in brain. However, the mathematical modeling did not support the presence of significant drug uptake via this route. In addition, it should be noted that this work examined total radioactivity and therefore might represent the disposition of both parent and one or more derived metabolites.

The fact that millions of people are afflicted with debilitating CNS disorders such as Alzheimer's and Parkinson's disease suggest that discovery and development of novel CNS agents will continue at a significant pace. It is imperative that new therapeutic regimens are able to reach relevant pharmacologic target within the brain. Nasal delivery may allow a drug to access a target in the brain more readily than by other routes of administration. However, the mechanisms governing this uptake are only beginning to be understood. In order to exploit this potential delivery route, efforts must be focused on increasing the fraction of the dose that reaches the CNS. A comprehensive characterization of the potential transporters and metabolic enzymes present at the "nose-brain barrier" is required in order to maximize the potential that this delivery route may offer.

REFERENCES

1. C. L. Graff and G. M. Pollack. Drug transport at the blood-brain barrier and the choroid plexus. *Curr Drug Metab* **5**: 95-108 (2004).

2. R. B. Kim, M. F. Fromm, C. Wandel, B. Leake, A. J. Wood, D. M. Roden, and G. R. Wilkinson. The drug transporter P-glycoprotein limits oral absorption and brain entry of HIV-1 protease inhibitors. *J Clin Invest* **101**: 289-94 (1998).

3. W. Loscher and H. Potschka. Role of multidrug transporters in pharmacoresistance to antiepileptic drugs. *J Pharmacol Exp Ther* **301**: 7-14 (2002).

4. E. M. Kemper, A. E. van Zandbergen, C. Cleypool, H. A. Mos, W. Boogerd, J. H. Beijnen, and O. van Tellingen. Increased penetration of paclitaxel into the brain by inhibition of P-glycoprotein. *Clin Cancer Res* **9**: 2849-55 (2003).

5. R. L. Juliano and V. Ling. A surface glycoprotein modulating drug permeability in Chinese hamster ovary cell mutants. *Biochim Biophys Acta* **455**: 152-62 (1976).

6. V. Ling. Multidrug resistance: molecular mechanisms and clinical relevance. *Cancer Chemother Pharmacol* **40 Suppl**: S3-8 (1997).

7. P. F. Juranka, R. L. Zastawny, and V. Ling. P-glycoprotein: multidrug-resistance and a superfamily of membrane-associated transport proteins. *Faseb J* **3**: 2583-92 (1989).

8. E. Beaulieu, M. Demeule, L. Ghitescu, and R. Beliveau. P-glycoprotein is strongly expressed in the luminal membranes of the endothelium of blood vessels in the brain. *Biochem J* **326 (Pt 2)**: 539-44 (1997).

9. F. J. Sharom. The P-glycoprotein efflux pump: how does it transport drugs? *J Membr Biol* **160**: 161-75 (1997).

10. A. R. Safa, U. S. Rao, S. L. Nuti, T. W. Loo, M. C. Bartlett, and D. M. Clarke. Identification and characterization of the binding sites of P-glycoprotein for multidrug resistance-related drugs and modulators. *Curr Med Chem Anti-Canc Agents* **4**: 1-17 (2004).

11. W. H. Frey, 2nd. Bypassing the Blood-Brain Barrier to Delivery Therapeutic Agents tot he Brain and Spinal Cord. *Drug Delivery Technology* **2**: 46-49 (2002).

12. A. A. Hussain, R. Kimura, and C. H. Huang. Nasal absorption of testosterone in rats. *Journal of Pharmaceutical Sciences.* **73**: 1300-1 (1984).

13. J. Henriksson, J. Tallkvist, and H. Tjalve. Uptake of nickel into the brain via olfactory neurons in rats. *Toxicol Lett* **91**: 153-62 (1997).

14. H. S. Chow, Z. Chen, and G. T. Matsuura. Direct transport of cocaine from the nasal cavity to the brain following intranasal cocaine administration in rats. *Journal of Pharmaceutical Sciences.* **88**: 754-8 (1999).

15. A. A. Hussain. Intranasal drug delivery. *Adv Drug Deliv Rev* **29**: 39-49 (1998).

16. S. Perlman, E. Barnett, and G. Jacobsen. Mouse hepatitis virus and herpes simplex virus move along different CNS pathways. *Adv Exp Med Biol* **342**: 313-8 (1993).

17. R. G. Thorne, C. R. Emory, T. A. Ala, and W. H. Frey, 2nd. Quantitative analysis of the olfactory pathway for drug delivery to the brain. *Brain Res* **692**: 278-82 (1995).

18. H. H. Chow, N. Anavy, and A. Villalobos. Direct nose-brain transport of benzoylecgonine following intranasal administration in rats. *Journal of Pharmaceutical Sciences.* **90**: 1729-35 (2001).

19. C. L. Graff and G. M. Pollack. P-glycoprotein attenuates brain uptake of substrates after nasal instillation. *Pharm Res* **20**: 1225-1230 (2003).

20. Y. Wang, R. Aun, and F. L. Tse. Brain uptake of dihydroergotamine after intravenous and nasal administration in the rat. *Biopharm Drug Dispos* **19**: 571-5 (1998).

21. T. Sakane, M. Akizuki, S. Yamashita, T. Nadai, M. Hashida, and H. Sezaki. The transport of a drug to the cerebrospinal fluid directly from the nasal cavity: the relation to the lipophilicity of the drug. *Chem Pharm Bull (Tokyo)* **39**: 2456-8 (1991).

22. L. Illum. Nasal drug delivery--possibilities, problems and solutions. *J Control Release* **87**: 187-98 (2003).

23. P. Arora, S. Sharma, and S. Garg. Permeability issues in nasal drug delivery. *Drug Discov Today* **7**: 967-75 (2002).

24. L. Illum. Transport of drugs from the nasal cavity to the central nervous system. *Eur J Pharm Sci* **11**: 1-18 (2000).

25. C. Dagenais, C. Rousselle, G. M. Pollack, and J. M. Scherrmann. Development of an in situ mouse brain perfusion model and its application to mdr1a P-glycoprotein-deficient mice. *Journal of Cerebral Blood Flow & Metabolism.* **20**: 381-6 (2000).

26. M. A. Wioland, J. Fleury-Feith, P. Corlieu, F. Commo, G. Monceaux, J. Lacau-St-Guily, and J. F. Bernaudin. CFTR, MDR1, and MRP1 immunolocalization in normal human nasal respiratory mucosa. *J Histochem Cytochem* **48**: 1215-22 (2000).

27. W. A. Banks, M. J. During, and M. L. Niehoff. Brain uptake of the glucagon-like Peptide-1 antagonist exendin(9-39) after intranasal administration. *J Pharmacol Exp Ther* **309**: 469-75 (2004).

28. A. Lazarowski, A. J. Ramos, H. Garcia-Rivello, A. Brusco, and E. Girardi. Neuronal and glial expression of the multidrug resistance gene product in an experimental epilepsy model. *Cell Mol Neurobiol* **24**: 77-85 (2004).

29. C. E. Inturrisi. Clinical pharmacology of opioids for pain. *Clin J Pain* **18**: S3-13 (2002).

Table A.1: Final model parameters associated with the brain distribution of [^{3}H]-verapamil after nasal instillation.

	Parameters in the absence of P-gp		Parameters in the presence of P-gp		Parameter Ratio
Parameter (hr^{-1})	**Estimate**	**CV%**	**Estimate**	**CV%**	
k_a	0.126	6.82	0.0835	24.8	0.663
k_{12}	1.32	10.8	1.19	43.5	0.902
k_{o1}	5.48	129	7.62	113.8	1.39
k_{o2}	1.21	46.9	3.22	78.5	2.66
k_{o3}	0.496	47.7	1.75	62.3	3.53
k_{o4}	0.584	47.0	1.23	48.8	2.11
k_{o5}	0.610	56.2	1.12	32.5	1.84
k_{o6}	0.151	78.9	0.872	78.2	5.77
k_{o7}	0.216	62.3	3.27	48.2	15.14
k_{o8}	0.0204	212	2.24	198.8	110
k_{o9}	0.0110	168	2.11	223.6	192
k_{o10}	0.0831	150	2.87	143.4	34.5
k_{o11}	0.319	78.3	0.983	87.2	3.08
k_{o12}	0.521	59.3	1.23	56.8	2.36
k_{o13}	0.186	61.2	0.822	48.8	4.42
k_{o14}	0.394	78.2	1.29	112.5	3.27
k_{o15}	0.451	34.6	1.89	89.8	4.19
k_{o16}	0.649	48.8	1.24	65.7	1.91
k_{o17}	0.893	52.1	2.74	49.9	3.07
k_{o18}	1.27	57.3	3.21	123.4	2.53
k_{o19}	1.89	47.5	3.78	65.4	2.00
k_{o20}	4.89	68.9	7.13	43.4	1.46
k_n	1.87	168	1.87	187.7	1
k_{np}	n/a	-	8.92	72.3	n/a
k_{1p}	n/a	-	4.32	68.2	n/a
F_{abs} (%)	2.03	78.5	2.03	84.8	n/a
	Diffusivity Factors				
Diazepam	3.12	43.6	n/a	-	n/a
Verapamil	2.52	58.8	2.52	84.3	1
Antipyrine	1.13	38.6	n/a	-	n/a

*[^{3}H]-verapamil only

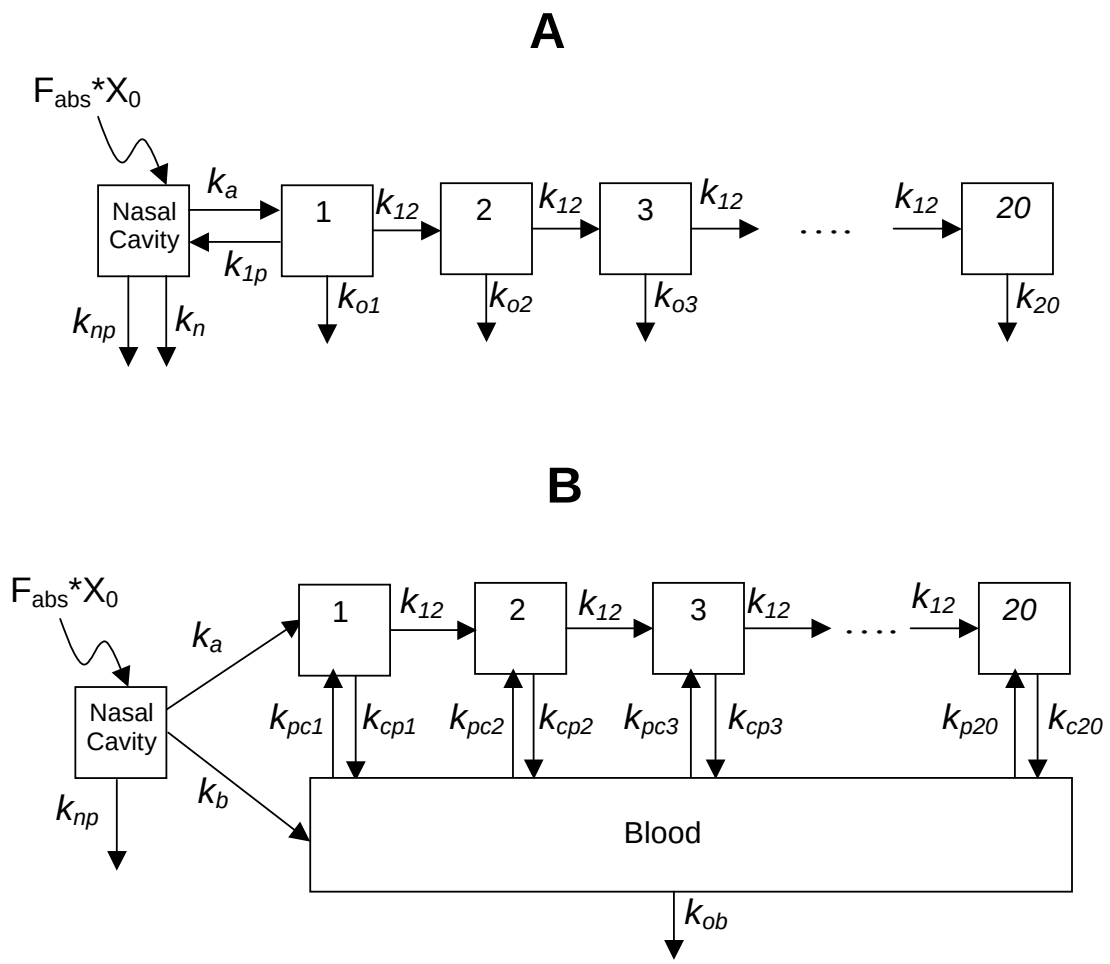

Figure A.1: Panel A. Scheme of the model for brain uptake and disposition following nasal administration via the olfactory epithelium. F_{abs} represents the fraction of dose absorbed with X_0 representing the dose. k_a represents the apparent first-order absorption rate constants into brain from the nasal cavity; k_n represents the first-order rate constant for non-P-gp-mediated flux from the nasal cavity; k_{1p} and k_{np} are first-order rate constants representing P-gp-mediated flux from the brain and nasal cavity, respectively; k_{12} represents the first-order rate constant for passive diffusion between adjacent slice compartments (in a rostral-to-caudal direction only); k_{oi} represents the first-order rate constant for the passive diffusion out of the i^{th} brain section. Diffusivity factors (D_{fj} for each compound j) were included in the final model structure to

account for the lipophilicity of each compound and were incorporated into k_a and k_{12}. **Panel B.** Scheme of the best model fit for brain uptake via systemic circulation following nasal administration. The parameters are the same as for model A with additional parameters representing absorption into blood (k_b), absorption rate constants for flux between blood and brain (k_{pci} and k_{cpi}) and flux out of blood (k_{ob}).

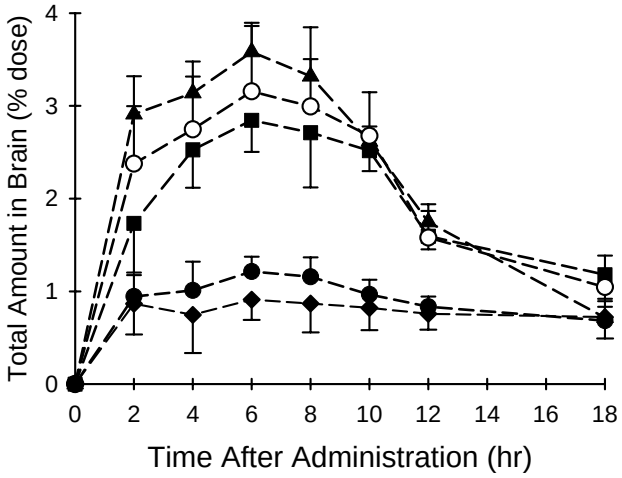

Figure A.2: Time course of [^{14}C]-diazepam (triangles), [^{14}C]-antipyrine (squares), [^{3}H]-sucrose (diamonds) and [^{3}H]-verapamil [circles, closed in *mdr1a(+/+)*, open in *mdr1a(-/-)* animals] following nasal administration represented as % dose in brain. Symbols represent mean ± SD (n=4).

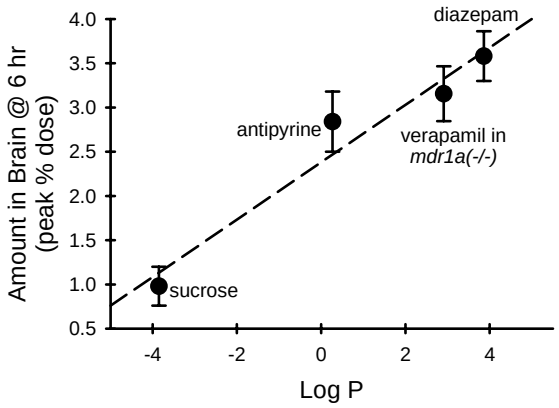

Figure A.3: Relationship between reported log P values and the peak amount of drug delivered to the brain following nasal administration. Data represent mean ± SD (n=4) and the line represents the linear regression through those points ($y=2.38x + 0.32$; $r^2=0.95$).

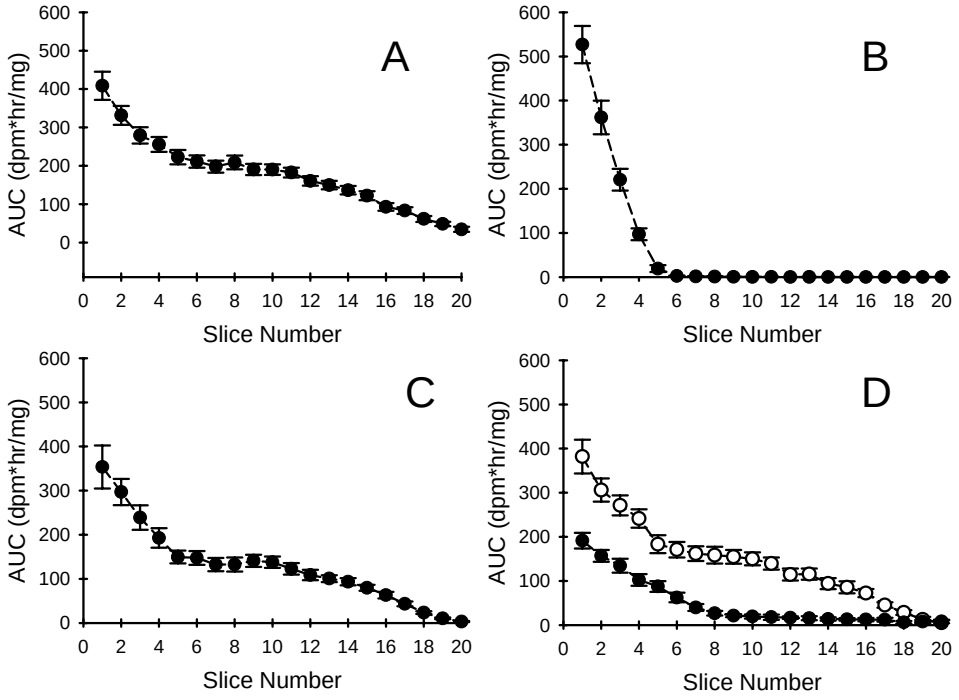

Figure A.4: Regional exposure (expressed as AUC0→18) resulting from the distribution of substrates following nasal administration. Symbols represent mean ± SD (n=4). **Panel A** describes the distribution of [^{14}C]-diazepam, **Panel B** describes the distribution of [^{3}H]-sucrose, **Panel C** describes the distribution of [^{14}C]-antipyrine, and **Panel D** describes the distribution of [^{3}H]-verapamil [• in *mdr1a(+/+)* and **o** in *mdr1a(-/-)* animals].

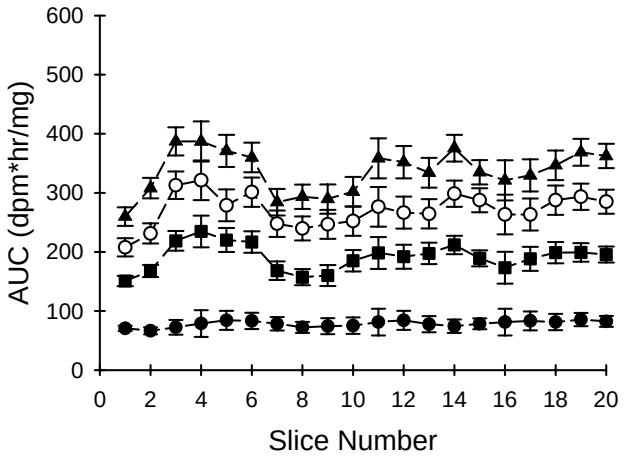

Figure A.5: Regional exposure of substrates (expressed as AUC0→10) following systemic administration. Triangles represent [^{14}C]-diazepam, squares represent [^{14}C]-antipyrine, and circles represent [^{3}H]-verapamil [open in *mdr1a(-/-)* and closed in *mdr1a(+/+)* animals].

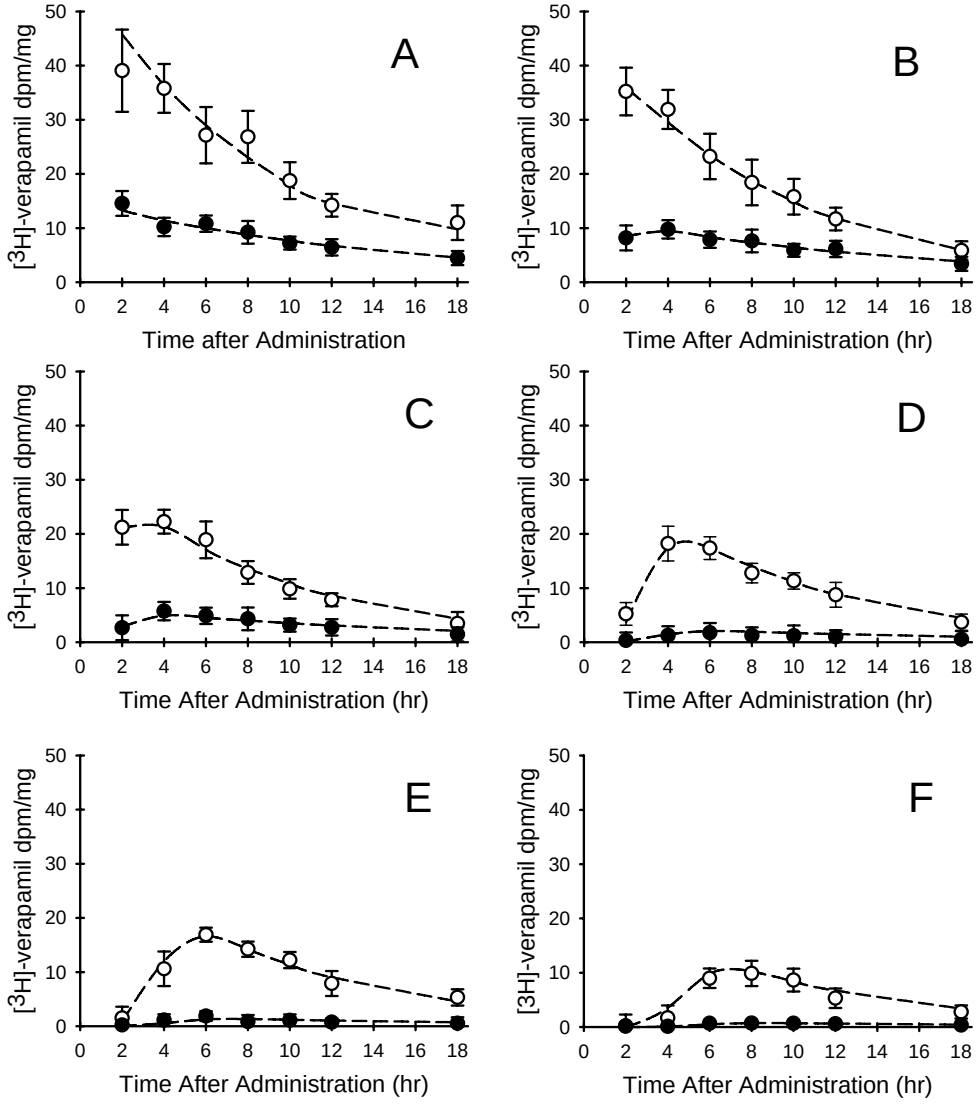

Figure A.6: Representative fit of the model to data from individual brain slices following nasal administration. Data are mean ± SD (n=4); the line indicates the model fit. Open symbols indicate [^{3}H]-verapamil in *mdr1a(-/-)* animals and closed circles indicate [^{3}H]-verapamil in *mdr1a(+/+)* animals. The individual slices shown are: slice #1 (**Panel A**), slice #3 (**Panel B**), slice #5 (**Panel C**), slice #9 (**Panel D**), slice #11 (**Panel E**) and slice #14 (**Panel F**). These slices were selected as representative of different brain regions and illustrate typical goodness-of-fit of the model to the data.

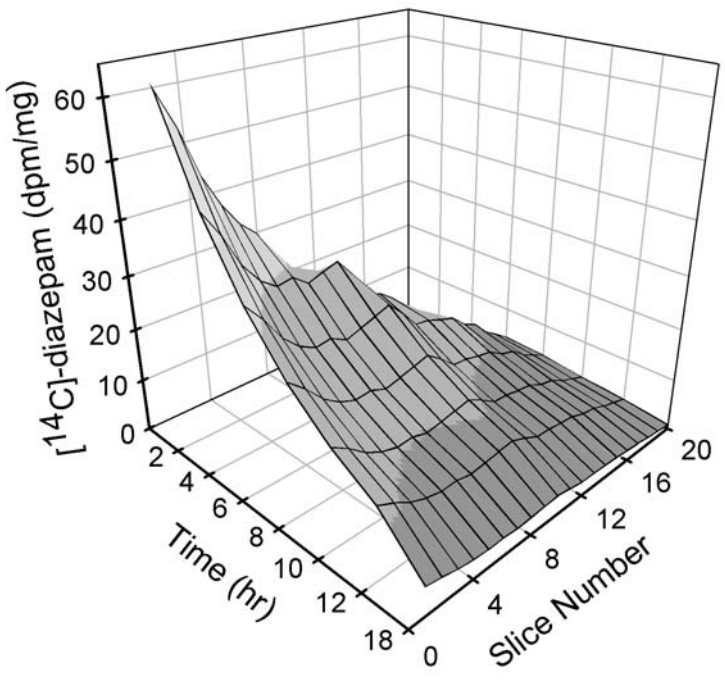

Figure A.7: 3D-representation of the brain disposition of [^{14}C]-diazepam following nasal administration accounting for the influence of time and region on substrate exposure showing the influence of both brain region and time after administration on substrate accumulation.

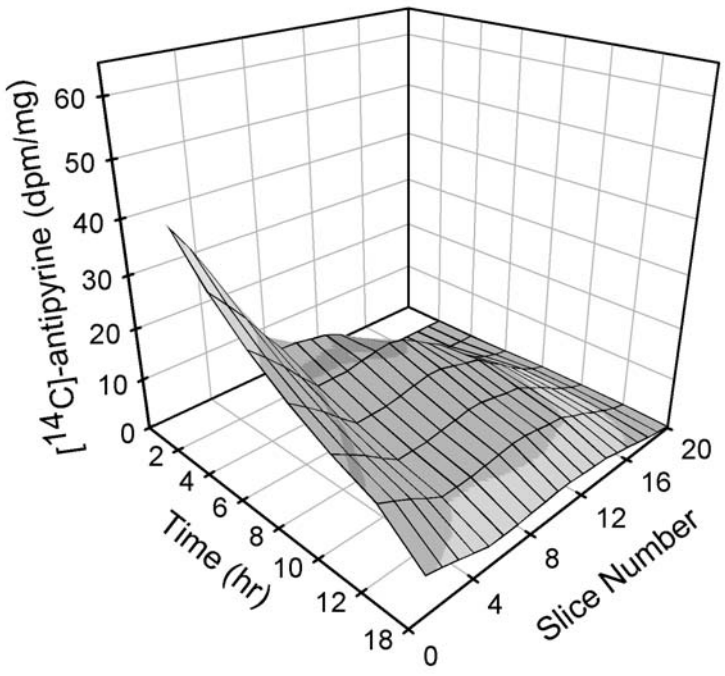

Figure A.8: 3D-representation of the brain disposition of [^{14}C]-antipyrine following nasal administration accounting for the influence of time and region on substrate exposure showing the influence of both brain region and time after administration on substrate accumulation.

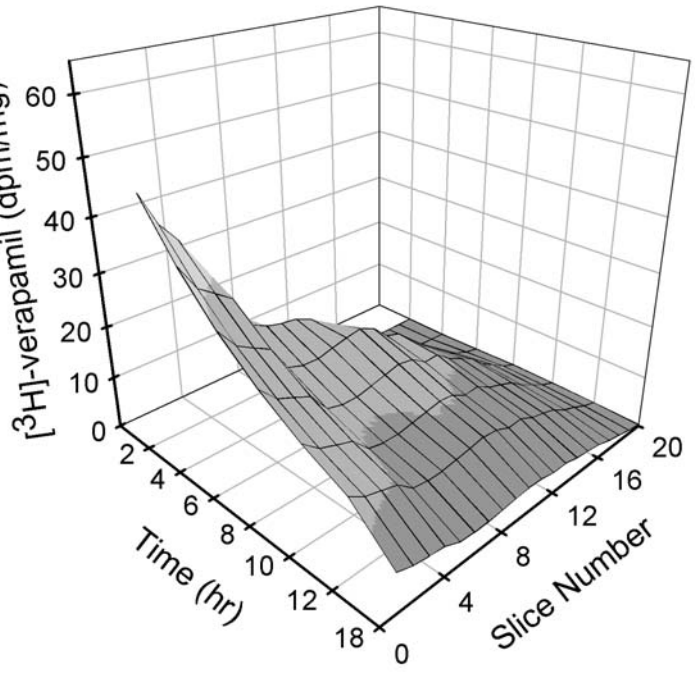

Figure A.9: 3D-representation of the brain disposition of [^{3}H]-verapamil (in mdr1a(-/-) mice) following nasal administration accounting for the influence of time and region on substrate exposure showing the influence of both brain region and time after administration on substrate accumulation.

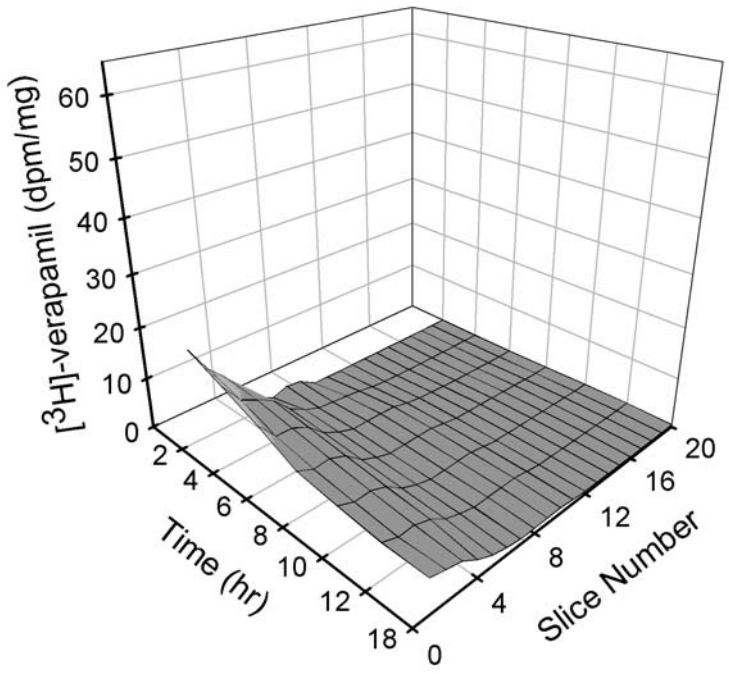

Figure A.10: 3D-representation of the brain disposition of [^{3}H]-verapamil (in *mdr1a (+/+)* mice) following nasal administration accounting for the influence of brain region, time after administration, and P-gp-mediated efflux on substrate exposure.

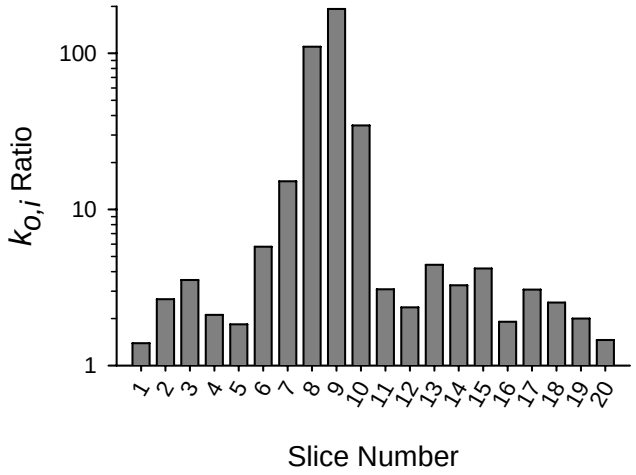

Figure A.11: P-gp effect of [^{3}H]-verapamil loss from individual slices (*i* = slice number). P-gp effect is expressed as the ratio of k_{oi} estimates in *mdr1a(+/+)* vs. *mdr1a(-/-)* animals. Note that the y-axis is shown as a log scale.